Sea Silk

Multiscale study of structure-function relationships in *P. nobilis* byssus and its traditional processing into golden yarn

vorgelegt von
M. Sc.
Delphine Pasche
ORCID: 0000-0002-4178-2251

von der Fakultät II - Mathematik und Naturwissenschaften
der Technischen Universität Berlin
zur Erlangung des akademischen Grades
Doktor der Naturwissenschaften
-Dr. rer. nat.-

genehmigte Dissertation

Promotionsausschuss:

Vorsitzender: Prof. Dr. Norbert Esser
Gutachterin: Prof. Dr. Birgit Kanngießer
Gutachterin: Prof. Dr.-Ing. Claudia Fleck
Gutachter: Prof. Dr. Dr.h.c. Peter Fratzl

Tag der wissenschaftlichen Aussprache: 5. Juli 2019

Berlin 2019

To *Pinna*

Was liegt am Strand und redet undeutlich?

Eine Nuschel

Kurzzusammenfassung

Auf der Suche nach nachhaltigen Alternativen zu Kunststoff, liegt ein immer größerer Fokus der Forschung auf biomimetischen Ansätzen und natürlichen Fasern wie Seide und Byssusfäden, den Haftfäden verschiedener Muschelarten. Byssusfäden sind ein beeindruckendes, widerstandsfähiges und selbstheilendes Material, welches z.B. das Überleben von Miesmuscheln in der Brandungszone ermöglicht.

Bislang wurden hauptsächlich Byssusfäden der Gattung *Mytilus* untersucht. Am viel besser studierten Material Seide ist jedoch zu erkennen, dass erst vergleichende Studien über Seide verschiedenen Ursprungs jene bahnbrechende wissenschaftlichen Erkenntnisse über den Aufbau der Fasern brachten, welche die Herstellung künstlicher Seide erst ermöglichten. Folglich ist auch die genauere Untersuchung von Byssusfäden anderer Muschelarten von hohem wissenschaftlichem Interesse. Die Byssusfäden der Steckmuschel *Pinna nobilis* (*P. nobilis*) sind in diesem Kontext besonders interessant, da sie sich in Morphologie und Funktion grundlegend von jenen der Gattung *Mytilus* unterscheiden. Des weiteren werden die Byssusfäden von *P. nobilis* in einem traditionellen Handwerk zu „Muschelseide“, einem goldenen Garn, verarbeitet. Die Herstellung von Muschelseide aus Byssusfasern erfolgt durch eine Behandlung, welche viel implizites Wissen über den Aufbau und die Eigenschaften der Byssusfäden beinhaltet.

Da die Eigenschaften von natürlichen Materialien von ihrer hierarchischen Struktur bestimmt werden, wurden im ersten Teil dieser Arbeit die Byssusfäden von *P. nobilis* mit Hilfe von Transmissionselektronenmikroskopie und Röntgenbeugung untersucht. Für einen weitergehenden Vergleich wurden die Byssusfäden von drei mit *P. nobilis* verwandten Muschelarten *Atrina pectinata*, *Pinctada fucata* und *Pinctada margaritifera* charakterisiert. Die Untersuchung zeigt, dass die Byssusfäden sowohl von *P. nobilis* als auch der drei anderen Arten aus hochgradig ausgerichteten Nanofibrillen bestehen. Diese Fibrillen wiederum bestehen aus einem ungewöhnlichen Baustein: Einer Helix aus globulären Proteinen, ähnlich wie auch bei Aktin oder den Pili von Bakterien. Als extrakorporale Bausteine von Materialien wurden vergleichbare Strukturen allerdings bisher nicht nachgewiesen.

Der zweite Teil dieser Dissertation untersucht die Beziehung zwischen der Protein-Helix als Baustein und den mechanischen Eigenschaften der Byssusfäden von *P. nobilis*. Dazu wurden sowohl Zugversuche allein, als auch in Kombination mit Röntgenstreuung (XRD) durchgeführt. Die Byssusfasern zeigten hierbei ein ungewöhnliches viskoelastisches Verhalten mit zwei Wendepunkten im Spannungs-Dehnungs-Diagramm. Die Verformung zu Beginn des Zugversuches kann mit der Streckung der Helices erklärt werden. Das Plateau nach dem ersten Wendepunkt ist wahrscheinlich auf das Brechen von labilen Bindungen (wahrscheinlich Metall-Protein-Komplexe) und durch den dadurch verursachten Längenzuwachs zurückzuführen. Ähnlich wie die Byssusfäden der *Mytilus*-Muscheln, sind auch die Fasern von *P. nobilis* in der Lage, durch Zugversuche verursachte mechanische Schäden teilweise zu heilen, wenn eine Regenerationszeit vorhanden ist. Die Beziehung von

Struktur und Funktion der Faser weist auch auf das Vorhandensein einer weiteren Komponente mit einer höheren Steifigkeit als die der Proteinhelices, hin.

Der dritte Teil der Dissertation befaßt sich mit der traditionellen Verarbeitung von Byssusfäden zu Muschelseide. Die Verarbeitung verursacht eine Farbänderung und verändert die mechanischen Eigenschaften. Im Labor ließ sich dies teilweise durch die Verwendung von Zitronensaft und Lösungen aus Zitronensäure reproduzieren. Die Farbänderung scheint mit einer Verringerung des Eisengehalts in den Fasern zusammenzuhängen. Die Veränderungen der mechanischen Eigenschaften konnten nur teilweise reproduziert werden, vermutlich weil nicht alle Aspekte der traditionellen Verarbeitung im Labor reproduziert werden konnten.

Insgesamt liefern die Ergebnisse dieser Arbeit erste wissenschaftliche Erkenntnisse über die eigenartigen Bausteine der Byssusfäden von *P. nobilis* und ihr Verhältnis zu den Fasereigenschaften. Die Arbeit zeigt außerdem die essentielle Rolle der labilen Bindungen aus Metall-Protein-Komplexe in verschiedenen Arten von Byssusfasern und fügt der Liste der natürlichen Materialien mit Metall-Protein-Komplexen interessante neue Struktur hinzu. Die Arbeit liefert mit der Charakterisierung des Einflusses auf die Fasern während der traditionellen Verarbeitung von Byssusfäden zu Muschelseide neue Einsichten in dieses traditionelle Handwerk.

Ich hoffe, diese Arbeit ist ein kleiner Schritt vorwärts auf dem Weg zur Entwicklung nachhaltiger Materialien und hilft das Wissen über die aussterbende Tradition der Muschelseidenherstellung zu bewahren.

Abstract

In search of sustainable alternatives to plastic, an increasing amount of research is focusing on biomimicry and natural fibers such as silk and byssus, the anchoring fibers of mussels. Byssus is an impressive self-healing and tough material which enables the survival of mussels in wave-beaten seashores. However, most of the understanding of byssus arises from deep study of Mytilus spp., while the success of silk research based on comparative studies underlines its importance for the extraction of design principles for biomimicry. Thus it is essential to develop the knowledge of byssus from other species. In this light, Pinna nobilis byssus is especially interesting, because it has very a different morphology and function than Mytilus, but also because it is the object of a long tradition of producing sea silk, an artisanal golden byssus yarn. Sea silk fabrication requires a traditional treatment, in which a lot of tacit knowledge on the byssus structure and properties is embedded. Because their hierarchical structure determines the properties of natural materials, the first part of this work consisted in the investigation of P. nobilis byssus structure using TEM and XRD. In order to enrich the comparison, I also characterized the byssus of three related species: Atrina pectinata, Pinctada fucata and Pinctada margaritifera. I discovered that the byssus of P. nobilis and all three related species was made of highly aligned nanofibrils comprised of an unusual building block: a helix made out of globular proteins, such as actin or bacterial Pili. To my knowledge, this is a structure never observed in an extra-organismic material so far. In the second part, I investigated the relationship between this building block and the mechanical properties of P. nobilis byssus. For this I used tensile testing alone and combined with XRD. This showed that the byssus of P. nobilis had an unusual viscoelastic behavior, with a tensile curve presenting two yield points. The initial deformation could be attributed to helix stretching whereas the plateau following the first yield point could be attributed to some hidden length and sacrificial bonds (likely metal-protein coordination). Like Mytilus, P. nobilis byssus experienced damage after undergoing yield, which partially self-healed after a resting period. This structure-function relationship investigation also suggested the presence of an additional phase, much stiffer than the superprotein helixes. Finally, the traditional processing of P. nobilis byssus to sea silk was seen to induce a change in color and a decrease in mechanical properties, part of which could be reproduced in the lab using simple lemon juice or citric acid solutions. The change in color seemed to be associated to a decrease in Iron, whereas the change in mechanical properties could not be completely replicated in the lab and may be due partially to other aspects of the treatment (e.g. saliva). These findings provide a first understanding of the peculiar building blocks of P. nobilis byssus and their relationship with the byssus properties. This work also pointed out the importance of sacrificial bonds and metal-protein coordination in different types of byssus while adding one more structure to the diversity of natural materials. Finally it also provides a completely new insight of the traditional processing of P. nobilis byssus into sea silk by characterizing its effect on the byssus structure and properties. By doing so, I hope that this work represents a small step further in the development of more sustainable materials as

well as allows to prevent the complete loss of knowledge associated with the dying tradition of sea silk production.

Table of contents

List of figures

List of tables

List of abbreviations

A. pectinata..... *Atrina pectinata*
A. rigida.....*Atrina rigida*
AFM.....Atomic force microscopy
Ala.....Alanine (amino acid)
Asp.....Aspartate (amino acid)
B. mori.....*Bombyx mori*
Cys.....Cysteine (amino acid)
DOPA.....3,4-dihydroxyphenylalanine
E.coli.....*Escherichia coli*
EDTA.....Ethylenediaminetetraacetic acid
EDX.....energy-dispersive X-ray spectroscopy
FFT.....Fast Fourier Transform
FTIR.....Fourier transform infrared spectroscopy
Glu.....Glutamate (amino acid)
Gly.....Glycine (amino acid)
Hyp.....Hydroxyproline (amino acid)
ICP-OES.....inductively coupled plasma optical emission spectrometry
Ileu.....Isoleucine (amino acid)
Leu.....Leucine (amino acid)
Lys .....Lysine (amino acid)
M. californianus.....*Mytilus californianus*
M. edulis.....*Mytilus edulis*
Met..... Methionine (amino acid)
microCT.....micro-Computer Tomography
P. fucata.....*Pinctada fucata*
P. margaritifera.....*Pinctada margaritifera*
P. nobilis.....*Pinna nobilis*
Phe.....Phenylalanine (amino acid)
PreCol.....prepepsinized collagen
PreCol-D.....Distal prepepsinized collagen
PreCol-NG.....non-graded prepepsinized collagen
PreCol-P.....Proximal prepepsinized collagen
Pro.....Proline (amino acid)
SAXD.....Small Angle X-ray Diffraction
SAXS.....Small Angle X-ray Scattering
SEM.....Scanning electron microscopy
Ser.....Serine (amino acid)
spp.....species
TEM.....transmission electron microscopy
Thr..... Threonine (amino acid)

Tyr..... Tyrosine (amino acid)
UHRTEM.....Ultra High Resolution treasmission electron microscopy
Val.....Valine (amino acid)
WAXD.....Wide Angle X-ray Diffraction
WAXS.....Wide Angle X-ray Scattering
XRD.....X-ray diffraction
XRF.....X-ray fluorescence spectroscopy

1 Introduction

After thousands of years relying solely on natural fibers[1,2], the invention of synthetic fibers like Nylon was perceived as a revolution[3–5] through all the new possibilities they offered with their durability and resistance. However, as the drawbacks of synthetic materials on the environment and health becomes increasingly noticeable[6], scientists are turning back to natural materials in search of sustainable replacements[7,8] and are rediscovering their advantages. Indeed, natural materials like silk, wood and byssus, the anchoring fibers of mussels, have many advantages including sustainable production, high mechanical properties and biodegradability. Along these lines, my thesis investigates the ancient fabric known as sea silk, which is fabricated from the byssus fibers of the noble pen shell mussel *Pinna nobilis* in an attempt to see what a deeper understanding of this material might hold for our future and what it may tell us about our past.

It was long believed that the use and production of tool, since about 2.5 million years ago marked the turning points between animals and humans. It has since been discovered that tool-making is not a strictly human endeavor since lower primates were also found to make and utilize tools[1], in contrary to clothing fabrication. The production of clothing remains, to date, exclusive to humans[1]. Along with their ability to produce fire, the fabrication of garments and textiles largely contributed to the survival and expansion of humans by helping them to endure various extreme climates[2]. Thus, the development of fibers, fabrics and clothing production has been tightly connected to human progress [9].

Clothing production started approximately in 500 000 BCE, in the form of animal skin and fur held together by leather lace[9]. Flax and wool are thought to have been among the first fibers used by humans for textiles: traces of spun and dyed flax fibers and goat hairs were dated to as early as 30 000 BCE[10]. The introduction of spinning and weaving allowed the use of resistant fibers like flax and nettle to produce sewing thread, baskets and ropes[10]. Around 8000BC, the first kind of knitting technique, called nalbinding, was created[11], and the basis of textile fiber processing was already largely in place: raw material processing in order to change its mechanical properties, fibers spinning with distaff and spindle to increase their resistance, weaving and knitting to produce a final material of desired shape. From about 4000 BCE[12,13], humans learned how to ret plant fibers in order to separate the fibrils and gain in flexibility. Moreover, most of animal and plant fibers known today were discovered relatively early on, including silk (about 6500BC)[14], cotton (around 5700-4450BC)[5,15] and hemp (around 5000BC)[16]. The first rudimentary looms appeared around 4400-3300BC[5,12], and after this, no major evolution occurred in textile production until the appearance of the spinning wheel around 1530[17]. Spinning and clothing production nevertheless remained a slow artisanal process until the invention of Spinning Jenny, the first mechanical spinning machine in 1767[18] and the invention of the automated loom in 1785[5,18]. Along with the industrial revolution, steam and waterwheel powered spinning machines and looms provoked a revolution in fabrics production in Western countries during the 19th century, moving textile production to big factories[5].

The next revolution in textile and other fiber-based materials, was provided by the arrival on the market of the first man-made fibers. The first successful artificial fiber was Rayon, in the beginning of the 20th century, obtained by reaction of Carbon disulfide and cellulose[5]. Since Rayon is cellulose based, it was still considered a semi artificial fiber, in contrary to Nylon, created in the 1930s from chemicals extracted from petroleum[3,4]. It became a great success in replacement of Japanese silk during the Second World War, first restricted to military application such as parachutes and ropes[4]. After the war, its application extended to an incredible amount of other objects like stocking, fabrics, tires[3,4]. This was followed by the creation of the first Polyester in 1941[4,5], which is nowadays the most used synthetic fiber. Man-made fibers soon spread across the whole world, with almost 50 million tons produced in 2015[19], due to their incredible mechanical and chemical properties[4]. More durable than natural fibers, it is also possible to tune them to make them wear resistant[20], water repellent[21,22] or fire retardant[23] for example.

However, petroleum-based products have introduced a number of unintended global complications due to the high release of greenhouse gases, the non-degradability of these materials and the rapid depletion of our limited oil resources. Therefore, it becomes urgent to find sustainably produced alternatives to current man-made synthetic fibers[6]. This shines a new light on natural fibers, plant or animal based, due to their renewable production, biocompatibility and degradability. In addition, the building blocks of most traditional textile fibers, including cellulose, keratin and silk proteins, have been found to have very interesting combination of properties: toughness and strength combined with a low density[24–30] which provides a promising role model toward the development of more sustainable materials, either by directly using (modified) natural materials, or producing synthetic ones using recombinant proteins produced by example by bacteria. Along these lines, byssus, the protein-based anchoring fibers of marine mussels, has been shown to have exemplary material properties including high toughness, wet adhesion and self-healing capacity, which have evolved presumably as an adaptive response to life in wave–beaten habitats[31–34]. Additionally, byssus from a certain species has also been used for about 2000 years as a textile called sea silk, although this practice has been largely abandoned during the Second World War[35]. Sea silk is made out of the byssus of *Pinna nobilis* (*P. nobilis*), a bivalve species living in the Mediterranean Sea. *P. nobilis* byssus is processed following a traditional artisanal protocol based on lemon juice, as evoked by Swinburne in 1785[36] and orally reported by the byssus artisan Chiara Vigo. Historically, this textile was regarded to be lighter and warmer than silk, but its most valued property was its golden color, especially when exposed to sunlight. Therefore, sea silk was reserved for rich and powerful people, such as kings and priests, and in the Roman Empire, only the ruling class was allowed to wear sea silk[37].

P. nobilis and its byssus had a mysterious aura and gave rise to diverse legends concerning its origin, such as the Chinese sea sheep legend, or the tale of the Syrian lamb[38]. This confusion is also expressed by the various names given to *P. nobilis* byssus throughout history and

languages. Indeed, byssus was historically used to designate different thin fabrics, especially from linen, cotton or silk[39], before being used to designate the anchoring fibers from mussels. According to Felicitas Maeder[40], the names to describe *P. nobilis* byssus were numerous in French, German, Italian and English languages, going from “poil de nacre” (Nacre hairs) and “Fischwolle” (fish wool) to “bisso marin” (marine byssus). Most of them referred to *P. nobilis* byssus and the fabrics produced from it as wool or silk. The hypothesis was put forth that this was because they were often added of one of the two in order to make them more resistant[41]. In this work *P. nobilis* fibers are referred as byssus when considered from a biochemical and ecological point of view, and sea silk when referring to their cultural aspect, especially after their traditional processing, according to the appellation in use in this different research fields.

Due to its long history as textile material, the byssus of *P. nobilis* has not only attracted the attention of the public and proved its utility for human usage, but it is also rich in tacit knowledge, like many other artisanal craftsmanships, including the treatment of plant fibers (flax retting) or silk. Tacit knowledge[42] is comprised of all the traditions and secrets of traditional craftsmanship that were transmitted orally and can only be passed from individual to individual. These kind of traditional methods are highly adapted to the structure and properties of the treated materials and its future application. This tacit knowledge is essential to the field of byssus research since the byssus of *P. nobilis* currently remains much less understood than byssus from other species from a structure-function perspective. For example, in contrast to marine mussels from *Mytilus* species (spp.), the hierarchical structure of the protein-based *P. nobilis* byssus has not been determined; nor has the exact effect and role of the traditional lemon juice treatment been elucidated.

Because of its usage as a traditional fabric and the intense interest in the byssus as technological material and bio-inspiration source[43–47], the byssus of *P. nobilis* lays at a peculiar crossroads between emerging technology and ancient culture. Accordingly, the aim of this work is to study *P. nobilis* byssus both as a potential role model for development of high-performance polymers of the future and as a traditional material that has played an important part in cultural traditions in ancient Mediterranean societies. To do so, I aim first to establish and understand the hierarchical structure of *P. nobilis* byssus and its relationship to its properties and function. In a second step, I will investigate the purpose and effect of the artisanal lemon juice treatment and how it contributes to transform the underwater anchoring mussel fibers into the golden colored fabrics fancied for centuries by ancient populations. In other words, I will study how the structure and properties of *P. nobilis* byssus are modified by the treatment to adapt the change in function from a mechanical and optical perspective.

1.1 Biological Materials Science and Bio-Inspired Materials

Generally speaking, the approach to investigating biological materials such as *P. nobilis* byssus is different from how one studies synthetic materials. This is because man-made

fibers and natural fibers have a fundamentally different origin. Whereas man-made fibers are the product of chemists working in a lab towards the goal of fabricating a material with defined properties, natural fibers are the results of eons of evolution and natural selection and are fabricated by a living organism from biomolecular building blocks such as polysaccharide chains and proteins. The study of natural materials is thus, in its essence, highly interdisciplinary crossing boundaries of evolutionary and organismal biology, chemistry, materials science and engineering. As some of these concepts might be new to the reader, they will be introduced and explained in section 1.2. Due to the complexity of natural materials, their scientific investigation is an iterative process, from fundamental research to mimicry, and over again. Silk is one of the best understood biological fibers from a structure-function perspective, which has led to the production of recombinant silk fibers that successfully mimic the structure and properties of natural silk[48]. Thus, silk research provides a useful guide for investigation of other biological fibers, including the focus of the current thesis on sea silk, and therefore, I will include a discussion of silk research.

1.2 The study of natural materials

Even if the foreseen end of oil reserves in about 50 years was to be postponed[49–52], the oil prices are very likely to rise in the near future as petroleum availability decreases[53]. In addition, it becomes more and more urgent to drastically reduce our CO_2 emissions in order to minimize the associated climate change and limit its impact on the population[54]. Yet material production is one of the big sectors generating CO_2 and other Greenhouse gas[55,56], due, on one hand, to the energy cost of their production, (extracted from fuel and gas), and on the other hand to the nature of the raw material (oil or metals). Moreover, both plastic and metal industries emit numerous harmful byproducts, and the non-biodegradability of plastic is a huge environmental problem: according to current production and waste rates, by 2050, 12 000 million Metric tons of plastic will be in landfill or in the nature[6]. Because of this, there is a lot of room for improvement in material science[56]. Additionally, nature offers a great variety of highly adapted solutions which has inspired and continues to inspire the development of numerous man-made materials, devices and tools. Innovative materials were inspired on one hand by natural structural designs: Velcro was inspired by observation of how burrs attach to animal fur[57], the hierarchically structured surfaces of lotus leaves have led to the development of superhydrophobic and self-cleaning surfaces[58–60], gecko foot pads have led to development of remarkable reversible adhesives capable of supporting of large loads, biocompatibility and enabling soft robotic grip (e.g. Geckskin®)[43,61–69] and the micro and nano-textured surface of shark skin has provided inspiration for hydro- and aero-dynamic surfaces of in realms ranging from aviation, automotive design and diving suits[70–74]. On the other hand, numerous cutting the edge materials were inspired by natural chemical features: bone-mending and wound-healing have inspired the invention of self-healing epoxies and composite[75] while plant-based movements have spurred invention of autonomic actuators based on swellable hydrogel components[76,77]. Each example clearly indicates the importance of nature as a role model for future design of advanced materials.

However, none of the above examples has exploited the power of nature to produce this incredible variety of high-performance materials in a very clean and efficient way. Yet, by combining the already proven inspiration offered by nature for the creation of technological materials with its sustainability, bio-mimicry, meaning taking inspiration from nature, could provide answers to some of today's problems[78] For that we need to manage to not only reproduce structures from natural materials, but also to produce them the way nature does, using bio-degradable and sustainable building blocks in an energy efficient clean process.

Indeed, in order to be able to learn from nature, it is essential to contemplate how nature produces these materials and how this is different from how humans produce materials[79]. Most man-made materials are designed for a specific purpose defined by the engineer, whereas elucidating this purpose is an integral part of the question when studying natural materials[79]. Thus, the questions posed by the synthetic materials scientist and biological materials scientist are different: -"what are the properties of the chemistry and structure I created, do they fit my purpose?" versus: - "what are the structure, chemistry and properties of this structure, and what is the purpose that they are fulfilling?" Indeed, natural materials have arisen through the process of evolution guided by natural selection and selective pressures and limited material resources in the natural environment have had a strong influence on determining the structure, function and composition of these materials. While falling short of true "optimization", the resulting materials combine effective and appropriate materials properties with the economic use of material and energy resources[79].

In addition, biological materials by their very nature must be comprised of a limited selection of building blocks, which must be either synthesized by the organism (e.g. biomolecules) or acquired from the local environment (e.g. ions). Biomolecular components produced within the living cells include polysaccharides (e.g. cellulose and chitin), proteins (e.g. collagen, keratin, silk fibroin) as well as lipids and fatty acids. It is not uncommon for these biomolecules to be combined with inorganic components such as metal ions or even minerals, as in the case of bone or mollusk shells[80]. These building blocks are assembled at moderate temperatures and pressure, which can be reached by an organism, via self-assembly from aqueous solutions. This is especially impressive considering the high heat and/or pressure required in man-made production of metals, plastics and ceramics. Moreover, the self-assembly of building blocks in natural materials produces very well-defined hierarchical structures, meaning that these materials are organized at different length scales[80]. Thus, structural studies of natural materials are particularly extensive due to the usual complexity of their hierarchical structure[79]. This can be well observed in the lobster's exoskeleton for example (Figure 1).

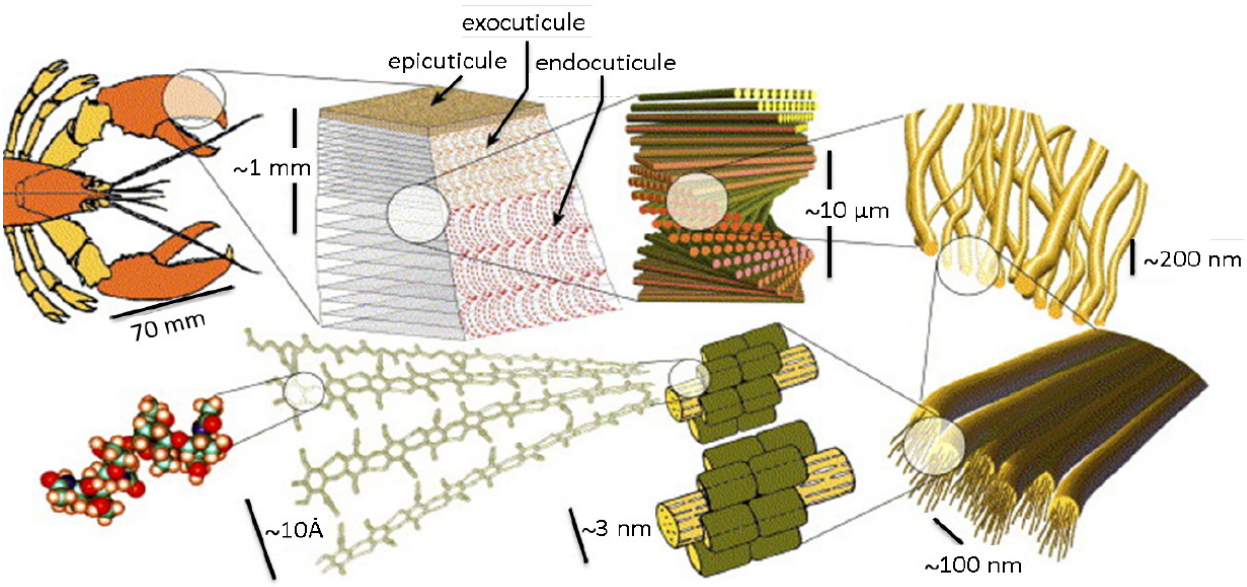

Figure 1 Lobster exoskeleton as an example of hierarchy of natural materials
Chitin (a) forms crystals (b) which are wrapped in proteins (c), forming long fibers (d). Those fibers are forming a planar branched network (e). Several of these planar structures organize into twisted plywood structure (f), which form the structurally and mechanically graded structure (g) of the lobster exoskeleton (h). Reproduced from Raabe et al [81] with permission from Elsevier.

In addition, it is always important to consider the concept of "evolutionary baggage" when studying biological material design. This is the term used to describe the fact that living organisms are not able to invent brand new material solutions to physical challenges out of the blue as humans are, but rather tend to repurpose (via evolution) existing building blocks already coded for in the genetic information. This is a simple result of the fact that evolution occurs via natural selection of random mutations to the existing genetic code that accumulate over time. Thus, these new materials do not respond to a need that was already present in the organism, but rather, they allow organisms to occupy new ecological niches or to become more effective in a certain function. In this sense, the function and the material were evolved together[82], as opposed to most man-made materials, which were engineered towards specific desired functions. However, the evolutionary baggage also means that not all features of a natural material are relevant for its function – some features have been retained during the evolution of the considered material.

Because of these differences, natural materials must be studied in a different way than man-made materials. The investigation of a natural material should focus on the relationship between structure and function, which is the crucial feature for every natural material, while considering the context of the ecological niche in which the organism lives and has evolved. In a biomimicry optic, the natural production process which allows the production of these hierarchical structures should also to be part of the study in order to be able to eventually produce similar structures in a renewable way. Engineering of natural materials has peculiar advantages not only in the cases where it is not possible to cultivate it naturally in adequate quantities (see the spider silk example in section 1.3), but it also allows to create diverse forms and features which extend the field of possible applications (silk foam or drug delivery

capsules). Moreover, biomimicry is an inherently iterative process: adapting biological material design principles into synthetic materials also improves or challenges the understanding of the hypothesized role of this feature in the natural system (Figure 2).

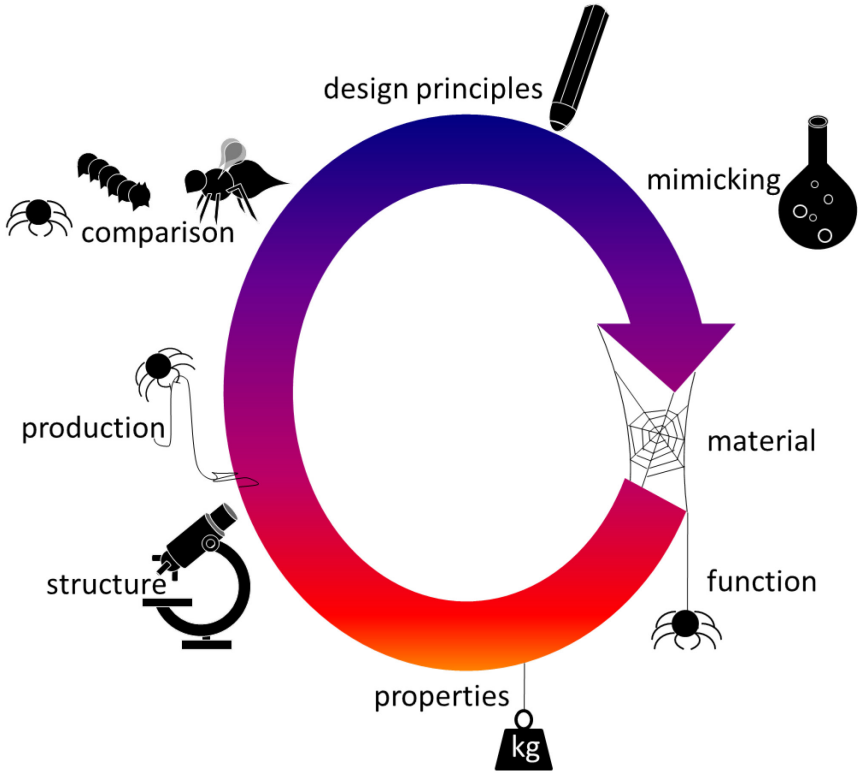

Figure 2 Schematic explanation of the iterative process of natural material study
from structure-function-properties-natural production relationship to mimicking through comparative study and the extraction of key design principles.

This iterative learning process is already quite advanced for certain natural materials, such as *Mytilus* byssus and spider/silkworm silk. In fact, silk provides a great example of a successful bio-mimicry process: after having been used for at least 8000 years in its natural (or slightly modified) state, it drew the interest of the scientific community about 100 years ago due to the impressive mechanical properties of spider silk, especially in terms of toughness[27,83]. This interest has continued strong since then, and silk biomimicry is now in the engineering phase, with companies and scientists finding more and more applications based on the production of artificial silk proteins. Because silk research is so advanced, there is a lot to learn from it to better inform research on other natural materials. Therefore, in the next paragraphs, I will provide an overview of silk research and biomimicry. This is especially relevant since silkworm silk from *Bombyx mori* and sea silk from *Pinna nobilis* have much in common with regards to historical background, value, traditional processing, tacit knowledge and fabric production.

1.3 The example of silk

1.3.1 Traditional treatment and usage of silk

Like *P. nobilis* byssus, silk produced by the silkworm *Bombyx mori* (*B. mori*) is a natural material which has a long history of human usage: the first discovered traces of silk fabrics go back far before sea silk to about 6500 BCE in China[14]. However, the ancient Chinese managed to keep sericulture techniques secret until 140 BCE. From that point on, this technology and material spread to the neighboring countries and eventually, was exported to Western countries, along the famous Silk Road, which enabled a lot of other goods and ideas to travel, emphasizing again how important developments in textile technologies were in human history [84,85]. By the 6th century, Europe was also producing silk based on silkworms smuggled out of China by two monks. Those worms were the source of the whole European sericulture until the 19th century, when a plague devastated the European silkworms cultures[86], and the production therefore moved back to Asia[87].

Traditionally, silk is made from cocoons of cultivated *B. mori* moths. Each female lays 300-400 eggs, which become larvae after 10 days. After six weeks, these larvae begin to spin a cocoon around themselves[88]. *B. mori* worm cocoons are made out of 600-1500 m of a single fiber consisting of two proteins: a fibroin core, which is the part used in fabrics and a gummy protein called sericin, which coats the fibroin core. Sericin also holds the silk together in its cocoon shape; therefore, it needs to be removed in order to be able to unravel the cocoon. This is made by throwing the inhabited cocoon in boiling water, sometimes with soap (this also kills the worm). Then, the end of the thread of several cocoons are gathered and reeled together to form a fiber[86–88]. Through this preprocessing, the silk fibers could then be woven into fabrics.

Analogous to sea silk, silkworm silk was mostly used to produce fabrics, which had a special meaning in the society, showing higher social class or royalty[89,90]. In China, embroidered pieces were worn by emperors, officials and priests as a way to distinguish them from the lower classes who could only afford to wear cotton or plain colored silk[90]. In Korea, people below a certain social class were even forbidden by law to wear silk at all[89]. This material was so valuable that people could even use it to pay taxes, and armies sometimes got paid in silk[91]. It was also very prized as a gift, and was a symbol of the emperor's wealth[87,89,90]. In Europe as well, silk was and remains a very luxurious material. Besides its usage as clothing, silk was also known for its useful properties in case of injuries: in ancient Greece, thousands of years ago, cobwebs were used to stop bleeding, and more recently, during the 20th century, silk was a prized suture material, due to its mechanical properties and biocompatibility[92,93].

1.3.2 Silk as a natural material and the interest of comparative studies

Beyond the extensively studied silkworms and spider, a large variety of insects also produce fibers that are also referred to as silks, including honey bees, glowworms, fleas and beetles,

although in some cases their biochemical and structural similarities to spider and silkworm silks is minimal[94]. Nonetheless, these various silk fibers are all composed of protein building blocks and are typically produced by different secretory glands situated at different locations within the organisms. Depending on the organism, silks can have applications as various as prey capture, web, sperm support, lifeline, nest building, cocoon covering, tunnels covering, rafts to support eggs on water[94](Figure 3).

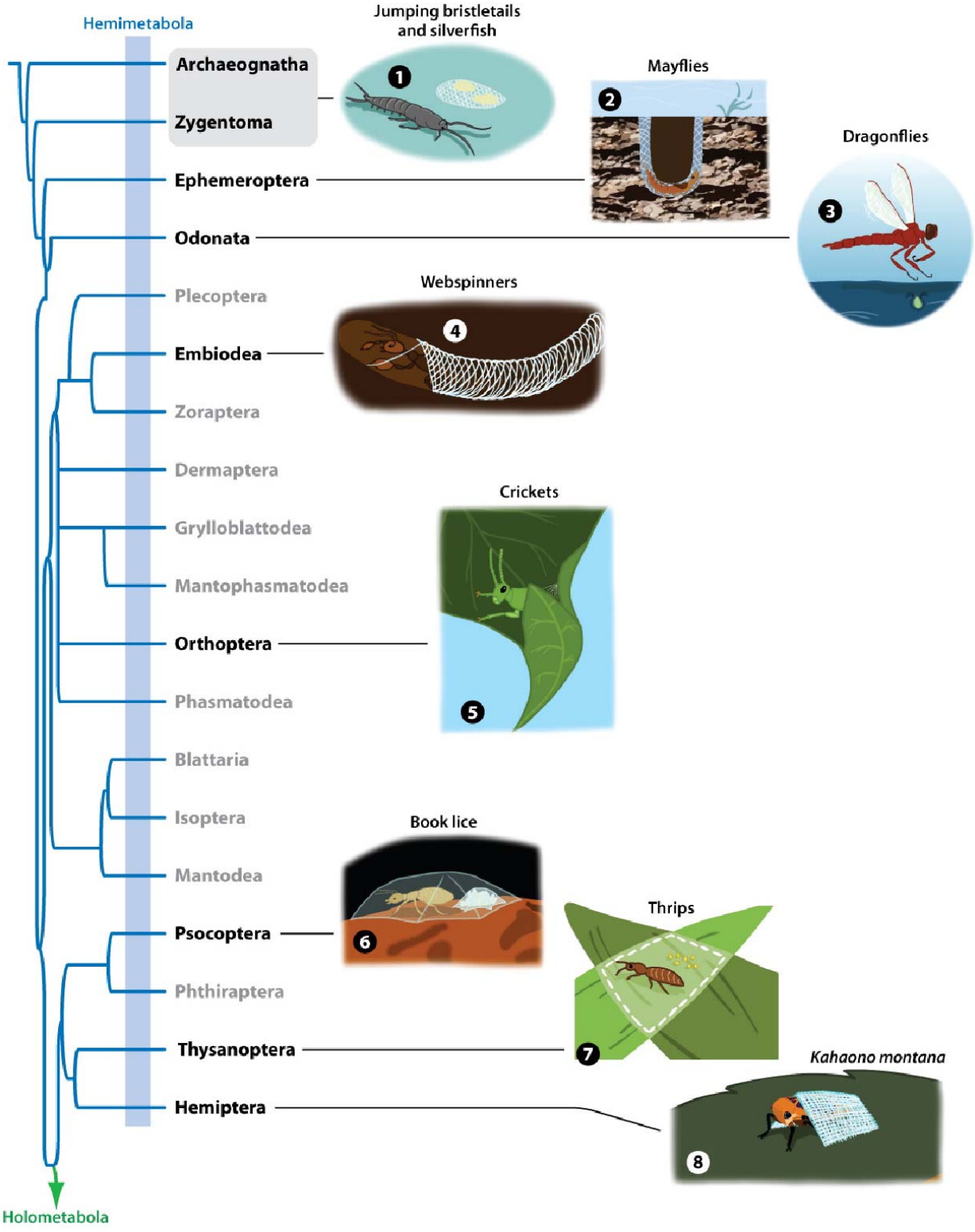

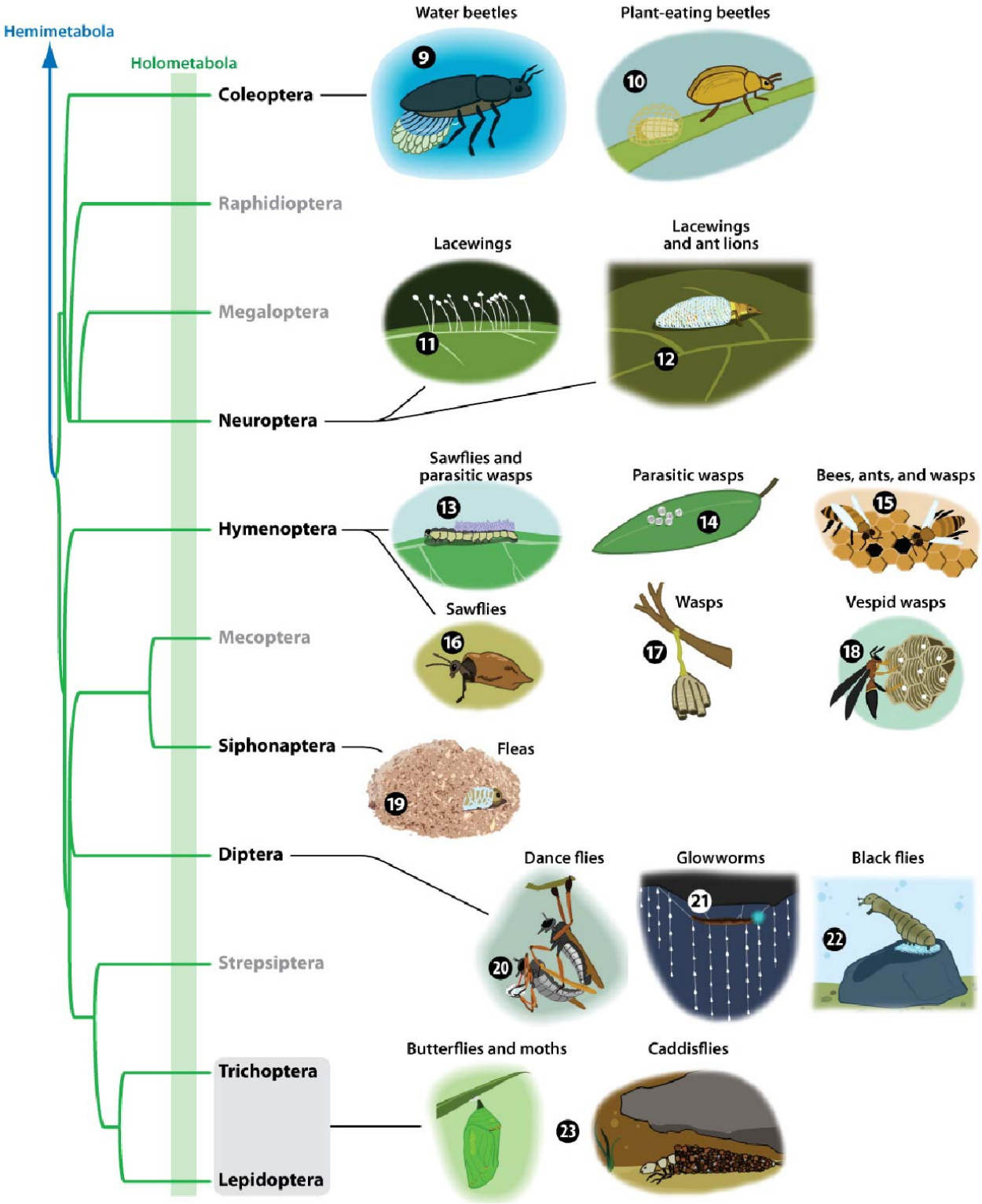

Figure 3 Diversity of insect silks: Phylogenetic relationship of silk-producing insects
There is a large variety in silk-producing insects and silk utilizations. Reproduced from Sutherland et al.[94] with the permission of the entomological society of America.

Not only is silk produced by a high variety of species for diverse applications, but also utilize different protein structures as diverse as: α-helices, extended β-sheets, cross β-sheets, collagen triple helices and polyglycine II [94]. All silks are made out of a combination of highly crystalline proteins and amorphous domains; however, the type of crystalline structures do not necessarily correlate with the purpose of the silk (although they will undoubtedly influence the properties). The various silk structures could however be related to the classification of the insects: so far, silk could be considered homologous (same structure and produced by a similar gland) within 14 of the 17 studied orders[94]. Sutherland concluded from these results that the high diversity in silk structures is probably the results of a convergent evolution. In other words, the many types of silks evolved independently in the different orders and reached a similar material solution because it was a highly effective one, rather than evolving one initial material adapted to different applications[94]. Sutherland argues that changing one crystalline protein structure into another is not so plausible. Indeed, this becomes more apparent if one considers how different protein folds might appear in the silk fibers of different species. Protein folding is directly determined by the sequence of the protein, the location and repetition of its bulky, hydrophobic and hydrophilic side chains geometrically determining what conformation the protein can adopt. Sutherland et al. explains that in most of the cases, it is not possible to change the secondary structure of a protein by exchanging only one of its amino acids, which would correspond to one mutation. Indeed, the change from one secondary structure into another one often requires several exchanges of amino acids; thus several mutations which are very unlikely to happen all at once. Therefore, a single mutation would rather only prevent the protein from folding into a crystalline structure and thus, impede the function of the material and the survival of the animal.

Thus, such comparative studies allow the discrimination between the essential biochemical features contributing to the material performances from less important ones, indicating that high crystallinity combined with some amorphous phase is the most essential silk feature for its production and function[95]. The achievement of high crystallinity is directly linked to the biochemical processing occurring within the organism during silk production[26]. One prominent model of silk assembly argues that silk proteins are stored as a highly concentrated aqueous solution within the insect which becomes ordered into a liquid crystalline phase during the drawing process (Figure 4b left). The loss of entropy due to the alignment of the protein solution into liquid crystals as it passes the spigot is compensated by a decrease in viscosity that helps the fluid to go through the spigot (or spinneret, the valve where the insect expels the silk, see Figure 4a)[96]. It is thought that the high protein concentration is important because it allows the production of a continuous thread as the liquid passes through the spigot (Figure 4a) by increasing the viscosity of the solution to a point where it is not breaking into droplets anymore. Insects start making silk by depositing a droplet of silk onto a surface and pulling on it by moving away. This creates additional shear forces that further align the proteins, and allows the creation of Hydrogen bonds between them[96]. Formation of hydrophobic interactions between proteins during silk formation

further leads to expelling of water. The alternative proposed mechanism (Figure 4b right) involves the formation of micelles due to hydrophobicity of the proteins within the insects, their coalescence into globules as the water content decreases and a deformation of the protein clusters due to shear forces during the spinning[97].

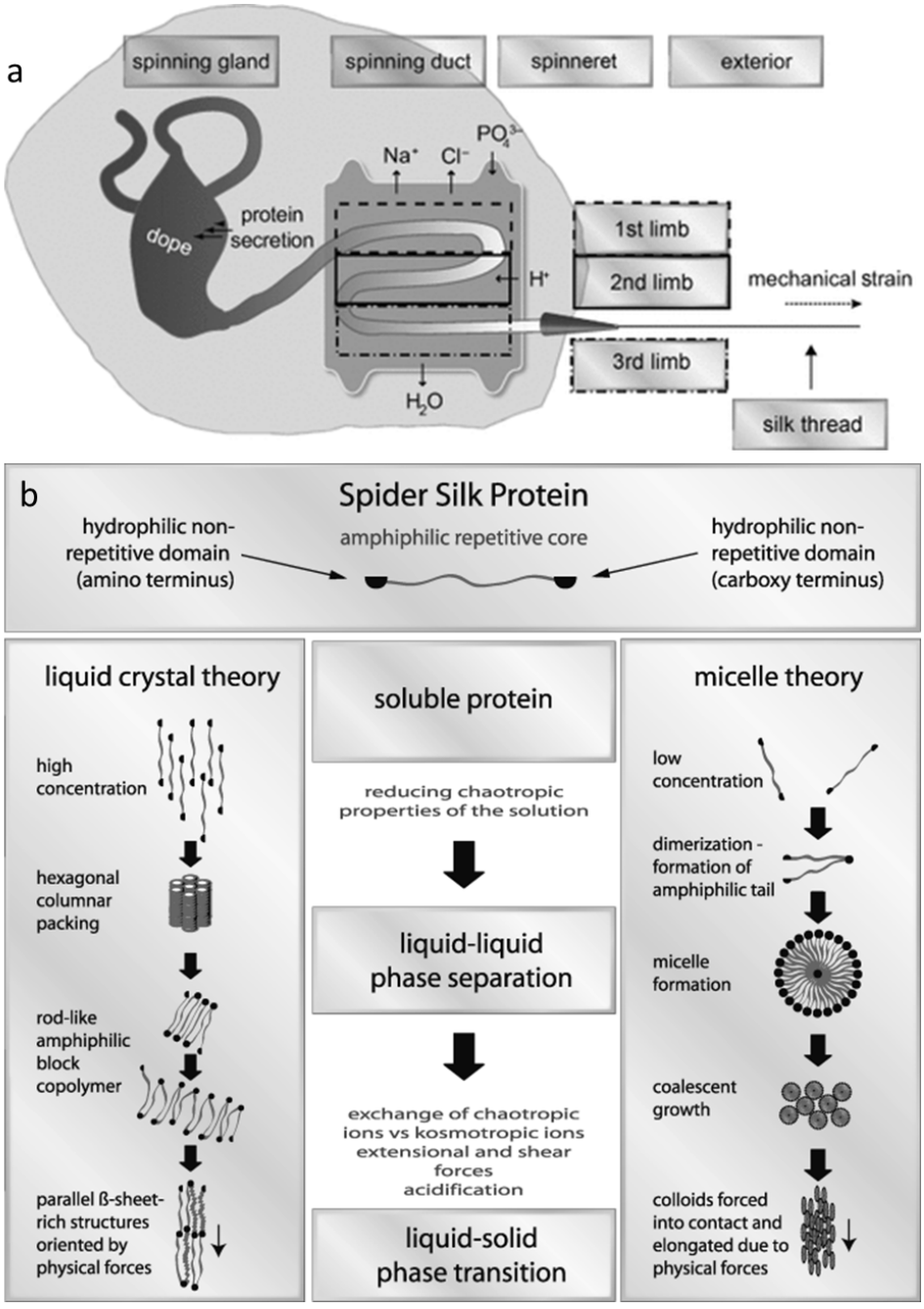

Figure 4 Silk biological production

(a) biological production of spider silk. (b) the two proposed pathways for protein self-assembly during silk production: left, the liquid crystal version from Vollrath and Knight[96], right, the micelle version from Jin and Kaplan[97]. Reproduced from[7] with the authorization from Wiley and Son.

The high crystallinity of the material achieved through the biological fabrication process is directly responsible for the toughness of silk[98]. Also here, it is interesting to notice that there are some similarities between silk and byssus in their production method: like silk, certain *Mytilus* byssus proteins are proposed to be stored as a liquid crystalline phase within the organism and undergo self-organization when secreted[99], even though the byssus producing organ looks quite different (this will be explained in detail in section 2.2.3). The organism also glues the first part of the fiber (namely the plaque) first, and then exerts a tension on it while producing the rest of the fiber to increase the alignment[99].

From this example, we can see that comparative study showed the convergent evolution nature of spider and insect silks, as well as the importance of the main common features to all silk types: high crystallinity, combined with an amorphous phase, and a special production process likely involving liquid crystals and high shear forces. Moreover, the comparisons between organisms which produce different kind of load-bearing fibers, like spiders and mussels, allow the drawing of general principles both for the design of the fibers and their production.

1.3.3 Silk bio-mimicry and applications

Silk has been the focus of an enormous amount of research (especially spider silk) since the 1990's due to its impressive combination of light weight, strength, toughness and stiffness. Indeed, silk has a higher weight-normalized toughness (energy dissipation during deformation reported to the weight of the material) than Kevlar or steel[27,28,88]. Moreover, like other protein materials, silk stretches when the ambient humidity increases, but interestingly, when the humidity reaches 70 %, it undergoes an irreversible supercontraction[27,100]. These properties combined with its biocompatibility and sustainable production out of aqueous solution make silk suitable for a large variety of applications besides traditional clothing: for example, sensors, materials for medical application, biocompatible coatings, lightweight high-resistance composites for transportation, technical clothing and electronics[26,101]. However, spiders, in contrary to silkworms, are less amenable to cultivation because they are predators prone to cannibalism. Also, despite the kilometers of silk they are producing, this remains a very small amount, due to the low diameter of the fibers [88]. Even *Bombyx* silk in its traditional production way is ethically problematic, since it requires the death of the larvae by throwing them in boiling water. These are many arguments in favor of a synthetic silk production in order to reach industrial quantities for commercial applications. Various organisms have been engineered to produce recombinant silk: the famous goat producing silk protein in its milk, but also plants and insect cells, *E.coli* and yeast[102,103]. Another advantage of recombinantly produced silk is the variety of shapes allowed besides fibers[104–107], even though the need for high alignment obtained through mechanical stimulation at the end of the process might make it difficult to reach high mechanical properties with 2D or 3D shapes. However, producing recombinant protein material for load bearing applications is tricky and the first artificial silk spinning processes produced only brittle fibers which required posttreatment to enhance their properties,

including annealing, alcohol bath treatment and post spinning straining to increase protein alignment[103]. This clearly revealed the importance of the natural processing of silk in achieving its final properties, and oriented the focus of researchers toward mimicking the natural production of silk[108] with success, since mechanical properties similar to natural spider silk have now been achieved[48,109].

A few companies took the challenge of developing bioengineered spider silk at an industrial scale[110]: AMSilk (Germany, 2004)[111], Spiber (Japan, 2008)[112], Bolt thread (USA, 2009)[113] and Kraig Biocraft[114]. They collaborate with several brands (Patagonia, North Face, Adidas, Stella McCartney, Airbus and Lexus) in order to produce leisure and technical clothing as well as material for transportation. However, none of these recombinant silk-producing companies has launched a product for mechanical application on the market so far. As observed by Service[115], the length of natural silk proteins (>600 kDa) makes them difficult to bioengineer recombinantly. Therefore most companies utilize truncated constructs of 50 to 200 kDa proteins, which likely impacts the mechanical performances of the resulting fibers. Moreover, the production costs remain prohibitively high, according to Kraig Biocraft[114]. However, despite its youth and imperfections, silk is the first natural material about to be engineered at industrial scales for mechanical applications, thus completing the silk cycle, from traditional application to studying its properties, assessing its structure-function relationship in order to be able to synthetically reproduce them. Even if bioengineered silk products are not perfect yet, they are paving the way for a new era of bioinspired materials. This first cycle from traditional usage to novel high-tech and sustainable application via research and mimicking and give a model and systematic to study similar materials.

1.4 Plan

Based on the previous considerations and the fact that almost nothing was known about the byssus of *P. nobilis* in terms of composition, structure and function, I decided to start by studying the hierarchical structure of *P. nobilis* byssus and its properties, in order to define the structure-function relationships so important in natural materials. This new understanding would then enable a more informed investigation of the traditional usage of *P. nobilis* byssus as sea silk and the effect of the traditional processing of byssus on its structure and properties. On the other hand, a deeper scientific understanding of the tacit knowledge associated with the traditional processing of *P. nobilis* byssus would surely provide additional information about the structure-function relationship of the threads, in an iterative process. Moreover, the characterization of the traditional processing of *P. nobilis* byssus would allow the preservation of this threatened craft by transforming it into explicit knowledge through its archiving and the elucidation of this long evolved artisanal process. Accordingly, this investigation is divided in three main parts: first, utilizing mainly transmission electron microscopy (TEM) and X-ray diffraction (XRD), I performed a comparative structural study of *P. nobilis* byssus and three related mussels (*Atrina pectinata* (*A. pectinata*), *Pinctada fucata* (*P. fucata*) and *Pinctada margaritifera* (*P. margaritifera*)) with

reference to the well-studied *Mytilus* byssus. As explained in section 1.2, comparative studies are critical in biological materials science to determine the nature of byssus evolution (i.e. whether or not it is convergent) and extract key material design features. Convergent evolution[116] is especially interesting regarding the discrimination between key features and evolutionary baggage. Indeed, if several species evolved separately similar biochemical features and structures in a similar material, one can suppose that these are critical for the function of the material, whereas in divergent evolution, common features might just be random part of the evolutionary baggage. In the second part, I described a structure-function relationship study combining XRD with *in situ* mechanical testing of the byssus of *P. nobilis*, in comparison with the well-characterized *Mytilus* byssus in order to observe how the differences between both translate into their properties, toward the extraction of common key properties for byssus function through the comparative study. Finally, in the third part, I described an investigation into how the traditional processing of *P. nobilis* byssus into sea silk modifies the structure and properties determined during part one and two by comparing this time native *P. nobilis* byssus fibers and treated ones. To achieve this goal, I have undertaken a multidisciplinary and multiscale investigation, going from nanometer to centimeter length scale and utilizing diverse techniques from biology, biochemistry and material science, such as XRD, vibrational spectroscopy, tensile testing and electron microscopy, which were all key techniques in the investigation of *Mytilus* byssus, silk and other natural materials.

2 State of the art

2.1 Byssus variety in relationship with the taxonomy of bivalves

Byssus is the name given to protein-based attachment fibers produced by most bivalves in their larval state. The majority of the bivalves appears to retain their byssus into adulthood: 20 out of the 34 bivalve superfamilies considered by Yonge[117] possess a functional byssus, and among the 270 genus listed in the Bivalve life habits database[118], 56 genera were always attached with a byssus, 31 genera possess a byssus only in some cases, 18 genera were attached by cementation, and 165 were unattached. However, similar to silk research, which mainly focused on certain species of spiders, mussel byssus research has largely concentrated on species from one bivalve order (Mitylidae), despite the high number of species from other superfamilies that possess a byssus at diverse stages of their lives. In fact, up to now, the byssus of only several tens of species have been at least partially investigated, but they belonged to only seven different superfamilies[119–124], and apart from Mytilidae species, the hierarchical structure of only one other species could be determined in any amount of detail[122]. Interestingly, analogous to silk, byssus from bivalves belonging to different orders exhibit significantly different composition, structure and performance[119,120]. For example, while the Mytilid mussels are based on collagenous building blocks[31], the byssus of the giant clam *Tridacna maxima* is comprised of four-stranded coiled-coil proteins[122], while Anomia oysters even possess a calcified byssus[125].

As discussed for silk in section 1.3, it is worth understanding the diversity of byssus structure-function relationships in order to extract relevant design principles responsible for the exceptional mechanics (e.g. high toughness and self-healing) of byssus fibers in general. Additionally, despite their differences in structure, composition and exact properties, the probability is high that all bivalve byssus are guided by similar basic rules. Thus, the knowledge of *Mytilus* byssus structure-function relationships could efficiently help the understanding of byssus fibers from other species and is therefore very useful as a reference in byssus comparative studies.

2.2 The byssus of *Mytilus* species

Mytilus mussels are probably the most widely spread mussels in the world, and include for example the well-known common mussel (also known as the blue mussel) *Mytilus edulis* (*M. edulis*)(Figure 5a and b).

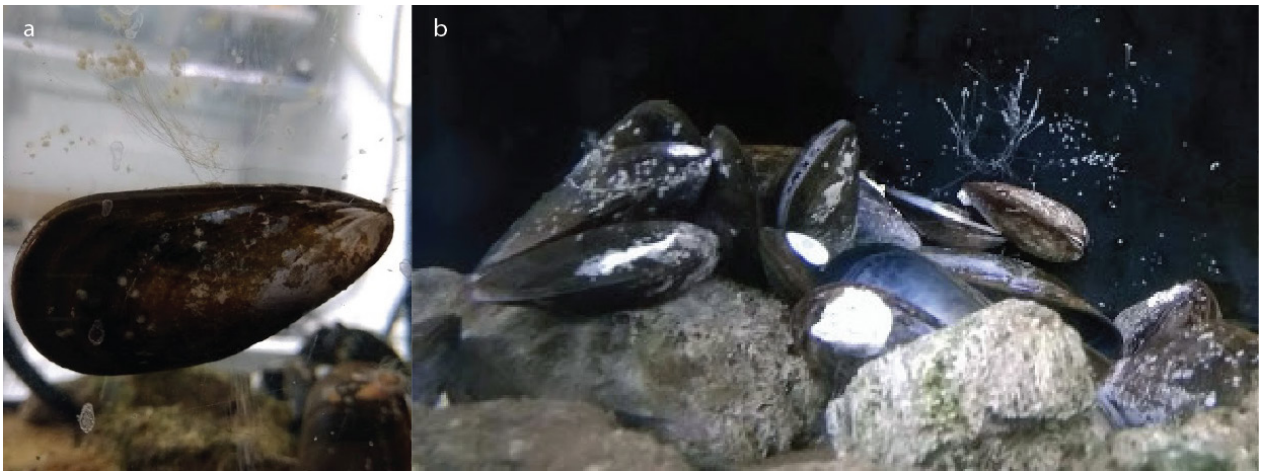

Figure 5 *M. edulis*, the blue mussel
(a) *Mytilus edulis* adhering to the aquarium glass by its byssus. (b) *Mytilus edulis* mussel adhering on rocks.

Mytilus mussels can survive life in wave-beaten seashore habitats on account of their byssus, which acts as a shock absorber, presenting an impressive combination of stiffness, strength and extensibility, in addition to their toughness and self-healing ability. Mytilus byssus is comprised of 20 – 100 protein threads attached to a stem. Each thread is about 0.1 – 0.2 mm in diameter, between 2 and 4 mm in length (for *M. edulis*)[31] and has three distinct parts (Figure 6a): a short and soft proximal part, followed by a long stiffer distal part terminated by an adhesive plaque. This adhesive plaque (Figure 6d) is thought to rely on 3,4-dihydroxyphenylalanine (DOPA), a post-translational modification of the amino acid Tyrosine (Tyr), for underwater adhesion. It has therefore been the subject of much research towards development of bioinspired adhesives in wet conditions[44,46]. However, the adhesive plaque seems not to be a determining feature for *P. nobilis* byssus attachment, which mostly occurs due to entanglement buried under the sediment[126]. Therefore, I am rather focusing on the fibrous threads of the byssus of *P. nobilis* as well as *Mytilus*.

Most research on *Mytilus* has concentrated on the distal part of the byssus threads because it is the most mechanically robust element of the byssus, almost all mechanical failure occuring at the adhesive plaque or in the proximal part[32]. Additionally, the distal part of the byssus has other mechanical characteristics crucial for the byssus function, such as its yield point, which allows shell re-alignment under forces, and extensibility so that all the threads become solicited, thus ensuring an homogeneous repartition of the load[32]. Moreover, the ability of the byssus to dissipate energy and to self-heal are vital properties for the mussel, which are assured only by the distal part of the byssus[127]. Finally, considering the byssus of *P. nobilis* has no proximal part, it seems logical to compare it with the distal part of the byssus fiber of *Mytilus* species, which makes up two thirds of the thread's length[127].

2.2.1 Composition/structure

The distal part of *Mytilus* byssus comprise a load-bearing core (Figure 6c) surrounded by a thin and stiff protective layer called the cuticle (Figure 6b). The composition, structure and properties of each part are described individually bellow.

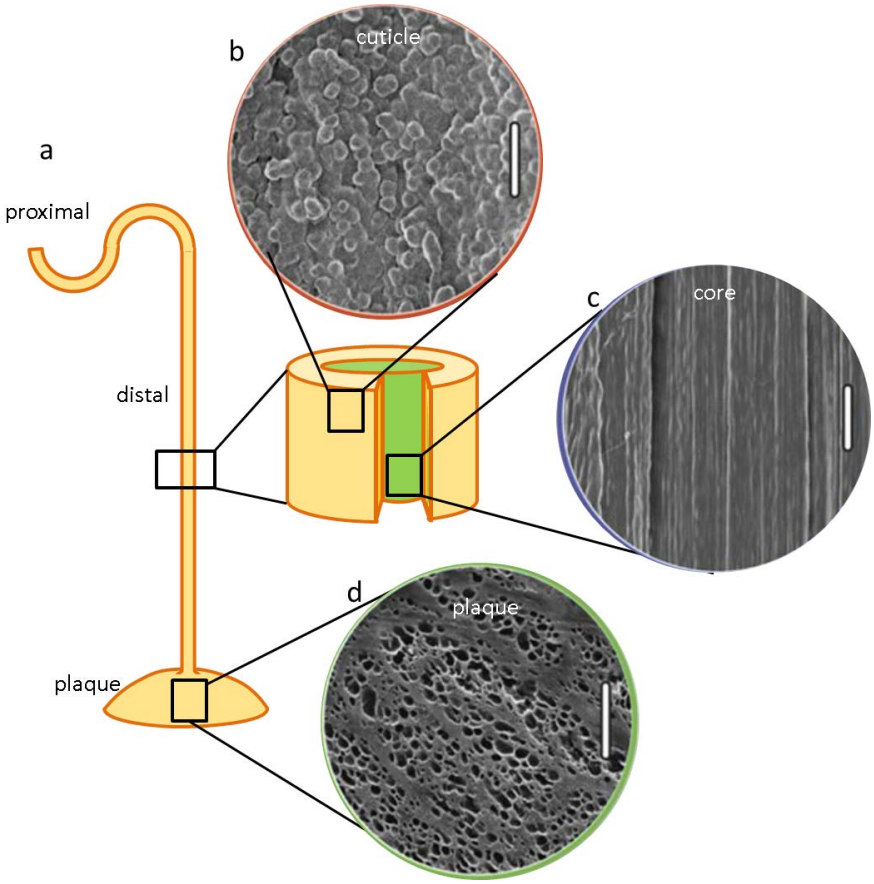

Figure 6 Morphology of *Mytilus spp*. byssus
(a) *Mytilus* byssus threads are made of three parts: proximal, distal and plaque. The distal part comprises a core protected by a layer called cuticle. Scanning electron microscopy (SEM) pictures show the structure of the cuticle (b), the core (c) and the plaque (d). Pictures b, c and d reproduced from Priemel et al [99]Available under public license. Published by Springer nature.

2.2.1.1 Core

The core (Figure 6c) is the load-bearing part of the byssus distal portion and is responsible for the self-healing, stiffness, toughness (energy absorbed when the thread is pulled to rupture) and extensibility mentioned above, but also for the high amount of energy dissipated by a thread during loading-unloading cycles, showed by the hysteresis between the loading and unloading curves[34,128,129] (Figure 7b). The energy dissipated during one cycle is given by this path difference[127] and plays a major role in avoiding mussels crashing on hard substrate during the unloading of the byssus after a wave, for example. The core is mostly made out of a family of unusual collagens known as PreCols [130–132] (Figure 7a). In particular, three variants known as PreCol-P, PreCol-D and PreCol-NG have been identified in threads [31,130]. The PreCols are named according to their concentration gradient along the byssus thread: the concentration in PreCol-P composition is elevated in the proximal region, whereas PreCol-D is enriched in the distal region. PreCol-NG in contrast is non-graded and uniformly spread along the thread. All the PreCol proteins are terminated by a flanking domain and a histidine rich domain (which contains a concentration in histidine about 10-fold higher than average proteins) at both ends (Figure 7a). The flanking domains of the three PreCol variants are very different: in PreCol-D, the flanking domain has a beta sheet structure, in Precol-P, it is rich in Pro and similar to rubbery proteins like elastin and PreCol-NG flanking domains are reminiscent of extensible flagelliform silk sequences[33]. The PreCols form triple helices which then arrange into 6+1 hexagonally packed bundles highly aligned along the fiber axis. In addition, the byssus core also contains a small amount (<1 wt%) of metal ions, especially Zn^{2+} and Cu^{2+}, which have been demonstrated to play an essential mechanical role in thread toughness and self-healing by complexing with histidine residues and forming intermolecular interactions within the histidine-rich domains belonging to adjacent PreCol (Figure 7a)[128,129,133]. Finally, the core contains about 2 % of matrix proteins, supposedly for spacing and lubrication between the PreCols.

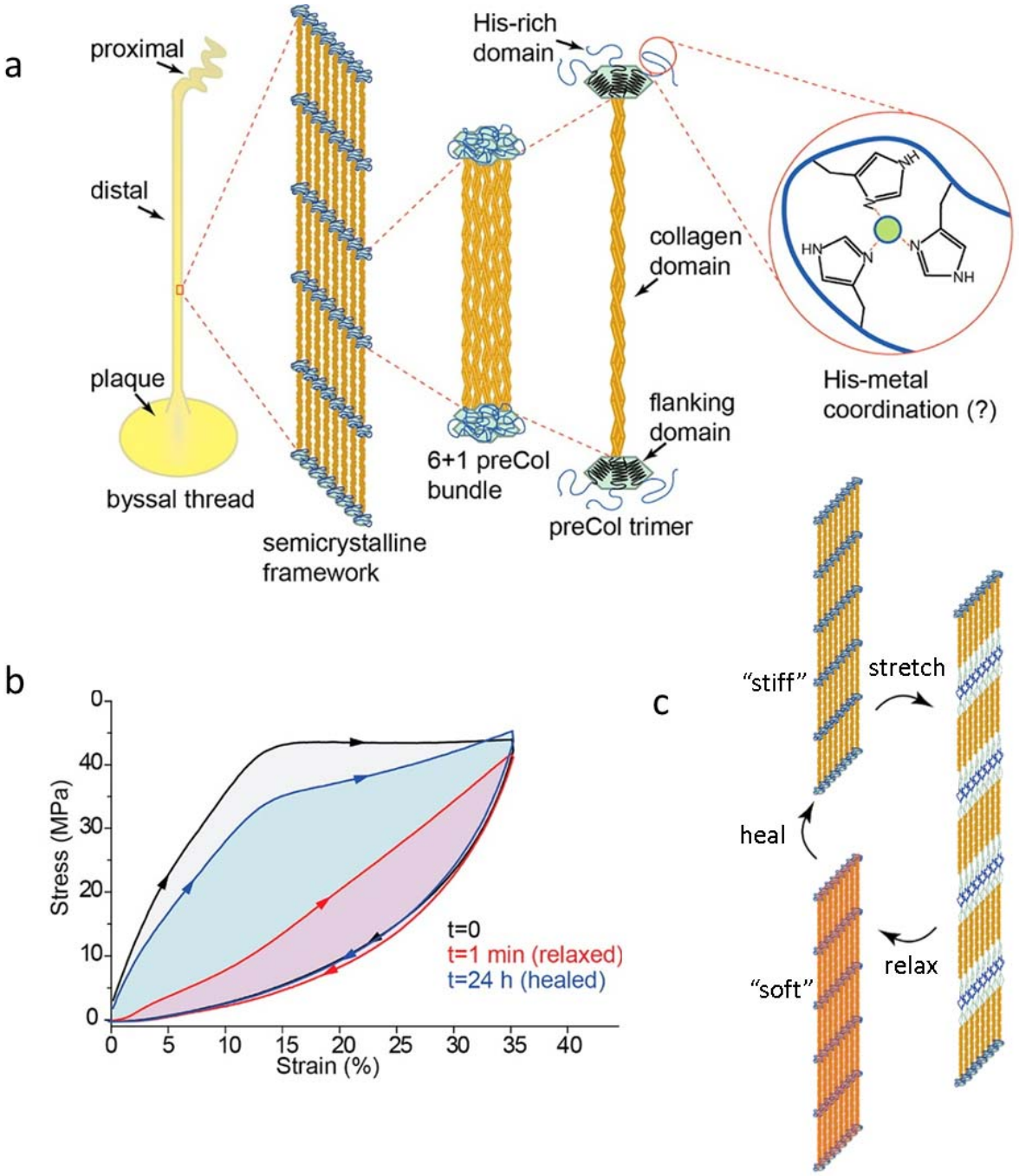

Figure 7 Structure-function relationship in *Mytilus* byssus

(a) The core of *Mytilus* byssus distal part is made of highly aligned PreCols terminated by a flanking and a histidine-rich domain. The histidine residues form reversible cross-links by complexion with metal ions. (b) stress-induced damage and self-healing of *Mytilus* byssus threads. (c) schematic explanation of the damaging and healing mechanism. Modified from Schmitt et al.[128] with the permission of the American Chemical Society.

2.2.1.2 Cuticle

The 5-10 µm thin cuticle surrounding the core (Figure 6b) is proposed to protect the fibrous core against mechanical abrasion, UV damage and bacterial degradation. The hardness and stiffness of the cuticle is up to 5-fold higher compared to the core; however, it can withstand strains of up to 100 %, which is unusual considering that typically hard materials are not extensible[47,134,135]. This was initially proposed to be due to its composite structure made out of micron size granules embedded in a matrix[135]. The granules have been observed to contain a high concentration of DOPA, whereas the cuticle matrix has a lower concentration in DOPA[136]. DOPA residues in the cuticle granules have been clearly demonstrated to interact with transition metal ions (e.g. Fe, V and Al) form strong, yet reversible cross-links that was long thought to contribute to cuticle stiffness and hardness[136,137]. However, recent investigations actually show that the granules have similar mechanical properties to the matrix in wet state, but that the matrix became stiffer during drying out while the granules kept their properties[123]. It is therefore thought that granules are able to retain water when the byssus is emerged, thus keeping their compliance when the surrounding matrix becomes stiff and brittle due to dehydration and acting as plasticizing inclusions. They might also receive most of the stress during cuticle stretching because they might be able to dissipate energy and self-heal due to their higher concentration in metal-DOPA complexes[123]. However, the structure-function of byssus cuticle is not fully understood yet, and still under investigation.

2.2.2 Mechanics and structure-function relationship of the mussel byssus core

The hierarchical structure of the distal part of mussel byssus thread determines its complex mechanical properties. The relationship between structure and properties could be assessed using a range of materials characterization techniques, most notably XRD combined with *in situ* tensile testing[34,129,138]. Under simple tensile loading, *Mytilus* byssus stress-strain curve exhibits three distinct regimes: a first stiff (E = 500-800MPa) elastic part terminated by a yield point at 10 – 15 % strain followed by a yield plateau, terminated by a post-yield stiffening. The byssus presents a large extensibility (up to 100 % in its wet state)[31,139]. However, the extension of the PreCol collagen is much lower than the macroscopic strain. XRD experiments indicate that the PreCols only extends by 2 % while the whole distal thread part stretches by 70 %[34]. Therefore, the extensibility of the thread is believed to arise from the unfolding of the preCol-D flanking domains and histidine-rich domains[128,129,133]. In this model, the yield plateau is due to the breakage of the sacrificial histidine-Zn bonds, which reveals the hidden length packed in the cross beta sheet flanking domains[129]. This also contributes to the large toughness of the byssus by dissipating energy while protecting the structural covalent bonds. Indeed, during the first cycle of a fatigue test, the byssus is able to dissipate up to 70 % of the applied energy (Figure 7b). But even though the proteins are able to fully fold back during the unloading, the histidine-Zn bonds do not immediately recover to their native cross-linking network structure, which leads to damage of the fiber associated to

a decrease in toughness and stiffness during subsequent loading cycles[128]. Nevertheless, the histidine-Zn bonding network recovers towards a more native-like configuration after a resting time of several hours, so that the initial mechanical properties are nearly recovered, in a self-healing process[128,129,140] (Figure 7b and c). The essential mechanical role of histidine-metal coordination was first suggested by metal removal with Ethylenediaminetetraacetic acid (EDTA), a chelating agent, and histidine positive charging by pH lowering[140], both leading to a decrease in mechanical properties and loss of yield point and self-healing ability, and could be confirmed using X-ray absorption spectroscopy[128].

2.2.3 Mussel byssus production

As already explained in section 1.3 for silk, the fabrication process of natural materials is extremely important for their final hierarchical structure and associated properties. The byssus is produced in the central groove of an organ called the mussel foot, which the mussel is able to stick out of its shell like a tongue (Figure 8a)[141,142]. The foot is used to explore the surface of attachment substrate, and once the mussel found a favorable place, it secretes the byssus proteins in an injection molding-like process, starting with the plaque directly attached to the substrate. Eventually, the mussel applies a final tension on the thread by the foot and release the newly formed thread into the seawater environment[142]. The whole process is quite fast and only lasts a 1 to 5 minutes[31,142]. Histology and transmission electron microscopy enabled investigation of the tissue along the groove of the foot, revealing three distinct glands that secrete the byssus plaque, core and cuticle (Figure 8b), which were called the phenol, collagen and enzyme glands, respectively[141] and newly renamed to plaque, core and cuticle glands according to the function of the proteins they produce[99]. The proteins are stored at low pH in vesicles within the glands, which prevent DOPA and histidine from forming crosslinks prior to the secretion of the proteins in the foot groove[143,144]. Birefringence indicates that the PreCols are already arranged within the vesicles in a liquid crystal organization[99]. During byssus thread production, all these vesicles are released into the foot grove, where their self-assembly is triggered by the change in pH due to the contact with sea water, and the incorporation of metal ions (Figure 9). However, the metal ions do not directly enter the already formed thread via contact diffusion from sea water, but seem to be rather stored and concentrated within the mussel and incorporated by the organism during byssus production[99]. Artificial induction of byssus formation by injection of KCl[99] into the mussel foot allowed the investigation of aspects of the assembly process that are governed by chemical and physical forces alone, as opposed to biologically controlled part, since the foot becomes essentially paralyzed. Induced threads lack the metal-proteins coordination crucial for its mechanical properties and its PreCols are only aligned on small portions (Figure 9). Their alignment on larger scale might require the mussel to actively pull on the freshly formed thread. The byssus fabrication process of the *Mytilus* mussel may also give some insight on the byssus fabrication of other species, because they all possess a similar foot presenting a grove, which they use to produce their byssus. However, this remains to be seen.

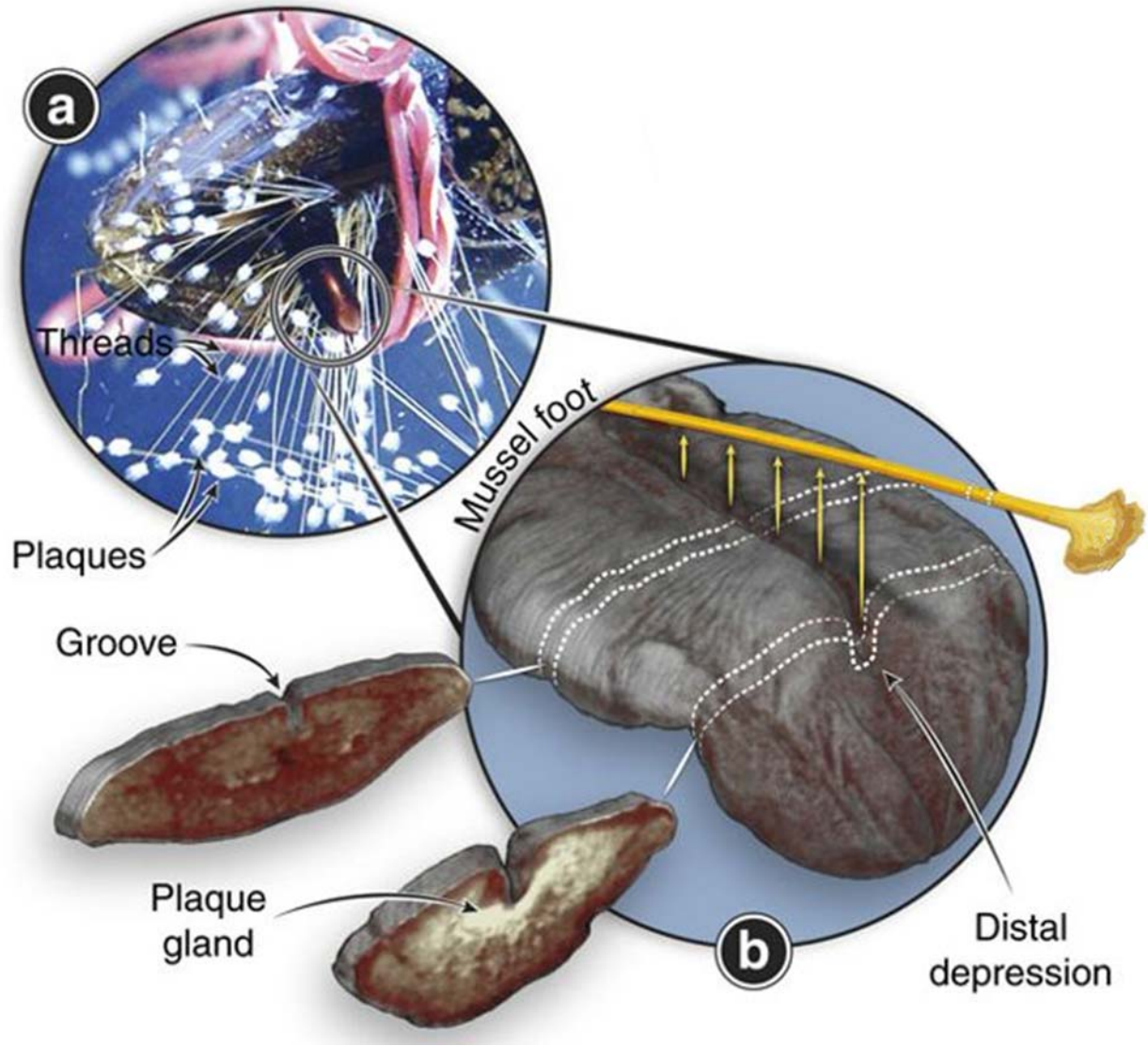

Figure 8 *Mytilus* byssus production system

(a) *M. edulis* specimen sticking out its foot to produce a byssus thread (b) micro-computed tomography (microCT) scan of *M. edulis* foot showing the grove where the proteins are secreted to form the thread, and cuts showing the glands producing the byssus proteins. Reproduced from Priemel et al.[99]. Available under public license. Published by Springer nature

Additionally, comparing the fabrication process of silk and byssus gives interesting insights of the key points in processing. In both cases, certain proteins are stored in aqueous liquid crystal phases and self-assembled when exiting the organism and the animal attaches the first part of the thread and exerts tension on it while producing it in order to align the proteins. However, because silk is produced in air and byssus in water, their production has a major difference: self-assembly of silk occurs via high shear forces, whereas a pH change is the triggers byssus proteins self-assembly[7,94,96,99,142].

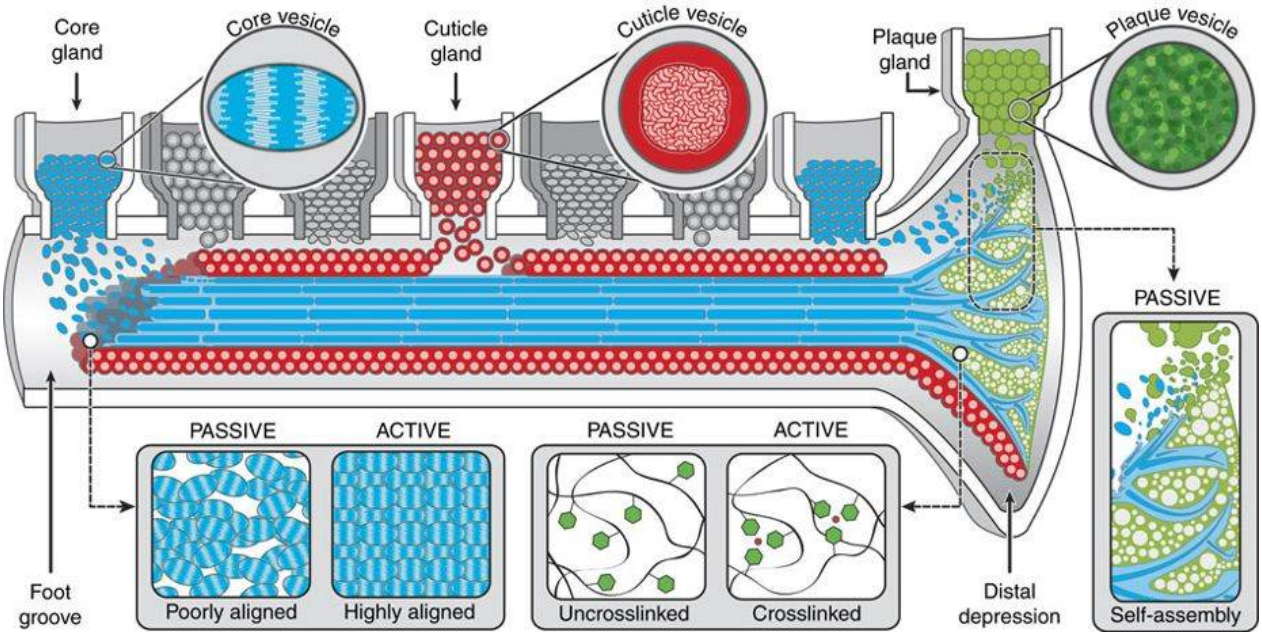

Figure 9 Schematic representation of the active and passive steps of byssus production
Reproduced from Priemel et al.[99] Available under public license. Published by Springer nature.

2.3 The byssus of *P. nobilis*

2.3.1 *P. nobilis* habitat, general data and the function of its byssus

At first sight, *P. nobilis*, also known as the Noble Pen shell, has very little in common with *Mytilus* mussels. It is a very large bivalve which can live up to 50 years[145]. The largest reported was 1.20 m long[146]. Like other bivalves, *P. nobilis* is a filtrating organism, but it lives completely underwater in a standing position, partially buried in the sandy ground of sea grass fields (Figure 10a)[37,126]. In order to keep the vertical position, vital for its survival, *P. nobilis* is anchored by its byssus (Figure 10b) which serves as roots to stabilize the shell in the unstable ground, prevent its uprooting by octopuses[147] and allow *P. nobilis* to withstand the high forces created by marine currents on the large surface of its shell[148].

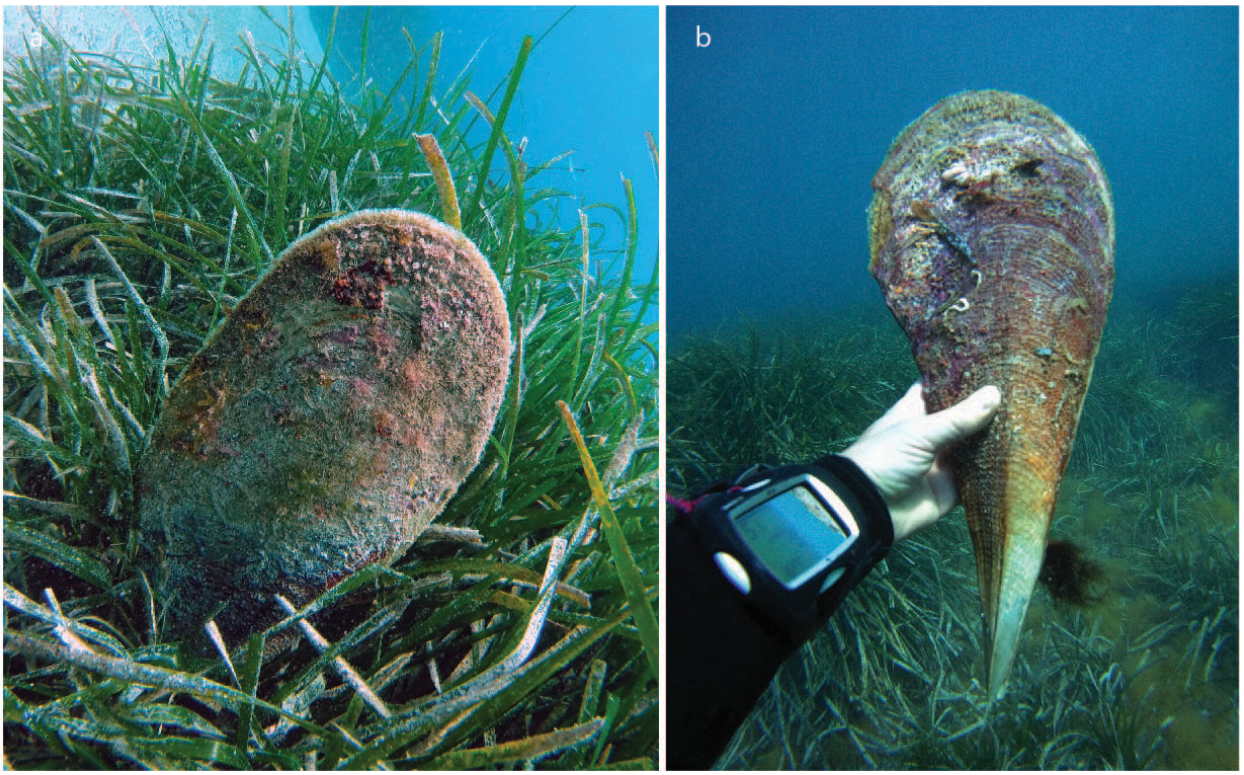

Figure 10 The noble pen shell *P. nobilis* and its byssus
(a) *P. nobilis* individual one third buried in a *Posedonia* field. (b) Whole *P. nobilis* shell showing its byssus protruding out of the shell on its right side. Rights: Sébastien Motreuil.

2.3.2 Byssus morphology

Perhaps because they have a slightly different function, the morphology of the byssus of *P.* nobilis also differs from the *Mytilus* one. *P. nobilis* byssus is made out of 20 000 to 30 000 thread protruding out of the shell under the ground[126,149]. These threads have an ovoid cross section[150] with a diameter around 30-50 µm. They are long (up to 15 cm out of the shell) and possess a small adhesive plaque at their extremity, which can stick to shell debris, dead leaves, roots and even sand grains[151]. Moreover, the threads are tangled in the substrate, which keeps their fixation role, even if the adhesive plaques are lost. Each thread protruding out of the shell has an additional 10 cm embedded in the foot retractor muscle, and is fixed in 4 different points within it. This system is also totally different from that of *Mytilus*, where the threads are attached to a stem, and is also reflected by the difference in the byssus producing gland system. Even if, like in *Mytilus*, *P. nobilis* byssus threads are formed in a furrow in the foot, the latter seems to possess one single gland responsible for the fabrication of the thread; the main gland[141], which forms "glandular islets" in the foot groove folds, separated by muscular fibers. At the border of the furrow are also various cells, called mucocytes, secreting substances probably involved in *P. nobilis* byssus. This system is definitely different from the three byssus glands of *Mytilus* byssus foot[99].

2.3.3 The composition of *P. nobilis* byssus threads

The amino acid composition of *P. nobilis* byssus threads is also quite different from *Mytilus* byssus. It has been measured numerous times by different groups[41,120,132,152,153], showing a high content (around 10 wt% each) in Proline (Pro), Glycine (Gly), Aspartate (Asp) and Serine (Ser), and a remarkably high amount of long side chain amino acid in comparison to the short ones[152]. Those results were obtained by direct hydrolysis of byssus threads, but it is also possible to obtain compositional information from the byssus producing glands by histological staining[141]. This method showed granules of a glycoprotein, rich in aromatic amino acids, and containing a monophenol (possibly Tyrosine (Tyr)), whereas the various mucocytes produce different substances: the cells directly in contact with the main gland secret a mucoprotein rich in sulfated acidic polysaccharides. In contact with the latter, a second type of cell produces two sorts of granules: the first one containing polysaccharides with sulfated groups, the other containing muccopolysaccharides with carboxylic groups[141]. Last, at the outside, in contact with the previous cells, there are other cells secreting neutral mostly mucopolysaccharides, and a few carboxylic ones. The presence of a quinonic tanning system similar to the one found in *Mytilus* has been suspected[141]. Finally, threads showed reaction to elastin antibodies[150].

2.3.4 Micro- and nanostructure of *P. nobilis* byssus threads

While the composition is undoubtedly important, research on the *Mytilus* threads clearly indicates that multiscale structural organization of protein building blocks within materials is essential in the determination of mechanical properties. However, structural information about the byssus of *P. nobilis* is sparse due to the technical limitations for characterizing such thin fibers and additionally, due to the inherent difficulty in gaining access to the material due to the fact that *P. nobilis* is considered an endangered species and is heavily protected. However, both XRD and polarized IR spectroscopy[131] confirmed that in contrast to *Mytilus*, *P. nobilis* byssus threads do not appear to contain collagenous proteins, consistent with amino acid compositional analysis. Interestingly, aged threads possessed more and sharper high angle diffractions than the "young" ones. SEM and TEM investigations showed a very aligned closely packed fibrillar structure within the threads[150].

2.3.5 Mechanical properties of *P. nobilis* byssus threads

There are only a few studies that have characterized the mechanical properties of the byssus of *P. nobilis*. Bouhlel et al,[120] observed a stress-strain curve that had a similar shape to the tensile curve of Mytilus byssus, comprising an initial elastic region, terminated by a yield point, followed by a plateau and by a post-yield stiffening region. The Young's modulus was higher than observed for *M. edulis* byssus, but the ultimate strength only about 30 % that of threads from *M. edulis*. On the other hand, the tensile tests performed by Lucas et al[132] showed a yield point in the traction curves of dried threads that did do not show up in the hydrated ones.

2.4 The byssus of other mussels

As mentioned in section 1.2, comparative study is highly effective and useful for differentiating between functionally important structural/compositional features vs. variations that are less impactful on material function. Moreover, it is already known that the core of byssus threads from *Mytilus* species (*spp.*) all share a similar structure and composition, based on collagen-like building blocks. Thus, it is highly intriguing to investigate if mussels belonging to the same order as *P. nobilis* (i.e. Ostreidea) share a similar structure with *P. nobilis* byssus. Therefore the byssus fibers of three other mussels were also investigated for comparative purposes: *Atrina pectinata* (*A. pectinata*), *Pinctada margaritifera* (*P. margaritifera*) and *Pinctada fucata* (*P. fucata*).

2.4.1 The fan shell *A. pectinata* and its byssus

A. pectinata is a mussel very similar to *P. nobilis*: they share a similar shape, habits and habitat; however, *A. pectinata* lives in the Chinese Sea, whereas *P. nobilis* lives in the Mediterranean Sea. Additionally, *A. pectinata* is much smaller than *P. nobilis* and does not tend to grow more than 50 cm in length. However, their byssus exhibit a very similar morphology, made out of numerous long and thin threads. Despite its availability in Asia,

where it is still eaten, *A. pectinata* byssus has not been the subject of many investigations. In fact, only a single article has been published that investigates the interface where the byssus is embedded into the adductor muscle and the soft tissues around it[154]. This study also presents tensile properties of the proximal part of the thread, which is embedded within the mussel.

2.4.2 The pearl oysters *P. margaritifera* and *P. fucata* and their byssus

P. margaritifera and *P. fucata* are pearl oysters cultivated all over the world – in Sudan, Australia, French Polynesia, Cook islands, the Philippines, China, Korea Japan and Mexico for *P margaritifera*, and in Sri Lanka, India, Thailand, China, Korea, Japan and Mexico for *P. fucata*. Both oysters live anchored by their byssus on hard surfaces in coral reefs or on rocky surfaces in calm areas. Wild *P. margaritifera* oysters have a size up to 14.7 cm and *P. fucata* up to 8.5 cm[155]. While several studies have been published on the byssus of *P. fucata*, no literature could be found about the byssus of *P. margaritifera*. The byssus of the *P. fucata* comprises 3–10 threads that are 1–2 cm long. They are made of three regions, a granular proximal part, a fibrillar distal part, made out of a core surrounded by a dense and smooth cuticle, and a trumpet shaped adhesive plaque[156] In the distal region, protein fiber clusters are separated by a less dense matrix. This region also contains voids, which increased in size when the byssus was treated with EDTA to remove the metals, but was recovered when the treated byssus was dipped in a Ca^{2+}-enriched solution[156]. The authors utilized Fourier transform infrared spectroscopy (FTIR) to investigate the structure of the proteins comprising the threads, reporting a mixture of different secondary structures, which they said changes with EDTA treatment. Moreover, EDTA treatment was associated with a decrease in mechanical properties while Ca^{2+} treatment resulted in the recovery of the native tensile properties. The authors concluded that Ca^{2+} ions play an important structural role in the byssus of *P. fucata*[156]. Moreover a thrombospondin-like protein was identified, which the authors believe could play a role in the metal binding in the byssus of *P. fucata,* since it was able to induce aggregation of the proteins produced by the oyster foot after KCl injection[157].

3 Studying hierarchical materials with X-ray Diffraction

The goals of the work in this thesis are two-fold: 1) to gain a deeper structure-function understanding of the Ostreida mussel byssus – in particular the threads of the noble pen shell mussel, *P. nobilis*, which is the source of the ancient fabric sea silk. 2) to determine how the structure-function relationships of the *P. nobilis* byssus threads are altered during the artisanal treatment that is utilized in sea silk fabric processing. Thus, it is absolutely essential to gain a multiscale understanding of the structural hierarchy across multiple length scales. Over the last ten years, one technique in particular has been highly successful in extracting the multiscale structure of byssal threads from *Mytilus* mussels[34,129], as well as other species (e.g. *Tridacna*[122]) – X-ray Diffraction. XRD is an incredibly powerful tool to observe and characterize regular structures. It is a key tool in the study of many materials including natural materials[158–161] and especially silk[28] and as mentioned mussel byssus[34,129].

3.1 X-ray, an electromagnetic wave

As the name implies, XRD utilizes X-rays to probe the structure of materials. X-rays are electromagnetic waves with a wavelength smaller than visible light (between 0.001 and 10 nm), which can be seen as a perturbation transferring energy through matter and space. It is generally described as a time dependent sinus function characterized by a phase, wavelength and amplitude. The real part of a 3D wave can be described by the equation: $\vec{E}(\vec{r},t) = \vec{E}_0 sin(\vec{k}.\vec{r} - \omega t - \phi)$ with $\vec{E}_0$ the maximum amplitude, $\vec{r}$ the space coordinate, t the time, $\vec{k}$ the wave vector, which is along the propagation direction of the wave, ω the angular frequency, and ϕ the phase constant, which is the offset of the wave at time zero. The particular case of a 1D wave is easier to represent graphically (Figure 11).

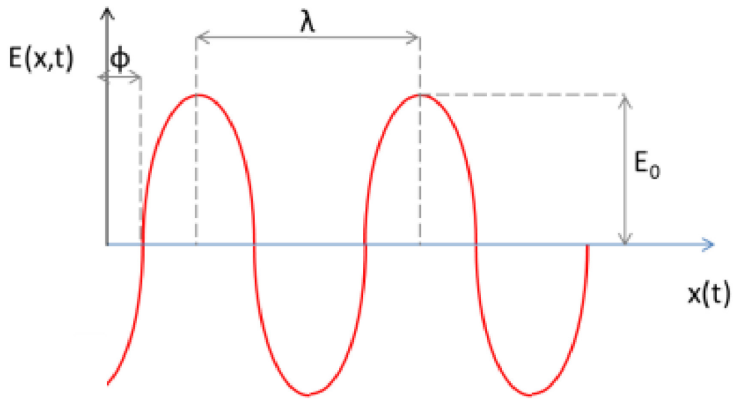

Figure 11 One dimensional representation of a light wave
representing graphically the wavelength λ, the phase offset ϕ and the amplitude E_0.

In this case, the wave is described by: $E(x,t) = E_0 sin(kx - \omega t - \phi)$ E_0 the maximum amplitude, x the space coordinate, t the time, k the wave number, ω the angular frequency, and ϕ the phase constant, which is the offset of the wave at time zero (see Figure 11). The wavelength λ is the distance between two subsequent maxima of the wave and is expressed as $\lambda = 2\pi/k$, and the Intensity of a wave is proportional to the square of its amplitude[162]. However, crystallographers often use a different definition of the wave vector: $\lambda = 1/k$, dropping the 2π factor to simplify further calculation.

X-rays and other light waves produce different interactions with matter, such as scattering, absorption, reflection and refraction. Depending on the energy (determined by the frequency) of the electromagnetic radiation utilized, the way light interacts with matter can be harnessed to gain information about the structure of matter from the subatomic scale up to higher level organization. For example, inelastic scattering of light (in the UV to near infrared range) is utilized in Raman spectrometry in order to probe vibrational states of molecules, while a related technique, Fourier Transform Infrared (FTIR) spectroscopy, measures the absorption of light in the infrared range by matter, which provides a spectroscopic footprint of vibrational modes of different molecules. Visible light absorption also allows, for example, the identification and quantification of substances thanks to UV-Vis spectroscopy, where the light absorbed at specific wavelengths is measured, which corresponds to specific electronic transitions within the analyzed chemicals[163].

Similarly, the interactions of X-ray radiation (both scattering and absorption) can be used to probe the molecular nature of matter, and as utilized in this thesis, the structural organization at the atomic to molecular scale. In particular, X-ray diffraction (XRD) probes the interference phenomenon between the different X-ray waves scattered by the periodic organization of molecular structure in a material. This information is used to deduce the interatomic or intermolecular distances in a sample. The most common use of XRD and the simplest to explain is its utilization to elucidate a crystalline structure; therefore, the basics of XRD by a crystal will be explained in this context in the next section.

3.2 Diffraction by crystalline structures

In order to understand, describe and analyze diffraction by crystalline structure, it is useful to first be able to characterize and describe the crystalline structure itself. A crystal is defined as a periodic and symmetrical arrangement of atoms (or molecules for biological materials) in 3D. This periodic arrangement is characterized by its unit cell, which is the smallest motif of atoms (or molecules) repeated throughout the crystal. The three axes $(\vec{a}, \vec{b}, \vec{c})$ of the coordinate system are defined along the edges of the unit cell (Figure 12a, b and c). Unit cells can have various shapes, depending on the arrangement of the atoms in the matter, as showed in Figure 12a, b and c. When extended and packed in 3 dimensions, the organization of atoms (or molecules) of the unit cells creates a 3-dimensional lattice, such that any given atom of the lattice has identical surroundings. Within the lattice, numerous sets of parallel planes can be defined, which are the elements interacting with X-

ray radiation (Figure 12e)[164,165] and therefore, need to be described and identified as well. The planes are described by their so-called Miller indices. The Miller indexes h, k and l (Figure 12d) of a given plane, are determined from the intersection of this plane with the unitary vectors $\vec{a}$, $\vec{b}$ and $\vec{c}$: if the plane intestects $\vec{a}$ in a point x, $\vec{b}$ in a point y and $\vec{c}$ in a point z, such that $0 < z \leq 1$, then the Miller idexes (h,k,l) are given by $h = \frac{1}{x}$, $k = \frac{1}{y}$, $l = \frac{1}{z}$. In the particular case where the considered plane is parallel to one of the unitary vectors, it is considered to cross at ∞, thus the corresponding Miller index is set to 0[164]. By convention, the set of Miller indexes for one plane are written between brackets and for negative indexes, the minus sign is placed above. As an example, a plane with miller indexes $h = 3, k = 1, l = -2$ is written $(31\bar{2})$. Parallel planes are considered equivalent, therefore a whole set of parallel planes are described by one single triplet of Miller indexes.

Now that we have discussed the basics of crystal structure, we can start to see how X-rays interact with crystalline structures and how this allows measurement of the distances within the crystal lattice. When an X-ray wave interacts with a plane in the crystal, each point of the plane scatters the wave and becomes the center of a new circular wave (Figure 13b), due to the interaction of the wave with the electrons. If the wave meets the surface with a random angle, it meets the plane at different points in different phases (Figure 13a). The scattered waves interact destructively (the crest of one wave meets the valley of another one) in all direction except the reflecting one, the direction presenting the same angle with the plane as the incoming plane wave (Figure 13b). The same will happen on the second plane of the same set (Figure 13c), the third one, and so on. If the waves resulting from the interactions with the different planes are not in phase, they will interfere destructively. For the scattered waves to be in phase, the path difference between the wave reflected by one plane and the wave reflected by the next plane has to be a multiple of the wavelength utilized, *nλ*. This is expressed by Bragg's law: $2dsin\,\theta = n\lambda$ with d the distance between the successive plans, θ the angle between the incident wave and the diffracting plane (same angle as between the diffracted wave and diffracting plane), λ the wavelength, and n, an integer giving the diffraction order (Figure 13d). A simplified illustration of this phenomenon envisages parallel planes in the crystal as mirror surfaces that partially reflect the incident X-ray wave, at an angle equal to the incident angle (i.e. specular reflection). Bragg's law is satisfied for a specific incident angle (θ) only if the spacing between subsequent reflecting planes in the direction of the wave vector is equal to a multiple of the X-ray wavelength (λ), resulting in constructive interference[166] (Figure 13 d). All other angles will result in destructive interference[165].

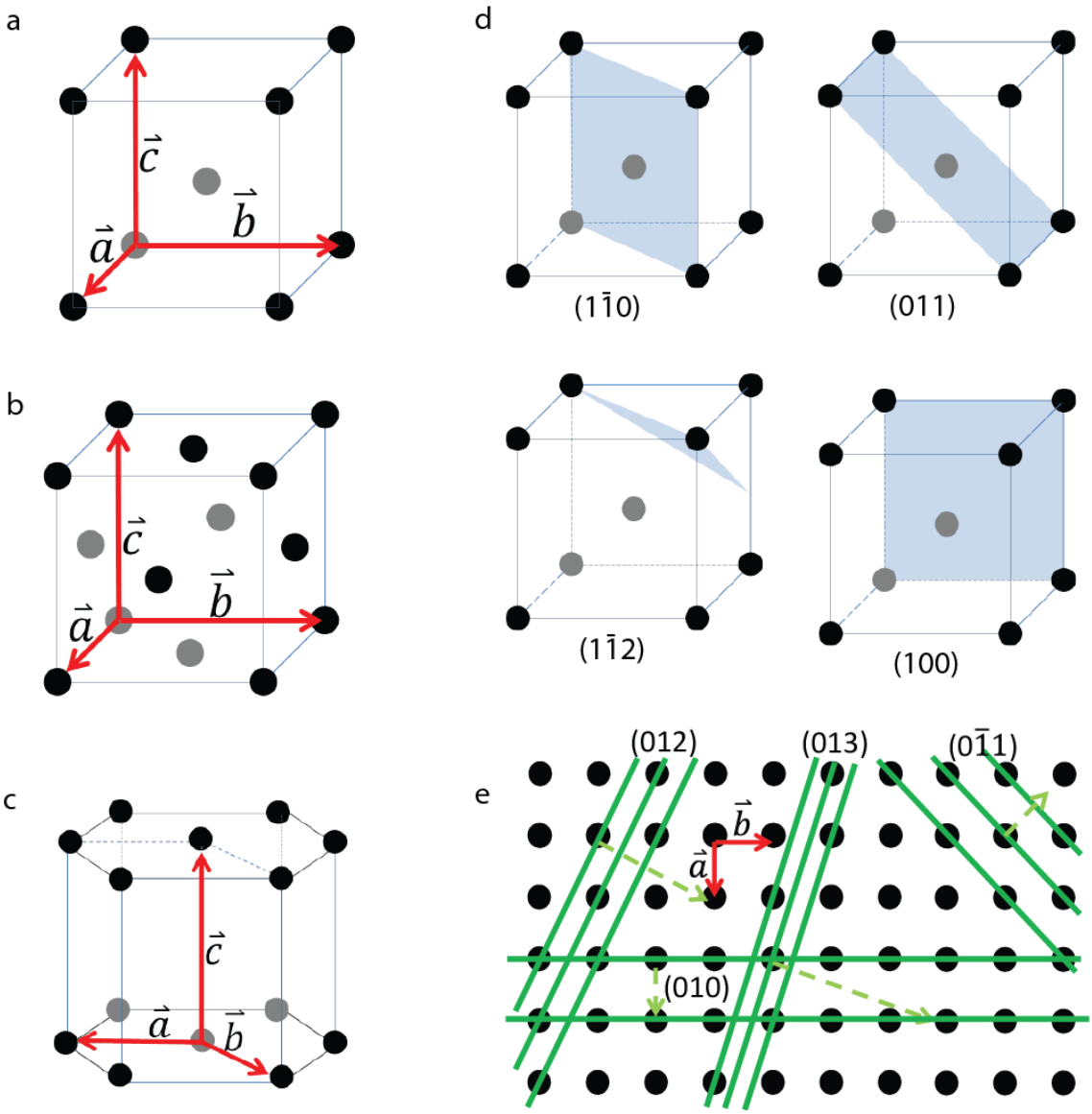

Figure 12 Unit cell, crystal lattice and representation of the Miller indexes

(a) cubic centered unit cell (b) face centered cubic unit cell (c) hexagonal unit cell (d) representation of different planes in a cubic centered unit cell with the corresponding Miller indexes written underneath e) one dimensional representation of the diverse planes in a crystal lattice. Each black dot represents an atom. In red are the unit vectors of the coordinate system, in green are different set of planes and their normal vector.

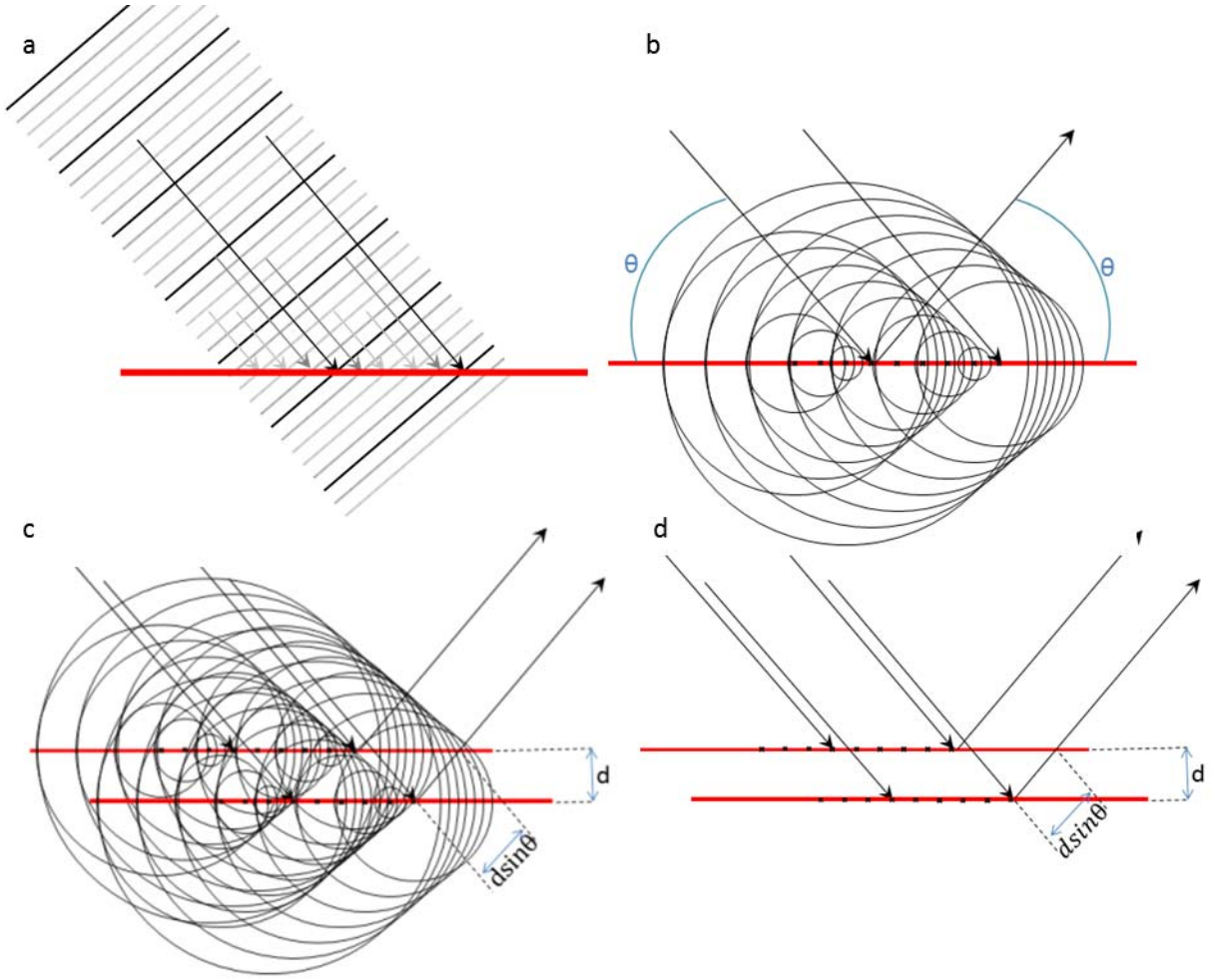

Figure 13 Diffraction by a regular structure, constructive and destructive interferences

(a) A plane wave meets the diffracting plane at different phases at different points. The black lines represent the crests of the wave, the grey lines, fronts of average and lowest amplitude. The arrows indicate the wave vector $\vec{k}$, and the red line represents the diffracting plane. (b) Each point of the incoming wave acts as the center of a new spherical wave (circular in 2D). The crests of the circular waves are shown as concentric circles (for clarity, the front of the incoming wave and the intermediate amplitudes are not shown any more.). These circular waves interact with each other, creating a new plane wave traveling in the mirroring direction of the incoming beam ($\vec{k}$ showed by the arrow). (c) In the same way, the next crystal plane will create a new plane wave with the same angle. However, the two waves created by the two crystal planes will interact positively only if there are in phase, meaning that the path difference between both is a multiple of the wavelength. This is the meaning of Bragg's law: a set of crystal planes diffract if $2dsin\,\theta = n\lambda$. (d) The same is represented in a simplified view, omitting the crests of the circular waves, and showing only the wave vectors $\vec{k}$ of the incoming and diffracted wave.

3.3 Characterization with X-ray diffraction

The angular dependence of X-ray diffraction is utilized in various X-ray diffraction setups in order to characterize unknown materials or phases[164,165]. In transmission, the basic principle is that the X-ray beam is directed on the sample, gets diffracted and is recorded on a detector placed behind the sample. The diffracted beams recorded on the detector create what is called a diffraction pattern. Knowing the distance between the sample and the detector, it is possible to calculate the diffraction angle 2θ, and use Bragg's law to determine d, the distance between the diffracting planes in the sample[166]. A schematic picture of a simplified XRD measurement set up in transmission with plane detector is given on Figure 14**.** However, most materials are almost transparent to X-rays; therefore, the diffracted beam has a very low intensity in comparison to the incoming beam since most of it is transmitted through the material. Thus, a beamstop has to be used in order to cut off the strong transmitted beam in order to avoid both damaging the detector and hiding the diffraction peaks.

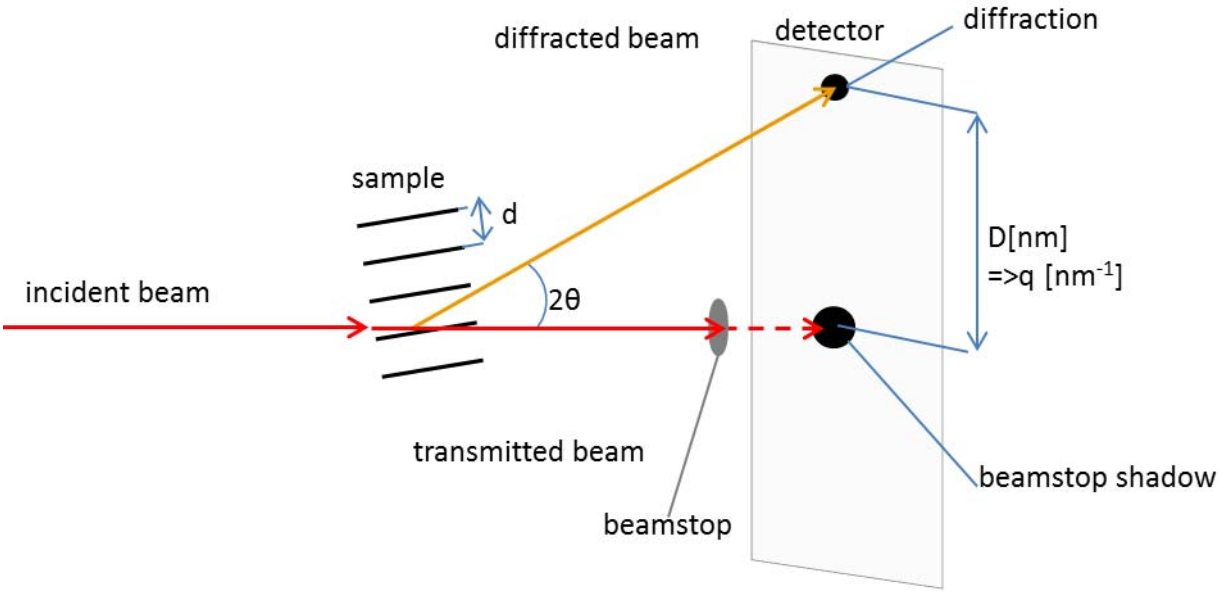

Figure 14 Scheme of XRD measurement setup
showing the diffraction by a single set of plans in Bragg's condition.

Knowledge of the sample-to-detector distance L and the distance D between the transmitted beam, which is also the center of the diffraction pattern, and the diffraction spot allows calculation of 2θ, the angle between incident and diffracted beam, thanks to the trigonometrical definition of the cosines: $\tan 2\theta = \frac{D}{L}$. Notably, the distance L can be varied in these experiments in order to probe different ranges of 2θ. The calculated diffraction angle can then be introduced into Bragg's law in order to calculate the distance between the diffracting planes d in the sample: $d = \frac{n\lambda}{2sin\,\theta}$ explained in section 3.2. The wavelength λ is directly given by the set up, but a reference sample has to be measured in the same conditions than the sample in order to calculate the distance between sample and detector L, and the position of the incoming beam. The reference sample is a well characterized

powder (e.g. quartz, silver behenate) with a known diffraction pattern. Because it is a powder it presents all the possible planes orientation, therefore all the possible diffraction angles 2θ are met, thus forming a diffraction pattern made of concentric circles, as further explained in section 3.5. The center of these circles is the position of the transmitted beam. The distances between the planes of the reference being known, it is possible to calculate the diffraction angle thanks to Bragg's law, and then use the trigonometric relationship given above to calculate the distance between sample and detector. The fitting of the diffraction pattern of the reference material also allows the determination from other geometrical parameters like a tilt from the detector in order to improve the analysis of the unknown sample diffraction pattern.

3.4 The Ewald sphere construction and the reciprocal lattice

The reciprocal lattice and the Ewald spheres are mathematical constructs helping to understand the interaction between the X-ray beam and the periodical lattice of the sample.

3.4.1 The reciprocal lattice

The reciprocal lattice corresponds to the Fourier transform of the real lattice. The unit vectors $\vec{a}$*, $\vec{b}$* and $\vec{c}$* of the reciprocal lattice are linked to the real lattice unit vectors $\vec{a}$, $\vec{b}$ and $\vec{c}$ by the following relationships: $\vec{a}^* \perp \vec{b}\ and\ \vec{c},\ \vec{b}^* \perp \vec{a}\ and\ \vec{c}, \vec{c}^* \perp \vec{a}\ and\ \vec{b}$ and $|\vec{a}^*| = \frac{1}{|\vec{a}|}$, $|\vec{b}^*| = \frac{1}{|\vec{b}|}$, $|\vec{c}^*| = \frac{1}{|\vec{c}|}$. Each point of the reciprocal lattice [h* k* l*] represents one plane (h k l) of the real lattice, meaning that the plane of the real space and the point in the reciprocal space have the same numerical coordinates but in a different reference system. As consequence, the length on the vector between the origin of the reciprocal space and a point of the reciprocal lattice $|\vec{d}^*|$ is reciprocal to the plane spacing d[166,167].

3.4.2 The Ewald sphere

The Ewald sphere is a graphical expression of Bragg's law[166,167]. It is a sphere of radius $\frac{1}{\lambda}$ in the reciprocal space whose origin is placed on the studied crystal (Figure 15). The sphere is traversed by the incident beam and the intersection of the sphere surface with the transmitted beam falls on the origin of the reciprocal lattice. It can be geometrically proven that each point on the Ewald sphere represents a plane of the direct lattice which is in diffraction condition: on Figure 15, the transmitted beam is represented by the vector between the center of the Ewald sphere C and the origin of the reciprocal lattice O. The diffracted beam has the same origin C and forms an angle 2θ with the transmitted beam and is drawn between the center of the Ewald sphere and the point of the reciprocal lattice corresponding to the diffracting plane B, therefore the distance between the center of the reciprocal lattice O and P is the reciprocal of the interplanar distances: $d^* = \frac{1}{d}$. Therefore $OA = \frac{d^*}{2} = \frac{1}{2d}$. And by definition $OC = \frac{1}{\lambda}$. The trigonometric relationships gives $\sin\theta = \frac{OA}{OC}$. OA and OC can be replaced by the above expressions: $\sin\theta = \frac{\lambda}{2d}$ or $\lambda = 2dsin\theta$. This means that a set of planes diffracts when the corresponding point of the reciprocal lattice is on the Ewald sphere[166].

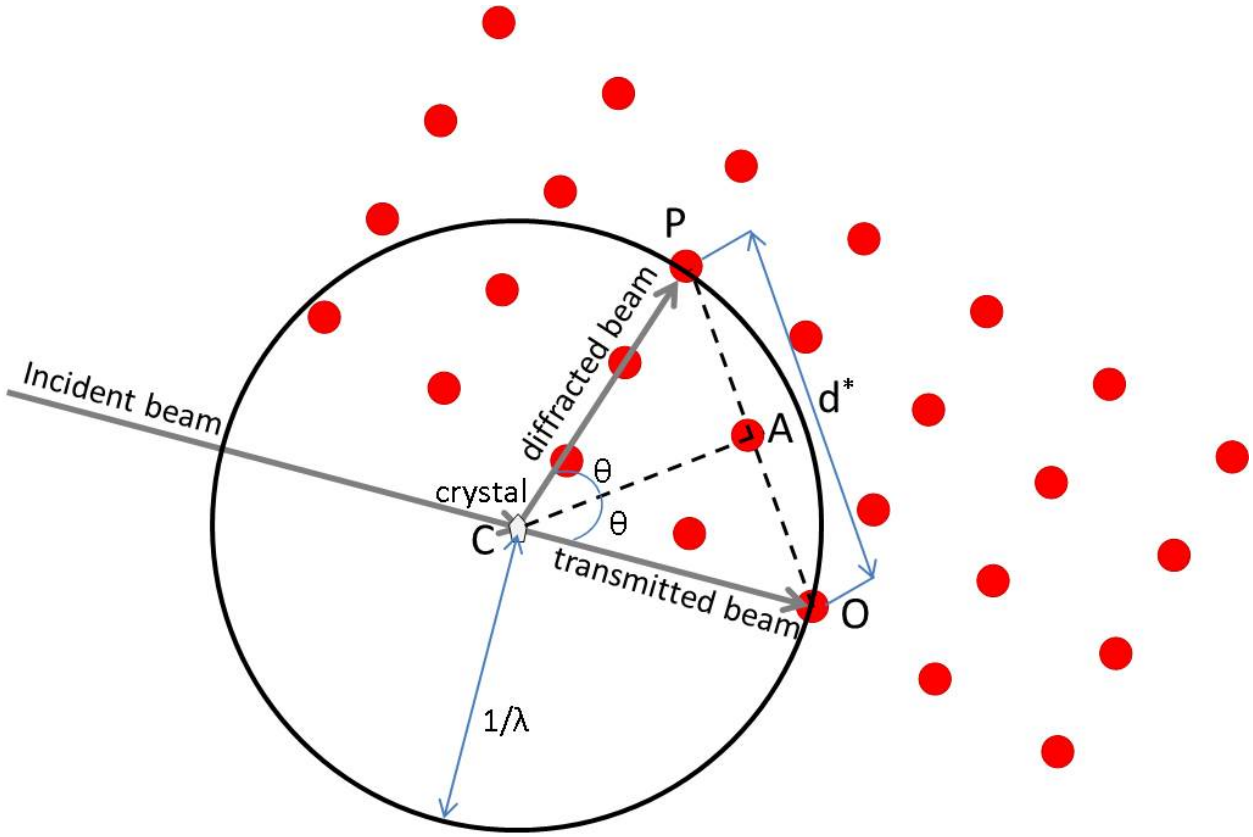

Figure 15 Construction of the Ewald sphere

The Ewald sphere is centered on the crystal C, with radius $\frac{1}{\lambda}$ and such that the intersection of the transmitted beam and the sphere falls on the center of the reciprocal lattice O.

The Ewald sphere displayed in Figure 15 corresponds to the crystallographic definition of the wave vector as evoked in section 29, but the physical description of the reciprocal lattice and the Ewald sphere actually both originally contained an additional 2π factor coming from the definition of the wave vector in physics $|\overrightarrow{k}| = \frac{2\pi}{\lambda}$ for the Ewald sphere, and from the Fourier series derivation of the reciprocal lattice. As a consequence, the scattering vector $\vec{q}$, sometimes used to describe the distances on the diffraction pattern in place of 2θ is derived from the physicist definition of the wave vector and therefore contains a 2π factor, as showed on Figure 16**.**

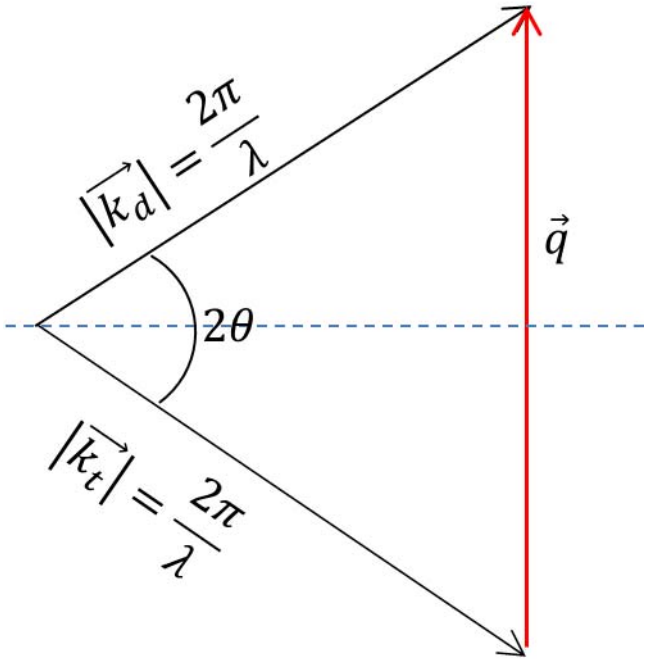

Figure 16 Definition of the scattering vector $\vec{q}$

The scattering vector $\vec{q}$ is sometimes used in order to normalize the diffraction pattern to the X-ray wavelength (λ) utilized (which can vary between different experimental setups) and thus, to enable fast comparison between different studies. The scattering vector is the difference between the diffracted and transmitted beam $\overrightarrow{k_d} - \overrightarrow{k_t} = \vec{q}$. By definition $|\overrightarrow{k_t}| = |\overrightarrow{k_d}| = \frac{2\pi}{\lambda}$. The trigonometric definition of the sinus gives $\sin\theta = \frac{|\vec{q}|}{2}\frac{\lambda}{2\pi}$ therefore $\overrightarrow{|q|} = \frac{4\pi \sin\theta}{\lambda}$, with nm^{-1} as unit. $\vec{q}$ is also quite useful because it describes sizes on a diffraction pattern in a way which is inversely proportional to the interplanar distances in the sample via the relation $q = \frac{2\pi}{d}$.

3.5 Measuring Setups

In order to characterize the symmetry of a material, it is important to get access to diffractions originating from different planes and orders. Several setups are able to achieve that: for example Laue setup, the rotating crystal method, or the powder diffraction method. In the Laue setup, a polychromatic X-ray beam is used, providing a range of wavelengths satisfying Bragg's condition for diverse planes and orders[164]. The rotating crystal method and powder diffraction utilize monochromatic X-ray beams. In the rotating crystal method, the X-ray beam and the detector are fixed, but the sample is turned around one, two or three rotation axes, in order to vary the planes that are in Bragg's condition[164]. Alternatively, the detector and incoming beam can be rotated around the sample in order to vary the angle θ and image different planes and orders. This is called the Bragg-Brentano geometry. Finally, in powder diffraction, a polycrystalline sample or a powder is used. In transmission, the incident beam is monochromatic and parallel, but because of the amount of grains of the sample, each possible orientation of a considered plane will be found in the sample, and each plane will simultaneously under diffraction condition (i.e. will satisfy Bragg's law) (Figure 17a)[164,168]. Due to the rotation of the diffracting planes around the axis of the incident beam, the resulting diffraction pattern is made of concentric circles (Figure 17b). This can be better visualized using the Ewald sphere. A change in orientation of a crystal leads to a rotation of the reciprocal lattice. In 2D, a powder would have all possible orientations and therefore, a 360° rotation of the reciprocal lattice around its center, the resulting reciprocal lattice is made of concentric circles as shown on Figure 17c. In 3D, the rotation of the reciprocal lattice occurs in all directions, thus the resulting reciprocal lattice is a set of concentric spheres. The interaction of this set of spheres with the Ewald sphere forms the concentric circles (Figure 17d) observed on the detector. Traditionally, a concentric film was used as detector, which was positioned around the sample (Debye-Scherrer diffraction setup)[166], or a CCD camera was moved around the sample. The actual version use either a source and detector moving along the vertical axis to cover all the possible 2θ angles or high energy X-ray sources, leading to reduction of the diffraction angles so that a simple plane detector can be used as showed on Figure 17[168].

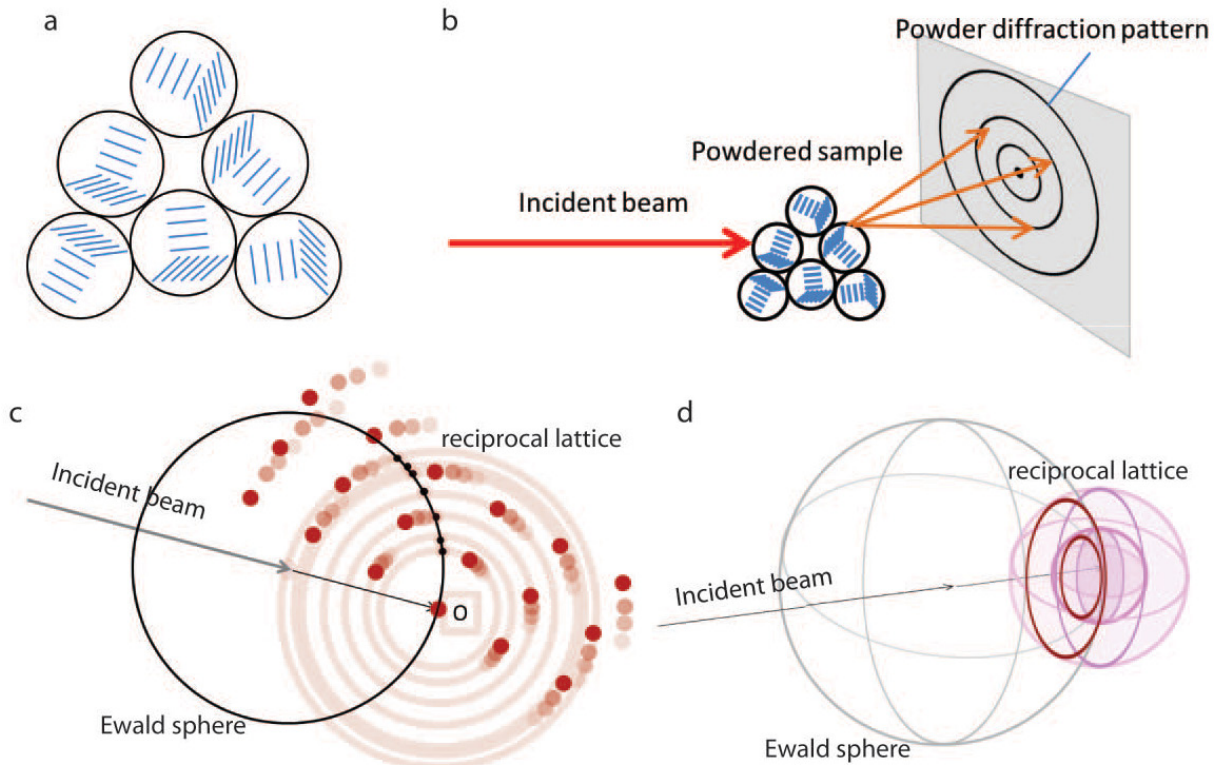

Figure 17 Powder diffraction and the Ewald sphere

(a) Schematic representation of a powder with two different sets of planes drawn in blue (b) Scheme of powder diffraction setup: a monochromatic incident X-ray beam reached the powdered sample at fixed angle. Due to the various orientations of the diffracting planes of the powder, they will all fulfill Bragg's law in some grains, and their various orientation around the axis of the incident beam creates concentric circles on the detector (c) explanation of powder diffraction using the Ewald sphere construct: the random orientation of the planes due to the high number of randomly oriented grains induces various rotations of the reciprocal lattice around its origin O, forming a set of concentric circles in 2D (d) and a set of concentric spheres in 3D. The intersection of the reciprocal lattice with the Ewald sphere is a set of concentric circles which will be projected on the detector.

This geometry can also be used for polycrystalline and fibrous samples[166]. Similarly to the grains of a powder, the crystalline domains of a polycrystal also present various orientations, whereas a fiber presents an axial symmetry around the fiber axis. As noticed before, such a simple setup can access different plans and orders in polycrystalline samples or fibers. Moreover, the approximations of the experiments also causes planes or higher orders which are not in exact Bragg's condition to also appear on the diffraction pattern, especially at small angles and when using high energy X-rays. Therefore, such a simple setup was used in this work, in combination with synchrotron radiation providing not only high energy but also high coherency and intensity useful to get diffraction patterns from protein-based biological samples, which produce weak diffraction peaks.

One normally also discriminates between Wide- and Small-Angle X-ray Diffraction. Indeed the distance between the sample and the detector (L) also determines the range of diffraction angles (and thus, d-spacings) that can be observed on the detector. By changing this distance L, one can probe different length scales from atomic structure to higher order

structural organization. Small structures diffract at larger (wider) 2θ angles; therefore, the detector needs to be placed close to the sample in order to be able to observe these diffraction peaks. On the other hand, larger structures diffract at smaller 2θ angles, and therefore, if the sample to detector distance L is too short, these diffraction peaks will be covered by the beamstop or the incident beam, and their spatial resolution will be low. Therefore, in this case, a larger sample-detector distance L should be utilized. The first case is called Wide Angle X-ray Scattering (WAXS) if 2θ is larger than 5°, or Wide Angle X-ray Diffraction (WAXD), and the second case Small Angle X-ray Scattering (SAXS), or Small Angle X-ray Diffraction (SAXD) when 2θ is smaller than 5°[167]. However, synchrotron beamlines offer such a good spatial resolution that it was possible to record diffraction patterns containing both the SAXD and WAXD region.

3.6 High energy sources-large Ewald sphere

The Ewald sphere construct permits one to easily understand what happens when the incoming beam is of high energy and thus, small wavelength λ. In this case, the diffracting angles 2θ become very small, and more planes become exactly or almost in diffraction condition. In other worlds, the radius of Ewald sphere $\frac{1}{\lambda}$ becomes very big, and therefore, the sphere gets very flat[167,168]. Thus the sphere intersects or touches more points of the reciprocal lattice explaining the fact that many more diffraction peaks can then be observed on the diffraction pattern for the same and unique diffracting angle 2θ *(*Figure 18).

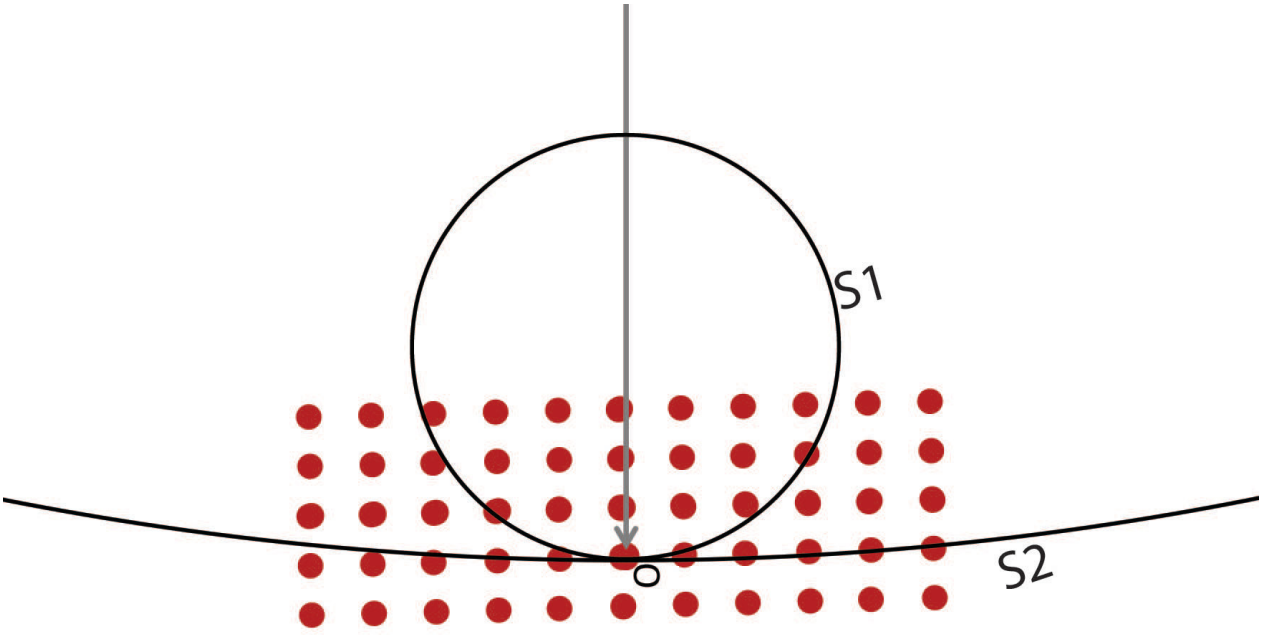

Figure 18 Effect of the energy of the X-ray on the Ewald sphere
Demonstration of the number of plane diffracted by high (S2) and low (S1) energy X Rays. S1 is the Ewald sphere for a low energy (long wavelength) x-ray, and S2 for a high energy (small wavelength) one. This construction graphically shows that high energy X-rays allow more planes to diffract[168].

3.7 Fiber diffraction

Many biological materials, in addition to byssus and silk, exhibit a fibrous structure comprised of well-ordered biomolecules, such as wood[169–171], hairs[172], tendon collagen[173] and muscles[174]. The diffraction pattern of a fiber and its analysis differs from those of typical crystalline materials in that they present an axial symmetry around the long axis. Diffraction patterns from fibers are obtained by placing the fiber axis perpendicular to the incoming X-ray beam (Figure 19a). On account of the axial symmetry of fibers, all the planes parallel to the fiber axis take all possible orientations along the fiber axis, and are therefore in diffraction condition (Figure 19b). The diffraction pattern can then show several orders of their diffractions (depending on ratio between wavelength and interplanar distances). On the other hand, the planes perpendicular to the fiber axis do not have an axial symmetry and therefore diffract as distinct spots when the Bragg condition is met (or almost, due to practical approximations). Therefore the diffraction peaks are arranged at regular interval on lines perpendicular to the fiber axis and called layer-lines. As in normal crystals, the position of the diffraction peaks on the layer lines can be related to the structure of the diffracting structure[167].

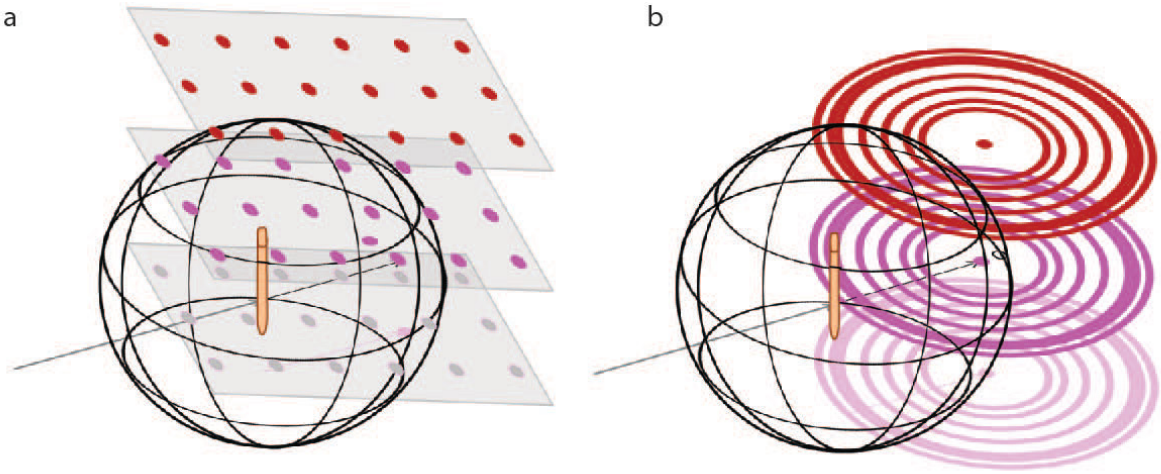

Figure 19 Interaction of the Ewald sphere and the reciprocal lattice for a fibrous sample
(a) Representation of the interaction between the reciprocal space of a monocrystal and the Ewald sphere (b) for a fiber, the reciprocal lattice is made out of several levels of concentric circles due to the axial symmetry of the fiber structure.

3.8 Diffraction by helical structures

One distinguishes between crystalline and non-crystalline arrangement of helices. In both cases, the helices all share a common axis, generally aligned along the axis of the fiber, called z axis, or c-axis. In the case of a crystalline arrangement, the helices are grouped in microcrystals where they present the exact same orientation. These crystals are then randomly oriented around the z axis. The diffraction pattern of such a structure is similar to the diffraction pattern of a crystal rotated around its z axis. It presents clear diffraction spots, which can be analyzed using Bragg's law, but they tend to overlap, making analysis difficult[175]. Therefore, in most of the cases, models need to be built, their diffraction pattern

simulated and compared with the experimental results, and the model corrected accordingly if needed. In case of non-crystalline arrangement of helices, the helices are still aligned along the z axis of the fiber, but their radial orientation is random. The corresponding segments of diffraction on the diffraction pattern are also arranged on layer lines, but they are broad. Their intensity on the layer line can be described using a Bessel function[176,177]. A Bessel function is the shape waves take in case of a cylindrical symmetry, and are made out of an initial strong peak followed by smaller ones (Figure 20). The position of the first peak depends on the order of the diffraction. A Bessel function of order zero begins in the middle of the diffraction patterns, and then shift to the side as the diffraction order increases. For a continuous helix, it was shown that the order of the Bessel function and the number of the layer line was the same. Because the order of the Bessel function increases as the layer line number increases, the first peak is displaced more and more to the side with increasing layer line, leaving more empty space in the middle of the diffraction pattern and creating the multiple"X" shape characteristic for diffractions by helical structures (Figure 21).

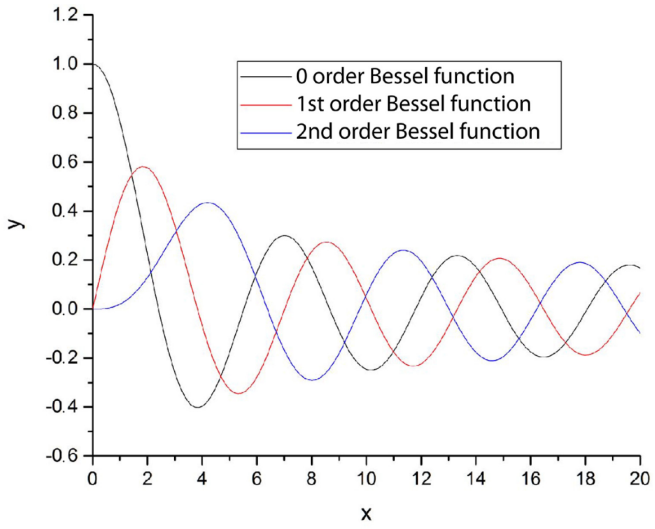

Figure 20 0, 1st and 2nd order Bessel function
showing the displacement of the first peak to the right, creating a lateral shift of the diffraction peak on the diffraction pattern.

In the case of real helices, made of distinct diffracting subunits (atoms or molecules), the diffraction pattern exhibits further helix crossings placed up and down on the meridian (the central vertical axis). The layer line of the first meridional diffraction after the central one is reciprocal to the rise per residue, or the axial distance between to subunits of the helix, while the distance between two layer lines is reciprocal to the pitch, which is the distance for the helix to make one full turn. The pitch, repeat size and distance between diffracting subunits is shown on Figure 21, both on a simulated diffraction pattern (Figure 21a) and on a projected helix (Figure 21b)[177].

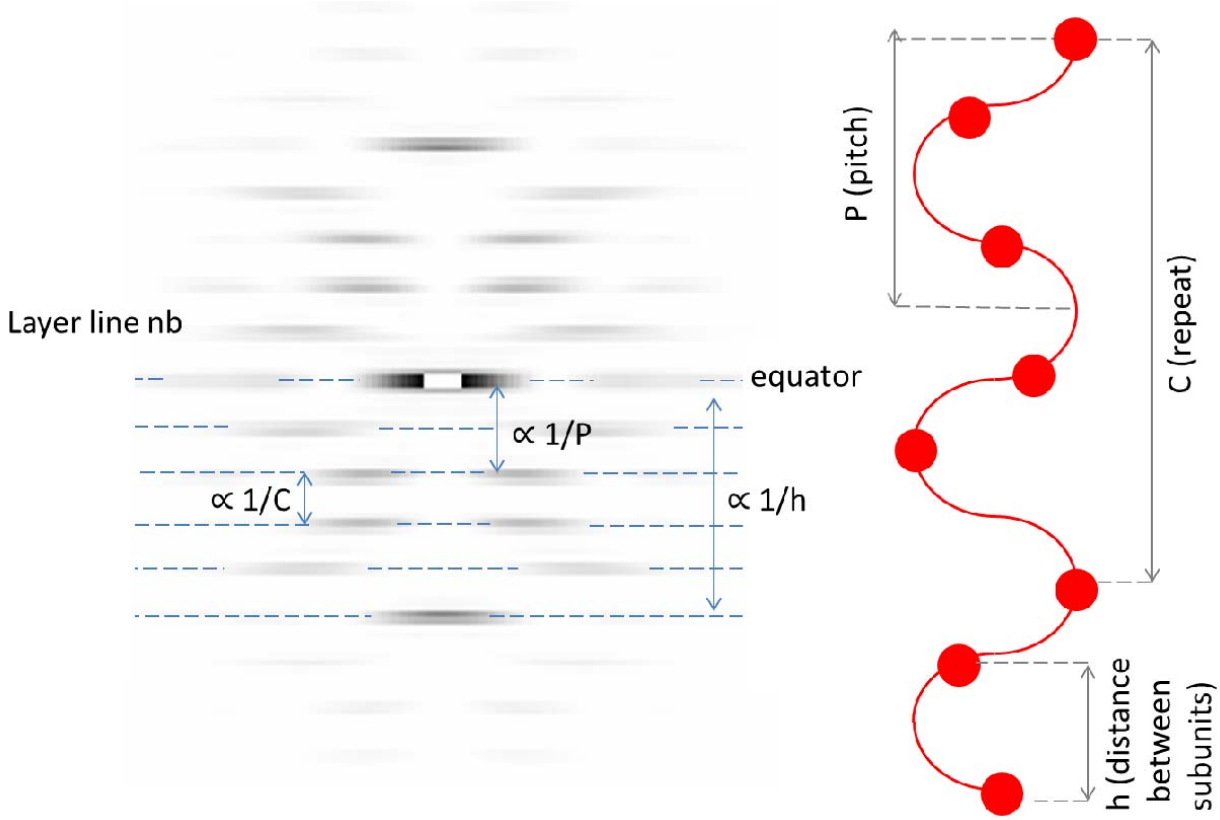

Figure 21 Diffraction patter of helical structures
(a) simulated diffraction pattern of a helical structure of 2.5 subunits/turn and (b) the projection of the corresponding helical structure.

3.9 Diffuse scattering

It is generally considered that the diffraction mentioned above is a special case of scattering, occurring in materials with periodic structure when the wavelength and the diffracting structure are approximately the same size. However, many materials are partially or entirely amorphous, lacking periodic structure, and can also be investigated using X-ray diffraction techniques. Their diffraction pattern reflects their internal unordered structure by exhibiting very diffuse diffraction rings instead of sharp and distinct peaks. Between these two extremes are a wide range of disordered states due to the movements of molecules or defects in a crystalline lattice, for example. The diffraction pattern shows an increasing degree of diffuseness as the order within a material decreases[178].

If we imagine that the atoms of a regular lattice get slightly moved away from their ideal position as for example in thermal motion, in random direction, this forms a slightly deformed lattice which has the effect to broaden the diffraction peak around Bragg's angle[179,180]. If the diffracting units are even more displaced from their original position, like in amorphous materials, and there are some missing ones, then the long-range order is destroyed, and there is only short range-order[165], which means that the position of one unit only depends of the position of its nearest neighbors, but that the position of two units situated far away from each other in the lattice an not be correlated anymore. In this case the broadening of the diffraction peak is even more dramatic[165]. The data from diffuse scattering can still be processed similarly to Bragg diffractions[181], but their exact analysis requires complicated modelling and simulations. The used principle is that the final scattering ring observed on the diffraction pattern is the sum of all the interactions between all the waves scattered by each diffracting unit, whose interaction depends on the distances between the scattering units[182] and necessitates previous information about the studied material. Information about simple non crystalline structures is obtained by numerically solving Debye's equation which describes the overall scattering considering the interferences between all the scattering units[182]:

$$I(s) = \sum_n^N \sum_m^N f_n(s) f_m(s) \frac{\sin[2\pi s r_{nm}]}{2\pi s r_{nm}}$$

With r_{nm} the distance between the scattering units n and m, $s = |(S - S_0)|/\lambda$ the magnitude of the scattering vector, with S_0 the wave vector of the incident beam and S the wave vector of the scattered wave, and f_n and f_m the atomic form factor, which depend on the energy of the incoming beam. This intensity function describes a Bessel function of zero order, and is the basis for simulation techniques used to get information out of diffuse scattering. However, this requires that one already has a model for the observed structure and idea of the position of the diffracting units, which was not the case in this work since I have been investigating a protein which was completely unknown.

4 Materials and parameters

4.1 Byssus

Most of the *P. nobilis* threads used in this work were collected from the wild in the bay of Villefranche-sur-mer, France and between the two Lérins Islands, France. Because *P. nobilis* is strongly protected (European Directive 92/43/CEE), prior to collection, all necessary permits were acquired from DDTM (Direction Départementale des Territoires et de la Mer, J. Banus) of Alpes-Maritimes department. Byssal threads were collected on site, without killing the animals. *P. fucata* and *A. pectinata* threads were collected in Namhae, Gyeongnam, South Korea and given by Jimin Choi. *Mytilus edulis* mussels were collected from the North Sea and kept in a saltwater aquarium at 16 °C. Freshly grown threads were collected from the tank-grown mussels. All threads were stored in Milli-Q water prior to measuring. Washed and treated byssus threads have been furnished by Chiara Vigo.

4.2 Inductively coupled plasma optical emission spectrometry (ICP-OES)

For metal content determination, approximately 5 mg of threads were freeze-dried and weighed prior to dissolution in 2 ml aqua regia overnight and heating at 180°C for 1 hour. The Aqua Regia was made by mixing 1/3HNO_3 (64 % Carl Roth, ROTIPURAN) with 2/3 HCl (37 %, Carl Roth, ROTIPURAN). The metal content was measured with inductively coupled plasma optical emission spectrometry (ICP-OES, PerkinElmer OPTIMA 8000) calibrated with a set of calibration standards in aqua regia (0.05, 0.2, 0.5 and 1 mg/L dilution of a 28 elements 1000mg/L ICP Multi-Element Standard Solution from Carl Roth). Three repetitions were effectuated for each sample and an independent standard at 1mg/L ICP Multi-Element Standard Solution (22 elements) from Carl Roth was used to check calibration and stability of the measurement. The ICP measurements presented in the comparative study are average of 3 samples for each species of *Pinctada* fucata and *Mytilus edulis* byssus fibers, 2 samples for *Pinctada margaritifera* byssus, 5 samples for *Atrina* and *Pinna* byssus. The results presented in the investigation of *P. nobilis* byssus traditional processing are made of 3 samples for each of the *in-lab* treated byssus (native, lemon juice and citric acid). 3 samples were use of native *Pinna* fibers provided by Chiara Vigo, 2 samples from instant treated fibers and 1 samples of each fully treated fibers (bisso trattato, fully treated and unknown treated).

4.3 Amino acid analysis

Amino acid analysis was performed using 1-2 mg of freeze-dried threads, which were hydrolyzed for 24 h in 6 N HCl (37 %, Carl Roth, ROTIPURAN) with 10 % phenol at 110 °C under vacuum. The amino acid composition of the samples was analyzed using a post-column ninhydrin-based amino acid analyzer (Sykam S433, Fürstenfeldbruck, Germany) after calibration with standard solutions from Sykam GmbH.

4.4 X-ray Diffraction (XRD)

For XRD experiments, threads were glued across a hole on a rigid plastic frame. Drying was minimized by placing threads between a Kapton foil with a hydrated tissue paper present. Wide and Small X-ray diffraction (WAXD and SAXD) measurements were conducted at BESSY Berlin (Elektronenspeicherring Gesellschaft m.b.H., Berlin, Germany) MuSpot beamline[183]. The X-ray wavelength was 0.82565 Å and the beam diameter was 50 µm. The diffraction patterns were collected on a 2D CCD detector (MarMosaic 225, Mar USA, Evanston, USA) with a pixel size of 73.24 µm and a frame size of 3072x3072 pixels. WAXD diffraction patterns were processed with dpdak, an open source XRD analysis tool[184], using the cake integration tool after background subtraction. SAXD diffractions were analyzed using ImageJ. Background was subtracted using the image subtraction tool. Then, the diffraction pattern was aligned with the image rotation tool, and a linear projection was effectuated of a rectangular selection drawn tightly around the diffraction spots. The integrated intensity vs q curves were plotted in Origin, and the peaks positions were measured by multiPeak fit, using Gaussian curves. Bragg´s law was used to calculate the corresponding spacings in the real space. Confirmation and refinement of the structure were done using the HELIX software[185], which is a simple tool simulating diffraction patterns of helical structures from a set of parameters introduced by the user. Three diffraction patterns from three different threads were used to measure the pitch of the helical structure, which is the peak position in real space multiplied by its layerline. All the visible diffractions from the helical structure on the three diffraction patterns were used in the calculation of the average helix pitch.

4.5 Transmission Electron Microscopy (TEM)

Threads were air-dried prior to embedding in LR White resin (Agar), polymerized at 60° C for 3 days and then cut into 100 nm slices (Leica Ultracut UCT). Grids were post-stained with 1-2 % uranyl acetate (aqueous solution) for 1-10 min and briefly rinsed in miliQ water. Bright field TEM images were obtained with a Zeiss EM 912 Omega at 120 kV and a Jeol JEM-ARM200F at 200 kV.

4.6 Tensile testing

An in-house tensile tester comprising an atmospheric chamber was used in combination with a HUMIGEN humidifier permit to keep the desired humidity within the tensile testing chamber. A 0.5 N load cell was used to measure the force for treated fibers testing, and a 2.5 N (Honeywell) load cell for the native byssus fibers. The tensile testing chamber possesses two windows allowing the use of a Keyence VHX-S550E microscope to record a video of the sample during testing.

For sample preparation, plastic frames were used, presenting a small hole in the middle. Samples were prepared by gluing both ends of a 5-6 mm long piece of fiber on both sides of the hole in the plastic frame using Polyurethane glue from Titebond. A second plastic frame

was placed on top, and clamps were used to press this sandwich together during glue polymerization. Prepared samples were kept in water overnight.

For testing, the clamp was removed, and the plastic frame sandwich containing the sample was placed on the sample holders so that the edges of the sample holders almost reach the edges of the hole of the plastic sandwich. The clamps of the machine were closed and the sides of the holes are melted using hot wire word burning pen. The clamped fiber sample was then rehydrated in deionized water. The water was removed with a pipet after 15 min, and Curcuma or coal was spread on the wet fiber so that grains stick to it and could be tracked on the video in order to measure the extension. The sample was left to equilibrate for 15 min at ≥90 % humidity prior testing.

During the test, the force was recorded by the load cell and the extensibility was measured on the video using a free tracking program called TRACKER. Force and extension were synchronized by aligning the force and image at the breaking point. Then the stress was calculated by normalizing the force by the cross area of the fiber, and the strain was calculated by dividing the displacement by the sample's initial length. All the tests were effectuated at a 83 µm/s (≈5mm/min) motor speed.

The fiber cross area was measured by aligning the sample vertically under the microscope (Keyence VHX-S550E) and taking a picture. ImageJ was use afterward to draw the contour of the cross section and measure its area.

10 fibers were used, coming for three different mussels for native byssus, and 10 fibers from 2 different fully treated batches (bisso trattato and fully treated). 3 fibers were used for the recovery test, 7 fibers were used for the tensile test of instant treated fibers, 6 for the citric acid treated fibers and 5 for the lemon juice treated fibers.

Cyclic testing and recovery were conducted in the same conditions. For cyclic testing, a 3% strain increase was applied between the successive cycles. For Recovery testing, the first cycle was effectuated by loading to about 30%, followed by a direct unloading to 0%strain. A second cycle was effectuated immediately to the same strain. After the release of the strain, some water was added on the bottom of the tensile tester chamber, below the sample, until the sample is completely soaked in water. The sample was left to rest for about 20 hours. After the resting period, the water was removed, the sample was re-stained with curcuma, and was left to equilibrate 15min at ≥90 % humidity. Finally, a last cycle was effectuated to the same strain than the first two cycles.

4.7 *In-situ* tensile testing at the synchrotron

The same setup was used while performing tensile testing combined with XRD, but the chamber was used in vertical position, and the windows were replaced by Kapton foil, which does not produce diffraction at same angles as *P. nobilis* byssus fibers. In this case, the samples were prepared the same way as for simple tensile testing, but after clamping them

in the sample holder, and melting the sides of the plastic stripes, the chamber was directly closed, and the samples were equilibrated at 70 % humidity for about 20 min. Measuring at 70 % humidity ensures that water does not condense on the sample or the windows, which would produce diffraction and deteriorate the signal. In this case, recording the extension could only be done via continuous record of the motor position, and the force was recorded by the load cell.

4.8 Fourier transform infrared spectroscopy-Attenuated Total Reflection (FTIR-ATR)

Thin (14 µm) sections of frozen thread embedded in ice were prepared using a cryo-microtome from Thermo Fisher Scientific™ Inc. (Microm HM 560). The cuts were laid on a glass slide and allowed to air-dry for 24 h. A FTIR microscope (Hyperion 2000, Brucker) was used for the measurements in ATR mode. A background signal was measured in the air after each change of place on the sample. Each sample was measured several times at different spots on different fibers in order to acquire 5 to 7 good spectra, which were averaged afterward. The tip of the ATR crystal was gently cleaned after each measurement with a little bit of ethanol on a thin paper towel. For data analysis, the background of each curve was individually removed using a Gummiband (7pts) method in OPUS and the results were exported to Origin for curve averaging and plotting.

4.9 Near Infrared Raman Spectroscopy

Thin (15 µm) cuts of frozen thread embedded in ice were prepared using a cryo-microtome from Thermo Fisher Scientific™ Inc. (Microm HM 560). The cuts were laid on a quartz slide and a 0.25 mm thin quartz coverslip (TED PELLA, Inc.) was laid on top and sealed using nail polish to prevent water evaporation. A confocal Raman microscope from WITec (CRM200), equipped with a near IR laser (wavelength 785 nm, Toptica Photonics AG) was used for measurement. Each sample was measured at several places on different fibers in order to acquire at least 5 good curves, using a Nikon 20x air objective (working distance 3.8 mm, numerical aperture 0.40). For Data Analysis, 3 to 5 similar curves were averaged using the spectrum calculator in the WITec software and exported as .txt file, which was loaded in OPUS for background removal using a 7pts Gummiband. The results were exported to Origin to produce the final graphs.

4.10 Color measurement

For visible light spectroscopy, a confocal Raman microscope form WITec was used in which the laser was replaced by a powerful white light made out of a blue, a red and a yellow LED combination (cool LED pE-100). The light spectrum was recorded using the spectrograph and CCD detector of the Raman microscope. Then a small bundle of fibers was put under the microscope, and the reflected light was measured. A white photography card (Ares Foto) was used as white reference. Origin was used to put the obtained curves into CIE 1931 XY

color space. For the *in-lab* treated fibers, 10 spectra were obtained on different fibers for each sample (=each treatment), for the traditional treatment, 9 fibers from native fibers provided by Chiara Vigo, 6 instant treated fibers, and 3 of each treatment (unknown treated, bisso trattato, fully treated) were measured.

4.11 Interdisciplinary and significance of the results

Due to the position of the present thesis at the interface of different disciplines, including biology and analytic sciences, it is important to discuss the meaning of the results, especially regarding the sampling size and the signal to noise ratio, which raise the question of the qualitative or quantitative nature of this work.

One also has to consider the probable source of the observed variation, and distinguish between natural variation and measurement error. For example the protein building the helical quaternary structure are expected to have a well-defined folding in order to be able to form this regular structure. This folded structure is determined by the genetically determined protein sequence and is unlikely to vary between different animals from the same species. Therefore the standard deviation of the measured helical pitch is very likely originating only from measurement error. In this case, a higher number of measurements would allow a decrease of the standard error and a better estimation of the real size of the structure. On the other hand, the metal content and mechanical properties of byssus have been observe to be subject to extremely large variations depending on the animal, its location and the season of byssus production[186], therefore the variation in metal content measured with ICP is likely more attributable to intrinsic biological variation. Finally, the byssus is made of various proteins and the proportion of the different proteins is likely to vary from one time to the other, which explains part of the variation in amino acid content and in mechanical properties, whereas measurement errors also play a part in the spread of the data.

In order to estimate the relevance of the results presented in this work, we can compare the sampling size and variation of the results to what is commonly used in the study of such natural materials. For example, we used 10 fibers for the mechanical characterization of native and traditionally treated *P. nobilis* byssus, whereas for the qualitative comparison of the instantly treated and the *in-lab* treated fibers, I used at least 5 fibers for each treatment, and 5 fibers for the recovery tests. Brazee and Carrington[119] used between 5 and 9 threads for recovery experiments in their byssus study, and from 5 to 16 fibers for simple pull to break tests, whereas Bell and Gosline[32] used 3 to 5 threads for the measurement of the Young modulus. Bouhlel et al.[120] used between 7 to 10 threads for a comparison of the mechanical properties of byssus fibers from different species. The same study included single fiber tensile tests of *P. nobilis* byssus and measured a Young modulus of 186 ± 68 MPa, so the deviation is about 36 % of the measured Young modulus. As a comparison, I measured a Young modulus of 566 ± 118 MPa, so a deviation of 20% of the measured Young modulus. As a side note, the difference in measured Young modulus can be attributed to the possibly

different strain rate, since stiffness is highly dependent on loading rate in *Mytilus* byssus[129] (not specified by Bouhlel et al), the fact that they discarded the fibers which broke at the fixing point (so they kept only the ones that had defects) and a different way to measure the fiber cross area, since I measured the area of the cross-section under a microscope, and Bouhlel et al used the average fiber diameter and estimated a circular cross-section. Part of the remaining spread in my data might be attributed to the measurement of fibers cross area. Indeed it was measured using a microscope to measure the area of the cross section, but if the surface is not exactly perpendicular to the fiber axis or the fiber is misaligned, the measured surface will have up to about 6% error for a 20° misalignment along only one axis (See Figure 22). The rest of the spread in Young modulus is likely related to a variation of the ratio of helixes to matrix proteins between the different threads.

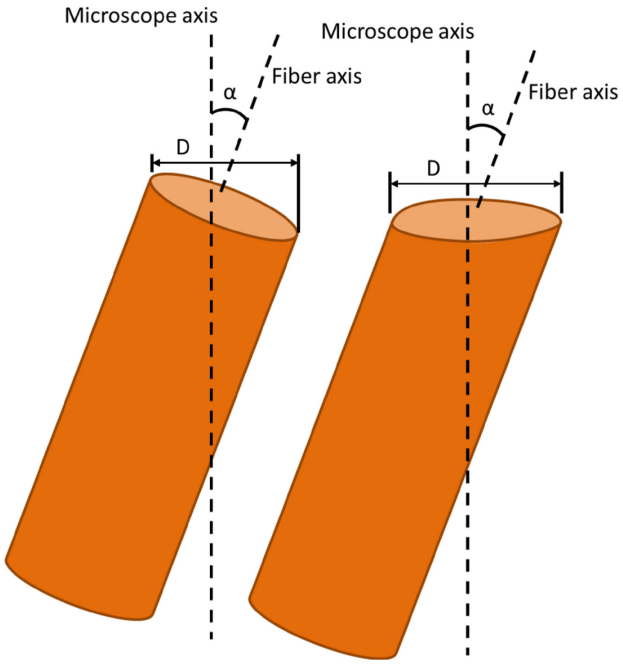

Figure 22 Error in section measurement. 2 cases of misalignment of the fiber compared to the axis of the microscope which can occur during the measurement of the cross-section for the calculation of the stress in the stress-strain curve, which can lead to up to 6% error for a misalignment of 20°

It is also useful to discuss the relevance of the analysis of the XRD with in-situ tensile testing, due to the variation in peak position. Indeed, there was a 1.7 pixels standard deviation of the scattering vector Q of the diffraction on the 3rd layer-line on three XRD measurements made on the same thread. This is about the same value as the difference in helix size between the measurements at two consecutive strains (See Table 1).

Table 1 Helix strain vs fiber strain. Scattering vector Q of the diffraction on the 3rd layerline for the different fiber strains, and statistics (R square and p) of the linear fitting of the helix strain vs fiber strain measurements of Figure 32.

n1		n2		n3		n4	
Fiber strain [%]	Q [pixels]	Fiber strain [%]	Q [pixels]	Fiber strain [%]	Q [pixels]	Fiber strain [%]	Q [pixels]
0	72.2	0	74.0	0	74.7	0	75.4
0.6	72.5	0.8	74.3	0.6	74.4	0.6	75.5
1.9	67.8	1.6	73.7	1.7	72.4	1.3	73.7
2.5	65.2	2.6	72.0	2.3	72.0	2.3	72.1
3.8	65.2	3.8	70.8	3.8	70.4	3.4	69.0
5	59.9	4.4	68.0	4.0	65.3	5.5	
5.6	57.7						
R^2	p	R^2	p	R^2	p	R^2	p
0.95	$2E^{-4}$	0.91	0.01	0.76	0.025	0.99	$5E^{-5}$

However, when considering the difference in scattering vector Q between non- consecutive fiber strains, it is clear that there is a change in Q bigger than the standard deviation. Also the value of p[a] (Table 1) showed that there was a relationship between the fiber strain and the helix strain (Figure 32) and the values of R squared (Table 1) show that despite the measurement error, the measurement points on the graph of helix strain versus fiber strain (Figure 32) could be fitted with a straight line. This confirmed that the helical building block gets stretched when the fiber is extended.

Finally, it is important to consider the results in the context of the work. This study is the first characterization of *P. nobilis* byssus and when comparing to the current knowledge of *Mytilus* byssus or spider silk, it has to be kept in mind that *Mytilus* byssus has been investigated continuously for the last 30 years, and spider silk for the last 50 years. Therefore it achieved important first steps for the understanding of *P. nobilis* byssus by finding out its building block and being able to relate this building bloc to the mechanical behavior of *P. nobilis* byssus. For this purpose, it is not crucial to measure the size of the building block with high precision, nor to know the very exact Young modulus of *P. nobilis* building block. Indeed, precise measurements of mechanical properties for example, are important to make predictions and are essentials for applications such as the design of load bearing structures, which was not the aim of this work. The purpose of this work was to characterize the structure and mechanical behavior of *P. nobilis* byssus, and to understand the principles driving byssus design. Quantitative data are important for this, because they allow the overlap results from different techniques (for example XRD and TEM), but in contrary to the design of load bearing structures, there was no need for a very precise determination of the considered quantities (sizes and mechanical properties).

[a] p is the probability tested by an ANOVA test that the fibers train and helix strain values are independent. So if $p<0.05$, indicates that the hypothesis that there is no relationship between the fiber strain and helix strain can be rejected.

5 Comparative analysis of hierarchical structure in Ostreida species byssus

5.1 Introduction

As explained in section 1.2, the mechanical properties of protein-based natural materials are highly dependent on their multiscale hierarchical structure. Especially in the case of *Mytilus* byssus, we saw in section 2.2.2 that special structural and chemical features (highly aligned PreCol, histidine rich and flanking domains) determines the self-healing capacity and high toughness of the core[187] by providing hidden length and sacrificial bonds[128,129,188]. Additionally, DOPA catechol has been observed to play a similar role on the mechanical properties of the cuticle by providing reversible crosslinks via protein-metal coordination. It is also thought to play a major role in the underwater adhesion of the plaque, which has already inspired the development of new synthetic materials such as adhesives for fetal surgery[46] and self-healing polymers[189,190]. These features are common to all species from the Mytilidae family studied so far; however, similar knowledge is lacking concerning the byssus of *P. nobilis* and any other species belonging to different families.

Due to the high potential of comparative investigation for the extraction of material key features as well as their evolutionary nature suggested by silk research (section 1.2)[94], I added other related species to this structural byssus study. The byssus of the fan mussel *A. pectinata* and the pearl oysters *P. fucata* and *P. margaritifera* (Figure 23) were chosen as objects of this study due to their different degree of relatedness. In addition to helping the extraction of key design features from byssus structure, the comparison of these different species will help assess the relationship between byssus structure and bivalve taxonomy, thus confirming or infirming the convergent nature of byssus evolution. *Mytilus* (*edulis* and *californianus*) byssus will be added to this study, the in-depth knowledge of their byssus structure-function properties offering important help in the assessment of the possibly important features of the byssus design from other species, if they present similarities, according to the hypothesis of convergent evolution.

All the bivalves studied in this work belong to the Pteriomorphia subclass (Figure 24). *Mytilus* mussels (Mytiloida order) are distantly related to the other four species which all belong to the order Ostreida. Within the Ostreida order, pearl oysters (*Pinctada*) and fan shells (*Atrina* and *Pinna*) belong to two different superfamilies (Pterioidea and Pinnoidea). *P. margaritifera* and *P. fucata* are the most closely related species in this study, since both belong to the Pinctada genus. *A. pectinata* and *P. nobilis* are slightly more distantly related species, both belonging to the Pinnidae family but two different genera. In line with these taxonomic divergences, these mussels also live in very different environments, as mentioned in section 2.1: *Mytilus* specimens are found in intertidal areas where they endure crashing waves, whereas Ostreida members live in calmer waters. The fan shell mussels from the Mediterranean Sea (*P. nobilis*) and from the West Pacific (*A. pectinata*) are very large

mussels (up to 1 m and 0.5 m, respectively). They live partially buried in sandy areas, where their byssus acts more like anchoring plant roots, which is in stark contrast to *Mytilus* mussels which anchor to hard substratum in the wave-swept rocky intertidal zone. *P. fucata* oysters have a size up to 8.5 cm, while *P. margaritifera* specimens can reach 14.7cm and both species live in coral reefs in protected areas of the Indo-Pacific ocean [155]. While little is known about the proteins comprising the threads of *P. nobilis, P. margaritifera* and *A. pectinata, P. fucata* threads are reported to contain a thrombospondin-like protein stabilized by Ca^{2+} [156,157], which greatly contrasts the collagen-based byssus of *Mytilus spp.*

In order to conduct an in-depth comparative investigation of the byssus ultrastructure from these species, I utilized a range of techniques including compositional analysis, XRD and TEM.

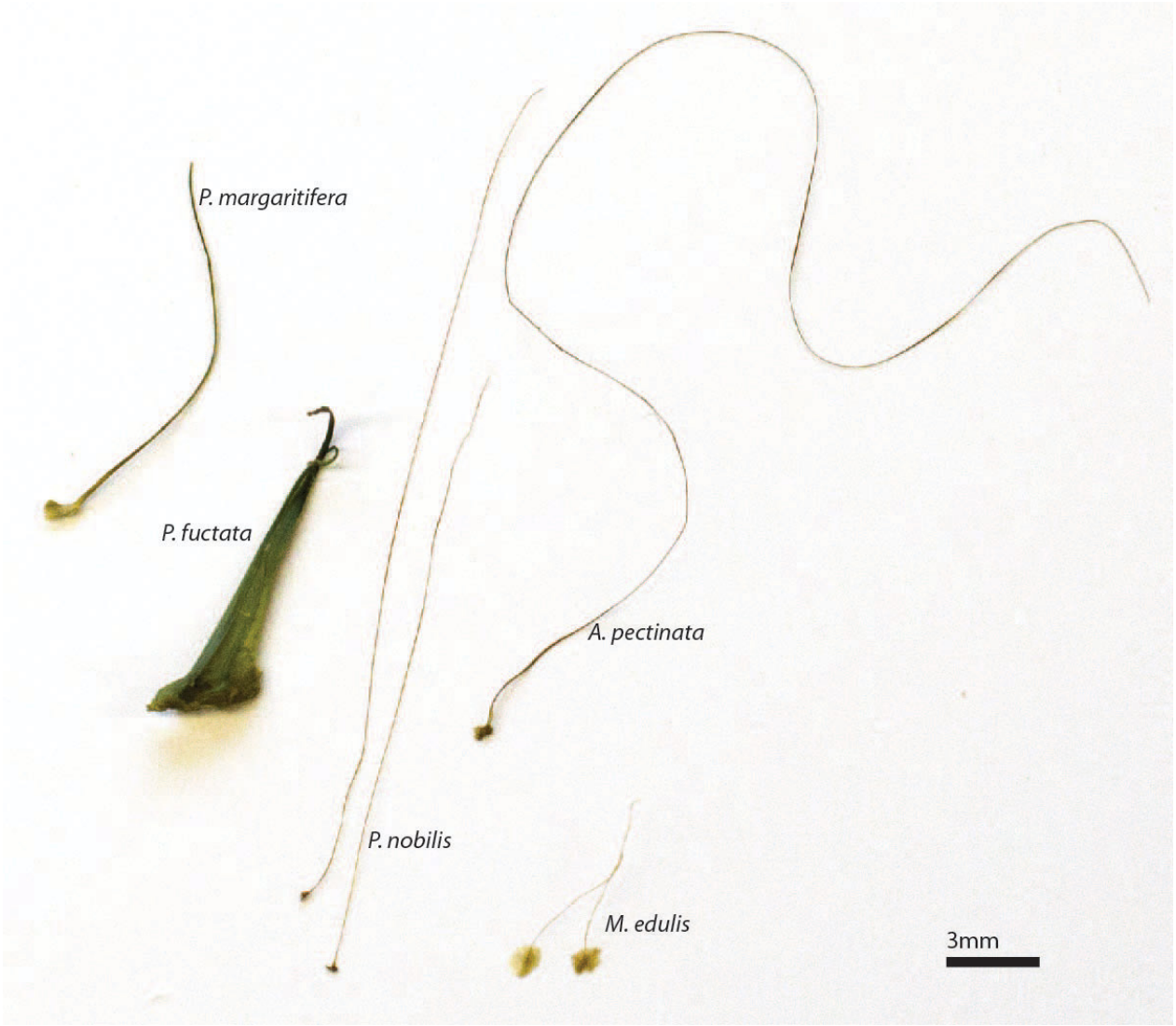

Figure 23 Comparative morphology of different byssal threads
Morphological variation between byssal threads investigated in this study, including pearl oysters (*P. margaritifera and P. fucata*) fan shells (*P. nobilis* and *A. pectinata*), and blue mussels (*M. edulis*). Modified from[191] to include *P. margaritifera* byssus. Published by The Royal Society of Chemistry.

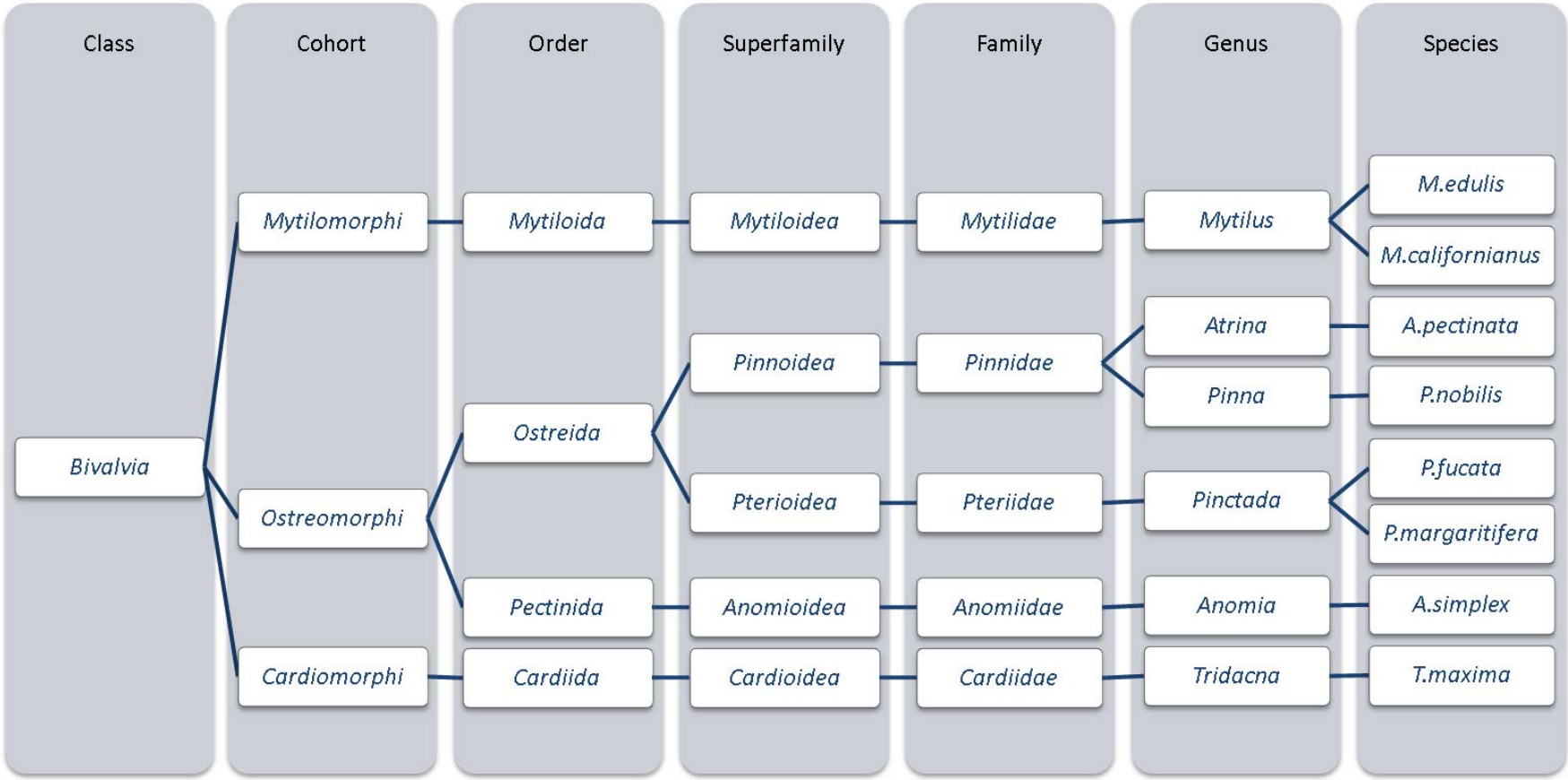

Figure 24 Taxonomic classification of some byssus-producing bivalves.

Classification of different mussels whose byssus structure has been studied thus far, according to Bieler et al.[192]. For simplification, some classification steps were omitted. Modified from[191] to include *P. margaritifera* byssus. Published by The Royal Society of Chemistry.

5.2 Results[b]

5.2.1 Byssus Composition (ICP-OES and amino acid analysis)

I used amino acid analysis to investigate the protein composition of *A. pectinata*, *P. fucata, P. margaritifera* and *P. nobilis* byssus and inductively coupled plasma optical emission spectrometry (ICP-OES) to characterize their inorganic content, and then compared the results with *M. edulis* byssus (Figure 25a and b).

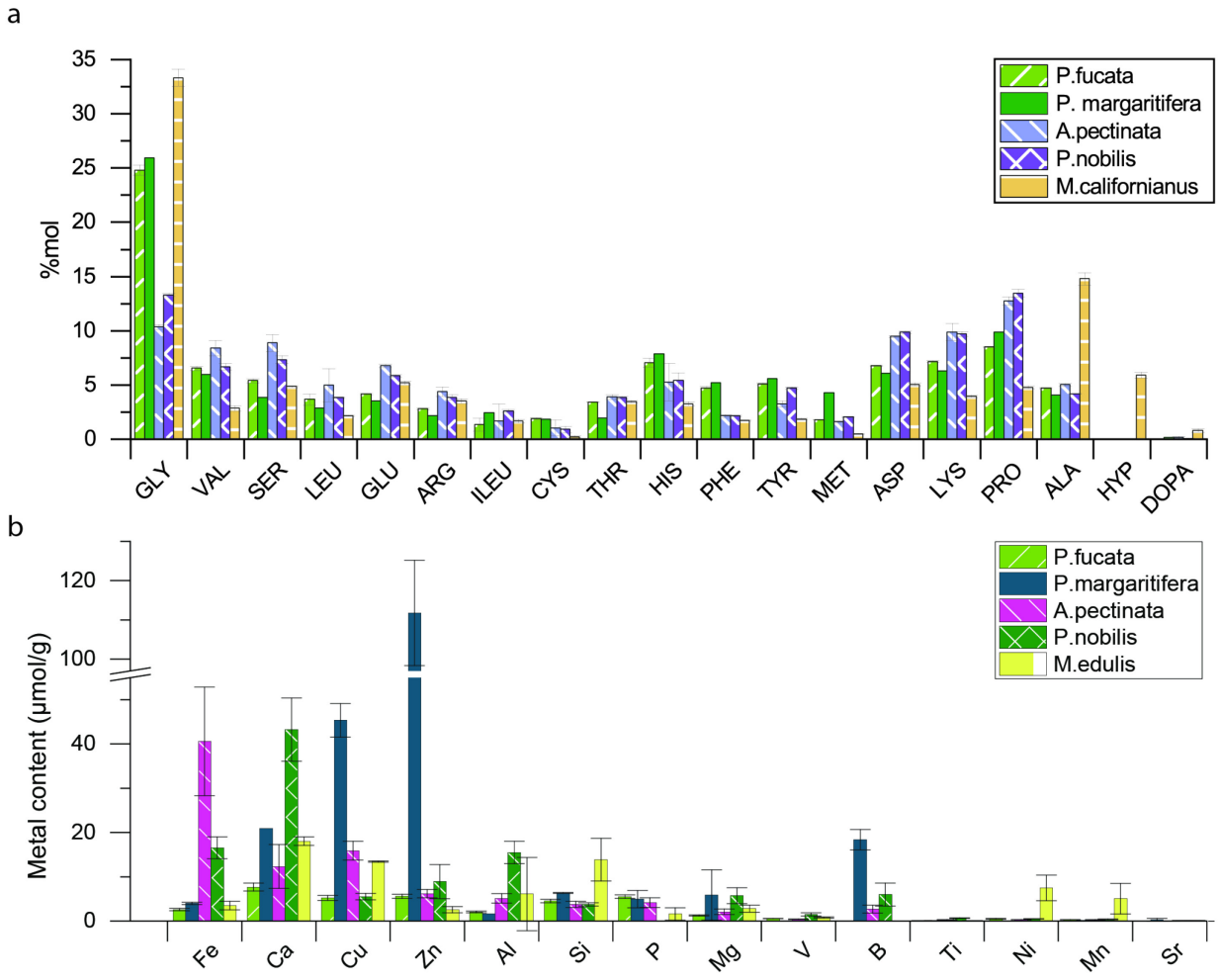

Figure 25 Comparative compositional analysis of different mussel byssal threads.
(a) relative amino acid composition of the byssus of *P. fucata*, *P. margaritifera A. pectinata*, *P. nobilis* and (for comparison) *Mytilus californianus* (*M. californianus*)[133], and (b) metal content in *P. fucata, P. margaritifera, A. pectinata, P. nobilis* and *M. edulis* byssus threads. The absence of standard deviation of the organic composition of *P. margaritifera* byssus is due to too low amount of material to replicate the experiment. Modified from[191] to include *P. margaritifera* byssus. Published by The Royal Society of Chemistry.

[b] The result and discussion of this chapter have been reproduced from[191] and modified to include *P. margaritifera* byssus. Published by The Royal Society of Chemistry.

Amino acid analysis showed that all four byssus are mainly composed of proteins (~80%), which is similar to *M. edulis* byssus. *P. nobilis* and *A. pectinata* byssus exhibit a similar protein composition, with a Glycine (Gly) and Alanine (Ala) content that is 2-3 fold lower than *M. edulis* byssus, and a complete absence of hydroxyproline (Hyp). This suggests that Pinnidae byssal threads, in contrast to those of Mytilids, are not based on collagen, as previously observed[120,131,141,152]. However, they do contain an elevated amount of Proline (Pro) (> 10 mol %), which is often associated with intrinsically disordered proteins (IDPs). While *P. fucata* and *P. margaritifera* byssus contain twice as much Gly as the Pinnidae mussels, they otherwise resemble them and the clear absence of Hyp still differentiate them from the *Mytilus* collagen-based byssal threads. Pinnidae byssus contains a total amount of metal ions (Figure 25 b) similar to *M. edulis* (4.7(±1.2) mg/g for *A pectinata*, 4.0(±0.7) mg/g for *P. nobilis* and 3.0(±0.5) mg/g for *M. edulis*), while *P. fucata* seems to contain a bit less (1.6(±0.2) mg/g) and *P. margaritifera* contains an intriguing high content in inorganics (11.6(±0.2) mg/g), especially Zn (7.3(±0.9) mg/g). However, it should be emphasized that metal content in byssal threads has been shown to vary considerably between different locations and season, even for threads from the same species[186,193,194], which complicates a purely quantitative comparison between the measurements in this study and with other studies[120]. Nonetheless, there are notable differences in the relative distribution of different metal ions between the different species.

5.2.2 WAXD/SAXD

Because amino acid analysis suggests that byssal thread proteins from the four non-mytilid species are not collagenous, I utilized WAXD to further investigate the conformation of proteins in the threads, and SAXD to observe and characterize the higher order organization of proteins. As previously observed[131,141,152], the typical collagen peak at D = 0.287 nm from *Mytilus spp.* byssus (arrow on Figure 26d), corresponding to the rise per amino acid residue of the triple helix, is absent from the diffraction pattern of *P. nobilis*, *A. pectinate*, *P. fucata* and *P. margaritifera* byssus (Figure 26a, d, g and j), as are other peaks arising from the triple helical backbone structure. In fact, there are no sharp peaks visible at all within the WAXD region of the diffraction patterns from *P. nobilis* (Figure 26a), *A. pectinata* (Figure 26d), *P. fucata* (Figure 26g) or *P. margaritifera* (Figure 26j). Rather, the fibers from all four species exhibit a diffuse halo from Q = 10 nm^{-1} to 25 nm^{-1}, which could originate from random-coil proteins or also from proteins with a mixture of many secondary structures with various orientations, as found in globular proteins. Notably, however, we do observe a series of sharp and ordered diffraction peaks in the SAXD area (Figure 26b, e, h and k) indicating that these proteins apparently arrange regularly at larger length scales. In fact, there is an X-shaped arrangement of diffraction peaks observed in the SAXD pattern from byssal threads from all four species, which is typical for helical structures, as explained in section 3.8. Because of their size, however, these helixes are not directly formed by one protein (the structure is much larger than a α-helix), but probably rather made of globular protein subunits arranged into a helical superstructure, as in bacterial pili[158] and actin[195,196].

Several important characteristics of this helical structure can be directly calculated from the position of the corresponding layer lines of the diffraction pattern (see section 3.8). For instance, the layer line of the first meridional diffraction indicates the number of subunits per repeat of the helix and the number of turns/repeat corresponds to the number of layer lines between the meridional diffraction and the neighboring ones[185]. In *P. nobilis* and *A. pectinata* byssus, the first meridional diffraction on the 2nd layer line indicates that the helix has two subunits per repeat, and the neighboring diffractions on the 3rd layer line indicate that the helix possesses one turn per repeat. Thus, both *A. pectinata* and *P. nobilis* byssus possess a helical superstructure with two protein subunits per turn. The byssus fibers of *P. fucata* and *P. margaritifera* generate a similar SAXD spectrum, except that the diffraction on the 3rd layer line is extinct. However, the distance between layer lines, which indicates the length of the repeat unit, are highly similar between the byssal threads from the four species (15.7(±0.4) nm for *A. pectinata*, 15.6(±0.4) nm for *P. nobilis*, 16.0(±0.3) nm for *P. fucata* and 15.5(±0.4) for *P. margaritifera*). Differences between the diffraction patterns were investigated using the HELIX software[185]. To do so, I tuned the different parameters (number and size of subunits, number and relative position of strands) until our simulated spectrum exhibit relative intensities close to the original central diffractions of the SAXD pattern (Figure 26c,f, i and l). For the simulated patterns presented in Figure 26n and o, I used the parameters given in Table 1. However, the improvement of the spectra simulation by addition and positioning of a second strand does not necessarily mean that the protein helices really contains two strands, but rather that the shape of the protein is such that it diffracts more like a pair of spheres, rather than like a single sphere (which is the approximation for the shape of the subunit in the HELIX software). This is not unusual considering the complex shape of the globular protein subunits found in bacterial pili[159], for example.

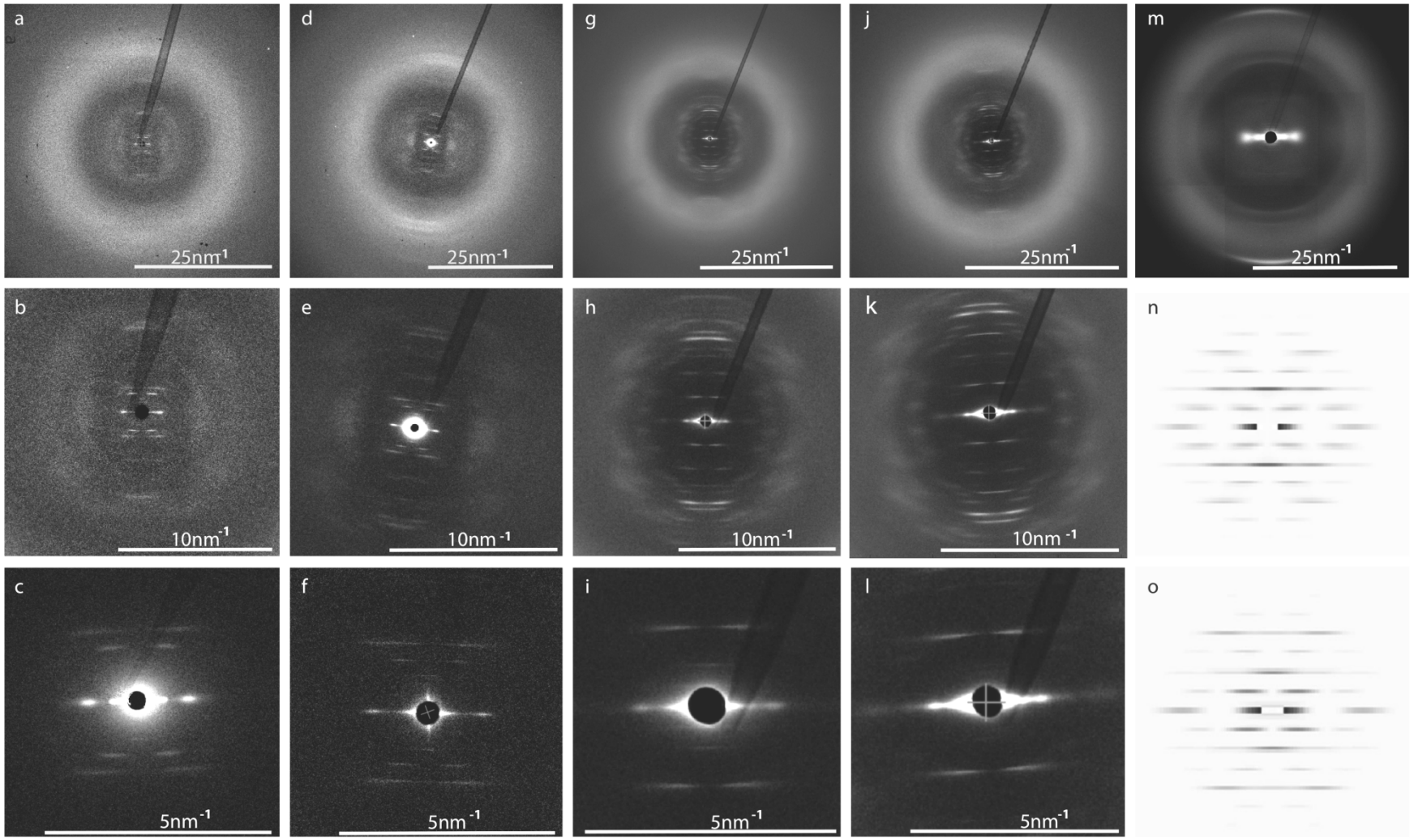

Figure 26 Comparative X-ray diffraction analysis of mussel byssal threads.

WAXD, zoomed WAXD and SAXD of byssal threads from *P. nobilis* (a – c), *A. pectinata* (d – f) and *P. fucata* (g – i) and *P. margaritifera* (j –l). (m) WAXD of *M. edulis* byssus. (n and o) Simulation of Pinnidae (h) and *Pinctada* (l) byssus diffraction pattern. Modified from[191] to include *P. margaritifera* byssus. Published by The Royal Society of Chemistry.

Table 2 Simulated helix parameters

Parameters used for the simulation of SAXD diffraction patterns of Pinnidae and *Pinctada spp.* byssus.

	Pinnidae	***Pinctada spp.***
Number of subunits levels	12	16
Axial separation of subunits [nm]	7.8	8.1
Number of strands	2	2
Azimuthal shift of second strand [°]	99	90
Axial shift of 2nd strand [nm]	1.8	2.1
Rotation angle between subunits [°]	180	180
Monomer center radial position [nm]	3	3
Subunit size (radius) [nm]	1.5	1.6

5.2.3 Organization of protein fibrils into macro-fibers (TEM)

To gain further support for the hypothesis that threads of *P. nobilis*, *A. pectinate*, *P. fucata* and *P. margaritifera* are comprised of globular proteins arranged helically into fibers, TEM was used to study the nanoscale ultrastructure of the fibers. In order to gain enough contrast, a small defocus was used, leading to a shift in the contrast transfer function allowing the wavelength corresponding to this structure size to be present in the image[197]. This enabled the observation of a clear fibrillar structure in longitudinal cross-sections of *A. fucata* and *P. nobilis,* as well as *P. fucata* and *P. margaritifera* (Figure 27a, d, g and m), which is also present on transversal cuts as small dense light circles with a dark-staining core (Figure 27b, e, h and n). This is also consistent with previous TEM[150] and SEM images of *P.nobilis* byssus[120,150]. The sizes of the structures I observed are consistent with the helix sizes predicted from our analysis of the WAXD/SAXD data. In all four species, the helical nanofibrils appear to be embedded in a matrix material, which appears unstructured; however, they are arranged differently in each thread type. In *P. nobilis*, the helical nanofibrils are dispersed in the matrix, whereas in *A. pectinata* and *P. fucata* and *P. margaritifera*, nanofibrils are grouped into bundles of different sizes. In *A. pectinata* byssus, these fibrils are closely packed, while in *P. nobilis*, *P. margaritifera* and *P. fucata* byssus, the packing is looser. A Fast Fourier Transform (FFT) of the TEM image allows a better characterization of the packing, and shows that locally, the fibrils in byssus of all three species present a well ordered hexagonal packing (Figure 27d, h, l), with a distance between fibrils of 10.6(±0.4) nm in *P. nobilis* fibers, 8.1(±0.7) nm in *A. pectinata* fibers, 10.4(±0.6) nm in *P. fucata* and 10.6(±0.7) nm in *P. margaritifera* fibers (calculated from the FFT). On larger length scales, however, the organisation was lost (Figure 27c, g, k and m).

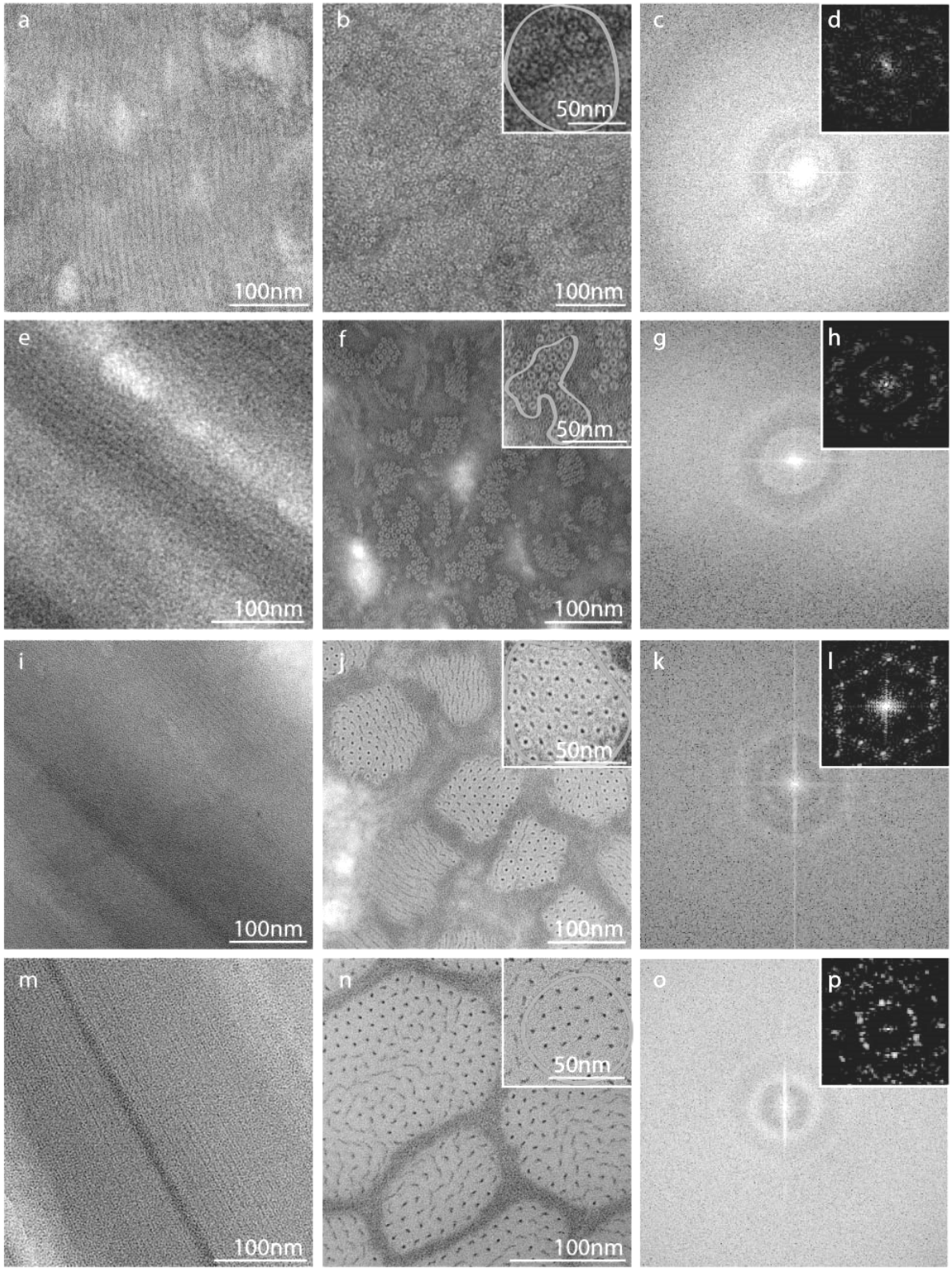

Figure 27 Comparative TEM investigation of different byssal threads.

TEM of longitudinal and transversal cut, Fast Fourier transform (FFT) of the transversal cut of *P. nobilis* (a, b, c and d), *A. pectinata* (d, e and f), *P. fucata* (g, h and i) and *P. margaritifera* (m, n and o) byssal threads. The inserts d, h, I and p show FFT analysis of small selections (in red on the insert in b, f and j) of the TEM image of transversal cuts of *P. nobilis, A. pectinata, P. fucata* and *P. margaritifera* threads. Modified from[191] to include *P. margaritifera* byssus. Published by The Royal Society of Chemistry.

5.3 Discussion[c]

Our investigation reveals that mussel byssal threads of the four species chosen from the order Ostreida possess a similar composition and ultrastructure to one another, which is entirely different from threads of Mytiloida mussels (Figure 28). Ostreida mussel byssus appears to be comprised of distinct nanofibrils assembled from globular protein subunits organized into a helical structure (Figure 28a). As already suggested in the literature[120,131,141,152], our compositional analysis indicates that Ostreida byssus fibers are not likely to be comprised of collagenous proteins. This conjecture was confirmed convincingly via analysis of WAXD and SAXD diffraction patterns from the threads of all four Ostreida species. WAXD patterns showed absolutely no evidence for the presence of triple helical collagen structure or any other periodic secondary structure, while SAXD patterns clearly indicate the presence of helical fibers, supported by TEM imaging.

This peculiar way of building fibers is shared between the four species investigated, with slight differences. There seems to be more similarities between the byssus ultrastructure of both the *Pinctada* species, which belong to the same family, than between the byssus of *P. nobilis* and *A. pectinata*, which only belong to the same superfamily, There are however closer similarities between *A. pectinata* and *P. nobilis* byssus than between them and *Pinctada spp.* byssus, which are less closely related, as clearly showed by the XRD patterns. Indeed, *A. pectinata* and *P. nobilis* byssal threads exhibit a similar biochemical composition, have the same size building blocks (as determined by SAXD analysis), and present very similar TEM images. The major difference between the two based on these data is the grouping of nanofibrils into bundles in the byssus of *A. pectinata*, while the nanofibers are more dispersed in *P. nobilis* byssus. Similarly, both *Pinctada* species presented a similar diffraction pattern, and thus, building block size, but their grouping into bundles was slightly different as observed in TEM. This results in a difference in the fibril/matrix ratio that may be responsible for the slight differences in amino acid composition between all the species since the matrix is likely to be made by different protein(s) than the fibrils, as is the case in *Mytilus spp.* byssus[198]. Simulation suggested that the distances between subunits of the protein helix of *Pinctada spp* byssus might be slightly larger than those in Pinnidae byssus, which likely indicates that the protein subunits are slightly bigger.

In any case, these findings strongly suggest that the species from the Pinnidae possess a very similar protein subunit for building the helical nanofibrils based on the fact that they are much closer on the evolutionary tree, whereas, although *Pinctada. spp.* byssus has retained the same general helical structure, the protein subunit is appreciably different from that of the Pinnidae.

[c] The result and discussion of this chapter have been reproduced from[191] and modified to include *P. margaritifera* byssus. Published by The Royal Society of Chemistry.

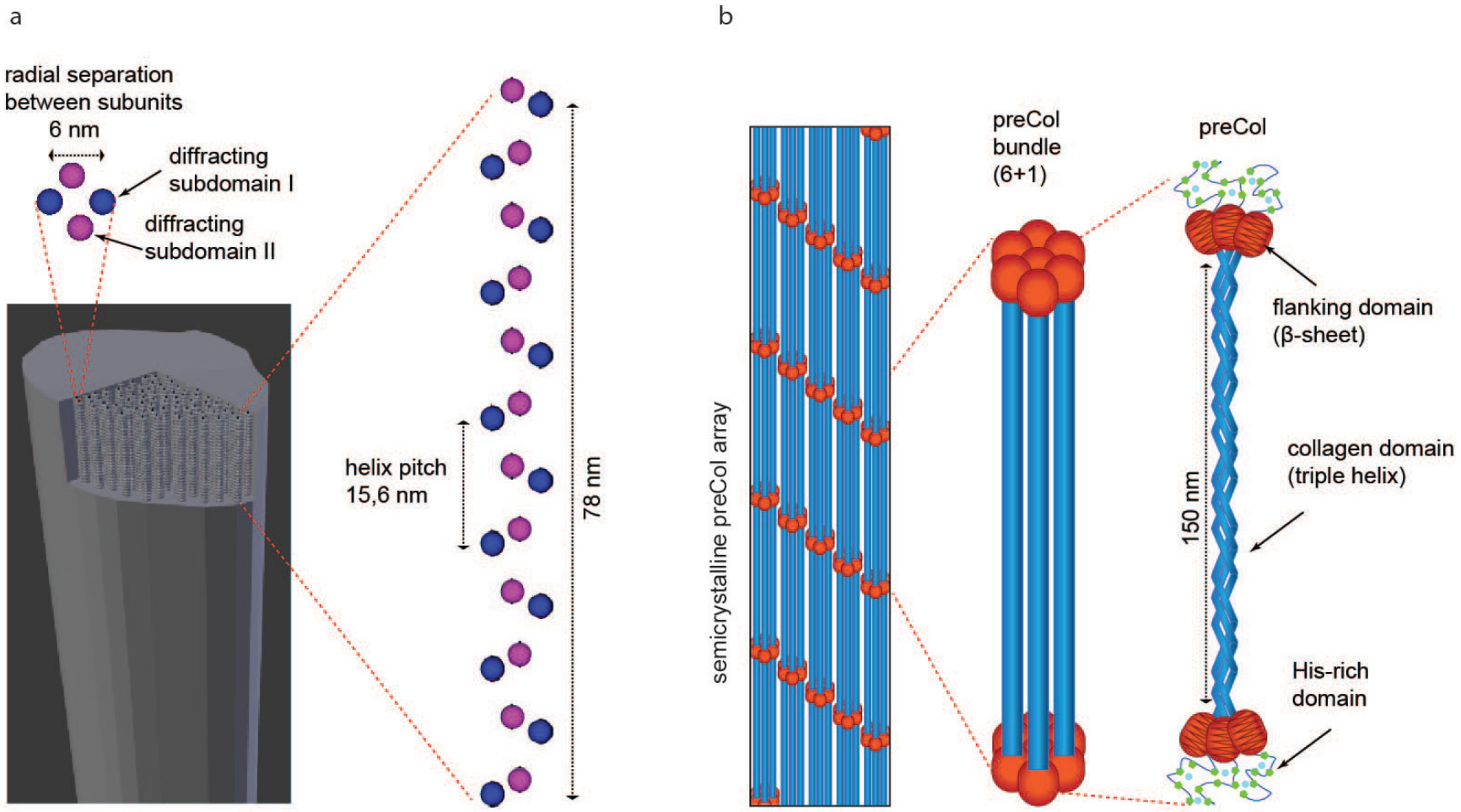

Figure 28 Proposed arrangement of the structural proteins in *P. nobilis* byssus.

(a) Minimal model of Ostreida byssus superhelix indicating diffraction centers based on SAXD measurements and simulations. Subdomains I and II are likely to belong to the same protein. (b) Current model of protein arrangement in *Mytillus spp* byssus. Reproduced from[191], **Published by The Royal Society of Chemistry.**

Investigations are underway to determine the sequence of these proteins; however, it has already been reported that byssal threads from *Pinctada spp.* may contain a thrombospondin-like protein[156], which is consistent with our model of globular protein building blocks. Thus, it stands to reason that the Pinnidae byssus building blocks may be similar. However, this must be further examined.

In spite of the differences between *Pinctada spp.* and Pinnidae mussel byssus, they are much more similar to one another than to Mytilid byssus. Indeed, Pinnidae and Pteriidae both belong to the same order (Ostreida), while *Mytilus spp.* belongs to a different order (Mytiloida) (Figure 24). The existence of morphological variations within different orders of the same cohort is confirmed by *Anomia* – like Pinnidae and *Pinctada*, *Anomia* belongs to the Pteriomorphia, but it possesses a mineralized byssus that is completely different, since it is 90 % calcified. These findings would argue, as for silk[94] for a convergent evolution of bivalve byssus fibers.

However, these differences in nanostructures might actually also be linked to the living environment of the mussel as previously suggested[120]: Ostreida prefers calm water and might not need the special chemical/structural features that allow *Mytilus spp.* mussels to survive in harsh environment with crashing waves. Even within *Mytilus spp.*, some species (e.g. *Mytilus californianus*) have apparently evolved to survive in higher wave impact zones than other related species (e.g. *Mytilus edulis* and *Mytilus galloprovincialis*)[140]. On the other hand, byssus macrostructure (number, thickness and length of threads) seems to be influenced by the mode of anchoring. For example, *Mytilus spp.* and *Pinctada spp.* are anchored on hard surfaces (rocks, coral), and therefore, they use a small amount of thick and short threads, whereas *A. pectinata* and *P. nobilis* evolved a different anchoring strategy as their byssus is buried in muddy or sandy sediments[120]. This may explain why they have an exceptionally high amount of long and thin threads (up to 30 000), whose attachment relies more on entanglement rather than adhesion.

Thus, as with the sheer diversity of different spider silks adapted to different physical requirements[100], many different forms of byssus have appeared throughout evolution. It seems likely that their properties may reflect both the systematic position within the class Bivalvia due to a possible converging evolution and the pressures of the ecological niche in which they live. This conclusion based on the micro-and nano-structure of byssus threads from related species seems to confirm a similar hypothesis suggested by Marcotte and co-workers based on compositional and mechanical analysis[120].

It is additionally notable, that similar to *Mytilus spp.* byssus, byssal threads of Ostreida mussels contain an elevated content of inorganic ions, especially calcium, iron, copper and zinc, although seasonal and regional dependence of inorganic content in byssus threads[199,200] prohibit detailed or quantitative comparison between species and with other studies. While it is well established that transition metal ions, such as Fe^{3+} and Zn^{2+} play a critical role in determining the tough and self-healing behavior of *Mytilus spp.* byssal threads

by forming metal coordination bonds with specific amino acid ligand in the byssus proteins (e.g. Histidine and DOPA)[201], the potential role of ions in the assembly and performance of Pinnidae byssus is not yet clear. Due to the very low DOPA content and the high content in charged amino acids, it was previously hypothesized that assembly and mechanics of *P. nobilis* byssus may rely on electrostatic interactions. However, it was recently reported for *P. fucata* that Ca^{2+} may induce thread assembly and that metal removal reduced mechanical performance of threads[157]; thus, it seems feasible that they may play a similar role in *Pinnidae* byssus given their structural and compositional similarity to *Pinctada spp.* threads. While the potential role of calcium ions remains to be established in Pinnidae threads, Fe-DOPA crosslinks have been reported to play a key role at the interface between *A. pectinata* byssus threads and soft tissue[154].

Perhaps the most perplexing finding of this study is the peculiar fibrillar superstructure in the Ostreida mussel byssus, which is built up from globular proteins arranged in a very well-defined helix (Figure 28a). Helical structures *per se* are not unusual in extraorganismic protein fibers. For example, fibrillar collagen is comprised of right-handed triple helices of three protein chains with left handed poly-proline II helical conformation[202], while coiled coil alpha helices are dominant in the intermediate filaments which comprise materials such as wool[203], gastropod egg cases[161] and even hagfish slime[204,205]. In fact, the byssal threads of the giant clam *Tridacna maxima* were discovered to consist of proteins arranged in a four stranded alpha helical coiled coil[122]. However, the discovery of a supramolecular helix of globular proteins that was deduced here from the SAXD patterns from the Ostreida mussel byssal threads is, as far as I know, unprecedented in an externally secreted macroscopic biological fiber. The only analogous structures fabricated extracellularly are single nanofibrils produced by bacteria known as pili. In some cases, bacterial pili can be used as an anchor to resist flow, as in the case of *E. coli* living in the urethra during urinary infections. In this case, the helical structure of the bacterial pili handles load from fluid flow by extending like a spring[206,207].

5.4 Conclusion

Through an in-depth comparative investigation of composition and ultrastructure, I have determined that byssal threads from Ostreida mussels including *P. nobilis*, *A. pectinata*, *P. fucata* and *P. margaritifera*, exhibit a peculiar protein superstructure in which globular proteins are organized into a helical building block. Globular protein helices were not previously observed as a structural motif in macroscopic biological fibers and are extremely different from the collagen-based structure of *Mytilus spp.* byssal threads. This finding suggests a convergent evolution of byssus design, with some divergent features such as macro-morphology to adapt specificity of the species environmental niche, such as the living substrate or the turbulence of the water.

6 Role of helical hierarchical structure in the mechanical behavior of self-healing byssus fibers of *Pinna nobilis*

6.1 Introduction

Mytilus byssus thread's ability to dissipate up to 70 % of mechanical energy and their capacity to self-heal following pseudoplastic mechanical damage[34,128,129,136,140,208] are of primary importance for their survival in the wave-beaten seashores. In contrast, subtidal bivalves such as the fan shell *Pinna nobilis* are not exposed to high energy crashing waves. As discovered in chapter 5, this might be related to their byssus structure, completely different from *Mytilus spp*. Collagenous threads[131,191], and one could accordingly think that their byssus plays a less important role. However, not only is *P. nobilis* a prey for cephalopods (e.g. octopus) who try to dislodge them[147], but they are such large mussels (up to 1 m or more in length) that the drag forces acting on them from subtidal currents can reach more than 45 N[148]. Therefore, the byssus also plays a crucial role in *P. nobilis* survival functioning as an anchoring system, as is also the case for *Mytilus* mussels.

Based on XRD studies, it was deduced in chapter 5 that *P. nobilis* byssus is comprised of globular protein superhelices, resembling bacterial Pili, embedded in an amorphous matrix[191]. Recent mechanical studies compared the tensile properties of *P. nobilis* byssus to other mussel species, including *Mytilus* ones[120], and showed that while the stress-strain curve appears superficially similar to *Mytilus* threads in their general shape, *P. nobilis* threads exhibited lower extensibility, strength and yield strain than *Mytilus*, which the authors attributed to observed differences in the fibers composition. However, these mechanical analyses did not include cyclic loading studies or investigation of self-healing capacity, which are key features in the byssus of *Mytilus* species. And of course, no link could be made so far between these mechanical observations and the newly discovered microstructure of *P. nobilis* byssus.

By comparison with other similar helical structures such as bacterial Pili, the peculiar structure of *P. nobilis* byssus suggests interesting structure-function relationships. As mentioned in chapter 5, bacterial Pili and mussel byssus have a similar function at different scales, suggesting that the helical structure of the nanofibrils within *P. nobilis* byssal threads might perform in a similar manner in its role as a sedimentary anchor, but on a macroscopic scale. In support of this hypothesis, single molecule force spectroscopy measurement of single bacterial pili with atomic force microscopy (AFM) exhibit an initial stiff region followed by a long yield plateau and finally a post-yield stiffening region[209], which is reminiscent of previously published tensile stress-strain curves of *P. nobilis* byssus fibers[120]. In single bacterial pili, the yield plateau was attributed to the unravelling of the higher order helix comprised of many globular subunits, while the post-yield stiffening was surmised to elongation of the unfolded helix[209]. At the macroscopic scale, the yield plateau observed in mechanical tests of *P. nobilis* threads could represent the successive unravelling of many

helical nanofibrils or from sliding of subunits in the matrix for example. Unfolding and elongation of alpha helical coiled coils results in a similar macroscopic stress-strain curve in materials such as wool[172], hagfish slime[204] and whelk egg capsules[161] adding further support to this putative structure-function model, and offering an interesting hypothesis for the start of the structure-function relationships in the byssus of *P. nobilis*.

Because *P. nobilis* byssus has an entirely different hierarchical structure, the in-depth elucidation of its mechanical behavior and the understanding of the relationship between mechanics and structure could not only lead to a novel concept of underwater attachment, but could also allow extraction of key design features, which could be common to both mussels. In order to develop an understanding of the structure-function relationship in *P. nobilis* byssus, I performed an in-depth structure-function investigation of *P. nobilis* byssus tensile behavior, including fatigue and self-healing properties. Moreover, these findings were interpreted in light of synchrotron X-ray diffraction studies combined with *in-situ* tensile testing, which has been successful with *Mytilus spp.* byssal threads[34,129,138].

6.2 Results

6.2.1 Pull-to break tensile testing

Simple pull-to-break tensile tests were used as a first way to characterize *P. nobilis* mechanical properties (Figure 29a). Interestingly, in contrary to previous observations[120,132], I observed two yield points, as in the byssus of *Atrina rigida* (*A. rigida*) (Pinnidae) and *Modiulus modiulus* (Mytilidae)[124]. As shown in Figure 29, the tensile curve of *P. nobilis* exhibits an initial linear stiff region, with a Young Modulus of 566(±118) MPa followed by a first yield point at 2.7(±0.4) % strain and 15(±4) MPa stress, leading to a much softer post-yield plateau (slope 66 (±5) MPa). This plateau is followed by a post-yield stiffening (slope: 257(±28) MPa), which is followed by a second yield point, at 30 (±4) % strain and 49 (±6) MPa stress. Most of the samples break during the post-yield plateau following the second yield point at 34 (±7) % elongation and 54 (±6) MPa breaking stress. All these characteristic values are summarized in Table 3. The spread in curves showed in Figure 29a and reflected by the standard deviations given in Table 3 originates partially from the difficulty to accurately measure the cross-section of the individual byssus fibers. Normalization by the Young's modulus (Figure 29b) provides a means of correcting this uncertainty and reveals that all the fibers exhibit an extremely similar behavior. The shape of this simple tensile curve already shows differences to those of *Mytilus* byssus, which is often taken as reference in byssus studies, since it is the best understood and characterized byssus system[32,34,127–129,187]. The tensile curve of *Mytilus* byssus only exhibits a single yield point; however, under the same loading conditions, it has a comparable stiffness in the initial region (Young modulus ~500 MPa for *M. californianus*[129]) but presents a higher yield stress and strain and breaks at higher strength and elongation[32,127]. One interesting feature of *Mytilus* byssus is its ability to dissipate energy during cyclic loading[127], which helps the animal to survive strong

forces from crashing waves. The mechanical hysteresis can be measured from cyclic tests (pulling and relaxing) as shown in Figure 29c, as the area within the loading and unloading curves, divided by the total energy under the pulling curve. During cyclic loading of *P. nobilis* threads, 66(±3) % of the energy is dissipated for a cycle at 36(±4) % strain. This is comparable to the energy dissipated by the distal region of *Mytilus* byssal threads (66 % for *M. californianus* byssus distal part cycled at 35 %[127]).

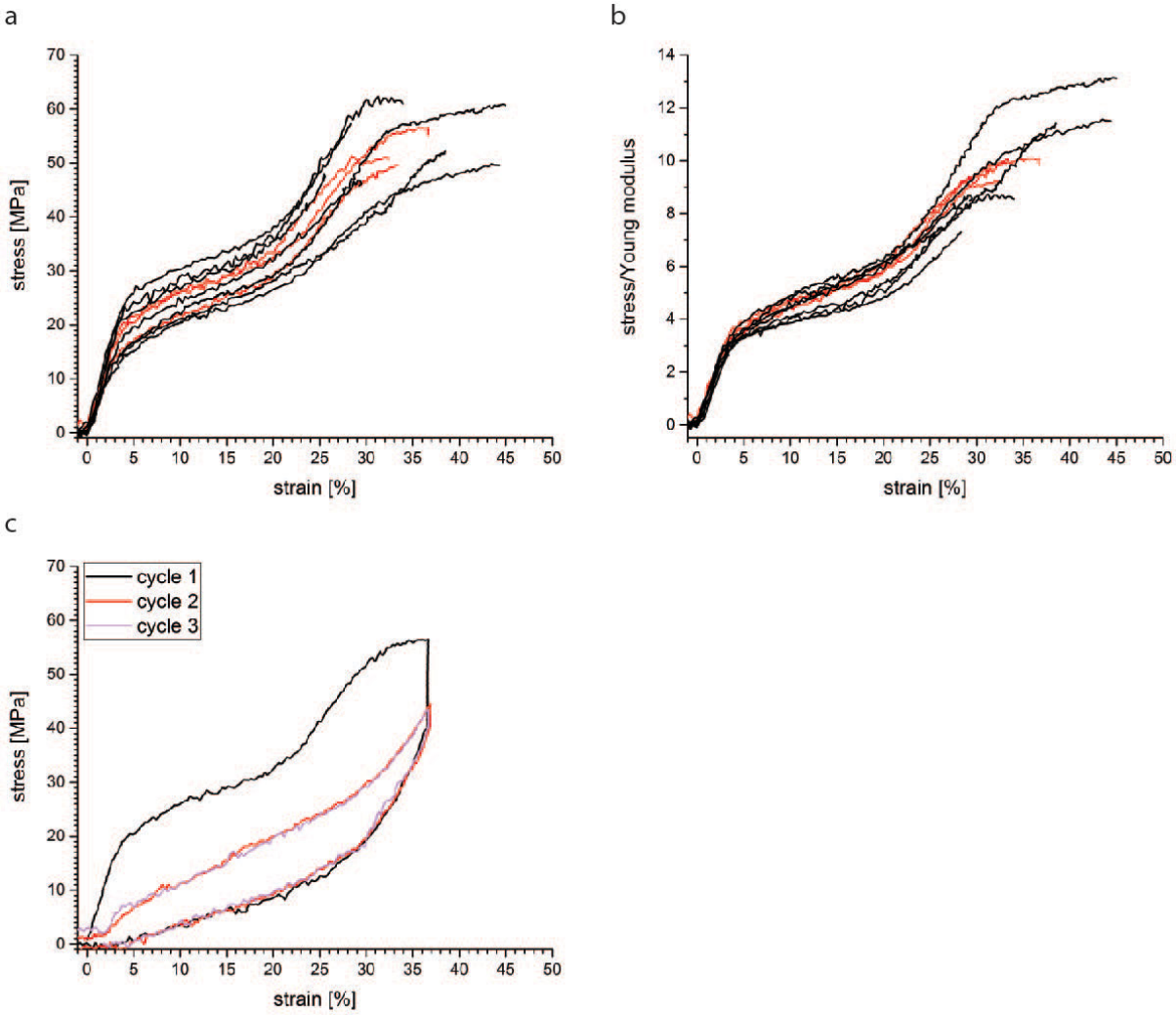

Figure 29 Stress-strain curve of single *P. nobilis* fibers

(a)Black curves were pulled to break whereas red ones were manually stopped and are therefore not included in the calculation of mean strain and force at break. Typical pull to break curves exhibit two stiff regions, two yield points, and two plateau. The spread in the curves is at most likely due to the difficulty of measuring the right cross section area of the single fibers. (b) The normalization of the stress by the Young Modulus allows a reduction of the data spread. (c) A typical cyclic curve for a sample pulled to about 35% strain and unloaded back to 0% strain (black), directly followed by a second cycle at the same strain.

If a thread is cyclically loaded, twice (or more) following a cycle past the second yield point (Figure 29c), the mechanical properties of subsequent loading cycles are significantly reduced. This behavior, which is reminiscent of the behavior of *Mytilus* threads[127], is indicative of molecular level damage in the protein network that is not recovered on short timescales. Specifically, there is a complete loss of yield behavior and the initial stiffness is reduced to 35(±12) % of its initial value.

Table 3 Characteristic values of *P. nobilis* byssus fiber tensile curve (10 samples tested)

	native Villefranche
Young Modulus (MPa)	566(±118)
Yield strain (%)	2.7(±0.4)
Yield stress (MPa)	15 (±4)
Plateau slope (MPa)	66(±5)
2nd stiff Modulus(MPa)	257(±28)
2nd Yield strain (%)	30(±4)
2nd Yield stress (MPa)	49(±6)
Maximal strain (%)	34 (±7)
Maximal stress (MPa)	54(±6)
Toughness (MJ/m^3)	11 (±3)

6.2.2 Cyclic testing

In order to further investigate the deformation and damage behavior of *P. nobilis* threads, I performed a fatigue test (Figure 30a) in which the maximal strain was increased by about 3 % at each loading cycle. Each cycle exhibits a decrease in initial stiffness; however, the envelope of this fatigue test, formed by the maximal strain and stress of all the cycles remains similar to the simple tensile curve showed in Figure 29a. As the strain is increased, the stress shows an exponential-like increase in response to strain. This happens earlier for the discharge curves (from about 20 % max strain) and in a more visible way (Figure 30a) than for the pulling curves. Figure 30b shows the normalized initial stiffness of each cycle versus the maximal strain of the corresponding cycle. This figure shows that there is a linear decrease in initial stiffness resulting from the gradual increase of strain until the cycle at 37 % max strain, after what the decrease slows down and the initial slope seems to stabilize between 10 to 30 % of the initial stiffness. Figure 30c shows the normalized initial unloading slope, which is the tangent to the unloading curve directly after the instant recovery[d].

[d] the instant drop of force showing at a small vertical part at the very beginning of the unloading curve

This graph shows a decrease in initial unloading stiffness to a minimum at about 20 % strain, which is the end of the plateau of the single traction curve. After this, the initial unloading stiffness exhibits a second increase. There might be a second local minimum around 32 %. Finally, Figure 30d shows the energy dissipated by each cycle in %. There does not seem to have any trend below 10 % maximal strain, but the dissipated energy seems to remain constant after this, with a possible maximum about 27-32 % maximal strain.

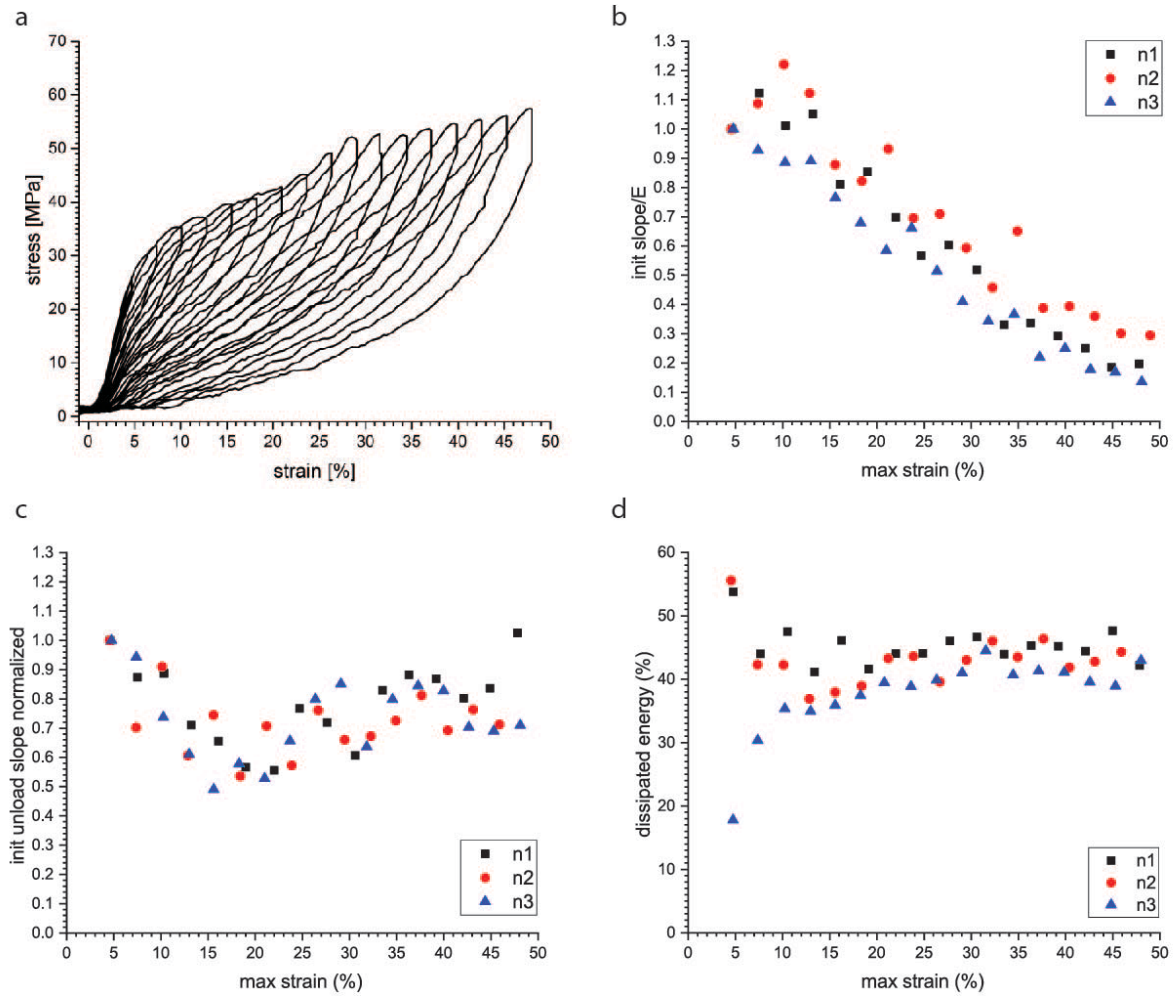

Figure 30 Fatigue tensile testing of *P. nobilis* byssus threads

(a) Typical fatigue test curve, with successive cycles with an increase of 3% of the maximal strain at each cycle. Despite the decrease in loading and unloading mechanical properties, the envelope drawn by the maximal strain-stress points is similar to a pulled to break curve. (b) The initial slope of the loading curve of each successive cycle of a fatigue test as shown in Figure 30a was divided by the Young Modulus of the first cycle and plotted versus the maximal strain of the considered cycle, for three different fibers. (c) The initial slope of the unload curve of each successive cycle of a fatigue test as shown in Figure 30a was divided by the unload slope of the first cycle and plotted versus the maximal strain of the considered cycle, for three different fibers. (d) The dissipated energy of each successive cycle of a fatigue test as shown in Figure 30a was plotted versus the maximal strain of the considered cycle, for three different fibers. The dissipated energy is equal to the area between the loading and unloading curves normalized to the area under the loading curve.

6.2.3 Self-healing

The ability to (partially) recover the plastic deformation inflicted by high deformations is one of the most interesting characteristics of *Mytilus* byssus. Therefore, I performed multi cyclic testing, with the 1st and 2nd cycle measured directly one after the other, and the 3rd cycle done after a 20 to 22 h resting period. Figure 31a represents a typical recovery experiment. It can be observed that the first cycle exhibits the two yield points observed in Figure 29, whereas the following cycle does not show any yield point. After the resting period, the first yield point came back, albeit lower, but the second yield point is still missing. Furthermore, I measured the dissipated energy for the three cycles of three different fibers (Figure 31b), which all show a clear recovery. Indeed, the average dissipated energy was 66(±3) % during the first cycle, 40(±5) % during the second cycle and 52(±6) % after recovery, during the third cycle. A decrease in initial stiffness could also be observed during the second cycle to 192(±67) MPa, which is 35(±12) % of its initial value. However, it recovered to 449(±128) MPa, or 83(±26) % of its initial value.

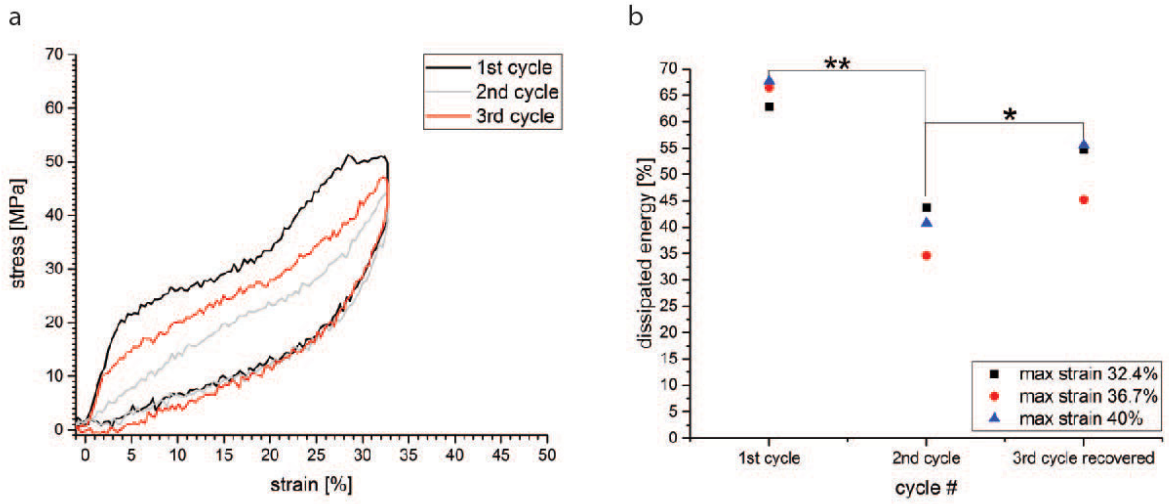

Figure 31 Recovery experiment on *P. nobilis* byssus fibers

(a) Recovery experiment, the 1st and second cycles were conducted directly one after the other, then an overnight rest was observed before conducting the 3rd cycle. (b) the dissipated area was plotted for each cycle, showing the decrease of mechanical properties associated to the second cycle, and their recovery after the overnight rest. One way ANOVA: ∗=p<0.05 ∗∗ =p<0.01. Tests effectuated on 3 fibers.

6.2.4 XRD with *in-situ* tensile testing

In order to understand the deformation mechanism of *P. nobilis* byssus at a molecular level, I used XRD coupled with *in-situ* mechanical testing. XRD was previously used to elucidate the hierarchical protein structure of *P. nobilis* byssus fibers, which are comprised of globular protein helices (chapter 5)[191]. The measurement of the position of the diffraction peaks characteristic for the helical structure during *in situ* mechanical testing will allow the following of the deformation of the fiber at the level of the helical building blocks. Figure 32a shows the SAXD pattern of *P. nobilis* byssus, which contains the information about the helical structure[191]. A line integration was made as shown by the red box on Figure 32a,

comprising the opposite peaks corresponding to the 3rd order diffraction of the helix. Those were chosen because they were the most distinct peaks. Line integration was performed for all the diffraction patterns taken during the tensile test, and plotted on Figure 32b. It can be directly observed that the diffraction peaks moved to smaller q values when macroscopic strain increased, but they also seem to get less defined until they completely disappear around 5-6 % macroscopic strain. After this, the samples were relaxed, and recovery of the peak could be observed (Figure 32b). From the peak position, it was possible to calculate the helix size at each strain, and therefore the strain of the helix at each macroscopic strain. The helix strain versus macroscopic strain of the fiber is plotted in Figure 32c. The helix strains are unexpectedly much larger than the macroscopic strain: e.g. for a macroscopic strain of 4 %, the helix strain can reach 14 %. The increase in helix strain was linearly fitted and had an average slope of 3.3(±0.1) %.

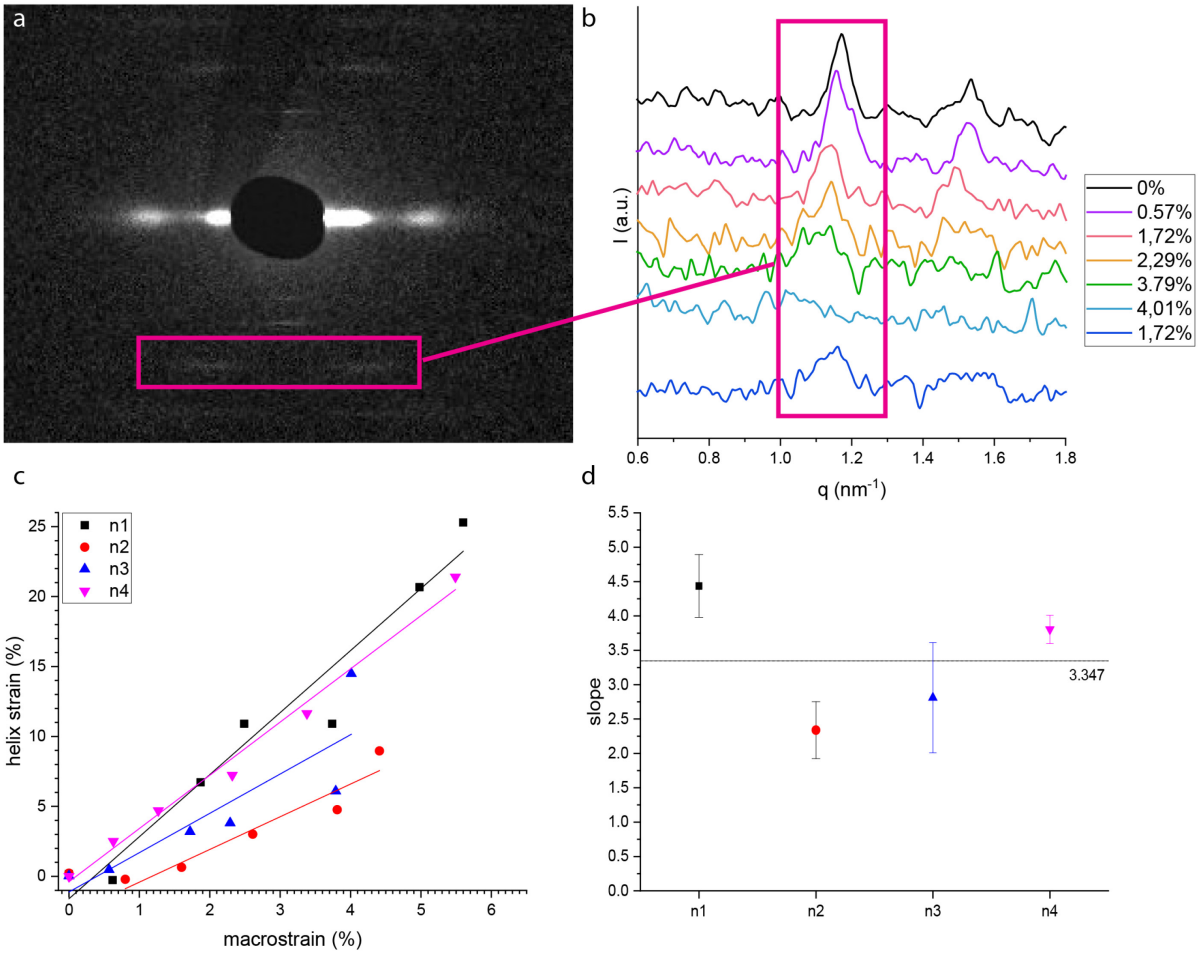

Figure 32 SAXD with *in-situ* tensile testing of *P. nobilis* byssus fiber

(a) Diffraction pattern of *P. nobilis* byssus fiber. The red rectangle shows the area integrated in order to measure the position of the 3rd order diffraction peak, (b) Intensity(I) versus position (q) resulting of the line integration around the 3rd and 4th order diffraction for successive strain during the in situ tensile testing experiment. (c) Helix strain was calculated from the position of the 3rd order diffraction at each macrostrain, for four samples, and the helix strain was plotted versus the macrostrain. Each sample set of acquired points was fitted with a straight line (the first point of Pinna 4 was omitted since the helix did not start stretching before 0.5 % fiber strain). (d) The slope of the linear fit and its standard error are plotted for each sample, and the horizontal line at a slope of 3.3 represents the average. Tests effectuated on 4 fibers.

Although it was not previously analyzed in depth, *P. nobilis* byssus also exhibits a signal in the WAXD region (q between 15 and 21 nm^{-1})[191]. Therefore, I performed additional *in-situ* tensile tests while measuring the WAXD signal. Here, a radial integration was performed in the meridional part of the WAXD ring, and in the equatorial one. The integration areas are showed by the two red selections on Figure 33a. The meridional integration curves for the different macroscopic strains are displayed on Figure 33b, and the equatorial integration curves are showed on Figure 33c. Some poorly defined peaks can be seen on top of the amorphous background (at q≅16 nm^{-1} and 18 nm^{-1}), which completely disappeared when the macroscopic strain reaches 25 %. Additionally, there is a peak around 12 nm^{-1}, which did not completely disappear, even when the macroscopic strain reached 35 %. In contrary, in the equatorial direction, no clear peak is visible, only the left side of the curve seems to flatten until the macrostrain reaches 5 %. Interestingly, the curve observed at 35 % strain is very similar in both directions (meridional and equatorial), probably corresponding to the amorphous background which can be observed under the weak peaks at lower strains.

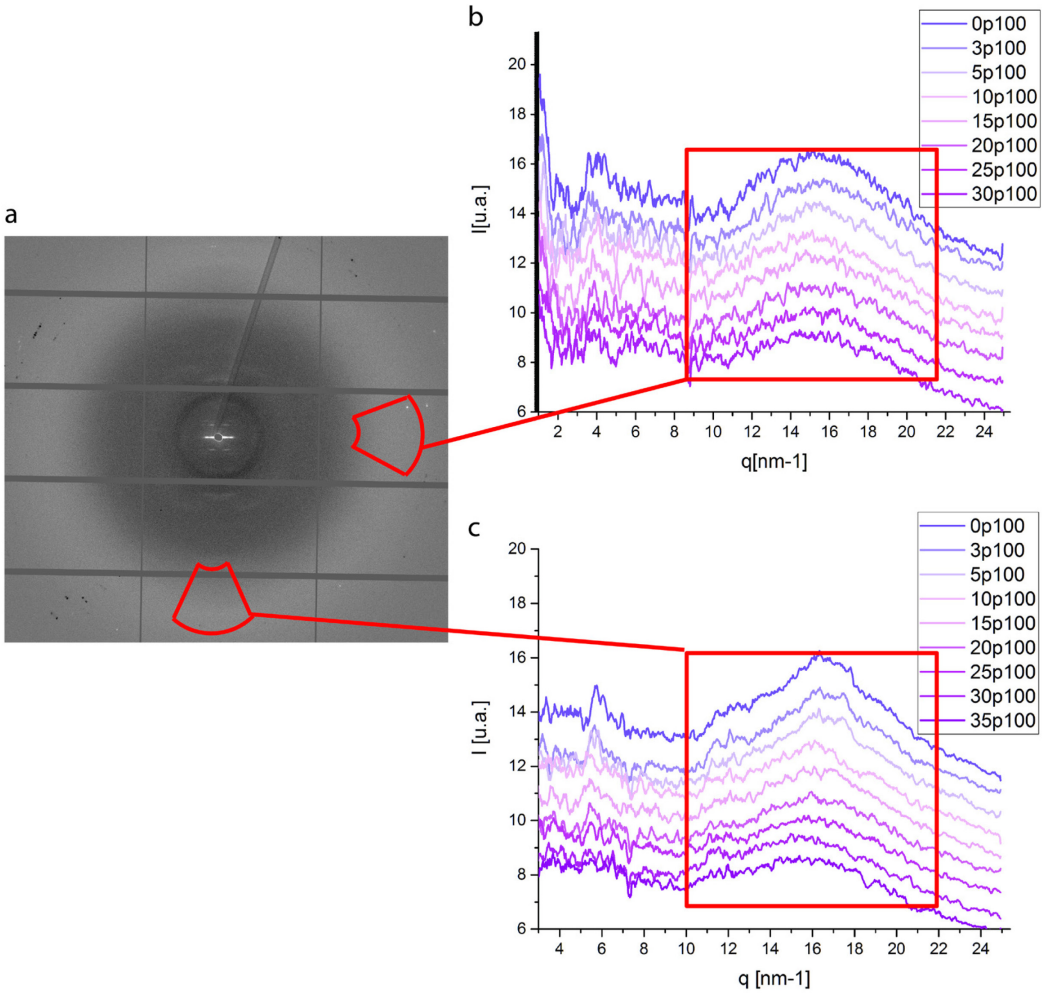

Figure 33 WAXD with *in-situ* tensile testing of *P. nobilis* byssus fiber

(a) WAXD diffraction pattern of a single *P-nobilis* byssus thread, with the equatorial and the meridional integration area shown by red boxes. (b) Integration of the amorphous ring in the meridional direction for the several strains does not show distinct peaks on top of the amorphous background. (c) equatorial integration of the pseudo amorphous ring in the WAXD area, for several strains during the tensile testing. Test effectuated on 3 fibers.

6.3 Discussion

Despite their different building blocks, the Young's modulus of *P. nobilis* byssus is comparable to the byssus of *Mytilus* species. However, in contrast to *Mytilus* threads and contrary to what was measured previously[120], the stress-strain curve of *P. nobilis* byssus fibers exhibits two yield points. Thus, the stress-strain curve can be divided in three parts: 1) the initial stiff region 2) the first yield point, plateau and the second stiff region and 3) the second yield point and plateau, for the following discussion of possible structure-function relationships.

6.3.1 Initial stiffness

XRD showed that the helical organization of the globular proteins previously observed[191] deform during the initial stiff part of the stress-strain curve of *P. nobilis* byssus up to about 5 % after which the diffraction peaks become unmeasurable. Interestingly, the strain of the helix measured on the diffraction pattern is on average 3.6(±0.4) fold higher than the strain of the whole fiber (Figure 32d). The diffraction pattern shows that the helices are highly aligned along the fiber axis; therefore, in order to compensate for the large helix strain, it seems plausible that there is a stiffer element in series with the helices, which has not been detected thus far. If this stiff element is in series with the helices, their length needs to make up about 72 % of the fibers length whereas the helices would make up only 28 % of it, assuming that the stiff part does not deform at all. This seems a plausible hypothesis for a first approximation of the ratio between the soft helices and the possible stiff domains in *P. nobilis* byssus considering the 2 % maximal deformation of the collagen domains forming the stiff part of Mytilus spp byssus[34]. However, this is the lower limit of the amount of stiff domain. In the case where the stiff domain would significantly deform, then the ration of stiff domain to helices should be even higher than the estimated 72 %. Cyclic testing showed that the deformation below the yield point is elastic, which was confirmed during SAXD experiment: the peak associated with the helical structure came back to its original position after relaxation (Figure 32b).

6.3.2 First yield point, first plateau and second stiff region

A plateau can have different possible origins: unfolding of the helix, such as in bacterial pili, or breaking of sacrificial bonds such as in Mytilus byssus. The signal originating from the helices disappear by 5 % fiber strain, which corresponds to the end of the yield region (Figure 29), meaning that the helices are probably completely stretched when the whole fiber reaches the end of the yield region. Therefore the pseudo-plateau deformation occurring from 5 % to about 25 % strain must be caused by another mechanism, in contrast to my initial hypothesis (section 6.1) based on the similarity in structure between *P. nobilis* helical building block and bacterial Pili. Upon further contemplation, it seems plausible that a similar structure behaves differently when free and alone, like bacterial Pili, than when embedded and constrained in a matrix within a bulk material, as in *P. nobilis* byssus.

The yield region around the yield point is probably caused by both mechanisms. As an additional argument against helix unfolding being responsible for the plateau, a simple calculation shows that the maximal strain of *P. nobilis* byssus helices if completely unfolded is 58 %. Indeed, the maximal length of a helix when unfolded is its contour length, which can be easily calculated using the construction on Figure 34. The helix can be considered on the surface of a cylinder with the same radius as the helix (3 nm in this case[191]), and of length equal to the pitch of the helix (15.6 nm for *P. nobilis* building block). If the cylinder is virtually cut vertically and unfolded so that it becomes a rectangle, the helix also gets unfolded and lays on the diagonal of this rectangle of sides with length 2π times the helix radius and helix length. Then, the Pythagorean Theorem is used to calculate the length of the diagonal which is the maximal stretched length of the helix. The difference between the stretched helix and the helix pitch normalized by the latter gives the maximal theoretical strain due to helix unfolding, which is about 58 %. Considering the fact that helix strain is 3.6 times larger than fiber strain, the helix would be completely unfolded by 16 % fiber strain, which is before the end of the plateau. Moreover, this value is likely smaller due to the geometrical constraint of protein chains, further supporting the idea that the plateau observed in the stress-strain curve is associated to another mechanism, the helices being completely unfolded by the end of the yield region.

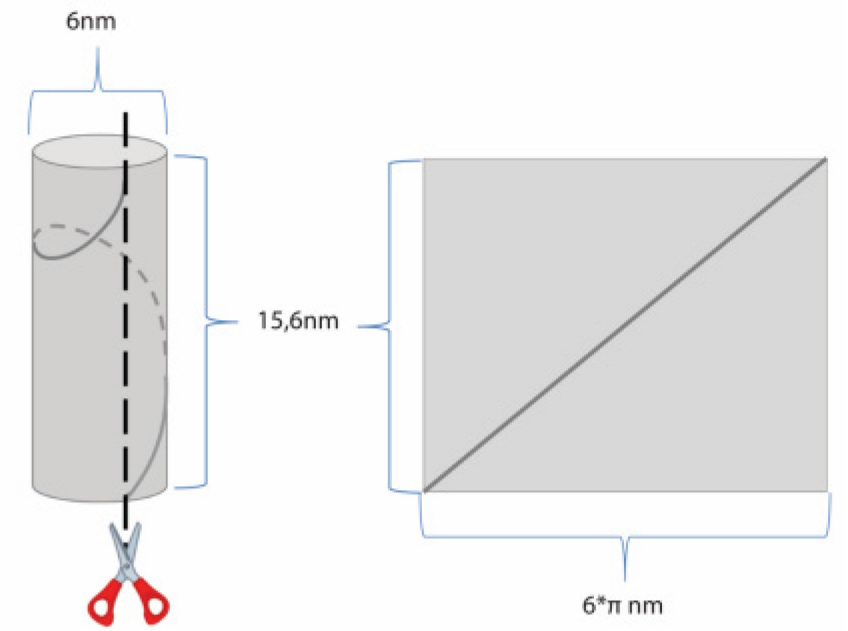

Figure 34 Estimation of the contour length of a helix

Before the yield point, the fiber is largely elastic during cyclic loading, suggesting that the uncoiling of the helix structure is a reversible process and that recoiling occurs rapidly, at least with respect to the strain rates utilized in this study. Past the yield point, however, cyclic testing exhibits a clear hysteresis, as well as a concomitant decrease in Young's modulus (Figure 30a and b) with increasing cycle strain, which is a hint that a damage is occurring within the material, which is not immediately recovered. However, when unloaded, the fiber can almost come back to its original length (Figure 30 and Figure 31);

therefore this damaging mechanism induces a reduction in mechanical properties but no permanent, plastic deformation. Since the helical signal is gone by 5 % macrostrain, the subsequent plateau is likely due to breakage of sacrificial non-covalent bonds, which rupture prior to the covalent bonds in the protein backbone. This is not unprecedented as metal-coordination bonds have been shown to act as reversible sacrificial bonds in *Mytilus* byssal threads[136,137,201,208]. In *Mytilus*, the breakage of the sacrificial bonds liberates some so-called hidden length which is responsible for the high extensibility of the byssus fibers.

Damage occurring to *P. nobilis* byssus fiber during cyclic testing also makes both the loading and unloading curve resemble more and more an exponential. Exponential stress-strain curves are typical for worm-like chain deformation[161,210]. The worm-like chain model is a commonly used mathematical representation of polymer (including protein) chain unfolding that accounts for the increasing force required to unravel the chain as the contour length is approached and is commonly used to fit AFM single molecule force spectroscopy protein unfolding data[211,212]. Indeed, the increasing force required to stretch the worm-like chain further arises from the decreasing entropy as the chains degree of freedom decrease due to its progressive alignment along the strain direction. This would support the hypothesis that during the plateau of the stress-strain curve of *P. nobilis* byssus sacrificial bonds break, liberating hidden length, which elongates further as worm-like chains. As mentioned one consequence of the worm-like chain model, is that the chains have a very low initial stiffness and a very high final stiffness. Therefore, the increasing content in low initial stiffness worm-like chains could explain the decrease of the fiber initial stiffness with increasing cycle maximum strain during cyclic testing (Figure 30b).

On the other hand, the final stiffness of a worm-like chain is related to the initial unloading slope (Figure 30c). Indeed, a stiff elastic element is difficult to deform and has therefore a high energy bringing it back to its original shape, therefore, a worm-like chain at low strain will have a low unload slope whereas a highly stretched worm-like chain will have a steep unload slope. Thus, an increasing content of liberated but not stretched worm-like hidden length could explain the decrease in initial unloading slope on Figure 30c up to about 20 % maximum cycle strain, which corresponds to the end of the plateau. Passed this point, stretching and therefore increase the stiffness of the worm-like chains could explain the increase in unloading slope up to the second yield point around 30 % strain (Figure 30c). However, cyclic testing shows that damaging continues even past the end of the plateau, during the second stiff region and the following plateau. It is not known if it still originates from breaking of further sacrificial bonds. It is feasible that the second plateau might correspond to unfolding of another domain held together by stronger bonds, but further knowledge of the structure of *P. nobilis* byssus is required in order to confirm this hypothesis. However, recovery experiments (Figure 31) suggest that the damaging occurring during the plateau of the tensile curve is not permanent, but that it can recover over time.

It is noteworthy that the peaks at 16 and 18 nm^{-1} observed on the WAXD diffraction pattern seem to start moving/disappearing above 5 % macrostrain (=yield region, disappearance of helix signal in SAXD). They are in the range of peaks usually associated with protein secondary structure and might therefore be associated to the structure and deformation of the hidden length. However, further investigation needs to be conducted in order to assess them. Cyclic testing also shows that pass the yield point, the slight decrease in toughness associated with damaging of the material is compensated by the additional energy needed to stretch the material to the next cycles strain, so that the toughness remains the same, despite the decrease in stiffness (Figure 30d).

6.3.3 Second yield point and final plateau

Based on our current evidence, it is difficult to confidently state what might be happening after the second yield point. Possibly, a further damaging of the material at the protein level, which could explain the sudden decrease in initial unloading stiffness (Figure 30c) right after the second yield point, even though it is not clear if there really is a minimum at 30 % strain. Furthermore, it was observed that the first yield point disappeared after the first cycle (Figure 31a) but reappeared after healing time, whereas the second yield point does not, showing that the phenomenon causing the first plateau is reversible with time, but that this is not the case for the damaging causing the second plateau (at least on the timescales of the current experiments), which suggest that they arise from different mechanisms.

6.3.4 Models

At this point, XRD measurement with *in-situ* tensile testing gives a clear hint that *P. nobilis* byssus fibers are not only made of the helical building blocks embedded in an amorphous protein matrix as previously observed in chapter 5[191], but that they contain a stiff element in series with these helical building blocks, and that the plateau observed in the stress-strain curve is probably associated with liberation of hidden length due to sacrificial bonds rupture. However, it is not known if the hidden length and sacrificial bonds are located within the globular proteins constituting the helices or within the stiff domains located between the helices, therefore I am presenting two possible models, one with the sacrificial bonds between the helices and the other one with the sacrificial bonds within the helices (Figure 35).

In the first version (Figure 35a) of the molecular model, the hidden length is contained in the globular proteins forming the helices and the stiff part connecting the helical domains would not deform. In this case, the first elastic part of the stress-strain curve would be due to unfolding of the helices, the plateau would be associated to the unfolding of some globular proteins, the second stiff region would be associated to the stretching of the free length provided by the unfolded globular proteins, whereas the second plateau might be due to the unfolding of a second domain of the helices. A similar plateau due to unfolding of several globular proteins is observed in the giant muscle protein titin[213]. The titin macroprotein

contains different domains, which unfold individually during single molecule AFM, which would support this version of the model. Furthermore, the helices might not be able to refold properly after the globular proteins unfolded, which would explain the decrease in initial stiffness and the disappearance of the yield point during cyclic testing. A simple way to investigate this would be XRD with *in-situ* cyclic testing, in order to see if the helix diffraction peaks are still recovered for strain far above the yield point.

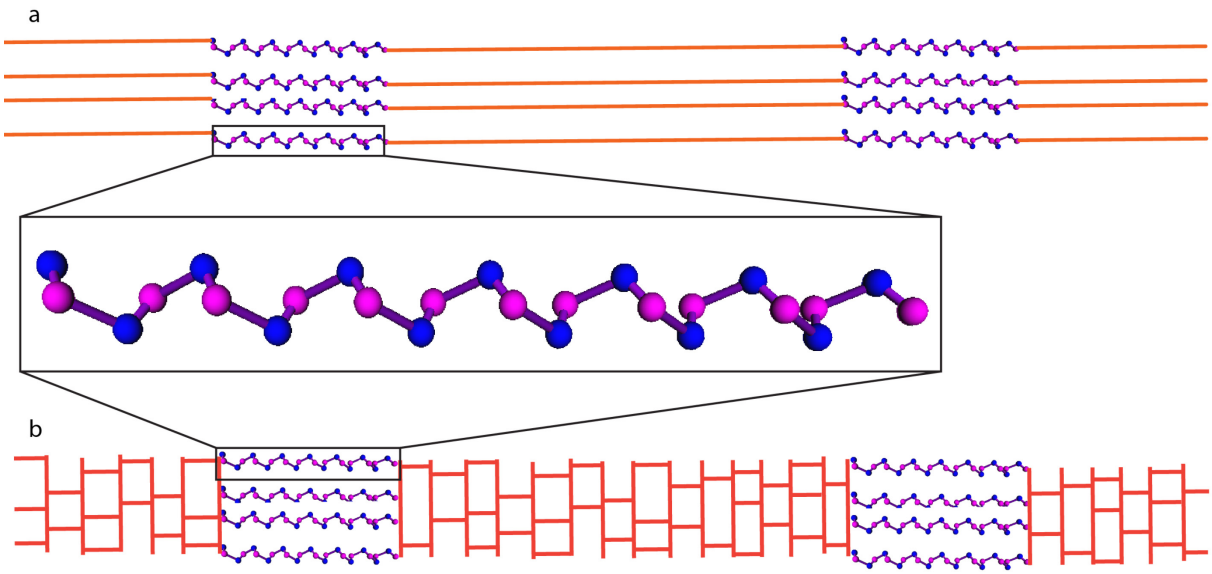

Figure 35 Two possible structures for *P. nobilis* byssus fiber proteins
The two models present a stiff and a softer phase, hidden length and sacrificial bonds as suggested by the tensile tests.in both versions, the stiff protein domain is intercalated between the helices, but in the version (a), hidden length provided by the globular proteins within the helix and the stiff part made out of straight and non-deforming proteins, whereas in version (b), the hidden length provided by the stiff part connecting the helices once the helices are stretched.

In the second version (Figure 35b), the hidden length would be contained in the stiff part connecting the helices. The first elastic deformation would again be due to the stretching of the helices, but in this case, the stiffness of the strained helices would be such that the stress would be transmitted to part connecting the helices, inducing brakeage of sacrificial bonds and liberating the length hidden within the connecting part. This would be the reason for the plateau. The second stiff region would be associated with stretching of the liberated hidden length, and the final plateau could be due to unfolding of the globular proteins in the helix. The presence of hidden length in domain connecting helices is reminiscent of the flanking domains of *Mytilus* byssus[129], even though there are some major differences: in *Mytilus* byssus, the protein helices are the stiffest part, whereas in *P. nobilis* byssus, the globular protein helices are the first to deform, and the length occupied by the connecting domain is much more important in *P. nobilis* than in *Mytilus* byssus.

In order to determine which version of the model is valid or if it is a combination of both or another mechanism altogether, more knowledge has to be acquired about the structure of the different domains and proteins present in the byssus of *P. nobilis*. Nonetheless, the

measurements performed in this work already provide very interesting insights into the deformation mechanism of *P. nobilis* byssus and showed that similarly to *Mytilus* byssus, the byssus of *P. nobilis* is likely to be made out of a soft and a stiff domain, this composite structure probably enables high extensibility without too much compromises about the toughness. Moreover, the presence of hidden length stabilized by sacrificial bonds seems to be a common feature between the byssus of *P. nobilis* and *Mytilus* and seems to be essential for the toughness, which allows them to survive marine currents or waves shocks and predators. Particularly interesting is also the comparison with the previous tensile tests of *A. rigida* byssus performed by Pearce and LaBarbera [124]. Indeed, *A. rigida* as well as *A. pectinata* (studied in chapter 5) and *P. nobilis* all belong to Pinnidae family. It was observed that *P. nobilis* and *A. pectinata* share a common helical building block, and that it is likely to be the case for other Bivalves belonging to the same family, like *A. rigida*. The fact that the tensile curve of *A. rigida* and *P. nobilis* look so similar tends to support this hypothesis. Indeed, they have the same overall shape, with two yield points, the same initial stiffness, although the yield point of *A. rigida* tensile curves occurs at slightly higher strains than *P. nobilis* byssus one and at an accordingly higher stress.

6.4 Conclusion

The combination of XRD and tensile testing enabled investigation of the relationship between the particular building blocks of *P. nobilis* byssus and its mechanical properties, and also suggested the presence of a stiff domain which could not be observed so far. The stress-strain curves of *P. nobilis* fibers have an unusual shape presenting two yield points, similarly to the byssus of the closely related *A. rigida*. The first elastic deformation could be attributed to helix stretching, while the post yield plateau may originate from breaking of sacrificial bonds, which liberate some hidden length. The plateau is followed by a second stiffening region which might come from the stretching of the liberated hidden length. The final plateau prior to material failure might be associated to unfolding of other domains or breaking of proteins. Even if the model is not complete yet, these findings are very interesting due to the unobserved structure of the byssus of *P. nobilis*, but also from the side of what can be learned from a comparative study between different species. Indeed, the combination of stiff and soft domains as well as the presence of hidden length stabilized by sacrificial bonds seems to be common to the byssus of *P. nobilis* and *Mytilus* species, and seem to be responsible for their toughness and their ability to self-heal. However, such studies should be conducted on mussel byssus possessing a different structure, such as *T. maxima*, which has been observed to be made out a fourfold coiled-coil, in order to determine if these features are essential features for all types of byssus.

7 Investigation of the traditional processing of *P. nobilis* byssus into sea silk

7.1 Cultural importance and scientific relevance of sea silk

As mentioned in section 1.1 many traditional natural fibers used for textiles and other materials require artisanal treatment to enable spinning and weaving. For example, as explained in section1.3, silk worm cocoons must be placed in boiling water to extract the silk fibers[88], while flax and hemp stems are macerated to degrade the pectin holding the fibers together[214]. Similarly, sea silk, which is derived from byssus fibers from the pen shell *P. nobilis*, is a valuable traditional fabric, which must undergo an artisanal treatment passed down through generations to achieve its characteristic golden color and in order to be woven into larger fibers.

Sea silk has a long and prestigious history among the ancient cultures of Europe and Northern Africa, and has developed its own mysterious lore associated with its origin. The first references to sea silk were made during the first century in the Hellenic world[38] and its golden color was highly regarded in the Roman and Greek culture which was very fond of yellow and used diverse dyes to color other fabrics[39]. *P. nobilis* byssus is referenced again in Greek texts from the 2nd century as "woolen stuff from the sea" and Chinese records from the 3rd century describing the eastern of Roman Empire refer to "a fine cloth said by some to originate from the down of a water-sheep"[38]. During the 4th century, sea silk was mentioned and admired for its color which was impossible to reproduce, and it was said to be superior to sheep wool. This is also the estimated age of the first sea silk fabrics found in Budapest, in the remains of the former Roman legionary town called *Auincum*. Sadly, this fragment was lost during the 2nd world war[38,215].

In the 6th century, the five governors of Armenia, received sea silk cloaks as a distinction from the Roman emperor[216]. Only Persian and Roman Emperors were allowed to wear sea silk[216]. References to sea silk are scarcer during the Middle ages; however, in the 10th century, the story of the sea-sheep made a comeback, this time in the Arabic world, under the form of an animal coming out of the sea at certain periods of the year, rubbing itself against rocks, leaving behind "a kind of wool of silken hue and golden color", which was so rare and valuable, that the Princes of Spain would keep it for themselves and forbid its exportation. For example, a robe made of sea silk at that time were said to cost more than a thousand gold pieces, which would be the equivalent of at least $400 000USD, or more than €350 000, according to the informal sources I could find. This story was told again in the 13th century. Due to its exorbitant price, there were attempts to imitate sea silk from the 4th century on, the most convincing of which was made of bird feathers[38].

During the 14th century, sea silk was also produced in Maghreb and worn by the Sultan of North Africa, and the secretaries of Egypt[39]. In 1681, there are reports that sea silk was still woven into valued fabrics used in the winter due to their warmth[39]. They were also said to

protect against damp and be soft and warm[216]. In the beginning of the 18th century, there was a considerable industry in Tarento, in Italy, with workers going as far as Sardinia and Corsica to get *P. nobilis* byssus that was mixed with up to 1/3 of silkworm silk in order to strengthen it before being knitted into various items. The feelings about it seemed to diverged, since it was reported to be uneven and not extraordinary fine, but also to be much more beautiful than wool and approaching the beauty of silk[39].

By the 19th century, sea silk became more common, and apparently, rich Italian family would wear scarf and gloves out of it on Sundays[215], and Jules Verne makes mention of sea silk in his famous book "20 000 Leagues Under the Sea"[217]. *Pinna* mussels were harvested for their byssus either by diving, or by fishing them from a small boat using a special tool, called Pernonico[216,218], comprised two semi-circular bars of iron held together, leaving a space between them. This metal construct was attached on one side to of a long wooden pole and to the other one to a rope. It was let down in the water, so that the *P. nobilis* shell would stand between the two metal parts, and twisted to loosen the shell from the ground, and then pulled back on board with the *P. nobilis*[216]. This is a time expensive process, and in the end, the sea silk industry was unable to expand and grow, due to the small amount of material available and the time necessary to process it and thus remained a local craft that finally declined, despite the effort of the locals to save it.

Nowadays, *P. nobilis* is an endangered and protected species and the tradition of sea silk is likely to become extinct as the old byssus artisans, who had the secret of byssus processing into fabrics, are disappearing. The process by which artisans transformed *P. nobilis* byssus into beautiful and comfortable fabrics has been passed through families, and is practiced today by only a few individuals, including the self-proclaimed Maestro di Bisso, Chiara Vigo (Figure 36). This treatment procedure seems to be crucial because it facilitates a complete change of function of *P. nobilis* byssus, from an underwater usage to a dry utilization, from single fibers made to entangle in sand to a thread which can be woven. Therefore, it stands to reason that the treatment might be associated with a change in properties and structure, thus giving insights not only on how to develop application for byssus and byssus inspired materials, but also on structural features of natural *P. nobilis* byssus fibers which still remain obscure so far. Therefore, understanding the processing of *P. nobilis* byssus fibers into sea silk is important not only from a historical and cultural point of view, but could allow us to gain important information about the structure and function of *P. nobilis* byssus and its application to human usage by taking advantage of the tacit knowledge developed over many centuries.

In order to understand how the aim of the traditional treatment allows this change in function of *P. nobilis* byssus, I performed here a comparative study of treated and native *P. nobilis* byssus fibers, using compositional analysis (amino acid analysis and ICP-OES), electron microscopy (TEM) and spectroscopy (Raman, FTIR, Visible-light) in order to determine any modification of the structure. In addition, I utilized tensile testing to compare mechanical

properties of native and treated *P. nobilis* byssus in order to assess changes that might be relevant for the processing of the fibers into fabrics. These investigations will help better understand the structure-function relationship of *P. nobilis* byssus fibers both in terms of mechanical properties and coloration that will help assess the importance and purpose of the traditional processing of sea silk. Understanding of the traditional processing will hopefully help to preserve this tradition at least in records if it comes to disappear completely along with the byssus artisans. Furthermore, in an attempt to better assess the effects of the artisanal treatment, I attempted to replicate it in the lab with simplified conditions, using only lemon juice and citric acid solutions and compared the properties of these *in-lab* treated fibers with *P. nobilis* byssus treated by Chiara Vigo.

Figure 36 Some examples of sea silk craftmanships

Chiara Vigo, byssus artisan, spins treated *P. nobilis* byssus fibers into a thread (a) that she mostly uses to web (b) traditional motives in linen (c), producing knitted pieces of clothing (d and e) demanding too much materials and time. The tie on picture (d) gives an idea on why byssus was used to knit gloves and hats for winter, whereas the piece of fabric on picture (d) shows the shimmering of the byssus in the sun which made byssus fabrics famous.

7.2 Traditional processing of sea silk

There are few and scarce reports of the traditional processing of sea silk. Yates[216] mentioned in 1843 the treatment of *P. nobilis* byssus only as washing in water, then soapy water, and then water again, before drying. Washing was also reported by Swinburne in 1785, as well as "dipping in lemon", which "provided the shine of lanna penna"[36].

Due to the lack of precise information about the traditional treatment, I rely only on the information provided by Chiara Vigo concerning this process. Her traditional artisanal treatment performed on *P. nobilis* byssus fibers to generate sea silk is an extended process, involving tap water, sea water, saliva, lemon juice and sometimes lavender. The process reported below is the traditional method used by Chiara Vigo, which was demonstrated during a visit to the Max Planck Institute in Golm. She brought dried fibers which had been desalted for 25 days in tap water, changed every 3 hours, days and nights (Figure 38a). Once in Golm, she started the next steps of processing. She indicated some of the steps below as optional, depending on the air quality, and said she had to do them because the air was too humid. The optional steps and elements (such as lavender) are written in grey.

1) The fibers were left for 5 minutes in a beaker with artificial sea water, and Chiara Vigo hummed over the water, because she believes that this modifies the water. Then she used her hands to wring the water out of the fibers.
2) The byssus fibers were then washed for 20 seconds in tap water, otherwise the debris and dust stick too much to the fibers
3) Chiara Vigo then used her fingernails to remove shells, roots and the adhesive plaques from the byssus.
4) Chiara Vigo chewed lavender leaves and flowers then spit it out onto the table surface.
5) At this point, she added an undetermined quantity of lemon juice (several ml based on estimation) by squishing a lemon above the chewed lavender (if no lavender was used, she would just use lemon juice) (Figure 38b).
6) Chiara Vigo then mixed the byssus with the mixture of chewed lavender and lemon juice, and taps it with her fingernails.
7) She rinses the threads in tap water (Figure 38c).
8) Finally, she wrings out the liquid and brushes the threads with a small metal brush.
9) At the end, she spins a single thread from the numerous treated fibers in the Z twist direction and doubles it again in the Z direction (Figure 38d). She said this works much better than the S direction.

Z and S are the terms used in fabric crafts and industries to describe the two possible fibers spinning directions, depending if the yarn forms a clockwise (Z twist) or counter-clockwise (S twist) helix[219]. Two spun threads can be twisted together in any of the directions (Z or S) to form a second ply [220]. In this case Chiara Vigo made a double Z two-ply and says that the first and second plies in opposite directions break the thread. An example of a double S two-ply is given in Figure 37.

Figure 37 Double S two-ply thread showing the counter clockwise spinning

I later discovered during a visit to her workshop in Sardinia that she actually leaves this thread in a mixture of sea water, saliva, lemon juice and algae (*Posedonia* sea grass) for several days before the sea silk actually takes its definitive color (step 10) (Figure 38).

Figure 38 Chiara Vigo proceeding to the traditional production of sea silk
Desalted byssus (a) is treated with lemon juice (b) and saliva, and then rinsed (c), before being spun into a thread (d) which was then left in a lemon juice, saliva and algae solution (e).

7.3 Sample description

At the outset, my goal was to assess what effect this treatment has on the structure and properties (mechanical and coloration) of the native byssal threads. Along these lines, I performed a similar set of characterization techniques on the following samples:

- **Native**: native byssus, acquired in May 2017 in the water off the coast of Villefranche, France and kept in deionized water prior to testing.
- **Chiara native**: native byssus given by Chiara Vigo, which she had already left in tap water for 25 days.
- **Instant treated** byssus fibers, which were treated in Golm by Chiara Vigo using the saliva-lemon juice mixture described above (step 1-8), but were not left in saliva, lemon juice and algae water for an extended period afterward.
- **Fully treated** byssus fibers, which were given by Chiara Vigo, spun and apparently fully treated, staying for 3 days in saliva, lemon juice algae mixture (step 1-10).
- **Bisso trattato** byssus given to me by Chiara Vigo as treated byssus, but not spun (step 1-8 and 10).
- **Unknown treated** was also given to me as treated byssus, through an intermediate person. The treatment procedure is not known. Their color observed with naked eyes lays somewhere between the instant treated and the fully treated fibers.

7.4 *In-lab* treatment

In an attempt to reproduce the key features of the treatment of *P. nobilis* byssus fibers by Chiara Vigo, I performed a simplified *in-la*b treatment. To do so, I took fibers from one mussel acquired in Villefranche, which was kept two years in deionized water, and separated it in four samples. Sample 1 and 2 were left 2.5 days in 120 ml deionized water, sample 3 in 90 ml deionized water with an additional 30 ml lemon juice (pH=2.2) and sample 4 in 120 ml of a 0.1 M citric acid solution (pH=2.2).

7.5 Results

7.5.1 Properties

Based on historical accounts of sea silk and discussion with Chiara Vigo, the primary effects of the artisanal treatment is a coloration change towards more golden tones and a mechanical change that improves processability. Therefore, I utilized visible light spectroscopy and tensile testing in order to detect any change in color or mechanical properties associated with the traditional treatment of *P. nobilis* byssus fibers.

7.5.1.1 Color measurement

A clear difference in color could be observed between the native and treated fibers already with naked eyes, as seen in Figure 39a and b. The native fibers given by Chiara Vigo appear dark brown to black. The Instant treated fibers present a similar color, but slightly lighter, whereas fully treated fibers and bisso trattato appear significantly lighter. However, the golden color of the treated fibers is especially enhanced when illuminated with direct sunlight at specific angle (Figure 39c and d) and is varying a lot according the incident angle of the sunlight on the threads (Figure 39d, right up and down are the same sample at the same spot, only slightly tilted). The color of the unknown treated byssus seems to lie between the one of the completely treated fibers and native ones, therefore, calling into question how fully it was treated. Indeed, Chiara Vigo, who gave me the treated fibers believes that the main point of the treatment is the instant treatment; therefore, she did not make the distinction between threads that were instantaneously treated and those that were soaked in lemon juice afterward. For this reason, the fibers received from her may range in the degree to which they are treated. The difference in colors observed with naked eyes can be partially quantified by acquiring a visible spectrum from a thread using the confocal microscope and detector of the Raman setup and replacing the laser source by a white source. The spectra obtained by this means can be transformed into (x,y) coordinate in a CIE 1931 color space and plotted on this space to be visualized (Figure 40). The native byssus fibers given by Chiara Vigo and the instant treated fibers have a similar color, whereas it can be seen that the fully treated fibers (fully treated and bisso trattato) lie more toward yellow hues (Figure 40a). Treated unknown fibers, however, have the same color as the native and instant treated fibers (Figure 40a). In order to compare the color of the diverse fibers in a more quantitative fashion, I calculated their “yellowness” which is the projection of their (x,y) position along the yellowness axis going from white to yellow on the CIE color surface as seen on Figure 41a. I also calculated the component perpendicular to the yellowness, which I called redness, since it lays almost along the green-red axis (Figure 41a). This calculation shows the shift in color associated with the treatment from Chiara Vigo as well as our *in-lab* treatments, indicating that treated fibers have increased yellowness in comparison with native fibers (Figure 41b and c), except the unknown treated, which exhibited a yellowness similar to native fibers. In contrast, the redness did not seem to change much with any of the treatments (Figure 41d and e).

Figure 39 The multiple colors of byssus

Traditional (a) and *in-lab* (b) treatment of *P. nobilis* byssus. The color of the fibers really appears in direct sunlight (d and e). The color of the fibers highly depends on their orientation regarding the light: (d) right up and down are the same sample at the same spot, only slightly tilted.

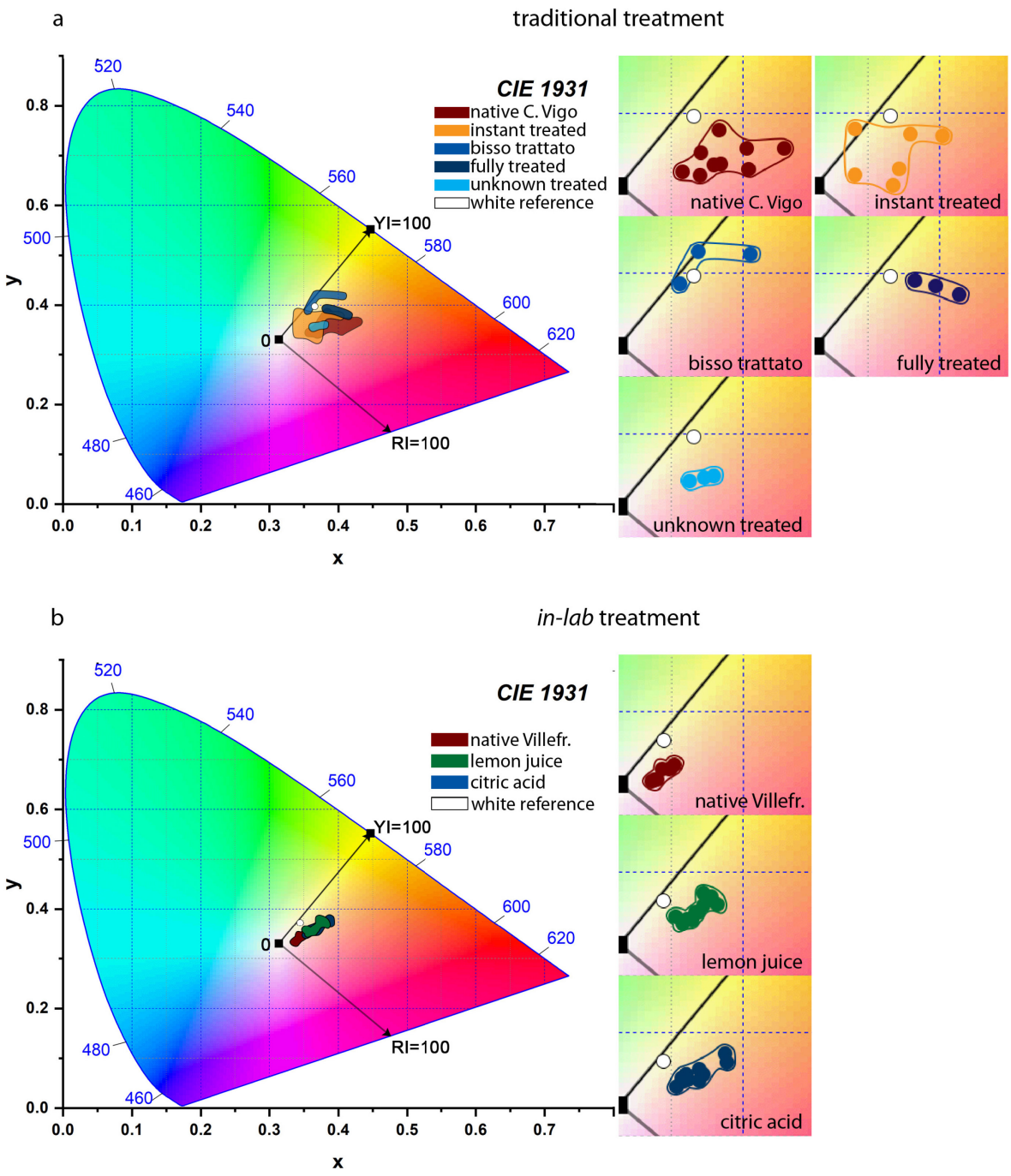

Figure 40 Visible light spectroscopy measurements plotted on a CIE 1931 color space

(a) plot of the fibers provided by Chiara Vigo (native and treated according to the tradition) on a CIE 1931 color space. The magnified area on the right shows the distribution of the measurements for each sample. (b) plot of the native byssus fibers from Villefranche, and the same fibers treated in the lab with lemon juice or citric acid on a CIE 1931 color space. The magnified area on the right shows the distribution of the measurements for each sample.

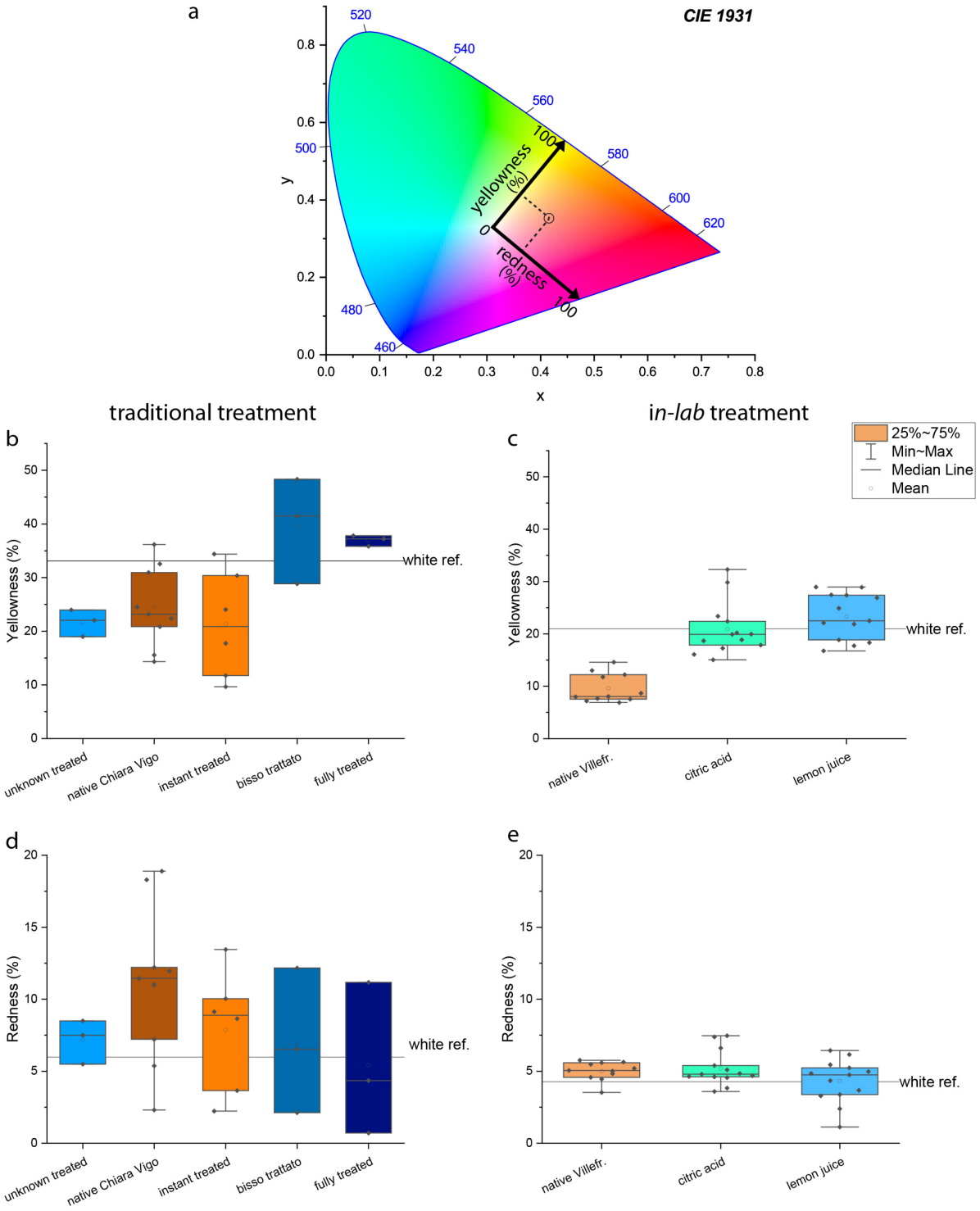

Figure 41 Yellowness and redness of the native and treated byssus

(a) graphical explanation of the new coordinate system expressing the yellowness and redness of the fibers. (b) and (c) show respectively the yellowness of the traditionally and *in-lab* treated fibers, (d) and (e) respectively show the redness of the traditionally and *in-lab* treated fibers, which represents their deviation from the axis between absolute white and complete yellow color. The value of the white reference is indicated as a line on all the plots.

7.5.1.2 Tensile testing

During her visit to our lab, Chiara Vigo stated that the artisanal treatment was essential for the mechanical properties of the yarn. In order to verify this assertion, I used single fiber tensile testing to compare the mechanical properties of native *P. nobilis* byssus fibers (Figure 42a), *P. nobilis* byssus fibers treated by Chiara Vigo in her workshop (fully treated and bisso trattato) (Figure 42b), which have most probably been soaking in lemon juice, saliva and Posedonia grass solution and fibers shortly treated by Chiara Vigo in our lab (step 1-9 of the treatment described in section 7.2, no soaking) (Figure 42c). Additionally, I measured the tensile properties of my *in-lab* treated fibers soaked in diluted lemon juice (Figure 42d) and citric acid solution (Figure 42e). At first look, the tensile curves of all the different treated fibers resemble those of native fibers in their general shape: they possess an initial stiff region followed by a yield point and a plateau terminated by a second stiff slope, in certain cases followed by a yield point. However, some differences can also directly be noticed: fully treated threads and bisso trattato possess a less defined first Yield point, a twofold decrease in yield stress and in initial stiffness and an increase in the stiffness of the plateau (Table 4). However, no change in yield strain, ultimate stress or ultimate strain was associated with the full treatment. Surprisingly, there was no decrease in toughness associated with the complete treatment (Table 4). The mechanical changes associated with the full treatment from Chiara Vigo are somewhat similar to the decrease in mechanical properties of native *P. nobilis* byssus fibers during cyclic testing in section 6.2.2., with a less distinct Yield point and a decrease in Young Modulus observed during the second cycle, which, in chapter 6, was associated with the damage of the fiber during the first cycle. The possible modification of the fiber tensile properties associated with the instant treatment from Chiara Vigo and the *in-lab* citric acid and lemon juice treatment are less obvious: some trends can be observed, even though they are too small to be considered significant according to the ANOVA test (Figure 43). Thus, this may represent an intermediate degree of mechanical change.

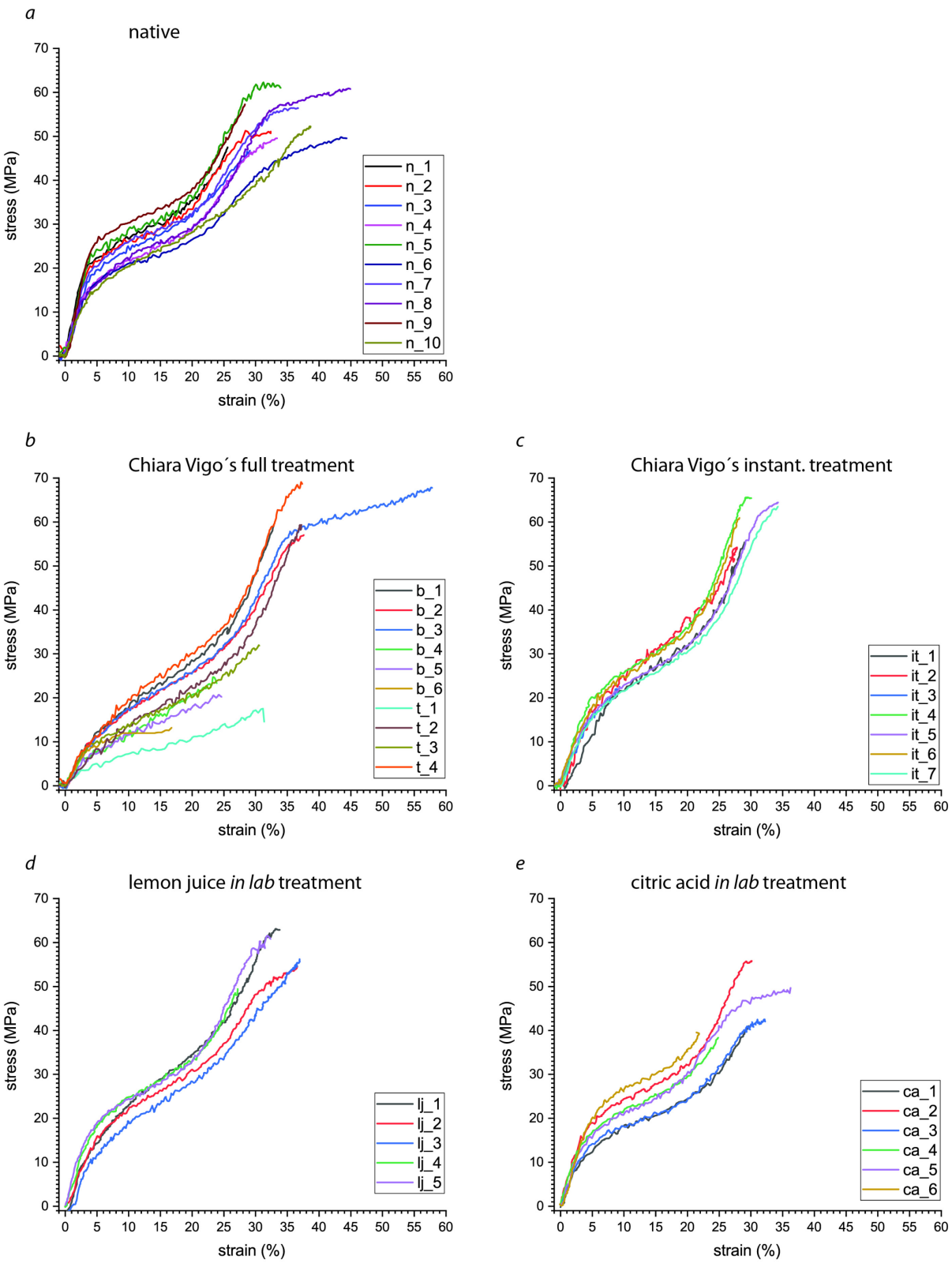

Figure 42 Tensile properties of native and treated byssus fibers

Comparison of tensile testing curve of (a) completely native *P. nobilis* fibers (taken from section 4.2.2), (b) treated *P. nobilis* fibers (b= bisso trattato, exact treatment unknown, t= 3 days in lemon juice) (c) *P. nobilis* fibers shortly treated by Chiara Vigo in our lab (d) *P. nobilis* fibers treated *in-lab* by me in lemon juice solution (e) *P. nobilis* fibers treated *in-lab* by me in citric acid solution.

Table 4 Comparison of the characteristic mechanical values of treated byssus

Completely native *P. nobilis* fibers (taken from section 4.2.2), treated *P. nobilis* fibers (bisso trattato, exact treatment unknown and 3 days in lemon juice) with *P. nobilis* fibers shortly treated by Chiara Vigo in our lab *P. nobilis* fibers treated *in-lab* by me in lemon juice solution and *P. nobilis* fibers treated *in-lab* by me in citric acid solution.

	native	fully treated	instant treated	Lemon juice	citric acid
# of samples	10	6	6	6	5
Young Modulus (MPa)	566(±118)	308(±78)	378(±61)	564(±198)	471(±86)
Yield strain (%)	2.7(±0.4)	2.9(±1.2)	4.3(±1.9)	2.8(±0.8)	2.7(±0.7)
Yield stress (MPa)	15(±4)	7 (±2)	14 (±4)	10 (±3)	12(±3)
Plateau slope [Mpa]	66(±5)	85(±15)	95 (±8)	93(±15)	71(±7)
2^{nd} Yield strain (%)	30(±4)				
2^{nd} Yield stress (MPa)	49(±6)				
Toughness (J/cm^3)	11 (±3)	11(±6)			
Maximal strain (%)	34 (±7)	39(±10)			
Maximal stress (MPa)	54(±6)	57(±13)			

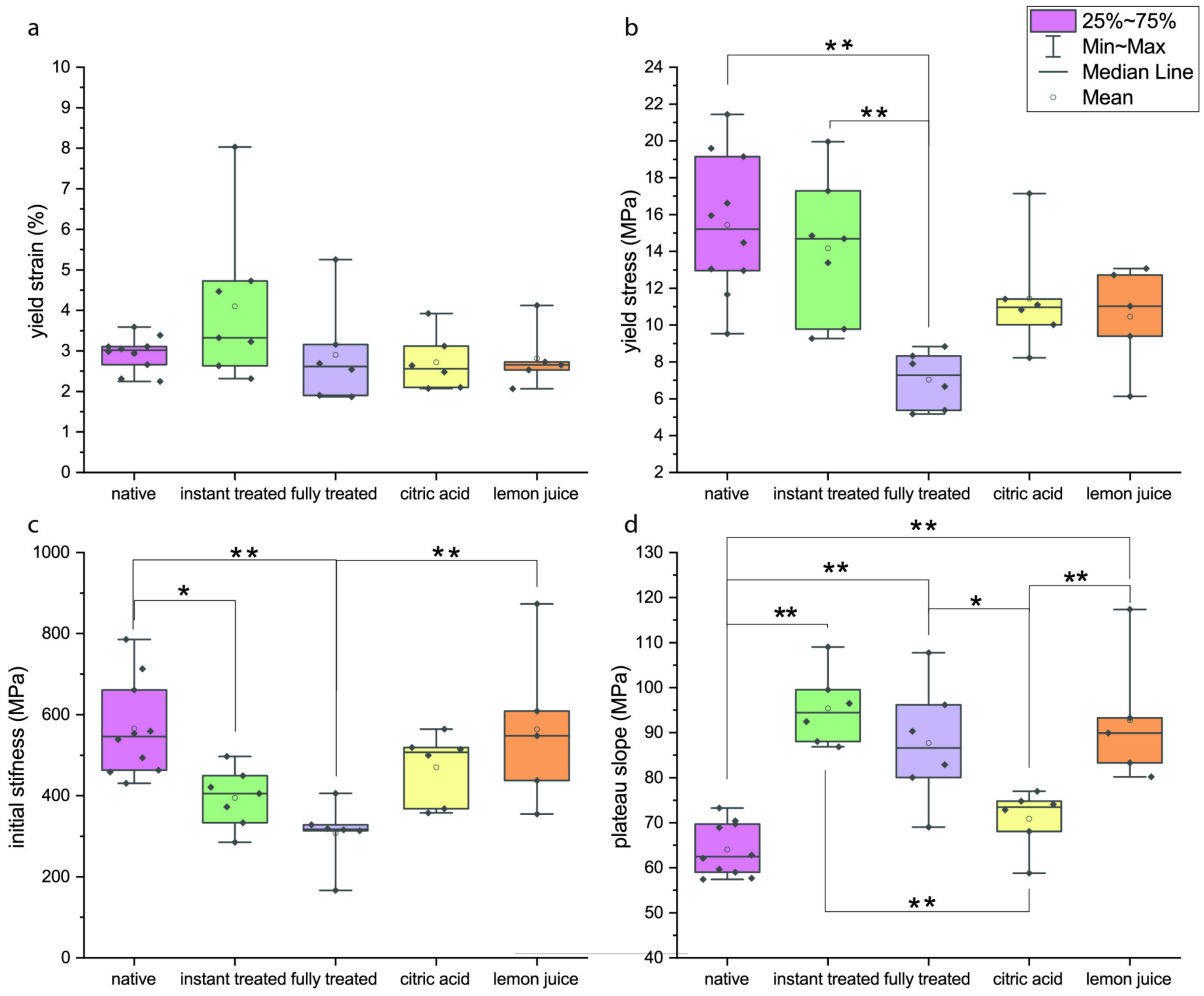

Figure 43 Effect of the treatments on characteristic mechanical values

Comparison of the characteristic mechanical values for native, instant treated, fully treated, citric acid and lemon juice *in-lab* treated fibers of *P. nobilis* byssus. (a) there is no statistical difference in yield point associated with any of the treatment (b) the yield stress of fully treated fibers is statistically lower than the native and the instant treated fibers (c) there was a statistical difference in initial stiffness due to both the instant and full treatment of Chiara Vigo. Also the lemon juice treated fibers are statistically different than the fully treated ones (d) the instant treated, fully treated and lemon juice treated fibers have a statistically steeper plateau than the native fibers. The citric acid fibers plateau slope is statistically different from the instant and fully treated fibers plateau. One way ANOVA: ∗=p<0.05 ∗∗ =p<0.01

7.5.2 Composition

In order to see if this difference in function could be explained by a change in composition, I measured the protein composition with amino acid analysis, and the elemental composition with ICP.

7.5.2.1 Protein composition (Amino acid analysis)

While the composition of most amino acids (e.g. Asp, Threonine (Thr), Glutamate (Glu), Gly, Ala, Methionine (Met), Isoleucine (Ileu) , Leucine (Leu), Phenylalanine (Phe)) does not seem to vary between samples, several other amino acids show slight variations (Ser, Cysteine (Cys), Valine (Val), Tyr, Lysine (Lys) and Pro) (Figure 44). However, these changes show no specific trends and fall within the normal variation associated with the technique. The fully treated fibers appear to exhibit a slightly higher His content, but this should be statistically confirmed.

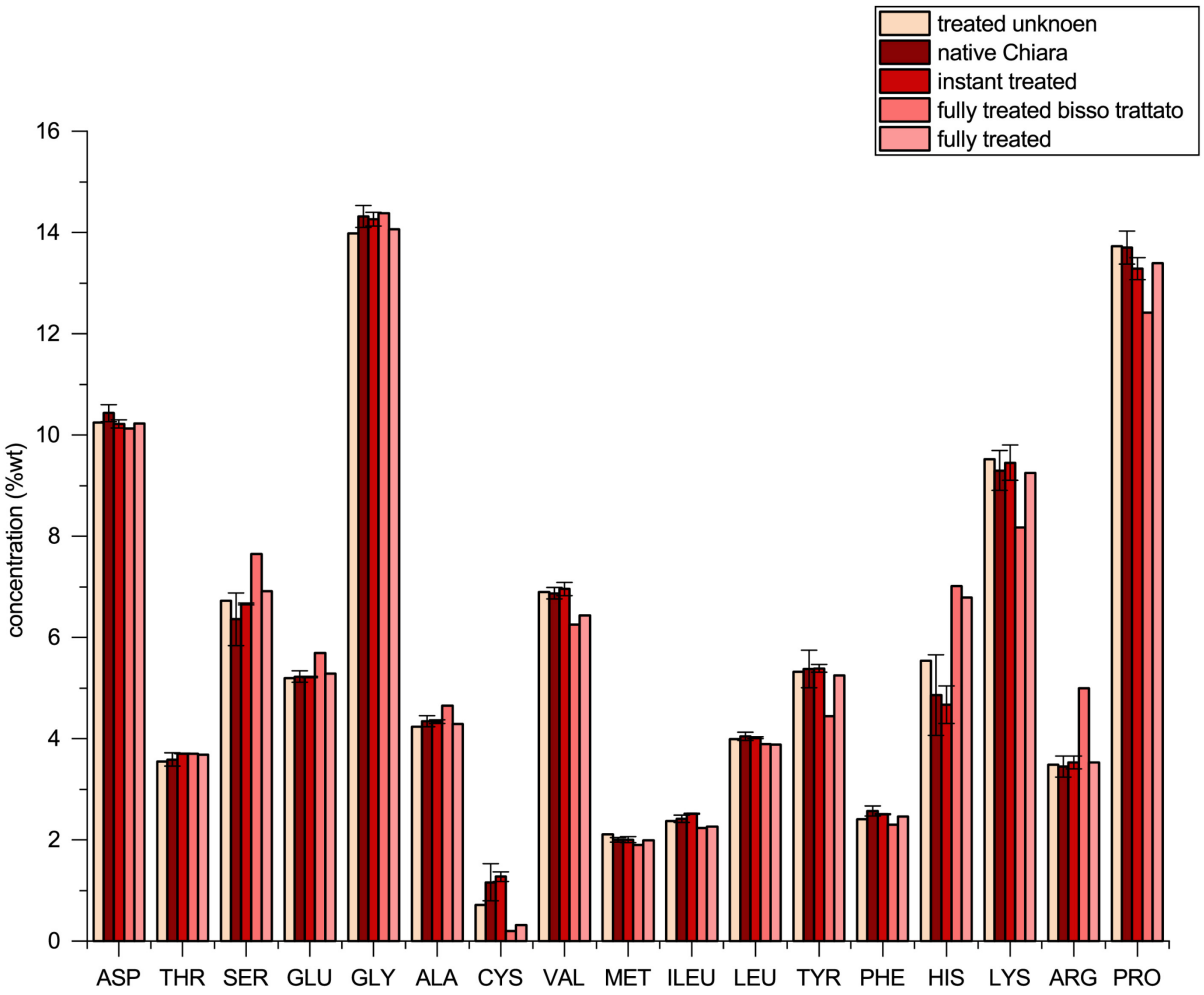

Figure 44 Amino acid analysis of different states of treatment of *P. nobilis* byssus fibers

7.5.2.2 Inorganic composition (ICP-OES)

In contrast to the organic composition, ICP-OES does show some notable changes in inorganic composition associated with the treatment performed by Chiara Vigo (Figure 45a). The variability in B and Si content seems to be completely independent of the treatment state. The concentration in Cu seems to be rather constant in all the fibers, independent of the treatment. However, Iron content seems to be related to the treatment state, as it is significantly lower in the two treated fibers which exhibited a distinct difference in color, whereas Ca is removed after instantaneous treatment. In contrast, Al appears also to be removed during the instantaneous treatment and the complete treatment (fully treated thread and bisso trattato). However, due to the high variation in native threads, it is not completely clear if this effect is real. It is also not clear what is happening with Magnesium, which seems to be removed by instant treatment and re-added during the soaking in the lemon juice, saliva, and algae solution. The concentration of Zinc is too low to notice any difference in concentration. In contrast, the unknown treated sample exhibits the same inorganic composition as the native samples. The *in-lab* treatment with citric acid and lemon juice allows a better characterization of the effect of the treatment on the inorganic composition of *P. nobilis* byssus (Figure 45b). A clear decrease in Ca, Al and Fe was associated with both lemon juice and citric acid treatment. Lemon juice was more efficient than citric acid at removing Fe, but less effective at removing Ca. There was no change in Cu and Si. No decrease in Mg could be observed with the citric acid either, but there was a clear increase in Mg and B after lemon juice treatment.

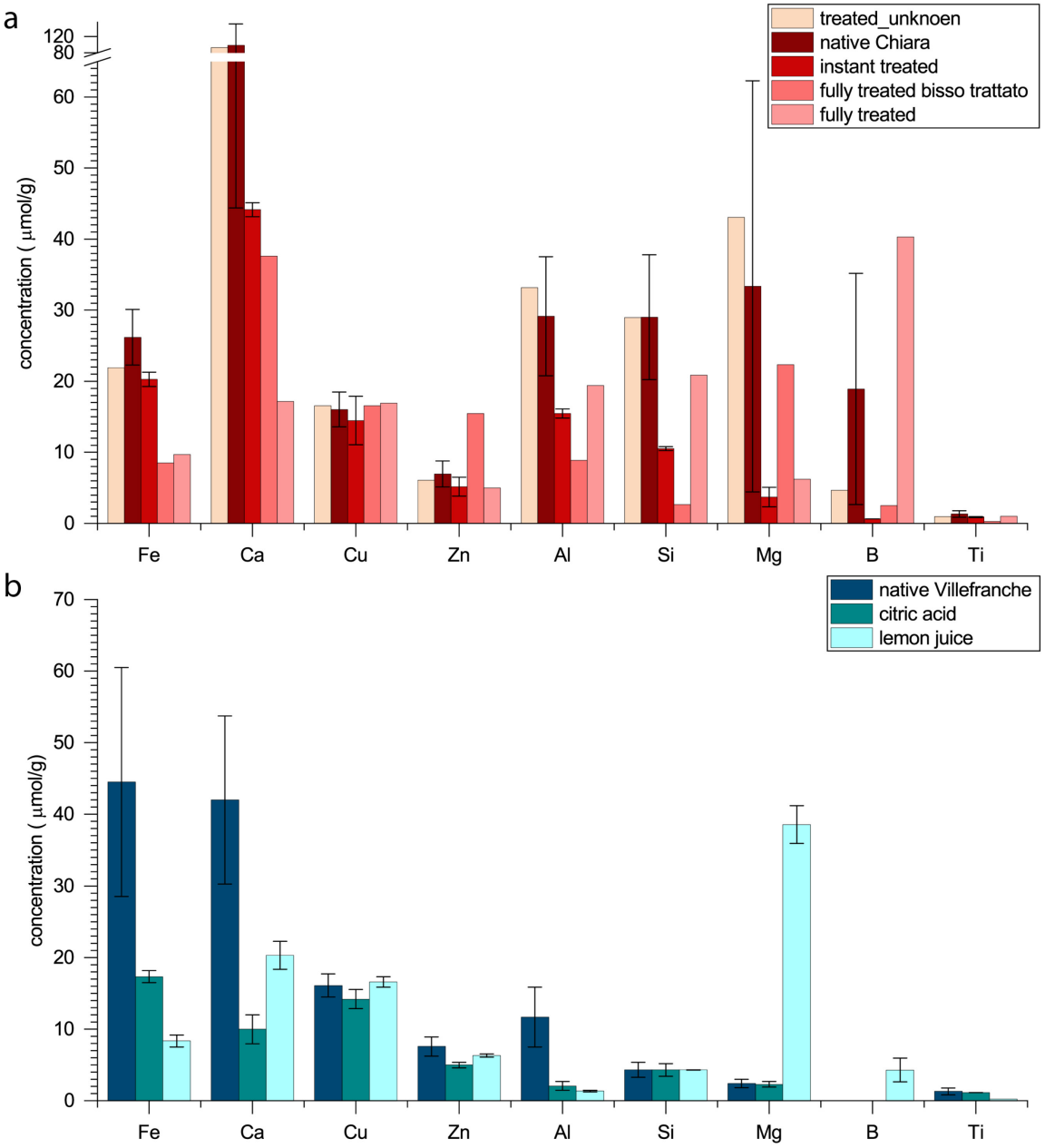

Figure 45 Inorganic composition of native and treated byssus

(a) inorganic content of the *P. nobilis* byssus having stand an unknown treatment, native *P. nobilis* fibers given by Chiara Vigo, fibers having stand the instant treatment from Chiara Vigo, fully treated fibers given by Chiara Vigo, fully treated fibers from Chiara Vigo, 3 days soaking in lemon, algae, saliva solution. (b) Inorganic composition of the native byssus from Villefranche compared with the same byssus after lemon juice or citric acid in-lab treatment.

7.5.3 Structure

FTIR and Raman spectroscopy were used to see if the change in properties and inorganic composition were associated with a change in protein structure at different hierarchical length scales.

7.5.3.1 FTIR

FTIR was used to observe any change in folding and structure of the byssus proteins due to the treatment. There seems to be a small change in the area between 950 and 1140 cm^{-1} (Figure 46), however, the variability of the signal from treated samples was so high in this area that it is not possible to draw exact conclusions. The other areas of the spectra look quite identical (Figure 46a) and the Amide I and II bands do not seem to present a different shape in any of the treated fibers (Chiara Vigo's treatment, *in-lab* lemon juice and citric acid). The Amide I band of the fully treated fibers might be slightly broader than the one of the native fibers (Figure 46b). In addition, a small shoulder is present at 1730-1740 cm^{-1} in treated fibers but not in native ones, which is often associated with C=O stretching as of carboxylate groups in amino acids (e.g. Asp or Glu)[221,222]. The Amide I band of the citric acid and lemon juice treated fibers may also be slightly broader (Figure 46c and d), however, this is a very small change which could also come from a slight difference in background and should not be over-interpreted. None of the in lab treated fibers show a clear shoulder around 1730-1740 cm^{-1}. Even though both curves are slightly higher than the curve of the native fibers in this area, it is not different enough to be sure it is real.

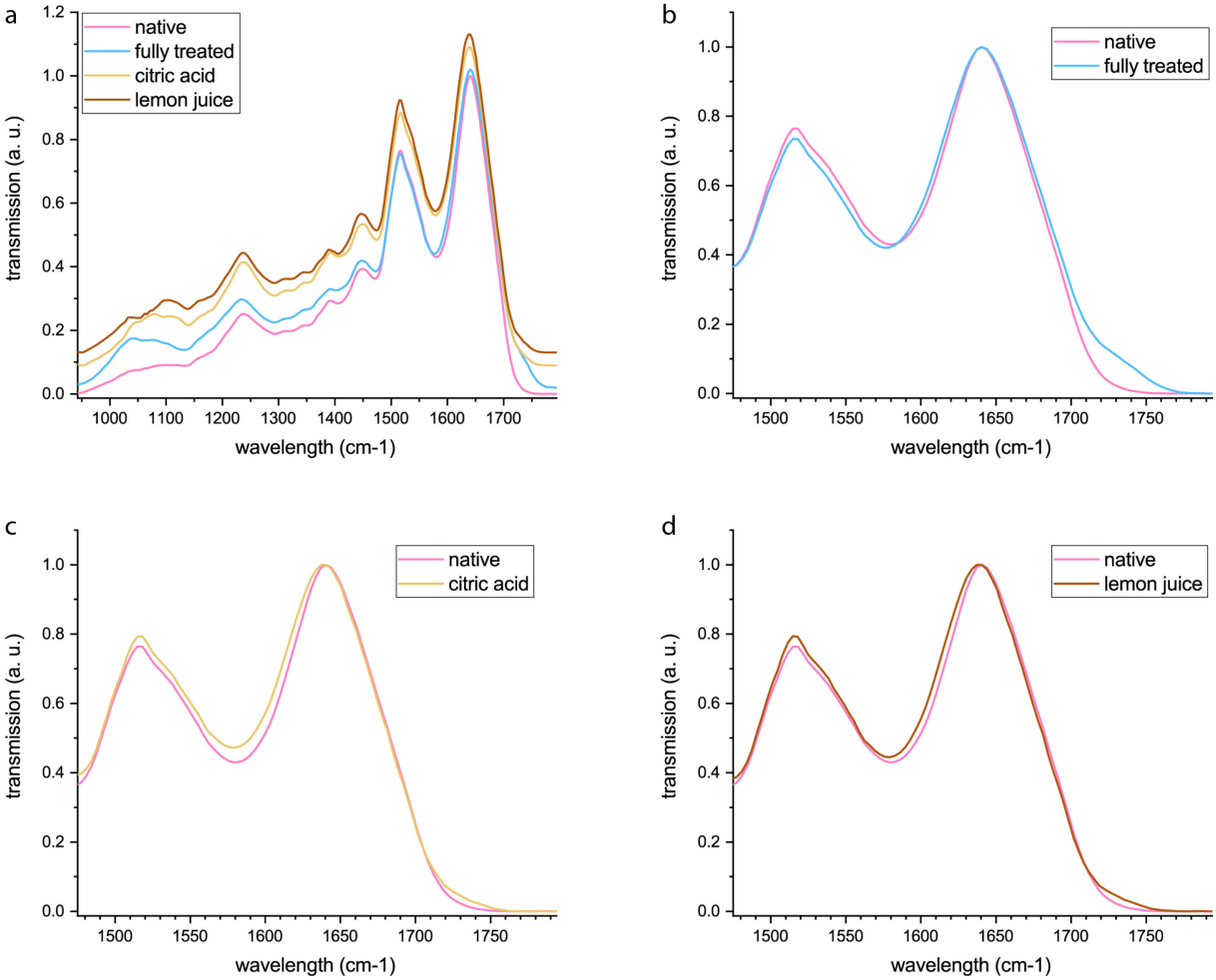

Figure 46 FTIR ATR spectra of native and treated byssus

Transmittance spectra of *P. nobilis* byssus fibers fully treated by Chiara Vigo, as well as in-lab lemon juice and citric acid treated fibers. (a). Amide I band comparison of fully treated with native fibers (b), citric acid with native fibers (c) and lemon juice treated fibers with native ones (d). Each spectra is the average of 7 spectra from 7 different samples.

7.5.3.2 TEM

TEM previously allowed the observation of specific nanoscale structural features in the byssus of *P. nobilis*, which were thought to be the helical nanofibrils observed in the XRD pattern as well (see section 5.2.3). Therefore, TEM was also used in order to observe if those structures would stand any modification after treatment. In particular, the small donut-shaped structures observed previously in transverse cross-sections, are believed to correspond to the cross section of a single helical fiber. While these entities are observed in both native (Figure 47a) and treated fibers (Figure 47b), their spacing is 8.8 (±0.8) nm on cuts of treated fibers, whereas it was measured to be 10.6 (±0.4) nm in native threads (measurements made on three images from one sample) .

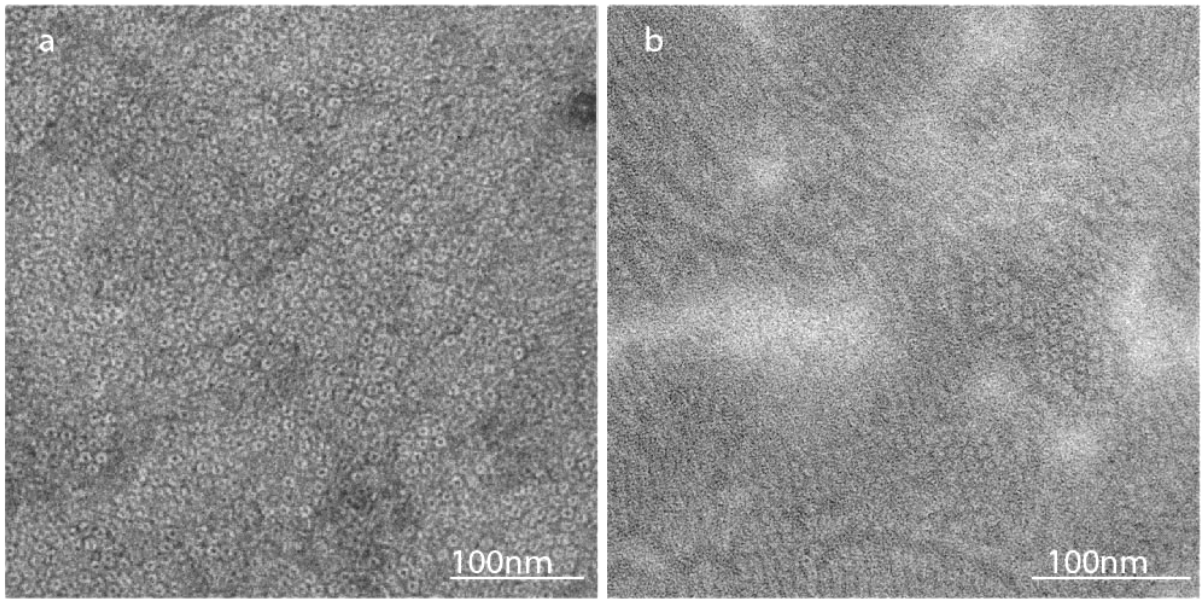

Figure 47 TEM investigation of native and treated *P. nobilis* byssus.
The donut shapes observed on TEM images of transversal cuts of native *P. nobilis* byssus fibers (a) could also be observed on fully treated (fully treated thread by Chiara Vigo, soaked 3days in lemon, saliva, algae solution) (b).

7.5.3.3 Raman spectroscopy

Raman spectroscopy has been successfully used to study the interaction between metal ions and proteins in *Mytilus* byssus, in which they are known to mechanically reinforce the cuticle. Furthermore, such Fe-based coordination complexes are known to absorb light in the visible range and thus, behave as chromophores (e.g. the heme group). Considering that the functional changes in mechanical properties and coloration in treated fibers are correlated with an observed decrease in Fe content, I measured near IR Raman spectrum of native and treated fibers in order to investigate the possible presence of catechol-based metal coordination and the loss thereof following the artisanal treatment. While the spectra quality are not excellent due to a high background fluorescence from the threads, Figure 48 reveals several clear peaks between 1100 and 1500 cm^{-1} which are slightly reminiscent of the resonance arising from DOPA-metal coordination[137]; however, I am cautious to assign them definitively since the presence of DOPA was not observed. Nonetheless, the peak

around 1455 cm^{-1} appears to decrease in intensity in all the treated fibers (treated by Chiara, and both of my in-lab treatments) (Figure 48). The peak around 1606 cm^{-1} does not seem affected by any of the treatment, neither its position nor its intensity. The peak at 1326 cm^{-1} appears to lose intensity with both lemon juice and Chiara Vigo's treatment and less with the citric acid. Finally, the peak at 580 cm^{-1}, which may also be a resonance Raman peak from the oxygen-metal interactions, also appears to lose intensity with all the treatments.

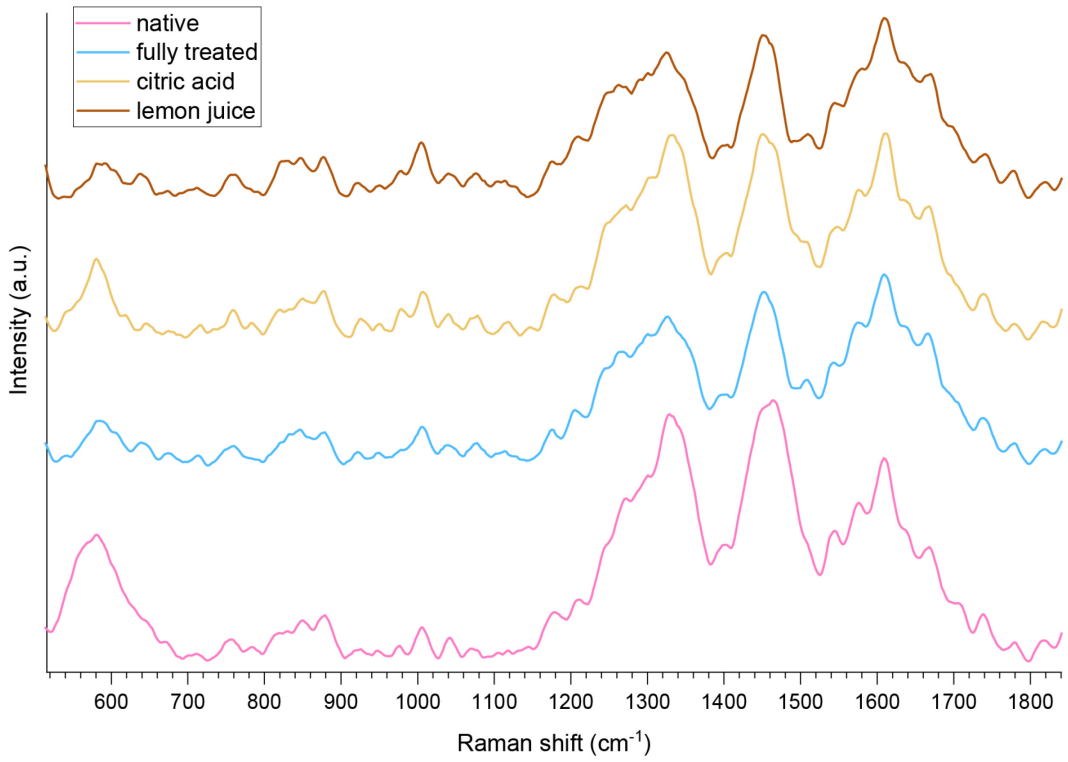

Figure 48 Raman spectroscopic investigation of the effects of the treatments
Raman spectra of native, fully treated by Chiara Vigo, citric acid and lemon juice *in-lab* treated *P. nobilis* fibers showing possible resonance peaks. Each spectra is the average of 7 spectra from different fibers.

7.6 Discussion

As stated by Chiara Vigo, her complete treatment affected both the mechanical properties and the color, turning the fibers from black to gold in the sunshine. There does not appear to be an associated change in amino acid composition; however, a clear decrease in Fe and maybe Al concentration was observed. Additionally, TEM imaging showed a possible change in structure spacing in the lateral direction, while FTIR and Raman spectra might show slight differences in particular chemical features. Part of these changes could be mimicked via in-lab treatment using lemon juice and citric acid, especially the color change; however, the mechanical properties did not completely reach those of the fibers treated by Chiara Vigo. These findings are summarized in Table 5. Interestingly, the different treatments had different effects on the mechanical properties and color, suggesting that these two

functional differences are determined by different biochemical features of *P. nobilis* byssus proteins. Therefore the rest of the discussion will be separated in three parts corresponding to the main changes occurring during Chiara Vigo's full treatment of byssus: the change in color, the decrease in initial stiffness and the increase in slope of the plateau of the tensile curve.

Table 5 Summary of the effect of the different treatments

Changesof the different properties and structural features in *P. nobilis* byssus associated with the treatments Ø= no difference to native fibers O=there is a difference, but weaker than for other treatment √= there is a clear/ significant difference. * the case of Ca is complicated, since part of it comes from crystalized sea water, and part seems to be bound within the fibers. **Mg and B in native from Villefranche are much lower than in the native fibers from Chiara, as low as in the instant treated fibers. The full treatment from Chiara and the in-lab lemon juice treatment increase Mg and B content, but the final concentration does not overcome the concentration in B and Mg in native fibers from Chiara Vigo. Therefore, the trend is unclear.

	Instant treated	Fully treated thread	Fully treated bisso trattato	In-lab lemon juice	In-lab citric acid
Yellowness	Ø	√	√	√	√
Redness	Ø	Ø	Ø	Ø	Ø
Initial stiffness	√	√	√	Ø	Ø
Yield strain	Ø	Ø	Ø	Ø	Ø
Yield stress	Ø	√	√	O	O
Plateau slope	√	√	√	√	O
Fe content	Ø	√	√	√	√
Ca content	Ø*	Ø*	√	√	√
Al content	√	√	√	√	√
Mg content	Ø**	√	O**	√	Ø
B content	√	O**	√	√	Ø
FTIR hydroxyl gr			√	Ø	Ø
TEM			√		
Raman peaks			√	√	O

7.6.1 Color change

All the fibers, native and treated, are situated in the reddish third of the CIE color plot. The native fibers given by Chiara Vigo and the instantaneously treated fibers are the same color; however, the fibers which were left 3 days in lemon juice ("fully treated"), and the fibers

called “bisso trattato” (treated byssus) by Chiara present a color which goes more toward yellow. The “unknown treated” sample seems to be exceptions, its color being much less yellow than the other treated fibers. A similar change in color could be obtained using lemon juice and citric acid *in-lab* treatment. Both *in-lab* treatments produced a similar color, which had the same yellowness than the byssus treated by Chiara Vigo, relatively to the white source, and no change in redness compared to native fibers. Table 5 is very useful for showing structural and compositional features of *P. nobilis* byssus showing a trend in their modification similar to the color change associated with the diverse treatments. Therefore, the part of Table 5 which is following the color modification trend is reproduced in Table 6.

Table 6 Color variation and other features following similar trends.
Biochemical/structural feature exhibiting a variation similar to the color change associated with the diverse treatments so far.

	Instant treated	Fully treated thread	Fully treated bisso trattato	In-lab lemon juice	In-lab citric acid
Yellowness	Ø	√	√	√	√
Redness	Ø	Ø	Ø	Ø	Ø
Fe content	Ø	√	√	√	√
TEM			√		
Raman peaks			√	√	O

The content in Fe seems to be well related to the threads yellowness: ICP shows a decrease in Fe after complete treatment by Chiara Vigo as well as after my in lab treatments involving both lemon juice and citric acid. Also, the resonance peaks observed on the Raman spectra follow the same trend, even though the change in peak intensity is a bit smaller in the case of citric acid treatment than for the fully treated and lemon juice treated threads. The signal observed in Raman spectroscopy recalls those of catechol, like DOPA in Mytilus byssus [137]. A wide range of pigments are based on DOPA[223–226] , which are able to interact with metal ions, making an argument for a pigmentary origin of the color. Moreover, catechol-Fe complexes emit in the blue-UV wavelengths[227]. TEM also shows a change, after treatment, of the spacing between the donut-shaped objects, probably representing the helical structures present in the byssus of *P. nobilis,* which is likely associated to a change in the structure of the helix or in the matrix material between the helical fibers.

7.6.2 Initial stiffness

The tensile curve of fully treated *P. nobilis* byssus fibers looks very similar to mechanically damaged native fibers, that is to say the second cycle during a cyclic tensile testing, with a reduced yield stress and initial stiffness. Therefore, the mechanism underlying the change in mechanics following the artisanal treatment might be similar and analogous to mechanical damage after yield (6.2.2). Interestingly, none of the other treatments led to a decrease in initial stiffness. Only FTIR and TEM show similar trends, even though the measurements need to be completed for the remaining treated fibers.

Table 7 Initial stiffness variation and features following similar trends
Summary of the biochemical features possibly associated to the decrease in initial stiffness due to the traditional processing of *P. nobilis* byssus fibers.

	Instant treated	Fully treated thread	Fully treated bisso trattato	In-lab lemon juice	In-lab citric acid
Initial stiffness	√	√	√	Ø	Ø
FTIR hydroxyl gr			√	Ø	Ø
TEM			√		

FTIR showed, however, that no drastic change in protein secondary structure happened after any of the treatments. However, the fully treated byssus exhibits a shoulder at 1730-1740 cm^{-1} which might indicate the presence of carboxylate groups in the treated byssus; however, it is unclear why they suddenly would appear in the treated threads. Since the initial stiffness was attributed to the stretching of the supramolecular helixes in chapter 6.3.1, the decrease in initial stiffness might be due to a decrease in stability of the helix, which could be caused by the breaking of some stabilizing bonds due to the full treatment of Chiara Vigo. Since a similar effect could not be reproduced with citric acid or lemon juice, another element of the treatment may to be responsible for the destabilization of the helix, most probably the saliva. The lavender could also play a role, but probably not the main one, since its use by Chiara Vigo is only occasional. Finally, the change in distance between the helixes observed in TEM cuts might reflect this effect, but could also be associated with a change of structure within the matrix proteins surrounding the helixes. Interestingly, the constancy on the yield strain gives a hint that the end of the elastic region is dictated by the maximal geometrical elongation of the helices, which does not seem to be influenced by the treatment.

7.6.3 Slope of the plateau

The slope of the plateau, interestingly, shows a similar increase after all the treatments, including the instant treated, even though the trend is much less clear concerning the citric acid treatment. The fact that the byssus fibers show an increase in plateau slope after all the

treatments but that only the fibers treated by Chiara show a decrease in initial stiffness are consistent with the conclusion of chapter 6, that the initial slope and plateau are controlled by different structural biochemical features, the first being attributed to the deformation of the supramolecular helixes, and the second to the breakage of sacrificial bonds and liberation of hidden length. The biochemical features following a trend similar to the change in slope of the plateau are reproduced in Table 8. Al content decreased for all treatments, as well as the intensity of the resonance peaks of the Raman spectra.

Table 8 Variation of the plateau slope and features following similar trends

Summary of the biochemical features possibly associated to the change in the slope of the plateau of the tensile curve from *P. nobilis* byssus after treatment.

	Instant treated thread	Fully treated bisso trattato	In-lab lemon juice	In-lab citric acid
Plateau slope	√	√	√	√	O
Al content	√	√	√	√	√
TEM			√		
Raman peaks			√	√	O

The decrease of the proposed unknown catechol resonance signal observed on the Raman spectra is weaker in the citric acid treated fibers than in the lemon juice and fully treated ones, suggesting that whatever is responsible for this signal (e.g. catechol-like molecules) are likely involved in the mechanical properties of the plateau. Interestingly, the slope of the plateau becomes steeper with the treatment. If some sacrificial bonds were already broken during the treatment, liberating some hidden length acting like worm-like chains, those might already get stretched during the plateau, thus increasing its slope. This hypothesis, however, should be further investigated. It is not quite clear yet if the change observed on the TEM picture is related to the change in slope of the plateau, nor what is happening with the concentration in Al. Since it is still as high in fibers treated by Chiara as in the native fibers from Villefranche, Al might not be linked with the change in plateau slope. An increase in yield stress could be observed for the complete treatment by Chiara Vigo, as well as maybe for our in-lab treated fibers. The yield stress is however highly depending on the behavior of the initials stiffness and the plateau. A steeper plateau seems to be associated with a smoother transition from the elastic regime to the plateau regime, and therefore leads to a decrease in yield stress. This effect is accentuated when the initial stiffness is reduced. The yield region being nothing else than the transition from one regime to the following, it does not make sense to look for other special biochemical features governing it.

7.6.4 Treatment action

In summary, the exposure to lemon juice of the traditional processing of *P. nobilis* byssus threads had the effect to change their color, giving them the goldish shade which made sea silk so valued in ancient times, but it also had a more practical effect. Indeed, from a functional point of view, the traditional treatment gives the fibers a softer and more flexible feeling by lowering their initial stiffness and yield stress, which may facilitate their knitting into fabrics and make these fabrics more comfortable on the skin. Interestingly, I was able to reproduce the change in color and in plateau stiffness by using a simplified treatment in the lab using lemon juice and citric acid. However these treatments did not affect the initial stiffness of the threads, therefore the destabilizing effect of the traditional treatment has to come from another of its constituents. The traditional treatment also involves saliva, which contains enzymes destined to digest food and denature proteins (proteolysis)[228] and which might destabilize the protein helix and induce the loss in initial stiffness associated with Chiara Vigo's treatment. Thus the processing of *P. nobilis* byssus fibers is a complex method which targets different specific features of the thread. By advancing the understanding of the structure-function relationship of *P. nobilis* byssus and its modification by the treatment, we might be able to fine tune each of the byssus features. This would be especially interesting for the eventuality of developing green material out of the byssus of pearl oysters, since it was observed to share the same structure than *P. nobilis* byssus and is a waste product of the pearl industry.

It is also interesting to note that this processing method was developed empirically through hundreds of years without any knowledge of *P. nobilis* byssus chemistry but is able to assess very specific chemical features of *P. nobilis* byssus which had not even been completely characterized yet, and that by taking advantage of the tacit knowledge, I was able to improve my scientific knowledge of the structure-properties relationship of *P. nobilis* byssus.

7.7 Conclusion

As stated by Chiara Vigo, the traditional treatment affected the color of the byssus but also its mechanical properties. This might partially be due to the effect of lemon juice which effectively removed certain metal ions probably involved in sacrificial bonds with some kind of chromophoric ligands. I could partially reproduce this effect in the lab using simple lemon juice or citric acid solutions. These chromophore-metal complexes may be involved in *P. nobilis* byssus color, however, the change in mechanical properties seem to be linked to another biochemical feature, and could not be reproduced completely in the lab. The saliva added by Chiara Vigo to her treatment might be responsible for the changes that could not be mimicked. The effect of the traditional treatment of *P. nobilis* byssus suggested the importance of the metal content for the color, but surprisingly, the change metal content could not really be linked to the modification of the mechanical properties. However, this last chapter also gives additional arguments for the proposed structure-function relationship proposed in chapter 6. It also shows that different aspects of the byssus properties can be

addressed separately using a specific treatment, which may be of importance in the eventuality of byssus as a green material for human application.

8 Work in progress and future directions

During this project, some experiments were started which could give more insight into the structure of *P. nobilis* byssus fibers, for example concerning the probable presence of a chromophore. However, these experiments would need to be pursued further in order to be able to draw conclusions and thus, lie outside the scope of the current thesis. However, since they might be useful for further work on *P. nobilis* byssus structure, they will be presented below.

8.1 Further analysis of the traditional treatment effect on *P. nobilis* byssus structure

8.1.1 XRD

As previously observed[34], XRD is a powerful technique to assess structure and structural changes in byssus, including *P. nobilis* fibers (section 5.2.2 and 6.2.4 of this work). Therefore I attempted to use XRD to characterize a possible change of the molecular structure of *P. nobilis* byssus, however the intensity coming from the treated fibers is so low that only one good diffraction pattern was obtained, and two additional ones had an extremely low intensity, so that these experiments should be repeated.

At first sight, the diffraction pattern of treated fibers shows a signal similar to native *P. nobilis* byssus fibers, with reduced intensity (Figure 49), and the partial or complete absence of signal coming from the helical structure in the SAXD region, maybe due to the very low signal intensity, out of the only three spectra which could be recorded, one of them which showed half of the helix peaks, the other two which did not exhibit any.

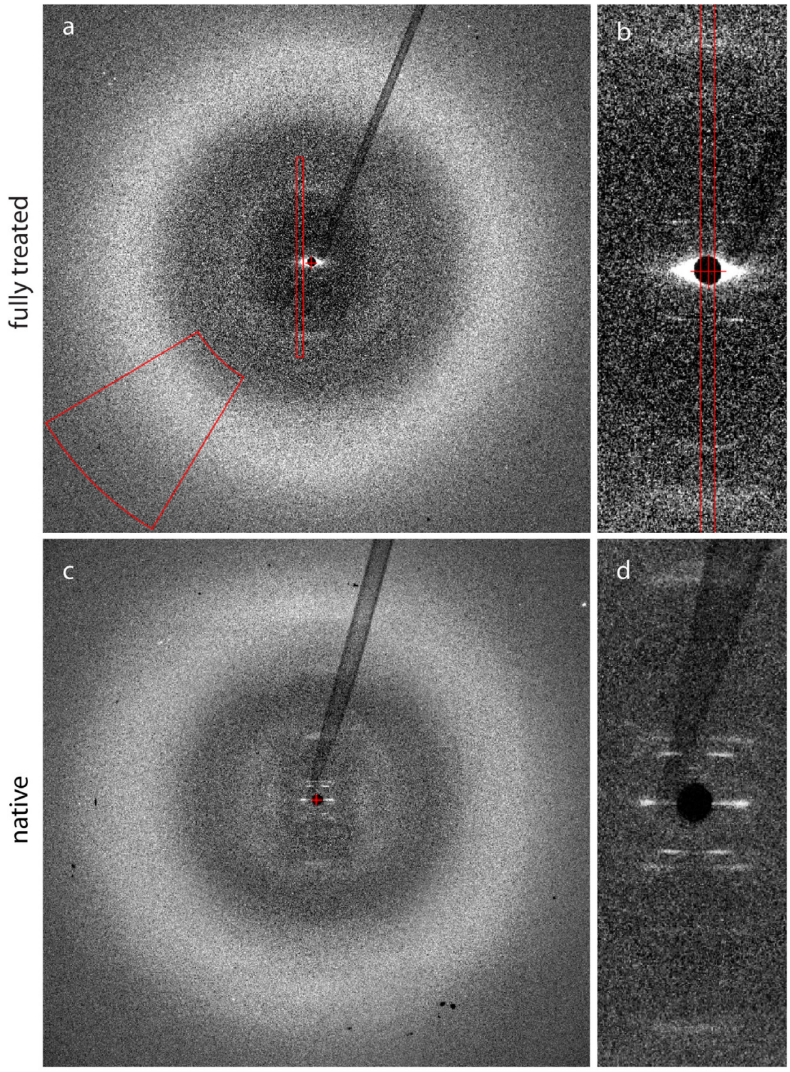

Figure 49 XRD investigation of traditionally treated byssus
WAXD (a) and SAXD (b) of treated *P. nobilis* fiber look very similar to WAXD (c) and SAXD (d) from native fibers.

Cake integrations were performed in the meridional and equatorial directions in order to assess the peaks positions (Figure 50a and b, respectively) in the WAXD area. As observed in chapter 6, the mechanical properties of treated fibers resemble those of mechanically damaged native fibers, therefore I compared the obtained spectra of treated fibers with those of un-stretched native fibers but also spectra of stretched fibers, in order to observe any resemblance or differences between these two causes (treatment and mechanical damage) leading to similar tensile properties (Figure 50d).

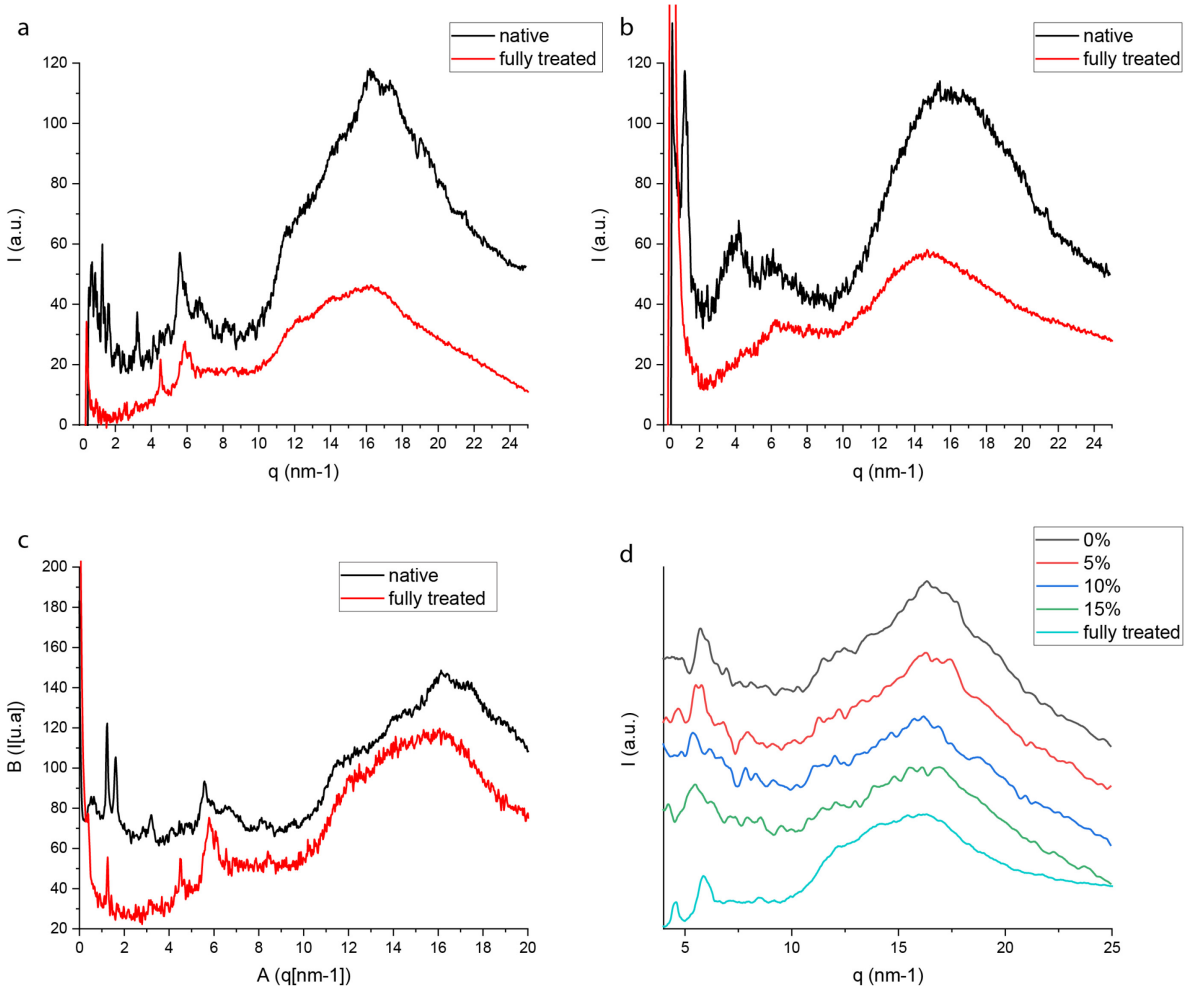

Figure 50 Integrated XRD spectra of traditionally treated byssus

Comparison of integrated XRD spectra of treated fibers with native byssus and mechanical damage thereof. Meridional (a) and equatorial (b) cake integration of native and treated WAXD signal. Line integration allows the observation of the SAXD signal coming from the helical structure of *P. nobilis* byssus in native and sometimes treated threads (c). The cake integration of treated fiber was also compared to the results obtained during in situ tensile testing (d).

The peak at 4.54 nm^{-1} has an intensity relative to the peak at 5.7nm^{-1} higher in diffraction pattern of treated fiber than in native ones, but does not seem to exhibit a shift in position. The 4.54 nm^{-1}peak is very weak in native byssus fiber, and disappears with the stretching. The peak at 5.7 nm^{-1} might be shifted to slightly bigger q values, thus smaller distances, after treatment whereas it gets shifted to smaller q values during fiber stretching. It is seems that

the bump/small peak observed at 3.2 nm^{-1} in native fibers, which starts to move around 15 % strain in tensile testing, is not visible in treated fibers. The peaks at 6.7 and 8.2 nm^{-1} present on native fibers also disappeared in treated fibers. Line integration (Figure 50c) confirms that when helix signal is present, there is only the third order, which is the brightest diffraction peak in native fibers. Its place probably did not change significantly compared to native fibers (q=1.25 vs 1.23 for native), however, further measurement would allow confirmation.

While it is not clear if there is a real change in the SAXD signal after treatment, or if the disappearance of the signal is due to the overall lower intensity, the WAXD region presents a clear change in shape associated with the treatment. The shoulders in the WAXD signal around 11.6 and 14.06 nm^{-1} remained after treatment, but the two peaks at 16.2 and 17.3 nm^{-1} also disappear after treatment, as well was the shoulder about 19nm^{-1} (Figure 50). This is more drastic than what occurs during fiber stretching, even though the shoulders at 11.6 and 14 nm^{-1} also tend to get more prominent when the fiber is stretched, because the signal coming from the area between 14.5 to 22nm^{-1} is losing intensity with the stretching.

8.1.2 TEM

A correction of the staining method of *P. nobilis* byssus threads allowed the observation of a banding pattern on both native and fully treated fibers, with no difference in size: each combination of light and dark part measures 161(±15) nm in native threads and 162(±5) nm in treated threads (Figure 51a and b, respectively). It is not completely impossible that these patterns are related to the alternation of stiff and soft phase suggested by the mechanical investigation in section 6.3. However, this is not the only explanation for such a pattern, and this should be investigated further, for example using Ultra High Resolution transmission electron microscopy energy-dispersive X-ray spectroscopy (UHRTEM-EDX) to observe an possible difference in organic composition between the dark and light parts of the banding pattern.

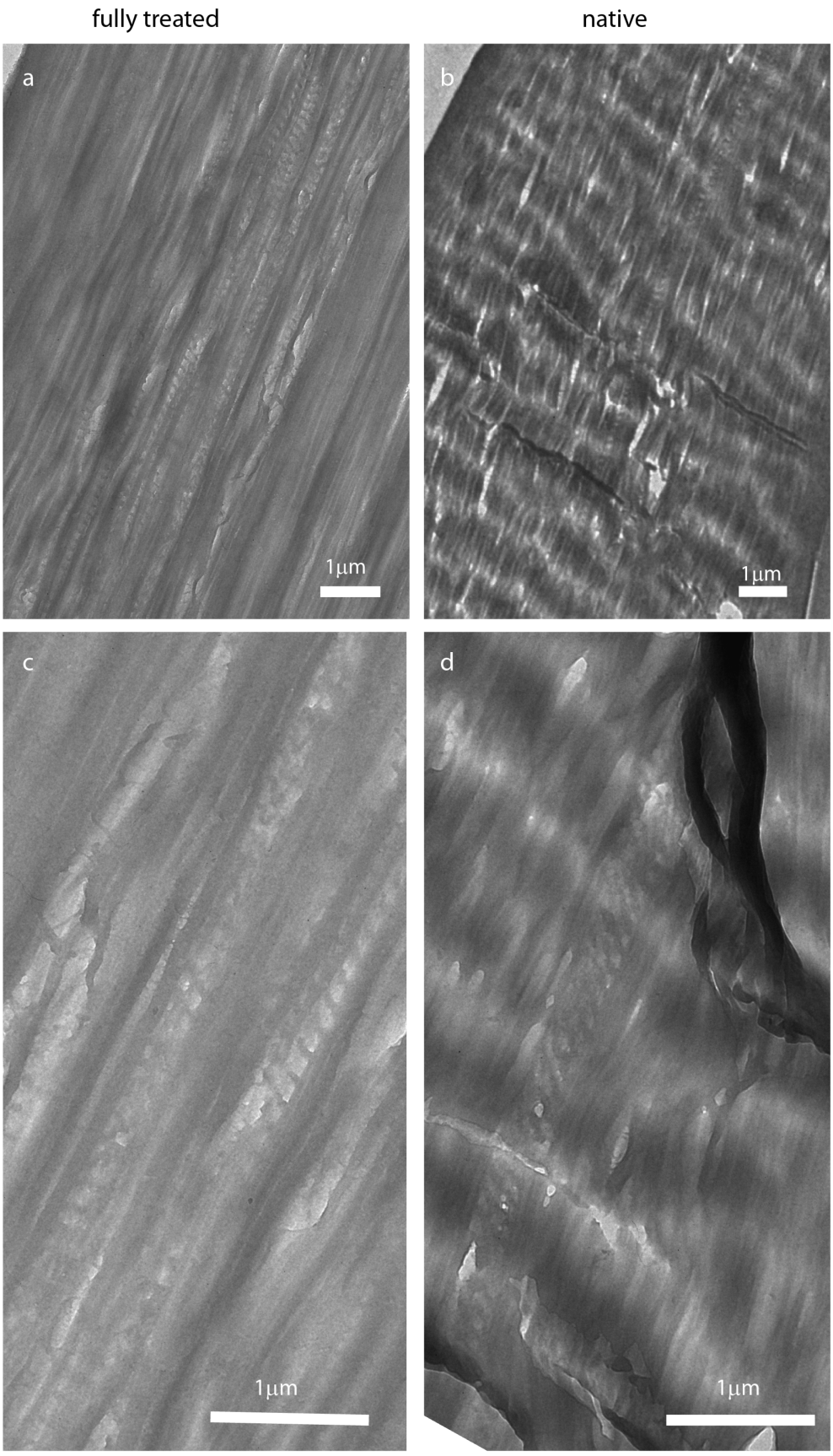

Figure 51 TEM of longitudinal cuts of native and treated byssus.
A corrected staining of fully treated and native *P. nobilis* byssus fibers showed a banding pattern on TEM pictures of longitudinal 70 µm thick cuts.

8.2 Catechol isolation using affinity chromatography

As DOPA plays a huge role in Mytilus byssus, and Raman spectroscopy gave a possible indication of the presence of a chromophore in the byssus of *P. nobilis*, I used affinity chromatography to purify possible catechols from byssus fibers of *P. nobilis*, using Boronate gel which specifically binds to cis-diols of sugars and catechols.

Therefore, about 0.01 g byssus fibers were hydrolyzed as for amino acid analysis, freeze-dried overnight and suspended in 1ml of phosphate buffer. The re-suspended samples were run through an Affinity column filled with Boronate gel (Affi-Gel Boronate Gel, Bio-Rad®), prepared according to the standard protocol as showed on Figure 52. The samples collected after elution were freeze dried overnight, re-suspended in 6 N HCl (37 %, Carl Roth, ROTIPURAN) and analyzed for amino acid composition as described in section 4.

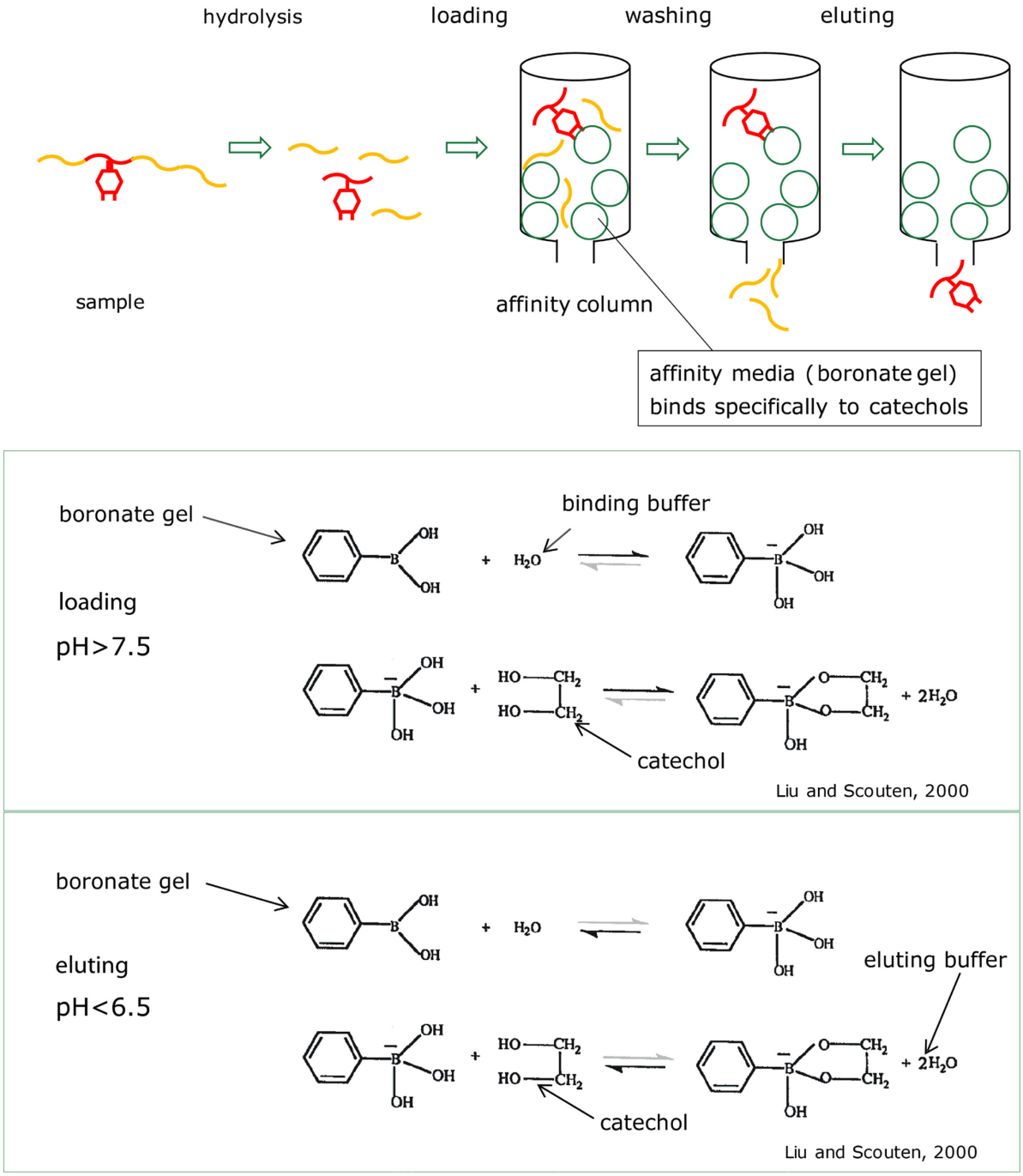

Figure 52 Principle of affinity chromatography.

After affinity chromatography, the consecutive amino acid analysis showed that only a very small amount of DOPA was present, but that the sample presented a high signal at the time corresponding to His (Figure 53). However, affinity chromatography with boronate gel is highly selective and not binding to His. Moreover, a closer look at the peak in the histidine region shows that the peak from the samples are slightly shifted to lower times compared to the reference, which is an additional hint that another catechol might be present but cannot be measured in the amino acid analyzer because it comes out almost at the same time than histidine. Alternatively, peak may arise from sugar groups, since they are also able to bind to boronate affinity columns, and there might be some in the byssus of *P. nobilis*. Indeed, I measured that the amino acid content in the thread was about 80% (section 5), Pujol et al.

detected the presence of carbohydrates[141] in *P. nobilis* byssus, and sugars have been observe to play a role at the interface between byssus and soft tissue in the byssus of the closely related species *A. pectinata*[154]. However, in the case of a sugar group, it would need to present an amine group in order to react with the ninhydrin used in the post-column functionalization during amino acid analysis. In any case, because of the presence of this unknown compound, the amount of histidine measured in whole *P. nobilis* byssus samples is probably over-estimated because of overlap with the histidine peak and that of the mystery group that binds the boronate column. Further analysis of the purified compound using Tandem Mass Spectroscopy should allow its identification.

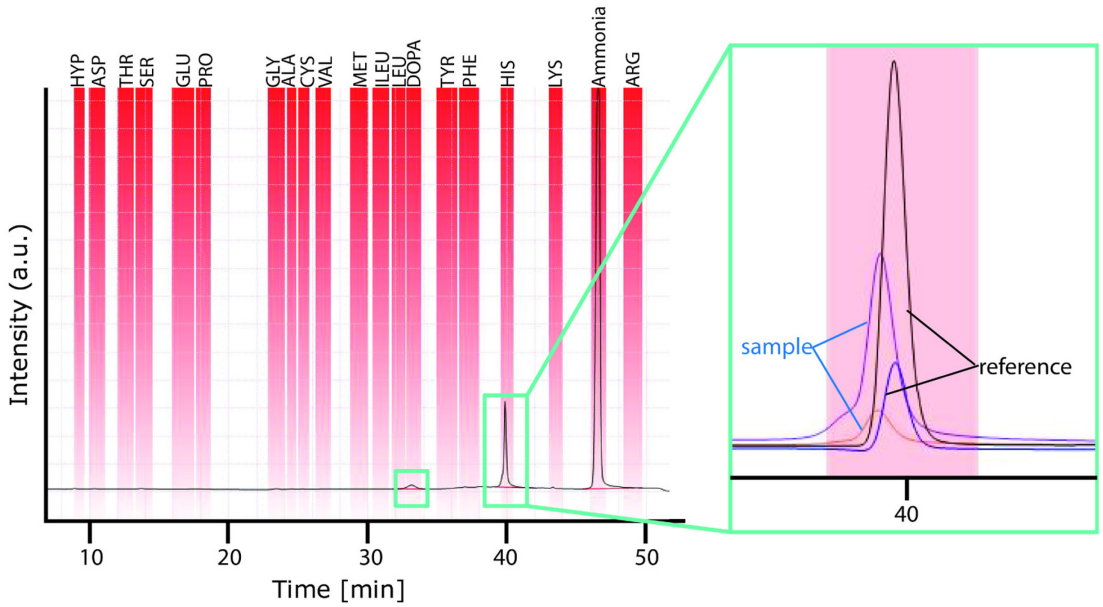

Figure 53 Results of amino acid analysis after affinity chromatography with boronate gel.
A very small DOPA peak could be observed, and a higher peak in the Histidine time area (left panel). However, a magnification of this peak (right panel) shows that the peak originating from the sample is slightly shifted toward smaller times.

8.3 The adhesive plaque

DOPA is mainly found in the cuticle and the adhesive plaque of *Mytil*us byssus[187], which already inspired bio-mimicking biocompatible glues. Analogous to *Mytilus* byssus, *P. nobilis* byssus fibers are also terminated by an adhesive plaque. Even if the adhesive plaque of *P. nobilis* byssus does not play a role as big as the adhesive plaque of *Mytilus spp*, it is able to stick to wet surfaces as well, like roots, shell debris or even sand grains[126]. Therefore, it is also of interest to investigate, according to the important principle of comparative studies. Here I present the findings from an initial investigation of *P. nobilis* byssus adhesive plaque using SEM, ICP-OES, Amino acid analysis and X-ray fluorescence spectroscopy (XRF).

8.3.1 Structure : SEM

The morphology of *P. nobilis* byssus adhesive plaque is quite different from the plate-like shape of Mytilus byssus adhesive plaque. *P. nobilis* byssus plaques are more arrow-shaped (Figure 54 a and b).

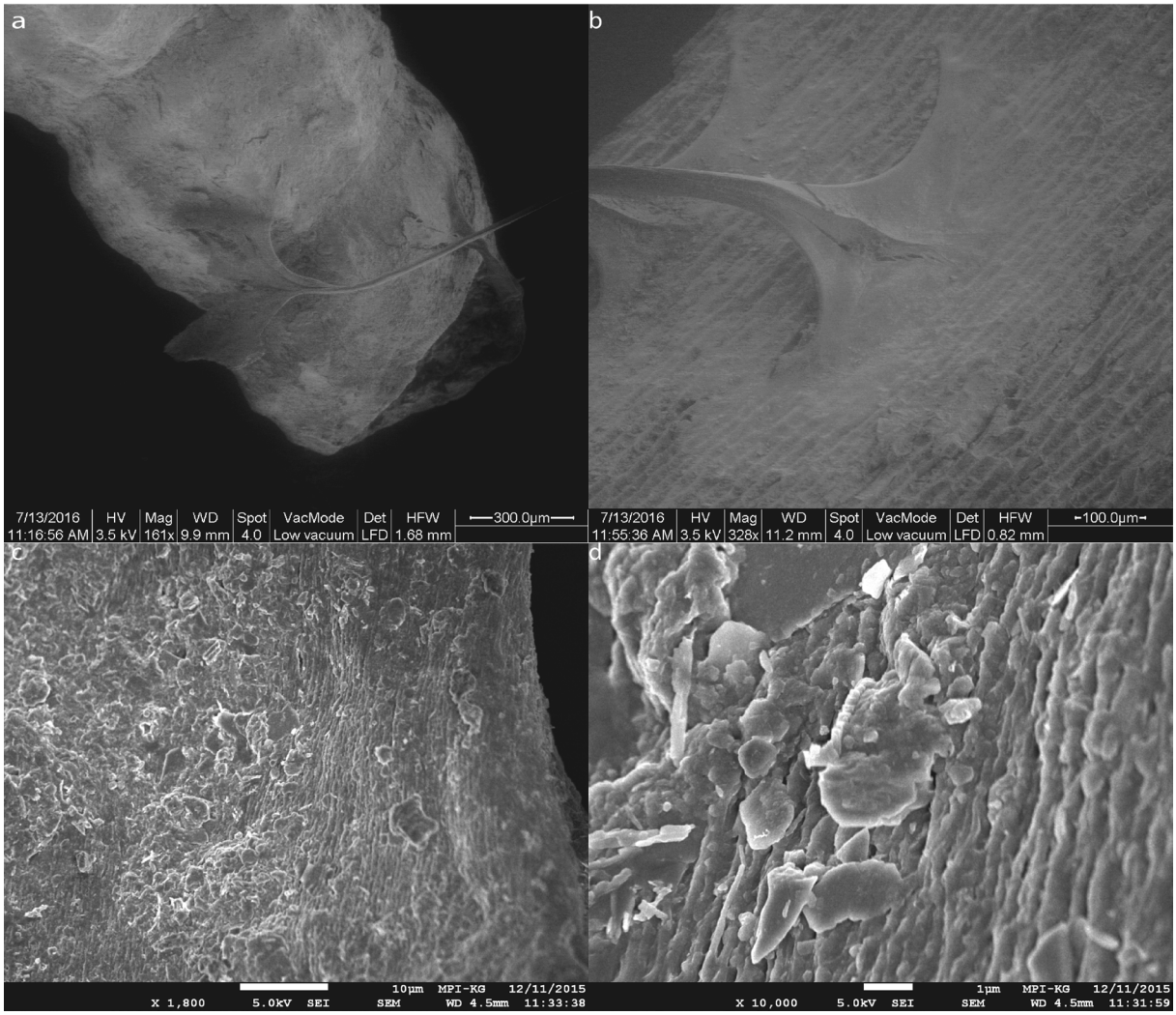

Figure 54 SEM investigation of *P. nobilis* byssus adhesive plaque
P. nobilis byssus plaque (a and b) has a unordered structure (c and d)

8.3.2 Organic content: Amino acid analysis

In *Mytilus*, the organic composition of the plaque differs from the thread[229]. Amino acid analysis might show a difference in composition between plaques and threads. However, this needs to be repeated in order to get statistics. If the differences are real, the plaques seem to contain more Gly and Leu, and the threads contain more Ser, however, neither the thread nor the plaque contains DOPA. Since DOPA is thought to play a major role in *Mytilus* adhesion[187,230]. *P. nobilis* byssus has to rely on another compound for its adhesion, giving further arguments to pursue the efforts toward the identification of the unknown catechol,

the presence of which was suggested by diverse techniques including Raman and Affinity chromatography (sections 7 and 8.2). Also interesting to notice, the plaque seem to have a slightly higher concentration in hydrophobic amino acids than the threads (more Gly, Leu, Ala, Phe, Gly, even if less Val, Met, Pro): they make up 48.4 (±1.1) % of *P. nobilis* byssus thread, and 52.7 % of the adhesive plaque (Figure 55).

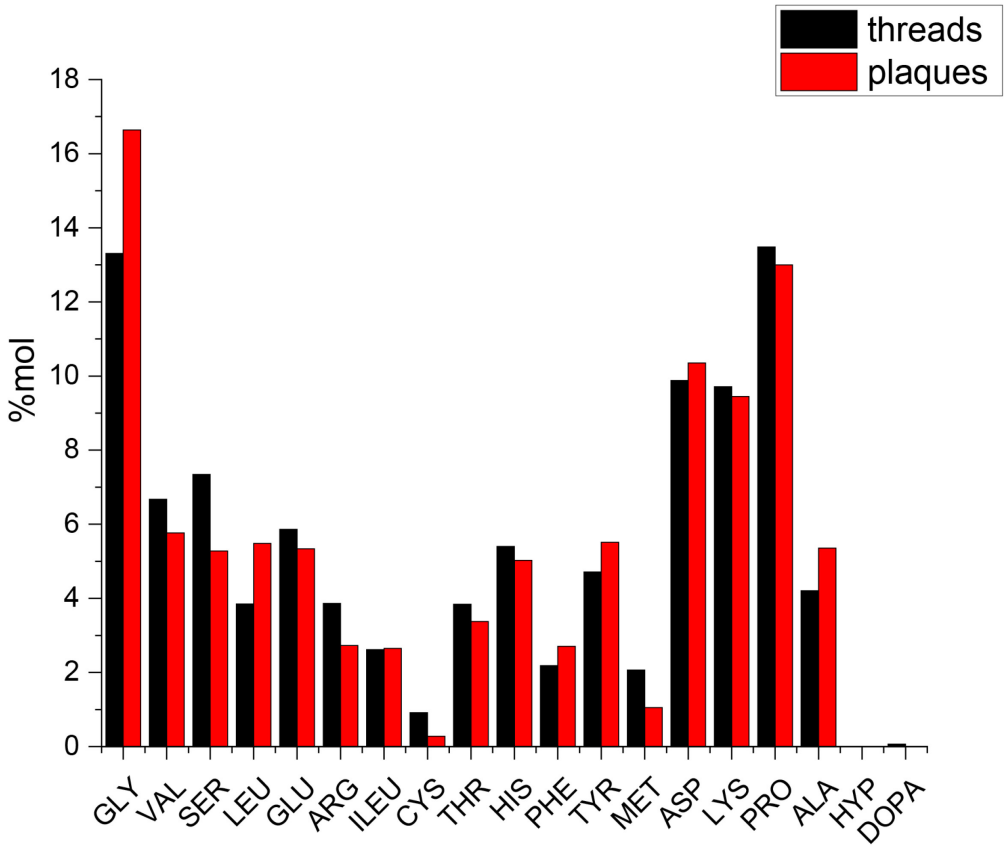

Figure 55 Amino acid analysis of adhesive plaque and thread of *P. nobilis*

Amino acid analysis might shows differences in composition between thread and plaque *in P. nobilis* byssus. However, the amount of plaques gathered was not enough to repeat this analysis.

Except the difference in Gly and Leu, there does not seem to be any significant difference in composition between plaques and thread. There is also no clear difference in the ratio of hydrophobic, polar, uncharged/acidic and basic amino acids between plaque and thread (Table 9).

Table 9 Repartition of the amino acid types in plaque and thread

Repartition of hydrophobic, polar, uncharged/acidic and basic amino acids in the thread and the plaque

	Thread (%mol)	Plaque (%mol)
hydrophobic	48.4(±1.1)	52.7
polar uncharged (without Asp and Glu)	16.8(±0.9)	14.4
uncharged/acidic (Asp+Glu)	15.8(±0.2)	15.7
basic	19.0(±1.2)	17.2

8.3.3 Inorganic content: ICP-OES

While this needs to be repeated for statistics, ICP-OES showed that the plaques contain 10-20 times more inorganic ions than the threads, especially Fe and Al (Figure 56), which interestingly are the metal that are removed during the traditional processing of *P. nobilis* byssus, and thought to be bound to the chromophore, which is therefore thought to be present in *P. nobilis* byssus fibers (section 7.6). This gives an additional argument to continue the research for the identification of the unknown catechol in *P. nobilis* byssus.

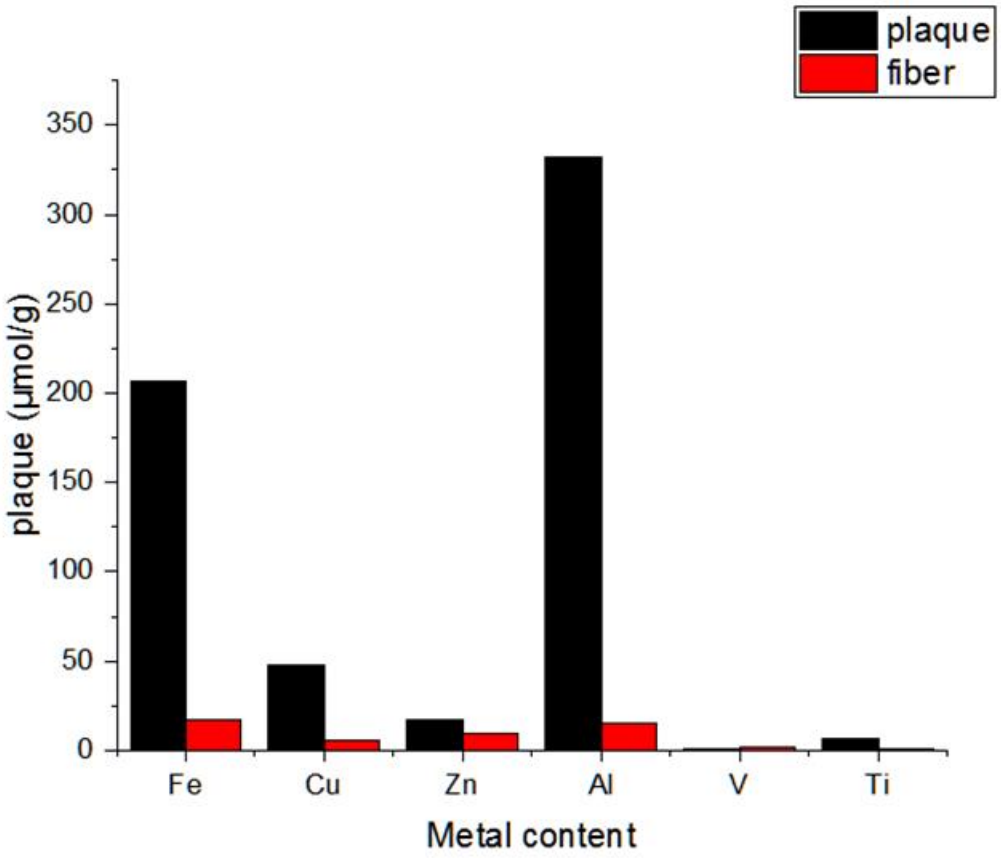

Figure 56 ICP shows that the plaques contain a lot more metals than the fibers
The content in Fe and Al is especially much higher in the plaque than in the thread (there are no error bars because plaques were not enough for several samples)

8.3.4 Metals localization: XRF

Micro X-ray fluorescence mapping[231] was performed in the BLiX lab of Prof. Kanngießer by Dr. Ioanna Mantouvalou and Tobias Drechsel. It was used to localize the inorganic elements along the fiber. XRF showed that the concentration in S, probably associated with amino acids like Cys or Met is present along the whole fiber (Figure 57a), whereas the concentration in Fe, Si and Ti is much higher in the plaque (Figure 57b, c and d).

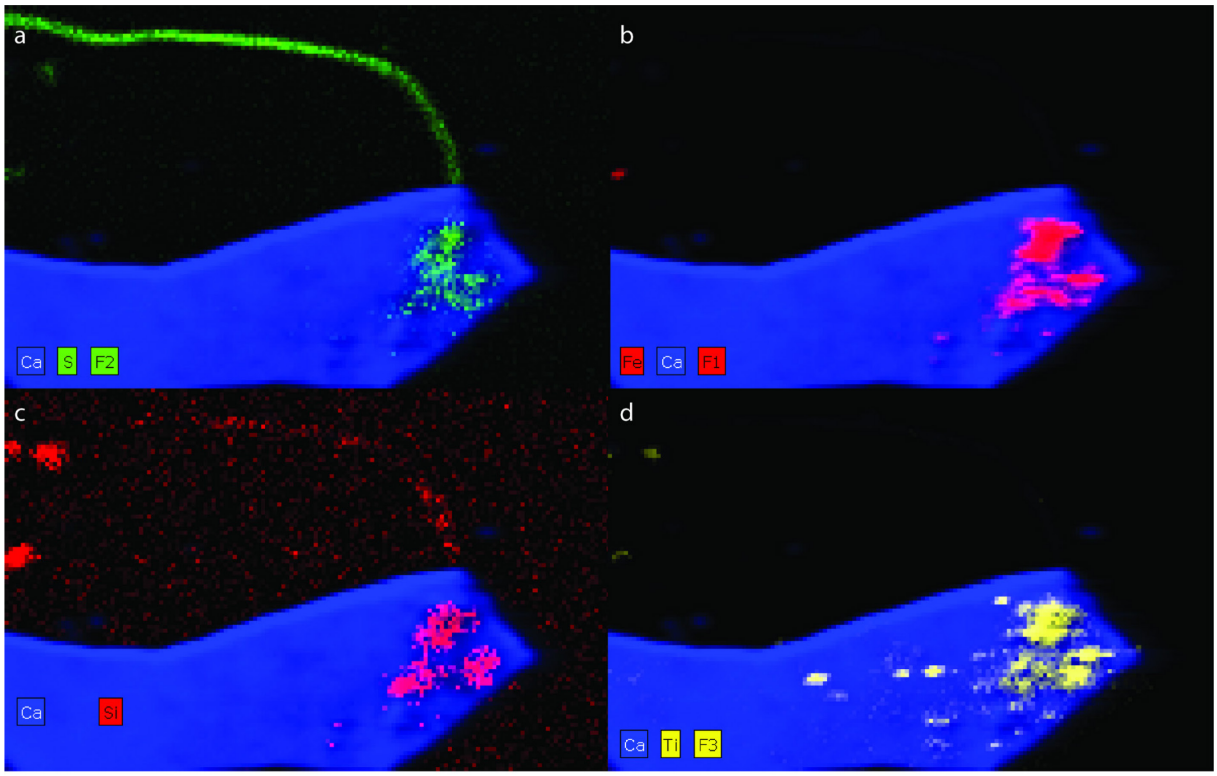

Figure 57 XRF mapping of inorganics along a byssus thread
Map of a *P. nobilis* byssus fiber attached by its plaque to a shell fragment. The latter appears violet due to its high Ca content. Panel a) shows the repartition of S along the fiber, b), c) and d) shows that Fe, Si and Ti, respectively, are more strongly concentrated in the plaque than in the thread.

8.4 Discussion

The absence in DOPA in the adhesive plaque of *P. nobilis* coupled with a high concentration in metals strongly argues for the presence of another compound playing a role similar to DOPA in Mytilus, in particular regarding mechanical properties of the cuticle and adhesion. These findings corroborate the presence of an unknown catechol found with affinity chromatography, thus opening very interesting perspective in the field of bio-mimicking. Indeed, DOPA is fascinating due to its water adhesion abilities, and hydrogels and glues were created using DOPA for adhesion and self-healing[45,187,189]. According to the principle of comparative studies, the finding of another amino acid modification able to perform underwater adhesion might greatly advance the research in this field.

8.5 Outlook

Despite the exciting first results presented in this thesis, research about the byssus of *P. nobilis* is still quite new and some aspects of this work need to be improved, completed or deepened. For example, further high resolution TEM and X-ray studies have to be made in order to determine the nature of this stiff phase that was deduced from the mechanical testing but could not be observed so far. Perhaps use of an even more coherent beam line with higher energy would allow the observation of more peaks on the XRD diffraction patterns. The usage of an Argon tube or any other way to avoid air scattering could also improve the quality of the spectra and allow better interpretation, more precise size

measuring and maybe the discovery of additional structural features. Transcriptome and comparison with the protein extracted from the byssus should allow us to identify the proteins present in *P. nobilis* byssus and from then, by comparison with other organisms where they are present, one might be able to tell what structures they usually build and which proteins are likely to constitute the stiff phase. Simulation could allow the determination of the folding of the proteins (secondary structure). This transcriptomic/proteomic approach would also allow the identification of the post-translational modifications in the byssus of *P. nobilis* and identify the "unknown catechol/chromophore". Also the results of affinity chromatography are still not clear, and the presence of a much higher Tyr content in the proteins of the gland than in the byssus would tend to indicate the presence of a post-translational modification of Tyr, either DOPA or something very similar. UHRTEM EDX could give information on the repartition of the inorganic material in the structure observed in TEM, and thus provide useful information concerning the localization of possible sacrificial bonds based on metal-protein complexes.

With the additional chemical knowledge provided by obtaining a protein sequence, it might be possible to isolate single superprotein helices from *P. nobilis* byssus, or produce them recombinantly, and perform single molecule atomic force spectroscopy to determine the exact mechanical properties of this building block. Furthermore, isolation/production and crystallization of the building blocks is very complicated, but would be incredibly informative, because it would permit the exact determination of their tertiary structure using single crystal XRD (Protein X-ray Crystallography). Concerning the structure-function relationship, *in-situ* cyclic tensile testing combined with XRD would allow determination of what is happening when the byssus has been damaged and the sacrificial bonds broken: does this prevent the helix to refold or not? If the helix was not refolding, it means that the sacrificial bond were probably within the helix. Moreover, some additional experiments could be done to gain a better understanding of the structure and the modification associated with the treatment. A metal recovery experiment using the treated threads would allow the confirmation of the hypothesis of the responsibility of the metal removal in the change of color. Finally, concerning the comparative study of byssus structure-function relationship, many more bivalve species should be studied in depth, as distant as possible from Ostreidea and Mytilus to confirm the nature of the key features of byssus in order to be able at some point to design bioinspired recombinant byssus materials offering relevant mechanical properties.

Additionally, the investigation of the knowledge associated with the traditional processing of *P. nobilis* byssus not only aids in the preservation of this historical practice, but also gives helpful insights on how to modify the mechanical properties and the appearance of byssus using a cheap ecological process. The first results presented in this work lead to think that with similar treatments and a better knowledge of its exact effect, it is possible to target very precise part of the mechanical properties, making natural byssus a fine-tunable material. Further investigation of the effect of the saliva on the thread mechanics should be

performed, and similar processing could also be tried on *Pinctada* and *Mytilus* byssus, with the aim to get a deeper understanding of byssus processing and be able maybe to use byssus form the pearl and food industries to create sustainable materials directly out of these waste products.

9 Conclusion

Considering that oil reserves are drastically decreasing and the environment increasingly threatened due to plastic waste, natural fibers have an important role to play, both as a traditional non-petroleum based material and as inspiration for new sustainable and high-performance alternative to today's plastics. Along these lines *P. nobilis* byssus fibers are especially interesting due to their traditional usage as valuable, light and warm clothing material on one hand and on the other hand as an inspiration for the development of new green materials due to the remarkable mechanical properties of byssus fibers, among others. However, the high mechanical properties of natural materials originate from their highly hierarchical structures; therefore the understanding of structure-function relationship is crucial for the understanding of natural materials. Moreover, comparative study is highly useful for identifying, among the numerous features of natural materials, which ones determine the properties and the features originating from individual variations among different species without real impact on the properties of the considered material in order to extract design principles.

For all these reasons, I performed, in this work, a study of structure-function relationship of the byssus fibers of *P. nobilis* in comparison with other bivalve species in order to understand the byssus of *P. nobilis* in the aim of extracting design principles for the development of bio-mimicking materials, but also in regard of its traditional usage as clothing material. Most traditional natural fibers, like flax hemp and silk for example, required an empirically developed treatment in order to adapt them for human usage and *P. nobilis* byssus is no exception: it had to be processed according to an ancient artisanal recipe to produce a change in function from underwater anchoring fibers to valuable soft and gold-shimmering pieces of clothing. This tacit knowledge offers a great insight toward a better understanding of *P. nobilis* byssus structure-function relationships. Therefore, this work also aimed at understanding the effect of the traditional processing on structure and properties the byssus of *P. nobilis*, which is interesting from a cultural point of view in order to record this tradition for the probable case where it will soon completely disappear, and also regarding the chemical modification of byssus material for human application. Thus this thesis had a double purpose: first study the structure-function relationship of the byssus of *P. nobilis* and compare it with other related bivalves, and second, study the effect of the traditional byssus treatment on these newly discovered properties.

Accordingly, I started by assessing the structure of *P. nobilis* byssus and compared it to the byssus of other bivalve species with different degree of relatedness: *A. pectinata*, which belongs to the same family as *P. nobilis*, *P. fucata* and *P. margaritifera*, which belong to the same order but different superfamily, and *Mytilus spp*, which are even more distantly related, since they belong to a different cohort. This permitted us to find out that Ostreida bivalves (*P. nobilis*, *A. pectinata* and *Pinctada spp.*) have a common building block made out of multiple globular proteins assembled into a helix. These helical building blocks were embedded in some kind of matrix material and highly aligned along the fiber‘s axis, however,

they were organized in a different way in the different species, grouped in bundles or not, with various bundle size. This difference in arrangement was also associated with a difference in ratio helixes/matrix material. Additionally, the findings of this structural study gave further arguments in favor of a probable convergent nature of byssus evolution, with different orders of Bivalves coming up with different building blocks to produce a similar tissue with similar functions because it is a highly effective strategy to survive and anchor in their environment. Finally, the comparative structural study showed that the building block used in the byssus was related to the order of the considered bivalve, while the macroscopic shape of the byssus was probably related to the anchoring mode used by the byssus: attachment for mussels living on hard substrates versus entanglement for mussels living in soft substrates. A few thick threads covered by a protective coating against abrasion being more adapted for attachment on hard substrates, whereas a high number of thin and long threads is more adapted to the entanglement anchoring mode efficient in soft substrates.

As a second step, the mechanical properties of *P. nobilis* byssus were investigated using single fiber tensile testing combined with *in-situ* XRD measurement, allowing to relate the mechanical properties to the structure discovered during the structural study, which allowed to understand their relationship but also to refine the model of the structure of *P. nobilis* byssus. First, a model could be established for the deformation mechanism: the helical macroprotein building block stretches like a spring during the first elastic part of the tensile curve. Then a plateau is reached in the tensile curve, during which some sacrificial bonds open, liberating some hidden length. The plateau is followed by a second stiffening, probably due to the worm-like chain stretching of the liberated hidden length. This is terminated by a second yield point associated with more damage to the material. Additionally, cyclic or fatigue testing showed semi-permanent damage caused to the fiber when stretched above the first yield point. Similarly to the well-studied *Mytilus* byssus, the byssus of *P. nobilis* partially recovered its initial mechanics after a resting period, in a self-healing process probably due to the reformation of the sacrificial bonds, which is not instantaneous. In addition, the assessment of the structure-function relationship of *P. nobilis* byssus fibers suggests the presence of an additional load-bearing structure within the byssus, which is stiffer than the observed globular proteins helixes. However it could not be observed so far. Moreover, this investigation of the function of *P. nobilis* byssus also allowed us to draw parallels with the deformation mechanism of the well-characterized Mytilus byssus, namely the importance of hierarchical structure, hidden-length and sacrificial bonds.

Finally, the last part consisted in the investigation of the traditional processing of *P. nobilis* byssus into sea silk on its structure and properties, so that it allows a change of function, from an underwater anchoring material, to a soft and elastic fiber for clothing production. This study showed that the treatment was responsible for the goldish color of sea silk, which caused this material to be so valued, especially in the ancient times. I also discovered that this artisanal processing reduces the stiffness of the fibers, which probably improves their workability and the comfort of sea silk clothing. The structure-properties comparison of

treated versus native fibers showed a probable involvement of metal-protein complexes in the change of color. The usage of a simplified *in-lab* treatment revealed that the change in mechanical properties had probably other origins than the modification of the color, and confirmed that the initial elastic region of the tensile curve, and the following plateau were governed by different key features of the biochemical structure of the fibers. Moreover, it also put in evidence the probable role of saliva in the initial softening of *P. nobilis* byssus by destabilizing the supramolecular helixes.

In summary, this work has led to the discovery of a previously unidentified paradigm in nature for building bulk fiber materials using helices made of globular proteins. This is a structure observed in muscles proteins and bacterial Pili for example, but has never been observed in a macroscopic extra-organismic material so far, and is completely different from the collagen-like building blocks of *Mytilus* byssus. However, *P. nobilis* and *Mytilus spp.* byssus share some common features, including sacrificial bonds and hidden length, which are crucial for their mechanical properties. These findings give arguments in favor of a convergent evolution of Bivalve byssus, as it is thought to be the case in silk as well[94]. By getting an idea of the structure of *P. nobilis* byssus and other Ostreida species, I observed that some features seem to be common to bivalves from different cohorts, having different building blocks, based on the comparison of *P. nobilis* and *Mytilus* byssus. These common features can be thought to be key features in byssus design and are probably common to all types of byssus. For example, all the species studied thus far seem to have a similar byssus macro-design comprise of fibers terminated by adhesive plaques; however, the presence of a stem and a proximal part seem to be specific to *Mytilus* byssus. All studied byssus fibers so far (including *T. maxima*[122]) exhibited a highly aligned fibrillar structure, even if their building blocks differ. A viscoelastic behavior dictated by the presence of sacrificial bonds and hidden length also seems to be a common feature so far, even if they can originate from different structural or chemical elements of the proteins or their higher scale organization. Both *P. nobilis* and *Mytilus* byssus possess two structural phases, one stiff and one softer, however, it has not been observed for the byssus of *T. maxima* so far[122], and I can only suppose it is the case for the other Ostreida mussels due to their similarity with *P. nobilis*. Finally, these features were responsible for a common high toughness and ability to self-heal after damage.

In addition to information about structure-function relationships, I gained insight on the effect of the ancient processing of *P. nobilis* byssus into sea silk and show that it goes beyond folklore. Indeed this long evolved piece of tacit knowledge results in a biochemical modification inducing a measurable change in both color and mechanical properties of *P. nobilis* byssus, probably in part by removing metals ions due to the low pH of the soaking solution. Like the processing of other natural materials (silk and plant-based fibers like flax and hemp), this process is specific to the nature of the fibers and allows a real change in function to adapt it to human needs. This was especially interesting considering the lack of knowledge on the structure and chemistry of *P. nobilis* byssus, and the completely empirical

nature of this processing, which led to this process being seen as mysterious and almost magical.

With these conclusions, this work provides a small extension of the general knowledge of natural materials structure-properties relationship in general, and of Bivalve byssus in particular, by adding a structure never observed before to the library of ways of building mechanically resistant natural fibers. I also gained a broader perspective on the evolution of mussel byssus and could extract some key design principles, which are of main importance in the perspective of developing bioinspired high properties protein-based sustainable materials. Moreover, understanding of the effect of the traditional processing on *P. nobilis* fibers will allow to preserve the knowledge empirically evolved for centuries, but also provides ideas to process *Pinctada* and *Mytilus* byssus, which are waste product from the food and pearl industries, in an easy and green way for human applications, or to modify the properties of other natural or synthetic protein material based on similar protein-metal interactions.

10 References

1. Ambrose, S. H. Paleolithic Technology and Human Evolution. *Science* **291**, 1748–1753 (2001).
2. Oakley, K. P. *Man The Tool Maker*. 115–118 (1943).
3. George B. Kauffman. Wallace Hume Carothers and Nylon, the first completely synthetic fiber. *Prod. Chem.* **65**, 803–808 (1988).
4. Aftalion, F. *A History of the International Chemical Industry*. (Chemical Heritage Foundation, 2001).
5. Fisher, C. H. History of Natural Fibers. *J. Macromol. Sci. Part - Chem.* **15**, 1345–1375 (1981).
6. Geyer, R., Jambeck, J. R. & Law, K. L. Production, use, and fate of all plastics ever made. *Sci. Adv.* **3**, (2017).
7. Heim, M., Keerl, D. & Scheibel, T. Spider Silk: From Soluble Protein to Extraordinary Fiber. *Angew. Chem. Int. Ed.* **48**, 3584–3596 (2009).
8. Kim, J. Cellulose as a Smart Material. in *Cellulose: Molecular and Structural Biology: Selected Articles on the Synthesis, Structure, and Applications of Cellulose* (eds. Brown, R. M. & Saxena, I. M.) 323–343 (Springer Netherlands, 2007).
9. Gilligan, I. The Prehistoric Development of Clothing: Archaeological Implications of a Thermal Model. *J. Archaeol. Method Theory* **17**, 15–80 (2010).
10. Kvavadze, E. *et al.* 30,000-Year-Old Wild Flax Fibers. *Science* **325**, 1359–1359 (2009).
11. Sagona, C. Two-needle knitting and cross-knit looping: early bronze age pottery imprints from anatolia and the caucasus. *Oxf. J. Archaeol.* **37**, 283–297 (2018).

12. Leuzinger, U. & Rast-Eicher, A. Flax processing in the Neolithic and Bronze Age pile-dwelling settlements of eastern Switzerland. *Veg. Hist. Archaeobotany* **20**, 535–542 (2011).

13. Maier, U. & Schlichtherle, H. Flax cultivation and textile production in Neolithic wetland settlements on Lake Constance and in Upper Swabia (south-west Germany). *Veg. Hist. Archaeobotany* **20**, 567–578 (2011).

14. Gong, Y., Li, L., Gong, D., Yin, H. & Zhang, J. Biomolecular Evidence of Silk from 8,500 Years Ago. *PLOS ONE* **11**, (2016).

15. Betts, A., van der Borg, K., de Jong, A., McClintock, C. & van Strydonck, M. Early Cotton in North Arabia. *J. Archaeol. Sci.* **21**, 489–499 (1994).

16. Ryder, M. L. Probable Fibres from Hemp (Cannabis sativa L.) in Bronze Age Scotland. *Environ. Archaeol.* **4**, 93–95 (1999).

17. Barlow, A. *The History and Principles of Weaving: By Hand and by Power*. (Low, Marston, Searle, & Rivington, 1878).

18. Gleason, C. *The Biography of Wool*. (Crabtree Publishing Company, 2007).

19. CIRFS: World Production by Fibre. Available at: https://www.cirfs.org/statistics/key-statistics/world-production-fibre. (Accessed: 23rd April 2019)

20. Chen, C. *et al.* Achieving high performance corrosion and wear resistant epoxy coatings via incorporation of noncovalent functionalized graphene. *Carbon* **114**, 356–366 (2017).

21. Teshima, K., Sugimura, H., Inoue, Y., Takai, O. & Takano, A. Transparent ultra water-repellent poly(ethylene terephthalate) substrates fabricated by oxygen plasma treatment and subsequent hydrophobic coating. *Appl. Surf. Sci.* **244**, 619–622 (2005).

22. Yan, H., Kurogi, K., Mayama, H. & Tsujii, K. Environmentally Stable Super Water-Repellent Poly(alkylpyrrole) Films. *Angew. Chem. Int. Ed.* **44**, 3453–3456 (2005).

23. Grand, A. F. & Wilkie, C. A. *Fire Retardancy of Polymeric Materials*. (CRC Press, 2000).

24. McKittrick, J. *et al.* The Structure, Functions, and Mechanical Properties of Keratin. *JOM* **64**, 449–468 (2012).

25. Wang, B., Yang, W., McKittrick, J. & Meyers, M. A. Keratin: Structure, mechanical properties, occurrence in biological organisms, and efforts at bioinspiration. *Prog. Mater. Sci.* **76**, 229–318 (2016).

26. Vollrath, F. & Porter, D. Silks as ancient models for modern polymers. *Polymer* **50**, 5623–5632 (2009).

27. Gosline, J. M., DeMont, M. E. & Denny, M. W. The structure and properties of spider silk. *Endeavour* **10**, 37–43 (1986).

28. Mukhopadhyay, S. & Sakthivel, J. C. Spider Silk – Providing New Insights in the Field of High Performance Materials. *J. Ind. Text.* **35**, 91–113 (2005).

29. Reddy, N. & Yang, Y. Properties and potential applications of natural cellulose fibers from cornhusks. *Green Chem.* **7**, 190–195 (2005).

30. Green, D. W., Winandy, J. E. & Kretschmann, D. E. Mechanical properties of wood. in *Wood handbook : wood as an engineering material.* **113**, 4.1–4.45 (Madison, WI : USDA Forest Service, Forest Products Laboratory, 1999).

31. Waite, J. H., Qin, X.-X. & Coyne, K. J. The peculiar collagens of mussel byssus. *Matrix Biol.* **17**, 93–106 (1998).

32. Bell, E. & Gosline, J. Mechanical design of mussel byssus: material yield enhances attachment strength. *J. Exp. Biol.* **199**, 1005–1017 (1996).

33. Qin, X. X., Coyne, K. J. & Waite, J. H. Tough tendons. Mussel byssus has collagen with silk-like domains. *J. Biol. Chem.* **272**, 32623–32627 (1997).

34. Harrington, M. J., Gupta, H. S., Fratzl, P. & Waite, J. H. Collagen insulated from tensile damage by domains that unfold reversibly: In situ X-ray investigation of mechanical yield and damage repair in the mussel byssus. *J. Struct. Biol.* **167**, 47–54 (2009).

35. Maeder, F. Landscape of Sea-Silk Traces of traditional production around Mediterranean Sea Felicitas Maeder Project Sea-silk, Natural History Museum Basel, Switzerland. in (2017).

36. Swinburne, H. *Voyages dans les deux Siciles*. (Chez Théophile Barrois le jeune, Libraire, Quai des Augustins, N. 18, 1785).

37. Turner, R. D. & Rosewater, J. *The Family Pinnidae in the Western Atlantic*. (The Department of Mollusks, Museum of Comparative Zoology, 1958).

38. Laufer, B. The Story of the Pinna and the Syrian Lamb. *J. Am. Folk.* **28**, 103–128 (1915).

39. McKinley, D. *Pinna and Her Silken Beard: A Foray Into Historical Misappropriations*. (Charles Babbage Research Centre, 1998).

40. Harich-Schwarzbauer, H. *Weaving and Fabric in Antiquity / Weben und Gewebe in der Antike: Materiality – Representation – Epistemology – Metapoetics / Materialität – Repräsentation – Episteme – Metapoetik*. (Oxbow Books, 2016).

41. Montegut, D. Moth or Mollusc? A Technical Examination of Byssus Fibers. *Mater. Technol. Art Conserv. Stud. Honor Lawrence J Majewski Occas. His 80th Birthd.* 186–203 (1999).

42. Castillo, J. A Note on the Concept of Tacit Knowledge. *J. Manag. Inq.* **11**, 46–57 (2002).

43. Lee, H., Lee, B. P. & Messersmith, P. B. A reversible wet/dry adhesive inspired by mussels and geckos. *Nature* **448**, 338–341 (2007).

44. Yang, M., Yamauchi, K., Kurokawa, M. & Asakura, T. Design of silk-like biomaterials inspired by mussel-adhesive protein. *Tissue Eng.* **13**, 2941–2947 (2007).

45. Fullenkamp, D. E. *et al.* Mussel-inspired silver-releasing antibacterial hydrogels. *Biomaterials* **33**, 3783–3791 (2012).

46. Kivelio, A. *et al.* Mussel mimetic tissue adhesive for fetal membrane repair: initial in vivo investigation in rabbits. *Eur. J. Obstet. Gynecol. Reprod. Biol.* **171**, 240–245 (2013).

47. Holten-Andersen, N. & Waite, J. H. Mussel-designed Protective Coatings for Compliant Substrates. *J. Dent. Res.* **87**, 701–709 (2008).

48. Bowen, C. H. *et al.* Recombinant Spidroins Fully Replicate Primary Mechanical Properties of Natural Spider Silk. *Biomacromolecules* **19**, 3853–3860 (2018).

49. *BP Statistical Review of World Energy*. (bp, 2018).

50. How Much Oil Is Left In The Earth? *NASDAQ.com* (2017).

51. *OPEC Annual Statistical Bulletin*. (Organisation of the Petroleum Exporting Countries, 2018).

52. Ledenko, M., Velić, J. & Karasalihović Sedlar, D. Analysis of oil reserves, production and oil price trends in 1995, 2005, 2015. *Min.-Geol.-Pet. Eng. Bull.* **33**, 105–115 (2018).

53. Chapman, I. The end of Peak Oil? Why this topic is still relevant despite recent denials. *Energy Policy* **64**, 93–101 (2014).

54. Jackson, R. B. *et al.* Warning signs for stabilizing global CO2 emissions. *Environ. Res. Lett.* **12**, 110202 (2017).

55. United States Environmental Protection Agency. Sources of Greenhouse Gas Emissions. *US EPA* (2015). Available at: www.epa.gov. (Accessed: 21st November 2018)

56. Olivetti, E. A. & Cullen, J. M. Toward a sustainable materials system. *Science* **360**, 1396–1398 (2018).

57. De Mestral, G. Velvet type fabric and method of producing same. (1955).

58. Liu, K. & Jiang, L. Bio-Inspired Self-Cleaning Surfaces. *Annu. Rev. Mater. Res.* **42**, 231–263 (2012).

59. Jiang, L., Zhao, Y. & Zhai, J. A Lotus-Leaf-like Superhydrophobic Surface: A Porous Microsphere/Nanofiber Composite Film Prepared by Electrohydrodynamics. *Angew. Chem.* **116**, 4438–4441 (2004).

60. Wu, L. Y. L., Shao, Q., Wang, X. C., Zheng, H. Y. & Wong, C. C. Hierarchical structured sol–gel coating by laser textured template imprinting for surface superhydrophobicity. *Soft Matter* **8**, 6232–6238 (2012).

61. GECKSKIN®. *GECKSKIN®* Available at: www.buygeckskin.com. (Accessed: 3rd April 2019)

62. Mahdavi, A. *et al.* A biodegradable and biocompatible gecko-inspired tissue adhesive. *Proc. Natl. Acad. Sci.* **105**, 2307–2312 (2008).

63. Menon, C., Murphy, M. & Sitti, M. Gecko Inspired Surface Climbing Robots. in *2004 IEEE International Conference on Robotics and Biomimetics* 431–436 (2004).

64. Murphy, M. P., Aksak, B. & Sitti, M. Gecko-Inspired Directional and Controllable Adhesion. *Small* **5**, 170–175 (2009).

65. Murphy, M. P., Kim, S. & Sitti, M. Enhanced Adhesion by Gecko-Inspired Hierarchical Fibrillar Adhesives. *ACS Appl. Mater. Interfaces* **1**, 849–855 (2009).

66. Brodoceanu, D., Bauer, C. T., Kroner, E., Arzt, E. & Kraus, T. Hierarchical bioinspired adhesive surfaces—a review. *Bioinspir. Biomim.* **11**, (2016).

67. Hawkes E. W., Eason E. V., Christensen D. L. & Cutkosky M. R. Human climbing with efficiently scaled gecko-inspired dry adhesives. *J. R. Soc. Interface* **12**, (2015).

68. Jiang, H. *et al.* A robotic device using gecko-inspired adhesives can grasp and manipulate large objects in microgravity. *Sci. Robot.* **2**, (2017).

69. Glick, P. *et al.* A Soft Robotic Gripper With Gecko-Inspired Adhesive. *IEEE Robot. Autom. Lett.* **3**, 903–910 (2018).

70. Bhushan, B. Shark Skin Surface for Fluid-Drag Reduction in Turbulent Flow. in *Biomimetics: Bioinspired Hierarchical-Structured Surfaces for Green Science and Technology* (ed. Bhushan, B.) 491–562 (Springer International Publishing, 2018).

71. Domel August G. *et al.* Shark skin-inspired designs that improve aerodynamic performance. *J. R. Soc. Interface* **15**, (2018).

72. Ibrahim, M. D. *et al.* The Study of Drag Reduction on Ships Inspired by Simplified Shark Skin Imitation. *Appl. Bionics Biomech.* (2018).

73. Chen, D., Liu, Y., Chen, H. & Zhang, D. Bio-inspired drag reduction surface from sharkskin. *Biosurface Biotribology* **4**, 39–45 (2018).

74. Molyneux, J. & Ransom, T. A. Wetsuits with hydrodynamic interlocking and kinesiologic features. (2019).

75. Hager, M. D., Greil, P., Leyens, C., Zwaag, S. van der & Schubert, U. S. Self-Healing Materials. *Adv. Mater.* **22**, 5424–5430 (2010).

76. Burgert Ingo & Fratzl Peter. Actuation systems in plants as prototypes for bioinspired devices. *Philos. Trans. R. Soc. Math. Phys. Eng. Sci.* **367**, 1541–1557 (2009).

77. Ionov, L. Biomimetic Hydrogel-Based Actuating Systems. *Adv. Funct. Mater.* **23**, 4555–4570 (2013).

78. Hwang, J. *et al.* Biomimetics: forecasting the future of science, engineering, and medicine. *Int. J. Nanomedicine* **10**, 5701–5713 (2015).

79. Fratzl, P. Biomimetic materials research: what can we really learn from nature's structural materials? *J. R. Soc. Interface* **4**, 637–642 (2007).

80. Meyers, M. A., Chen, P.-Y., Lin, A. Y.-M. & Seki, Y. Biological materials: Structure and mechanical properties. *Prog. Mater. Sci.* **53**, 1–206 (2008).

81. Raabe, D., Sachs, C. & Romano, P. The crustacean exoskeleton as an example of a structurally and mechanically graded biological nanocomposite material. *Acta Mater.* **53**, 4281–4292 (2005).

82. Thanukos, A. How the Adaptation Got its Start. *Evol. Educ. Outreach* **2**, 612 (2009).

83. Benton, J. R. ART. VIII.-The Strength and Elasticity of Spider Thread. *Am. J. Sci.* **24**, 75 (1907).

84. Hansen, V. *The Silk Road: A New History*. (Oxford University Press, 2012).

85. Foltz, R. *Religions of the Silk Road - Premodern Patterns of Globalization*. (Palgrave Macmillan, 1999).

86. Cherry, R. H. History of Sericulture. *Bull. Entomol. Soc. Am.* **33**, 83–85 (1987).

87. silk | Definition & History. *Encyclopedia Britannica* Available at: www.britannica.com. (Accessed: 5th March 2019)

88. Murugesh Babu, K. *Silk: Processing, Properties and Applications*. (Elsevier, 2013).

89. Cartwright, M. Silk in Antiquity. *Ancient History Encyclopedia* (2017). Available at: www.ancient.eu. (Accessed: 7th March 2019)

90. Liu, X. *The Silk Road in World History*. (Oxford University Press, 2010).

91. Frankopan, P. *The Silk Roads: A New History of the World*. (Bloomsbury Publishing, 2015).

92. Minoura, N., Aiba, S.-I., Gotoh, Y., Tsukada, M. & Imai, Y. Attachment and growth of cultured fibroblast cells on silk protein matrices. *J. Biomed. Mater. Res.* **29**, 1215–1221 (1995).

93. Halsted, W. S. Ligature and suture material: The Employment of Fine Silk in Preference to Catgut and the Advantages of Transfixion of Tissues and Vessels in Control of Hemorrhage Also an Account of the Introduction of Gloves, Gutta-Percha Tissue and Silver Foil. *J. Am. Med. Assoc.* **60**, 1119–1126 (1913).

94. Sutherland, T. D., Young, J. H., Weisman, S., Hayashi, C. Y. & Merritt, D. J. Insect Silk: One Name, Many Materials. *Annu. Rev. Entomol.* **55**, 171–188 (2010).

95. Gosline, J. M., Denny, M. W. & DeMont, M. E. Spider silk as rubber. *Nature* **309**, 551 (1984).

96. Vollrath, F. & Knight, D. P. Liquid crystalline spinning of spider silk. *Nature* **410**, 541–548 (2001).

97. Jin, H.-J. & Kaplan, D. L. Mechanism of silk processing in insects and spiders. *Nature* **424**, 1057–1061 (2003).

98. Keten, S., Xu, Z., Ihle, B. & Buehler, M. J. Nanoconfinement controls stiffness, strength and mechanical toughness of β-sheet crystals in silk. *Nat. Mater.* **9**, 359–367 (2010).

99. Priemel, T., Degtyar, E., Dean, M. N. & Harrington, M. J. Rapid self-assembly of complex biomolecular architectures during mussel byssus biofabrication. *Nat. Commun.* **8**, (2017).

100. Blackledge, T. A. *et al.* Reconstructing web evolution and spider diversification in the molecular era. *Proc. Natl. Acad. Sci.* **106**, 5229–5234 (2009).

101. Omenetto, F. G. & Kaplan, D. L. A new route for silk. *Nat. Photonics* **2**, 641–643 (2008).

102. Scheibel, T., Huemmerich, D. & Gat, U. Synthesis of spider dragline and/or flagelliform proteins. (2011).

103. Koeppel, A. & Holland, C. Progress and trends in artificial silk spinning: a systematic review. *ACS Biomater. Sci. Eng.* **3**, 226–237 (2017).

104. Demura, M. & Asakura, T. Porous membrane of Bombyx mori silk fibroin: structure characterization, physical properties and application to glucose oxidase immobilization. *J. Membr. Sci.* **59**, 39–52 (1991).

105. Liu, Y., Ling, S., Wang, S., Chen, X. & Shao, Z. Thixotropic silk nanofibril-based hydrogel with extracellular matrix-like structure. *Biomater. Sci.* **2**, 1338–1342 (2014).

106. Muller, W. S., Samuelson, L. A., Fossey, S. A. & Kaplan, D. Formation and properties of silk thin films. *ACS Symp. Ser. USA* (1994).

107. Kim, S. H., Nam, Y. S., Lee, T. S. & Park, W. H. Silk Fibroin Nanofiber. Electrospinning, Properties, and Structure. *Polym. J.* **35**, 185–190 (2003).

108. Andersson, M. *et al.* Biomimetic spinning of artificial spider silk from a chimeric minispidroin. *Nat. Chem. Biol.* **13**, 262–264 (2017).

109. Heidebrecht, A. *et al.* Biomimetic Fibers Made of Recombinant Spidroins with the Same Toughness as Natural Spider Silk. *Adv. Mater.* **27**, 2189–2194 (2015).

110. Salehi, S. & Scheibel, T. Biomimetic spider silk fibres : from vision to reality. *The Biochemist* **40**, 4–7 (2018).

111. AMSilk. Available at: www.amsilk.com/home. (Accessed: 3rd April 2019)

112. Spiber Inc. *Spiber Inc.* Available at: www.spiber.jp. (Accessed: 3rd April 2019)

113. Bolt Threads – Microsilk. Available at: www.boltthreads.com/technology/microsilk/. (Accessed: 3rd April 2019)

114. Spider Silk Technology Company | Kraig Biocraft Laboratories. Available at: www.kraiglabs.com. (Accessed: 16th April 2019)

115. Service, R. F. Silken promises. *Science* **358**, 293–294 (2017).

116. Roberts, M. B. V. *Biology: A Functional Approach*. (Nelson Thornes, 1986).

117. Yonge, C. M. On The Primitive Significance of the Byssus in the Bivalvia and its Effects in Evolution. *J. Mar. Biol. Assoc. U. K.* **42**, 113–125 (1962).

118. Todd, J. A. Bivalve Life Habits Database. (2001). Available at: https://fossils.its.uiowa.edu/database/bivalves/Bivalve_eco.html. (Accessed: 6th March 2019)

119. Brazee, S. L. & Carrington, E. Interspecific Comparison of the Mechanical Properties of Mussel Byssus. *Biol. Bull.* **211**, 263–274 (2006).

120. Bouhlel, Z. *et al.* Interspecies comparison of the mechanical properties and biochemical composition of byssal threads. *J. Exp. Biol.* **220**, 984–994 (2017).

121. Lucas, J. M., Vaccaro, E. & Waite, J. H. A molecular, morphometric and mechanical comparison of the structural elements of byssus from Mytilus edulis and Mytilus galloprovincialis. *J. Exp. Biol.* **205**, 1807–1817 (2002).

122. Miserez, A., Li, Y., Cagnon, J., Weaver, J. C. & Waite, J. H. Four-Stranded Coiled-Coil Elastic Protein in the Byssus of the Giant Clam, Tridacna maxima. *Biomacromolecules* **13**, 332–341 (2012).

123. Monnier, C. A., DeMartini, D. G. & Waite, J. H. Intertidal exposure favors the soft-studded armor of adaptive mussel coatings. *Nat. Commun.* **9**, (2018).

124. Pearce, T. & LaBarbera, M. Biomechanics of byssal threads outside the Mytilidae: Atrina rigida and Ctenoides mitis. *J. Exp. Biol.* **212**, 1449–1454 (2009).

125. Eltzholtz, J. R. & Birkedal, H. Architecture of the Biomineralized Byssus of the Saddle Oyster (Anomia sp.). *J. Adhes.* **85**, 590–600 (2009).

126. García-March, J. R. Aportaciones al conocimiento de la biología de Pinna Nobilis Linneo, 1758 (Mollusca Bivalvia) en el litoral mediterráneo ibérico. (Universitat de Valencia, 2005).

127. Carrington, E. & Gosline, J. M. Mechanical design of mussel byssus: Load cycle and strain rate dependency. *Am. Malacol. Bull.* **18**, 135–142 (2004).

128. Schmitt, C. N. Z., Politi, Y., Reinecke, A. & Harrington, M. J. Role of Sacrificial Protein–Metal Bond Exchange in Mussel Byssal Thread Self-Healing. *Biomacromolecules* **16**, 2852–2861 (2015).

129. Reinecke, A., Bertinetti, L., Fratzl, P. & Harrington, M. J. Cooperative behavior of a sacrificial bond network and elastic framework in providing self-healing capacity in mussel byssal threads. *J. Struct. Biol.* **196**, 329–339 (2016).

130. Qin, X. & Waite, J. H. Exotic collagen gradients in the byssus of the mussel Mytilus edulis. *J. Exp. Biol.* **198**, 633–644 (1995).

131. Fitton Jackson, S. *et al.* The Byssus Threads of Mytilus Edulis and Pinna Nobilis. in *Nature and Structure of Collagen* 106–116 (Butterworths Scientific Publications, 1953).

132. Lucas, F., Shaw, J. T. B. & Smith, S. G. 30—The Chemical Constitution of some Silk Fibroins and its Bearing on their Physical Properties. *J. Text. Inst. Trans.* **46**, T440–T452 (1955).

133. Schmitt, C. N. Z. The Role of Protein Metal Complexes in the Mechanics of Mytilus californianus Byssal Threads. (University of Potsdam, 2015).

134. Holten-Andersen, N., Fantner, G. E., Hohlbauch, S., Waite, J. H. & Zok, F. W. Protective coatings on extensible biofibres. *Nat. Mater.* **6**, 669–672 (2007).

135. Holten-Andersen, N., Zhao, H. & Waite, J. H. Stiff Coatings on Compliant Biofibers: The Cuticle of Mytilus californianus Byssal Threads†,‡. *Biochemistry (Mosc.)* **48**, 2752–2759 (2009).

136. Harrington, M. J., Masic, A., Holten-Andersen, N., Waite, J. H. & Fratzl, P. Iron-Clad Fibers: A Metal-Based Biological Strategy for Hard Flexible Coatings. *Science* **328**, 216–220 (2010).

137. Schmitt, C. N. Z. *et al.* Mechanical homeostasis of a DOPA-enriched biological coating from mussels in response to metal variation. *J. R. Soc. Interface* **12**, (2015).

138. Krauss, S., Metzger, T. H., Fratzl, P. & Harrington, M. J. Self-Repair of a Biological Fiber Guided by an Ordered Elastic Framework. *Biomacromolecules* **14**, 1520–1528 (2013).

139. Aldred, N., Wills, T., Williams, D. N. & Clare, A. S. Tensile and dynamic mechanical analysis of the distal portion of mussel (Mytilus edulis) byssal threads. *J. R. Soc. Interface* **4**, 1159–1167 (2007).

140. Harrington, M. J. & Waite, J. H. Holdfast heroics: comparing the molecular and mechanical properties of Mytilus californianus byssal threads. *J. Exp. Biol.* **210**, 4307–4318 (2007).

141. Pujol, J. P. Le complexe byssogène des mollusques bivalves, histochimie comparé des sécrétions chez Mytilus Edulis L. et Pinna Nobilis L. *Bull. Sciété Linneenne Normandie* 308–331 (1967).

142. Waite, J. H. The formation of mussel byssus: anatomy of a natural manufacturing process. *Results Probl. Cell Differ.* **19**, 27–54 (1992).

143. Harrington, M. J. & Waite, J. H. pH-Dependent Locking of Giant Mesogens in Fibers Drawn from Mussel Byssal Collagens. *Biomacromolecules* **9**, 1480–1486 (2008).

144. Rodriguez, N. R. M., Das, S., Kaufman, Y., Israelachvili, J. N. & Waite, J. H. Interfacial pH during mussel adhesive plaque formation. *Biofouling* **31**, 221–227 (2015).

145. Elodie Rouanet, S. T. From youth to death of old age: the 50-year story of a Pinna nobilis fan mussel population at Port-Cros Island (Port-Cros National Park, Provence, Mediterranean Sea). *Sci. Rep. Port-Cros Natl. Park* **29**, 209–222 (2015).

146. Zavodnik, D., Hrs-Brenko, M. & Legac, M. Synopsis on the fan shell Pinna nobilis L. in the eastern Adriatic Sea. *Espèces Mar. À Prot. En Méditerranée* 169–178 (1991).

147. Fiorito, G. & Gherardi, F. Prey-handling behaviour of Octopus vulgaris (Mollusca, Cephalopoda) on Bivalve preys. *Behav. Processes* **46**, 75–88 (1999).

148. García-March, J. R., Pérez-Rojas, L. & García-Carrascosa, A. M. Influence of hydrodynamic forces on population structure of Pinna nobilis L., 1758 (Mollusca: Bivalvia): The critical combination of drag force, water depth, shell size and orientation. *J. Exp. Mar. Biol. Ecol.* **342**, 202–212 (2007).

149. Butler, A., Vicente, N. & De Gaulejac, B. Ecology of the pterioid bivalves Pinna bicolor Gmelin and Pinna nobilis L. *Mar. Life* **3**, 37–45 (1993).

150. Diana, A. *et al.* The byssus threads of Pinna nobilis: A histochemical and ultrastructural study. *Eur. J. Histochem.* **61**, 280–286 (2017).

151. García-March, J. R. & Vicente, N. Protocole d'étude et de surveillance des populations de Pinna Nobilis dans les aires marines protegées. (2006).

152. Pujol, J. P., Rolland, M., Larsy, S. & Vinet, S. Comparative study of the amino acid composition of the byssus in some common bivalve molluscs. *Comp. Biochem. Physiol.* **34**, 193–201 (1970).

153. Abderhalden, E. Die Monoaminosäuren des 'Byssus' von Pinna nobilis L. *Z. Für Physiol. Chem.* **55**, (1908).

154. Yoo, H. Y. *et al.* Sugary interfaces mitigate contact damage where stiff meets soft. *Nat. Commun.* **7**, 11923 (2016).

155. Hwang, J. J., Yamakawa, T. & Aoki, I. Growth of wild pearl oysters Pinctada fucata, Pinctada margaritifera and Pinctada sugillata (Bivalvia: Pteriidae) in Taiwan. *Fish. Sci.* **73**, 132–141 (2007).

156. Liu, C. *et al.* Extensible byssus of Pinctada fucata: Ca2+-stabilized nanocavities and a thrombospondin-1 protein. *Sci. Rep.* **5**, (2015).

157. Liu, C., Xie, L. & Zhang, R. Ca2+ Mediates the Self-Assembly of the Foot Proteins of Pinctada fucata from the Nanoscale to the Microscale. *Biomacromolecules* **17**, 3347–3355 (2016).

158. Folkhard, W., Marvin, D. A., Watts, T. H. & Paranchych, W. Structure of polar pili from Pseudomonas aeruginosa strains K and O. *J. Mol. Biol.* **149**, 79–93 (1981).

159. Gorgel, M. *et al.* High-resolution structure of a type IV pilin from the metal-reducing bacterium Shewanella oneidensis. *BMC Struct. Biol.* **15**, 4 (2015).

160. L. Kreplak, J. Doucet & F. Briki. Unraveling double stranded α-helical coiled coils: An x-ray diffraction study on hard α-keratin fibers. *Biopolymers* **58**, 526–533 (2000).

161. Harrington, M. J. *et al.* Pseudoelastic behaviour of a natural material is achieved via reversible changes in protein backbone conformation. *J. R. Soc. Interface* **9**, 2911–2922 (2012).

162. Demtröder, W. *Experimentalphysik 2: Elektrizität und Optik*. (Springer-Verlag, 2013).

163. Leng, Y. *Materials Characterization: Introduction to Microscopic and Spectroscopic Methods*. (John Wiley & Sons, 2009).

164. Schwarzenbach, D. & Chapuis, G. *Cristallographie*. (PPUR presses polytechniques, 2006).

165. Suryanarayana, C. & Norton, M. G. *X-Ray Diffraction: A Practical Approach*. (Springer US, 1998).

166. Hammond, C. *The Basics of Crystallography and Diffraction*. (Oxford University Press, 2001).

167. Leng, Y. X-Ray Diffraction Methods. in *Materials Characterization* 45–77 (John Wiley & Sons, Ltd, 2010).

168. Liss, K.-D., Bartels, A., Schreyer, A. & Clemens, H. High-Energy X-Rays: A tool for Advanced Bulk Investigations in Materials Science and Physics. *Textures Microstruct.* **35**, 219–252 (2003).

169. Fernandes, A. N. *et al.* Nanostructure of cellulose microfibrils in spruce wood. *Proc. Natl. Acad. Sci. U. S. A.* **108**, 1195–1203 (2011).

170. Keckes, J. *et al.* In-Situ X-ray Diffraction as a Tool to Probe Mechanical Phenomena Down to the Nano-Scale. *Adv. Eng. Mater.* **8**, 1084–1088 (2006).

171. Rowell, R. M. *Handbook of Wood Chemistry and Wood Composites*. (CRC Press, 2005).

172. Kreplak, L., Doucet, J., Dumas, P. & Briki, F. New Aspects of the α-Helix to β-Sheet Transition in Stretched Hard α-Keratin Fibers. *Biophys. J.* **87**, 640–647 (2004).

173. Kastelic, J., Galeski, A. & Baer, E. The Multicomposite Structure of Tendon. *Connect. Tissue Res.* **6**, 11–23 (1978).

174. Hall, J. E. *Guyton and Hall Textbook of Medical Physiology*. (Elsevier, 2015).

175. Fiber Diffraction. Available at: https://www.mpimf-heidelberg.mpg.de/emeritusgruppen/biophysik/fiber_diffraction. (Accessed: 8th January 2019)

176. Ramachandran, G. N. Analysis of the x-ray diffraction pattern of helical structures. *Proc. Indian Acad. Sci. - Sect. A* **52**, 240–254 (1960).

177. Knupp, C. & Squire, J. M. HELIX: A helical diffraction simulation program. *ResearchGate* **37**, 832–835 (2004).

178. Welberry, T. R. Diffuse x-ray scattering and models of disorder. *Rep. Prog. Phys.* **48**, (1985).

179. Warren, B. E. *X-Ray Diffraction*. (Courier Corporation, 2012).

180. Welberry, T. R. & Goossens, D. J. Diffuse scattering and partial disorder in complex structures. *IUCrJ* **1**, 550–562 (2014).

181. Meisburger, S. P., Thomas, W. C., Watkins, M. B. & Ando, N. X-ray Scattering Studies of Protein Structural Dynamics. *Chem. Rev.* **117**, 7615–7672 (2017).

182. Feng, R. *et al.* X-ray scattering from amorphous solids. *J. Non-Cryst. Solids* **383**, 21–27 (2014).

183. Paris, O. *et al.* A new experimental station for simultaneous X-ray microbeam scanning for small- and wide-angle scattering and fluorescence at BESSY II. *J. Appl. Crystallogr.* **40**, 466–470 (2006).

184. Benecke, G. *et al.* A customizable software for fast reduction and analysis of large X-ray scattering data sets: applications of the new DPDAK package to small-angle X-ray scattering and grazing-incidence small-angle X-ray scattering. *J. Appl. Crystallogr.* **47**, 1797–1803 (2014).

185. Knupp, C. & Squire, J. M. HELIX: a helical diffraction simulation program. *J. Appl. Crystallogr.* **37**, 832–835 (2004).

186. Moeser, G. M. & Carrington, E. Seasonal variation in mussel byssal thread mechanics. *J. Exp. Biol.* **209**, 1996–2003 (2006).

187. Harrington, M. J., Jehle, F. & Priemel, T. Mussel Byssus Structure-Function and Fabrication as Inspiration for Biotechnological Production of Advanced Materials. *Biotechnol. J.* **13**, (2018).

188. Arnold, A. A. *et al.* Solid-State NMR Structure Determination of Whole Anchoring Threads from the Blue Mussel Mytilus edulis. *Biomacromolecules* **14**, 132–141 (2013).

189. Holten-Andersen, N. *et al.* pH-induced metal-ligand cross-links inspired by mussel yield self-healing polymer networks with near-covalent elastic moduli. *Proc. Natl. Acad. Sci.* **108**, 2651–2655 (2011).

190. Enke, M. *et al.* Self-healing response in supramolecular polymers based on reversible zinc–histidine interactions. *Polymer* **69**, 274–282 (2015).

191. Pasche, D. *et al.* A new twist on sea silk: the peculiar protein ultrastructure of fan shell and pearl oyster byssus. *Soft Matter* **14**, 5654–5664 (2018).

192. Bieler, R., Carter, J. G. & Coan, E. Nomenclator of bivalve families; with a classification of bivalve families by R. Bieler, J. G. Carter & E. V. Coan. *Malacologia* **52**, 113–133 (2010).

193. Szefer, P. *et al.* A comparative assessment of heavy metal accumulation in soft parts and byssus of mussels from subarctic, temperate, subtropical and tropical marine environments. *Environ. Pollut.* **139**, 70–78 (2006).

194. Szefer, P. *et al.* Distribution and relationships of trace metals in soft tissue, byssus and shells of Mytilus edulis trossulus from the southern Baltic. *Environ. Pollut.* **120**, 423–444 (2002).

195. Cooper, G. M. Structure and Organization of Actin Filaments. in *The Cell: A Molecular Approach.* (Sunderland (MA):Sinauer Associates, 2000).

196. Hanson, J. & Lowy, J. The structure of F-actin and of actin filaments isolated from muscle. *J. Mol. Biol.* **6**, 46–60 (1963).

197. Williams, D. B. & Carter, C. B. *Transmission Electron Microscopy: A Textbook for Materials Science*. (Springer US, 2009).

198. Sagert, J. & Waite, J. H. Hyperunstable matrix proteins in the byssus of Mytilus galloprovincialis. *J. Exp. Biol.* **212**, 2224–2236 (2009).

199. Coombs, T. L. & Keller, P. J. Mytilus byssal threads as an environmental marker for metals. *Aquat. Toxicol.* **1**, 291–300 (1981).

200. Szefer, P., Kim, B.-S., Kim, C.-K., Kim, E.-H. & Lee, C.-B. Distribution and coassociations of trace elements in soft tissue and byssus of Mytilus galloprovincialis relative to the surrounding seawater and suspended matter of the southern part of the Korean Peninsula. *Environ. Pollut. Barking Essex 1987* **129**, 209–228 (2004).

201. Degtyar, E., Harrington, M. J., Politi, Y. & Fratzl, P. The Mechanical Role of Metal Ions in Biogenic Protein-Based Materials. *Angew. Chem. Int. Ed.* **53**, 12026–12044 (2014).

202. Pauling, L. & Corby, R. B. The structure of fibrous proteins of the collagen gelatin group. *Proc. Natl. Acad. Sci.* **37**, 272–281 (1951).

203. Gruen, L. C. & Woods, E. F. Structural studies on the microfibrillar proteins of wool. Interaction between alpha-helical segments and reassembly of a four-chain structure. *Biochem. J.* **209**, 587–595 (1983).

204. Fudge, D. S., Gardner, K. H., Forsyth, V. T., Riekel, C. & Gosline, J. M. The Mechanical Properties of Hydrated Intermediate Filaments: Insights from Hagfish Slime Threads. *Biophys. J.* **85**, 2015–2027 (2003).

205. Elizabeth A Koch, Spitzer, R. H., Pithawalla, R. B. & Parry, D. A. D. An unusual intermediate filament subunit from the cytoskeletal biopolymer released extracellularly into seawater by the primitive hagfish (Eptatretus stouti). *J. Cell Sci.* **107**, 3133–3144 (1994).

206. Hospenthal, M. K. *et al.* Structure of a Chaperone-Usher Pilus Reveals the Molecular Basis of Rod Uncoiling. *Cell* **164**, 269–278 (2016).

207. Fällman, E., Schedin, S., Jass, J., Uhlin, B.-E. & Axner, O. The unfolding of the P pili quaternary structure by stretching is reversible, not plastic. *EMBO Rep.* **6**, 52–56 (2005).

208. Schmidt, S. *et al.* Metal-Mediated Molecular Self-Healing in Histidine-Rich Mussel Peptides. *Biomacromolecules* **15**, 1644–1652 (2014).

209. Miller, E., Garcia, T., Hultgren, S. & Oberhauser, A. F. The Mechanical Properties of E. coli Type 1 Pili Measured by Atomic Force Microscopy Techniques. *Biophys. J.* **91**, 3848–3856 (2006).

210. Kratky, O. & Porod, G. Röntgenuntersuchung gelöster Fadenmoleküle. *Recl. Trav. Chim. Pays-Bas* **68**, 1106–1122 (1949).

211. Zhang, W. & Zhang, X. Single molecule mechanochemistry of macromolecules. *Prog. Polym. Sci.* **28**, 1271–1295 (2003).

212. Janshoff, A., Neitzert, M., Oberdörfer, Y. & Fuchs, H. Force Spectroscopy of Molecular Systems—Single Molecule Spectroscopy of Polymers and Biomolecules. *Angew. Chem. Int. Ed.* **39**, 3212–3237 (2000).

213. Li, H. & Fernandez, J. M. Mechanical Design of the First Proximal Ig Domain of Human Cardiac Titin Revealed by Single Molecule Force Spectroscopy. *J. Mol. Biol.* **334**, 75–86 (2003).

214. Sharma, H. S. S. & Sumere, C. F. van. *Biology and processing of flax*. (M Publications, 1992).

215. Scales, H. *Spirals in Time: The Secret Life and Curious Afterlife of Seashells*. (Bloomsbury Publishing, 2015).

216. James Yates. On The Raw Materials Used For Weaving. in *an account of the art of weaving among the ancients* 472 (1843).

217. Verne, J., Davies, D. S. & Carabine, D. K. *Twenty Thousand Leagues Under the Sea*. (Wordsworth Editions, 1992).

218. Gilroy, C. G. *The History of Silk, Cotton, Linen, Wool, and Other Fibrous Substances:* (Harper & Brothers, 1845).

219. *Textiles and Fashion*. (Elsevier, 2015).

220. Okey, S. *Spin to Knit*. (Interweave, 2006).

221. Movasaghi, Z., Rehman, S. & Rehman, D. I. ur. Fourier Transform Infrared (FTIR) Spectroscopy of Biological Tissues. *Appl. Spectrosc. Rev.* **43**, 134–179 (2008).

222. Woodill, L. A. & Hinrichs, R. Z. Heterogeneous reactions of surface-adsorbed catechol with nitrogen dioxide: substrate effects for tropospheric aerosol surrogates. *Phys. Chem. Chem. Phys.* **12**, 10766–10774 (2010).

223. Barnard, W. & Waal, D. de. Raman investigation of pigmentary molecules in the molluscan biogenic matrix. *J. Raman Spectrosc.* **37**, 342–352 (2006).

224. Grotewold, E. The Genetics and Biochemistry of Floral Pigments. *Annu. Rev. Plant Biol.* **57**, 761–780 (2006).

225. Himasnshu Paliwal, Sachin Goyal, Shivali Singla & Shashi Daksh. Pigments from natural sources: An overview. *Int. J. Res. Pharm. Pharm. Sci.* **1**, 1–12 (2016).

226. Micillo, R. *et al.* 'Fifty Shades' of Black and Red or How Carboxyl Groups Fine Tune Eumelanin and Pheomelanin Properties. *Int. J. Mol. Sci.* **17**, 746 (2016).

227. J. Sever, M. & J. Wilker, J. Visible absorption spectra of metal–catecholate and metal–tironate complexes. *Dalton Trans.* **0**, 1061–1072 (2004).

228. Tiwari, M. Science behind human saliva. *J. Nat. Sci. Biol. Med.* **2**, 53 (2011).

229. Benedict, C. V. & Waite, J. H. Composition and ultrastructure of the byssus of Mytilus edulis. *J. Morphol.* **189**, 261–270 (1986).

230. Silverman, H. G. & Roberto, F. F. Understanding Marine Mussel Adhesion. *Mar. Biotechnol. N. Y. N* **9**, 661–681 (2007).

231. Kanngießer, B., Malzer, W. & Reiche, I. A new 3D micro X-ray fluorescence analysis set-up – First archaeometric applications. *Nucl. Instrum. Methods Phys. Res. Sect. B Beam Interact. Mater. At.* **211**, 259–264 (2003).

11 Acknowledgments

First, I sincerely thank my supervisors Matt and Peter. You know how much you helped me, probably not how I appreciate for your trust, support and patience.

Vielen Dank auch an meine Doktormutter Birgit für deine Unterstützung und Geduld.

Grazie Chiara, maestro di bisso. Sei la star di questo lavoro, dopo Pinna, e senza di te questa tesi non sarebbe esistita. Grazie per la vostra fiducia e spiegazioni. Grazie Chiara, Giuseppe e Devis per il tempo piacevole e interessante a Sant'Antioco.

Danke auch an:

Jeannette und Alex als beste Quatschbuddies, die den Alltag im Büro deutlich besser machen. Ik dank u Alex ook voor uw altijd nuttige advies. Jeannette, zusätzlich Dank für die verschiedenen AAA und ICP Messungen.

Elena und Rona, für eure Mühe mit dem TEM und *Pinna* freut sich über das Interesse an ihren Haaren. Danke an Heike für die Hilfe mit REM.

Clemens, Nils, Franzi, Tobi, daß ich von eurer Erfahrung profitieren konnte, die ihr immer lieb und geduldig geteilt habt.

Dr. Ioanna Mantouvalou and Tobias Drechsel for the XRF und Chris für die ganz nette antworten zu meine Panik Fragen.

Danke Chenghao und Stefan für die BESSY Messungen, Isabell für deinen Enthusiasmus und deine Hilfe und Korrekturen.

I want to thank Dong Soo and Jimin for having me in Korea. Thank you Jimin also for the nice discussions.

Thank you Shahrouz for the visible light spectroscopy.

Mille mercis à Frédéric et Sébastien pour les super et instructif moments passé à Villefranche. Merci aussi d'avoir rendue possible ma première rencontre avec *Pinna* en chair et en nacre, ainsi que mon premier (et j'espère dernier) mal de terre.

Danke René für deine geduldige Hilfe beim Ausdrucken.

Je remercie Pauline, Dennis, Pompon et Martin pour votre présence, votre écoute, votre soutien et votre effet positif sur mon moral. Martin, Pompon et Pauline, vous êtes des relecteurs en or.

Merci Clemens de t'être occupé de moi ces derniers temps, pour ta patience et ta présence.

Merci á François, Laura, Gritte, Grand-Maman, Etienne et Prof Demartines d'avoir été là au moment de ma vie où j'en avais le plus besoin. Sans vous rien n'aurait été possible.

Finally, I also have to thank all the people from the institute and excuse myself to the people I might have forgotten to cite here.